

DEVELOPMENT OF A FAIL SAFE DESIGN OXIDATION
RESISTANT REINFORCED CARBON SYSTEM FOR THE WING
LEADING EDGE OF A SPACE SHUTTLE VEHICLE

PHASE III FINAL REPORT
VOLUME II TECHNICAL

VSD REPORT NO. T143-5R-30008

JUNE 1973

NASA-JSC CONTRACT NO. NAS9-12763

DRD NO. 3

B. A. Forcht

B. A. Forcht
Project Manager
Approved by

VOUGHT SYSTEMS DIVISION
LTV Aerospace Corporation
P. O. Box 5907
Dallas, Texas 75222

X74-10172

FOREWORD

This final report was prepared by the LTV Aerospace Corporation, Vought Systems Division for NASA/JSC Contract NAS9-12763, Development Of A Fail Safe Design Oxidation Resistant Reinforced Carbon System For The Wing Leading Edge Of A Space Shuttle Vehicle. This work was performed under the direction of the Thermal Technology Branch of the Structures and Mechanics Division with Mr. F. S. Coe, III as the Program Director.

The following individuals were directly responsible for performing the program tasks and in the preparation of this final report: Don While - Project Engineer; Bill Agan and Dwain Bennett - Structures; Jim Medford and Wes Whitten - Thermal; Ed Matza, Frank Tarsia and Al Hill - Design; Bob Bost - Dynamics; Dick Rogers and Kelly Adams - Testing; Ike Harder, Don Rogers, Benny Tillison, Dave Shuford, and Bob Scott - Materials and Processes; Lou Karkos - Manufacturing Project Leader; Jack Vought, Zeke Williams, Stan Whitcher and Tom Mays - Manufacturing; Bob Miller - Quality Control Project Leader; and John Fenton and Roy Littlejohn - Quality Control.

This report is prepared in five volumes. Volume I contains a summary of the wing leading edge program. Volume II provides a detailed technical discussion of the Phase III program. It is arranged in accordance with the major tasks performed under this contract during the period 24 April 1972 through 15 June 1973. Volumes III, IV, and V are appendices, containing backup material and more detail technical data on certain tasks.

TABLE OF CONTENTS

<u>Section</u>		<u>Page</u>
1.0	TECHNICAL DISCUSSION OF TASKS	1
1.1	TASK 1 - FAILSAFE LEADING EDGE	1
	1.1.1 Design	2
	1.1.2 Fabrication	74
	1.1.3 Quality Assurance	87
	1.1.4 Thick Laminate Development	99
1.2	TASK 2 - INSULATION DEVELOPMENT	105
	1.2.1 Materials Evaluation	105
	1.2.2 Parametric Analyses	116
	1.2.3 Vibration Tests	125
1.3	TASK 3 - SUPPORT LUG THERMAL TEST	131
	1.3.1 Parametric Analysis	132
	1.3.2 Initial Test	134
	1.3.3 Design Configuration - Lug Support Test	138
	1.3.4 Test Analysis	141
	1.3.5 Polyimide Fiberglass Temperature Limit	146
1.4	TASK 4 - SEAL STRIP JOINT - GAS LEAK TEST	149
	1.4.1 Alternate Design Concepts	150
	1.4.2 Test Plan and Gap Configurations	155
	1.4.3 Instrumentation Design and Installation Development	161
	1.4.4 Test Conditions and Procedure	166
	1.4.5 Test Results	170
	1.4.6 Thermal Analysis	172
	1.4.7 Conclusions	181
1.5	TASK 5 - THICK LAMINATE MATERIAL FOR NASA EVALUATION	187
1.6	TASK 6 - DOCUMENTATION	189

TABLE OF CONTENTS (Cont'd.)

<u>Section</u>		<u>Page</u>
1.7	TASK 7 - DESTRUCTIVE EVALUATION OF A PHASE II LEADING EDGE	191
1.8	TASK 8 - NON-DESTRUCTIVE EVALUATION OF COATING THICKNESS	201
1.9	TASK 9 - COATING CRAZING INVESTI- GATION	207
1.9.1	Crazing History	207
1.9.2	Technical Discussions with Outside Consultants	209
1.9.3	University of Washington Investigations	210
1.9.4	Chemical Analysis	211
1.9.5	Thermal Expansion	212
1.9.6	Material System Modifications	213
1.9.7	Summary of Results	214
1.10	TASK 10 - FABRICATION OF THICK PLY LAMINATES FOR NASA TEST	217
1.11	TASK 11 - FABRICATION OF 13-PLY LAMINATES FOR NASA TEST	219
1.12	TASK 12 - FABRICATION OF ONE ADDITON- AL FAILSAFE LEADING EDGE	221
1.13	TASK 13 - DESTRUCTIVE EVALUATION OF A PHASE III FAILSAFE LEADING EDGE	223
1.14	TASK 14 - THICK LAMINATE PROPERTY DETERMINATION	231

LIST OF FIGURES

<u>Figure</u>		<u>Page No.</u>
1	Phase III Wing Leading Edge - Full Size - Two Segment Assembly	3
2	Heatshield System Installation	5, 6
3	Drawing Breakdown	8
4	RPP Panel Assembly - Fail Safe Wing Leading Edge	9, 11
5	RPP Panel Support Design	15
6	Test Article Final Assembly - Wing Leading Edge	17, 18
7	Ultimate Design Loads	23
8	Design Properties Used - RPP Bare and Coated, Room Temperature - Warp Direction	25
9	RPP Property Variation with Temperature Coated 13-Ply Material - Warp Direction	27
10	Perspective of NASTRAN Leading Edge Model	28
11	Summary Margins of Safety - Boost Phase	29
12	Summary of Margins of Safety - Entry Phase	31
13	Summary of Margins of Safety - Oxidized Leading Edge Cruise Maneuver	33
14	Leading Edge NASTRAN Buckling Model	34
15	Buckle Mode Shapes	36
16	Summary of Margins of Safety - Support Structure	37
17	Entry Design Trajectory	39
18	Heating Rate Distribution Around Leading Edge	39
19	Comparison of Skin Inside Temperatures - Oxidation Analysis	41
20	Thickness Loss for 2400 Seconds - RPP Density = 80 lb/ft ³	41
21	Skin and Insulation - Maximum Temperatures	42
22	Skin Temperature Distribution (Outside Surface)	42
23	Rib Temperature Distribution	45

LIST OF FIGURES (Cont'd.)

<u>Figure</u>		<u>Page No.</u>
24	Windward Side Support Joint Temperatures - Entry Time = 400 seconds	45
25	Heatshield Analysis Maximum Temperatures	47
26	Maximum Temperatures from Heatshield Analysis	47
27	Temperature Response - Heatshield Analysis	47
28	Peak Temperatures in Lower Lug Insulation and Support Bracket - Side View	51
29	Peak Temperatures in Lower Lug Insulation and Support Bracket - Top View	51
30	Peak Temperatures in Lower Lug Support	52
31	Peak Temperatures in Upper Lug Insulation and Support Bracket - Side View	54
32	Peak Temperatures in Upper Lug Insulation and Support Bracket - Top View	54
33	Predicted Temperatures Windward Side - RSI Panel	56
34	RPP Lug Test - Final Predictions vs Test Data	58
35	Post Test Predictions - Effect of Change in Contact Coefficient	58
36	Predicted Temperatures - Leeward Side - Lug Area	60
37	Random Vibration Environment - Boost Phase	62
38	Acoustic Environment	62
39	First Heatshield Mode Shape - $f = 144$ HZ	64
40	Second Heatshield Mode Shape - $f = 290$ HZ	64
41	Effects of Isolator Thickness and No. of Tiles on Insulation Peak Stress - Canted Heatshield	65
42	Insulation Stress Distribution - Canted Heatshield Weak Direction	65
43	Upper Access Panel Distribution of Stress in Dynaquartz (weak direction)	67

LIST OF FIGURES (Cont'd.)

<u>Figure</u>		<u>Page No.</u>
44	Acoustic Test Leading Edge and Test Fixture	70
45	Acoustic Test Leading Edge Installed in Progressive Wave Facility.	70
46	Hole Damage After Acoustic Test - Countersunk Floating Side	72
47	Acoustic Test Leading Edge Support Lug Beef-up	73
48	Bushing Details Acoustic Test - Leading Edge	73
49	Process Sequence for Coated RPP	77, 78
50	Lay-up Molds	79
51	Restraint Tooling	82
52	Graphite Tooling	83
53	Support Structure and RPP Panel	86
54	Assembly Fixture with Support Structure in Build-up Stage	86
55	Panel Width Tolerance and Measurements	91
56	Panel Thickness Tolerance and Measurements - Coated Condition	93
57	Lug and Rib Tolerance and Measurements - Comparison of L. H. Ribs of Coated Panels	95
58	Coating Thickness Measurements	96
59	Panel Surface Straightness - Measured Along Element Lines	98
60	Typical Temperature Response	122
61	Heatshield Panel Thickness	123
62	Heatshield Vibration Response	123
63	Initial Heatshield Test Component	126
64	Second Heatshield Test Component	128
65	Second Heatshield Test Component After Successful Test	130
66	Early Support Joint Design	133
67	Support Bracket Concepts	133

LIST OF FIGURES (Cont'd.)

<u>Figure</u>		<u>Page No.</u>
68	Initial Support Lug - Component Test	135
69	Lug Bolt for Component Test	136
70	Design Configuration - Support	139
71	Test Results - Design Support Lug Thermal Test	140
72	RPP Lug Test - Final Predictions vs. Test Data	140
73	Polyimide Fiberglass Laminate Test Data	147
74	Comparison of Phase II Joint Seal Design versus Initial Thermal Analysis Model	151
75	Typical Expansion Joint Seal Concepts	153
76	Refinements Made to Phase II Joint Seal Design	154
77	Seal Gap Test Configuration Matrix	156
78	Gap Heating Test Model	157
79	Calibration Model for Seal Strip Joint Leak Test	159
80	Teflon Model for Seal Strip Joint Leak Test - Shown After Test	160
81	Seal Joint Leak Test Model Location and Orientation in Plasma Arc Facility	167
82	Chordwise Heating and Pressure Distributions from Calibration Model	169
83	Thermal Model with Sample Temperature Locations	175
84	Detailed Temperatures - 7 Assembly Stagnation Line	180
85	Heating on -1 Assembly	182
86	Heating on -2 Assembly	183
87	Heating on -3 Assembly	184
88	Heating on -7 Assembly	185
89	Destructive Evaluation of Phase II Leading Edge	192

LIST OF FIGURES (Cont'd.)

<u>Figure</u>		<u>Page No.</u>
90	Eddy Current Statistical Model 1.6MHZ Equipment	205
91	Eddy Current Statistical Model 5 MHZ Equipment	205
92	Crazing Evaluation Program Task - Flow Table	208
93	Cutting Plan - Destructive Test - Phase III Leading Edge	224

LIST OF TABLES

<u>Table</u>		<u>Page No.</u>
1	Static Structural Analyses	22
2	Process History of Thick RPP Laminates	101
3	Physical Properties of Thick RPP Laminates	103
4	Physical Changes in Insulation After 15 Minute - 2500°F Cycles	107
5	Tensile Strength of RTV560 - 64 Hour Cure	113
6	Tensile Strength of RTV 560 - 7 Day Cure	113
7	Comparison of Fail Safe Leading Edge Heatshield Concepts	120
8	Design Properties Used - RPP Bare and Coated - Room Temperature - Warp Direction	143, 144
9	Ceramic Cement Adhesion Test Matrix	162
10	Stagnation Line Gap Heating Test Results	171
11	43° Off Stagnation Line Gap Heating Test Results	171
12	Comparison Between Calculated and Measured Gap Heating Temperatures	176
13	Physical Properties Phase II Leading Edge and Control Specimens	194
14	Mechanical Strength Comparison, Phase II Leading Edge (Average Values)	195
15	Elastic Modulus Comparison, Phase II Leading Edge (Average Values)	198
16	Schedule of Specimens Shipment	203
17	Physical Properties Phase III Leading Edge and Control Specimens	225
18	Mechanical Strength - Phase III Leading Edge	227
19	Strength Comparison - Phase III Leading Edge	229
20	Strength Data - Phase III Coated RPP	233
21	Strength Data - Bare 8-Ply RPP	236
22	Shear Modulus	236
23	Elastic Modulus - Phase III Coated RPP	236

1.0 TECHNICAL DISCUSSION OF TASKS

This volume describes the technical work involved in the execution of the fourteen major program tasks undertaken during the Phase III program. Each of these tasks are discussed in the order in which they were identified in the contract. Additional details on some of the tasks are provided in the appendices of Volumes III, IV, and V. Conclusions and recommendations are included in the summary document, Volume I.

1.1 TASK 1 - FAILSAFE LEADING EDGE

The objective of this task was to design, fabricate, and deliver two complete leading edge assemblies, consisting of the RPP leading edge, support brackets, support structure, and insulation system. The leading edge was to be "failsafe" with respect to thermal/oxidation performance, meaning that the leading edge would be designed for one safe entry to landing, assuming no coating on the outer surface of the leading edge at initiation of entry.

Inherent in this task was the requirement to develop a process for the fabrication of thick (up to 0.5 inch) RPP laminates to provide sufficient material so that even after significant material loss from oxidation during entry a sufficient amount would remain to ensure structural integrity for cruise maneuver and landing loads.

The approach to this task was straightforward from a design standpoint. Computer analyses were employed to establish design thicknesses and to verify overall design performance. Details of the structural and dynamics analyses and thermal analyses are presented in Appendices B and C, respectively. A full scale mock-up was used to aid design and demonstration of spatial and internal access features. Because of the thicknesses and thickness variations (12 to 34 plies) involved in the leading edge, a trial unit was fabricated to establish tooling and lay-up procedures. Thick laminates present fabrication difficulties because of entrapped decomposition gases, which can cause delamination. Because of this difficulty,

a number of processing approaches were initiated in an effort to arrive at an acceptable or best approach. Several of these approaches proved successful.

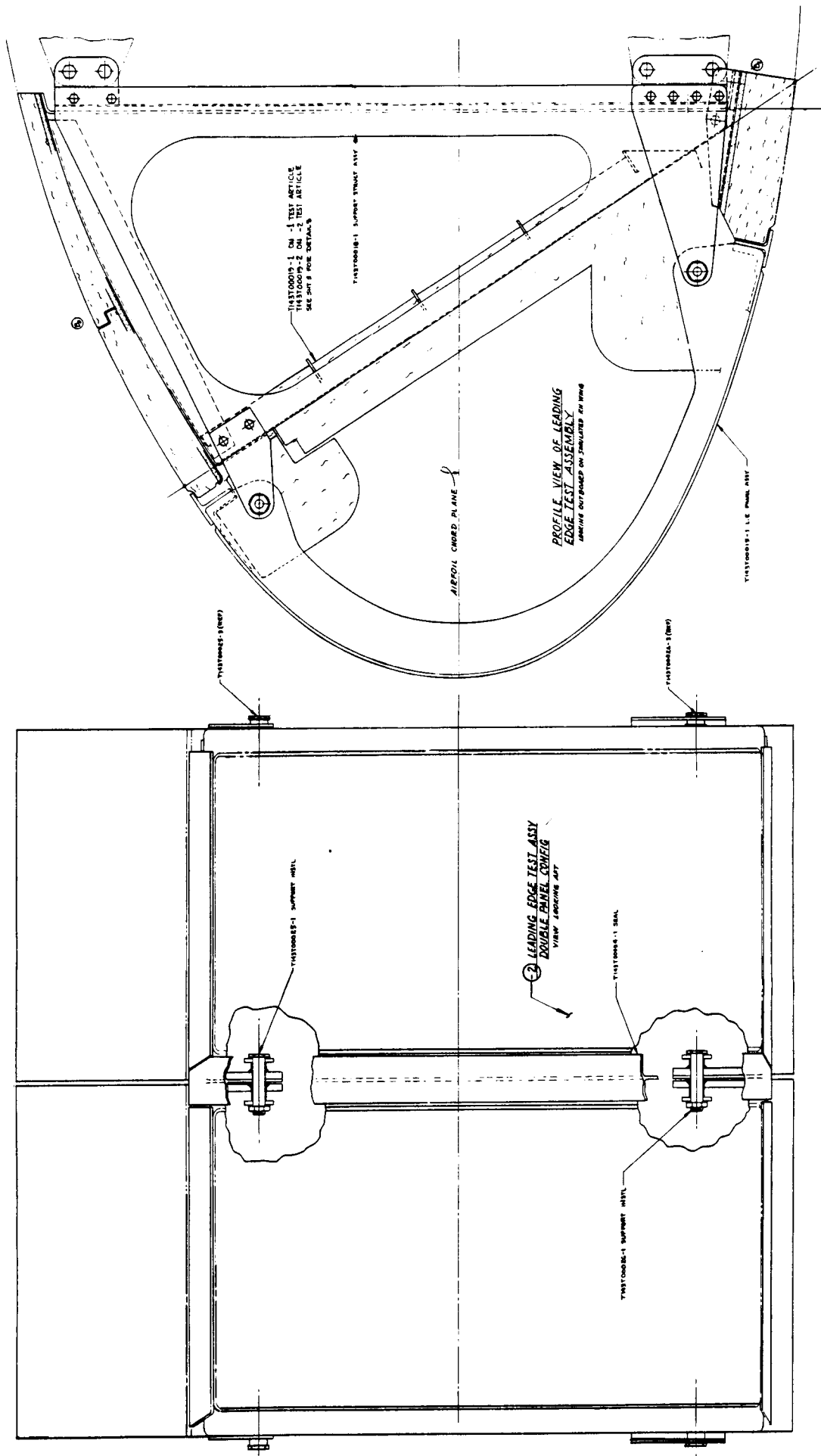
1.1.1 DESIGN

This section of the report describes the leading edge assembly design details and associated rationale. Supporting structural, thermal, and dynamic analyses are then summarized to establish credence to the design. Specific component tests such as heatshield, support brackets, and gap heating are covered under Tasks 2, 3, and 4 respectively.

1.1.1.1 Design Description

The basic configuration of the RPP portion of the leading edge assembly retained the geometry from the Phase II program, including external lines, trailing edge trim lines, width, locations of support bolts, and geometry of joggles. The purpose of this was to limit cost by preserving the applicability of Phase II lay-up tooling. Basically the only changes made to the RPP portion of the leading edge from the Phase II design were thicknesses and detail support attachment hole geometry. T-seal geometry remained exactly as the Phase II design and, in fact, a Phase II T-seal was used as part of the delivered dual-segment assembly for reasons of economy.

The geometry of the leading edge was derived from a cut taken normal to a 60° swept leading edge at a 310 inch long chordline with NACA-0012-64 airfoil. This produces a leading edge radius of 8.0 inches. The front beam was located 24 inches aft of the leading edge while RPP trim lines were established at 18 inches aft of the leading edge on the lower surface and 7 inches aft of the leading edge on the upper surface. Thus, a "J" section RPP component cross section was defined, as illustrated in Figure 1. This configuration permits access to upper and lower support bolts through the upper RSI access panel and provided a part size that could be coated in the current 24 inch diameter furnace.



30 **FIGURE 1 PHASE III WING LEADING EDGE FULL SIZE TWO SEGMENT ASSEMBLY**

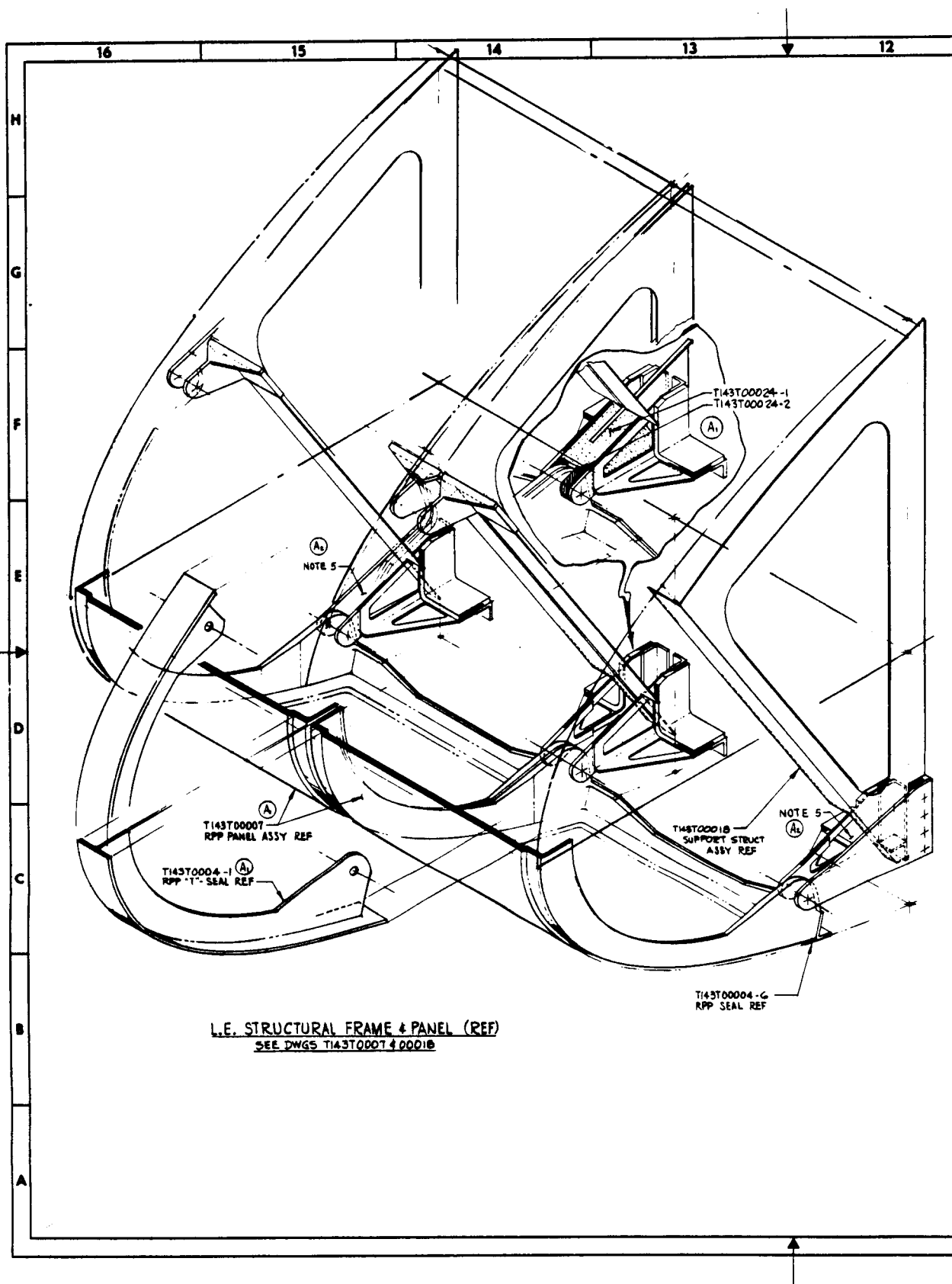


FIGURE 2 HEATSHIELD SYSTEM INSTALLATION

Preceding page blank



۶۵۹

The ground test configuration, shown in Figure 1, was derived from a layout depicting a "flight vehicle design" of a leading edge integrated with a typical Shuttle wing structure. The flight design was gleaned from Rockwell International and Grumman data supplied to VSD. The ground test configuration, also shown isometrically in Figure 2, is a simplified version of a flight design, configured to obtain minimum cost without excessive weight penalty.

The assembly consists of the RPP leading edge, which is supported at four points by the lug support brackets. A truss shaped structure supports the upper support brackets. The wing front spar is simulated by an aluminum panel at the aft end. Various insulation assemblies are used to protect the support brackets, titanium truss structure and front beam. Upper and lower panels simulate RSI panels on the vehicle.

Access to the attachment bolts is through the upper RSI panel. The canted heatshield is removed to gain access to the RPP compartment, and the clamshell support bracket insulation assemblies. Removal of this insulation exposes the attachment bolts.

The right hand side (looking forward) of each leading edge assembly is held fixed against side movement. The opposite side is permitted to expand by sliding on the attachment, which closes the built in expansion gap. The T-seal covers the gap to restrict direct flow of hot gas into the leading edge cavity. The sliding side of the leading edge requires countersunk attachment holes to clear the bushings that hold the fixed side of each leading edge in place. This is clearly shown in Figure 1.

The drawing family tree of all drawings comprising the leading edge assembly is given on Figure 3. Each of these components will be discussed individually starting with the RPP leading edge.

RPP panel - Details of the RPP are provided in Figure 4. This drawing shows how each ply of the lay-up is to be configured and positioned. It is typical of an RPP lay-up drawing. Trim lines for each ply, where not dimensioned, are determined from a stable drawing, which is scaled by shop and inspection personnel.

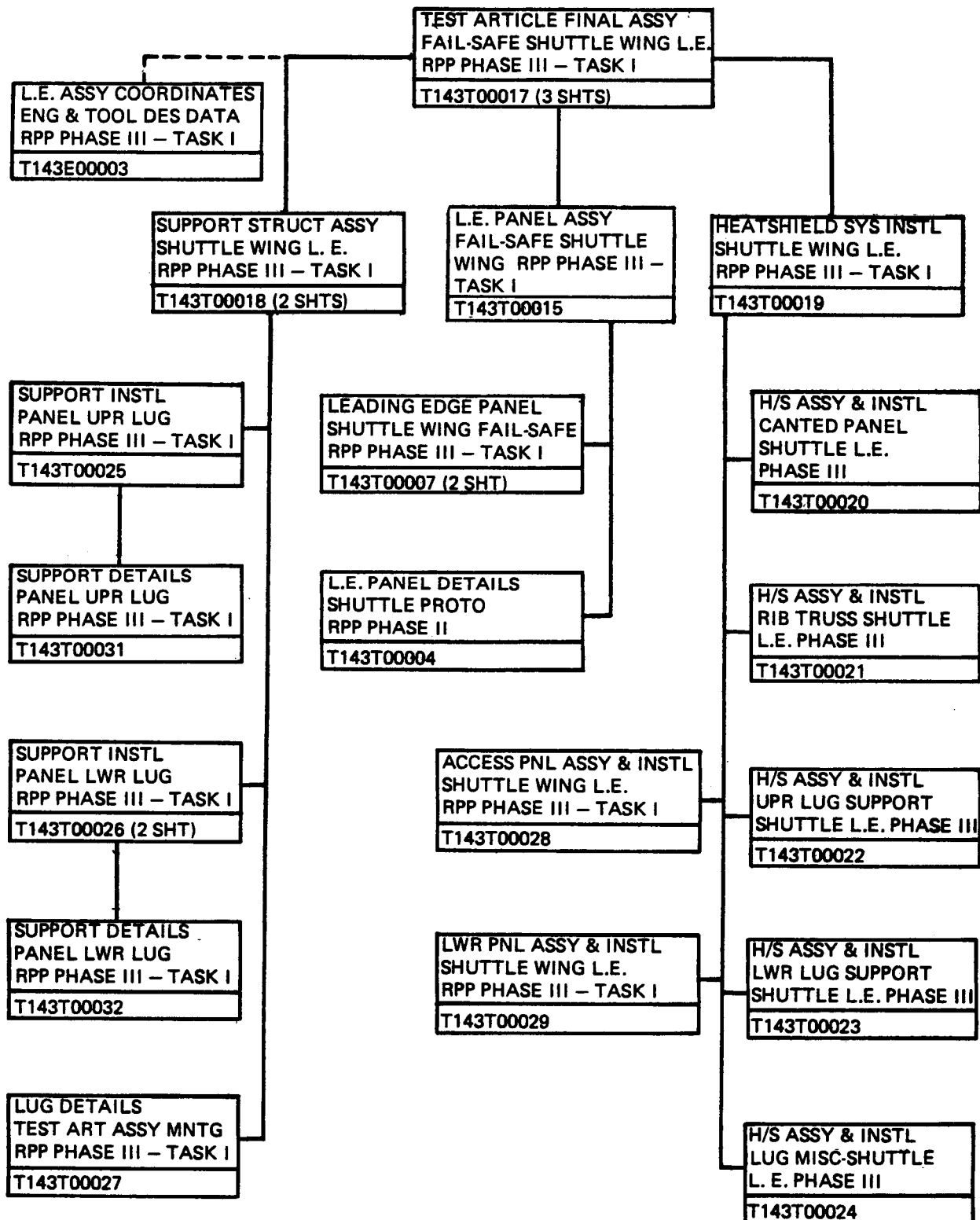


FIGURE 3 DRAWING BREAKDOWN

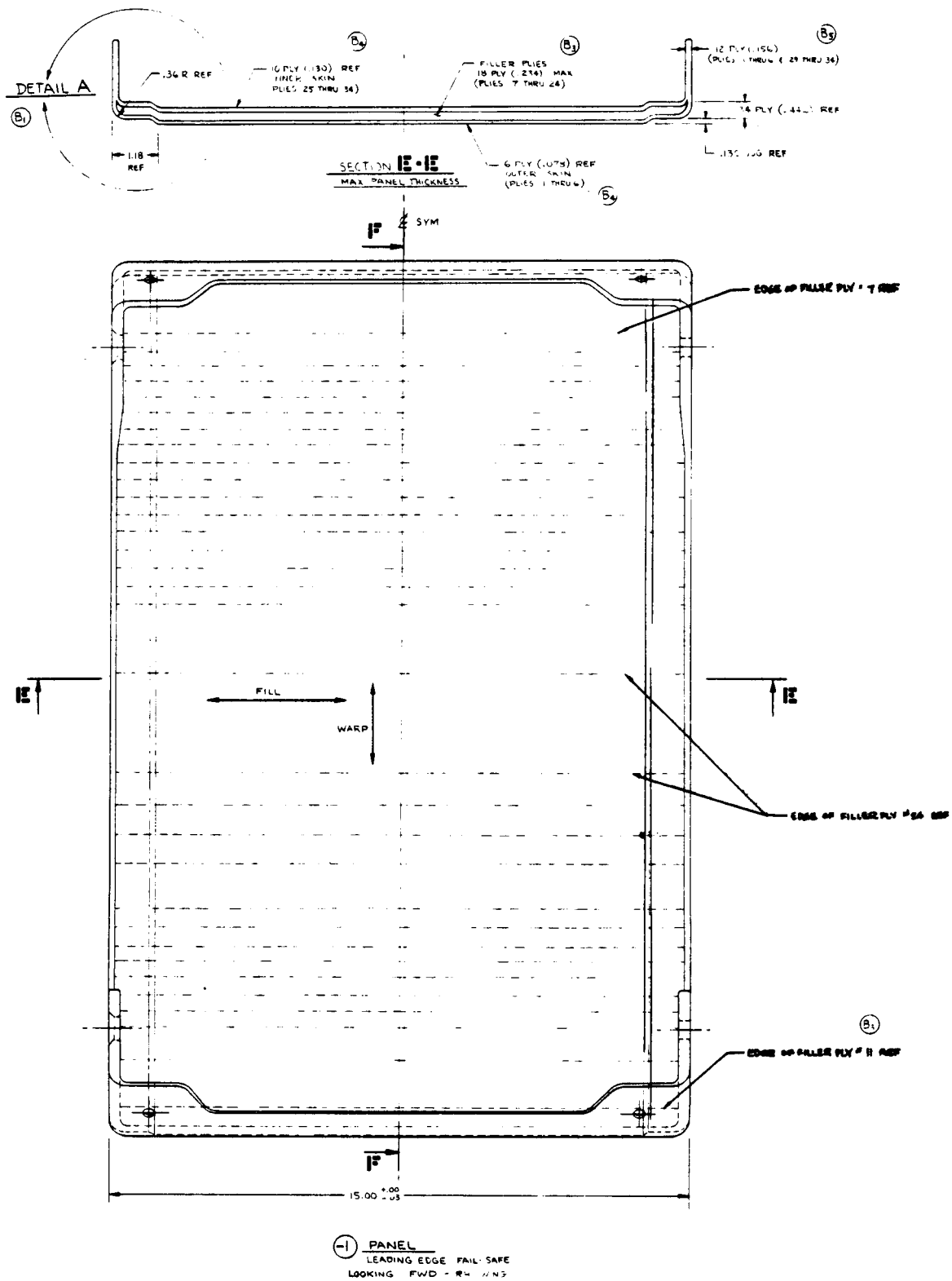


FIGURE 4 RPP PANEL ASSEMBLY — FAIL SAFE WING LEADING EDGE



The skin panel, ribs, and spars are all integrally laid up to form an integrated structure for maximum reliability and stiffness. This approach avoids bonding or riveting of primary structural elements to form the component. This design has two primary advantages as compared with designs employing multiple ribs or intercostals: (1) tooling and lay-up costs are lower and (2) interlaminar tensile stresses are maintained at manageable levels, because critical corner bending moments approach zero, as the corners tend to act as simple supports.

The skin thickness varies from 34 plies in the stagnation area to 20 plies at the windward trailing edge and 16 plies at the leeward trailing edge. These thicknesses were selected to accommodate loss of coating, oxidation during entry with a 20 per cent margin, and sufficient remaining material to permit cruise maneuvering and landing without failure. The skin build-up is such that the oxidized condition results in continuous plies for load carrying. Thus, "filler" plies are sandwiched between continuous outer and continuous inner plies. This avoids raw edges and prevents peel.

Ribs remain at a nominal 12-ply as was used on the Phase II leading edge. However, overlapping splices are used in the Phase III design for tailoring the cloth in the "shrink" rib flanges. This results in a variable flange thickness.

Lug regions are built up to 23 plies as compared to the 17 plies used in Phase II. The added thickness was intended to accommodate edge radii to reduce chipping possibilities and to permit chamfer of attachment holes, while maintaining static bearing stresses low. This design shows high margins statically, but when one of the Phase III leading edges was tested under acoustic noise loading conditions, it was found that wallowing of the chamfered holes and edge chipping of the other holes occurred. Thickening the lug regions and enlarging the hole diameters proved to be an acceptable production fix as demonstrated in a retest. Lug region thickness is 34 ply (0.45 inch).

As in Phase II, T-section seals are used at the trailing edges to overlap the RSI. In the interest of economy, trailing edge seal design was exactly like Phase II to utilize existing lay-up tooling. These T's are bonded in place and further secured with RPP rivets as in Phase II. Improved tolerance control and tooling resulted in bonded joints with no delaminations. This is in contrast with Phase II where local edge bond delamination was experienced on all three leading edges.

Support Structure - The support structure is that structure bridging the gap between the wing front beam and the RPP panel (exclusive of support brackets which are covered separately). The support structure is illustrated in Figures 1 and 2. Side members are triangular shaped 0.040 inch titanium to form a truss. Titanium is employed because temperature at the forward portion of the truss can reach nearly 600°F.

Titanium flanges are employed to provide support for the upper RSI panel. Gussets which were designed into these flanges at the corners to provide increased stiffness, when the door is removed, proved highly effective. A central portion of each side flange (not shown) is removable to permit removal of the canted heatshield. This approach, though increasing access time through the heatshield, greatly simplified the insulation design by eliminating the need for "picture frame" insulation on the aft side of the canted heatshield.

The titanium is insulated from the aluminum front beam with strips of laminated polyimide fiberglass at each joint.

Support Brackets - The RPP leading edge component is tied to the wing through two lug type joints on top and two on the bottom (Figure 2). The upper brackets are attached to the titanium support structure, while the lower brackets bypass the titanium and tie directly into the aluminum front beam. This was done to produce greatest design simplicity, maximum stiffness, and longest heat path.

The upper bracket is a straightforward steel weldment, gusseted to provide side stiffness. Since it operates in a low temperature region of the

leading edge (1000°F) and ties to titanium, there is no heat flow problem. A backup fitting on the aft side of the titanium is employed to transfer loads from the support bracket into the titanium sheet metal.

The lower bracket on the other hand operates in a 2000°F region of the leading edge and must drop this temperature to below 350°F at the aluminum structure. Therefore, thermal requirements, rather than structural requirements, dominate the design. A suitable design was produced by virtue of three main features:

- (1) Long conduction paths in the Inconel 718 fitting. Structural stiffness is retained even with a long bracket through the use of a wide base where it is anchored to the front beam.
- (2) Low conduction area in the Inconel fitting. This was achieved by using a truss, tripod arrangement to maintain structural integrity, while minimizing cross sectional area.
- (3) Introduction of an insulator. Polyimide fiberglass is employed within its temperature limits at the cool end of the bracket where it is most effective. It is applied in series with the structural path so that conduction area is minimized while the conduction path is maximized. Thus, it is much more effective than sandwiching an insulator between two structural members, which is the usual approach. The design is so effective that relatively thick (0.25 inch) polyimide fiberglass can be used to maintain low operational stress levels for high reliability.

The bracket design is shown in Figure 5, where the Phase III design is contrasted with a proposed production design. The primary difference between the two designs is that by virtue of the need for the Phase III test articles to be assembled as either single or dual-segment configurations, each support fitting must be a separate unit. On a flight vehicle, adjacent leading edge segments would share a single support bracket, which could be fabricated as a casting.

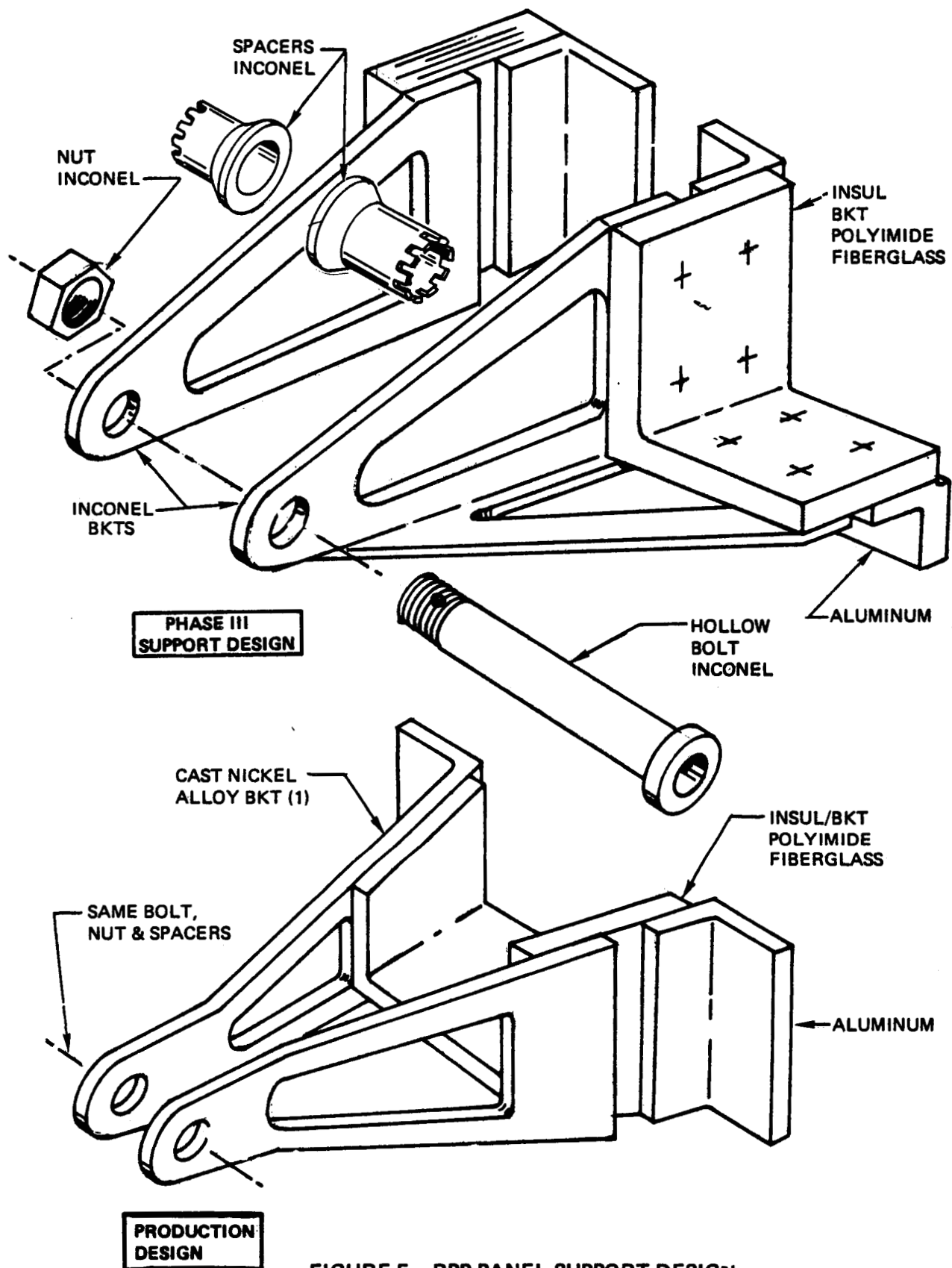


FIGURE 5 RPP PANEL SUPPORT DESIGN

Because of the design of the bracket, a metal fastener and spacers are employed without the need for ceramic insulators as initially envisioned. This is a significant feature of the design, because it eliminates potentially unreliable, brittle ceramic insulators. Results from the acoustic noise test (reference Section 1.1.1.4) strengthen this contention, where even the coated RPP suffered wear and chipping. It doesn't appear feasible to employ ceramics unless these are close fitting and trapped or encased so that in the event fracture is encountered, pieces are not lost.

Entry temperature tests discussed under Task 3 confirmed the ability of the bracket design to restrict aluminum temperature to an acceptable level. In the most representative test aluminum temperature peaked at 231°F, well within the 350°F allowance.

Heatshield Assemblies - Heatshield assemblies are the individual insulation assemblies consisting of insulation, strain isolator, and support structure. There are heatshields to protect the support brackets and a main, canted heat shield that protects the aluminum front beam.

The insulation used in Phase III was an alternate material because RSI desired for this application could neither be obtained nor could be afforded. As a result, VSD elected to use Johns-Manville's Dynaquartz insulation because it is thermally representative of RSI and has a temperature capability in excess of the 2300°F required. The canted heatshield employs 10 lb/ft³ Dynaquartz, while the insulation around the lugs uses an experimental 15 lb/ft³ Dynaquartz. The increased density was required, because heat inputs into the insulation required excessive thickness of the 10 lb/ft³ material to protect bondlines from overheating. Even with the 15 lb/ft³ density, support structure was required to provide heat sink capacity to maintain acceptable bondline temperatures.

Both upper and lower lug insulation systems are similar, Figures 2 and 6, in that they employ: titanium support structure which, as noted, serves also as heat sink; a silicone foam strain isolator, Raybestos-Manhattan RL1973 (20 lb/ft³), which functions to relieve thermal

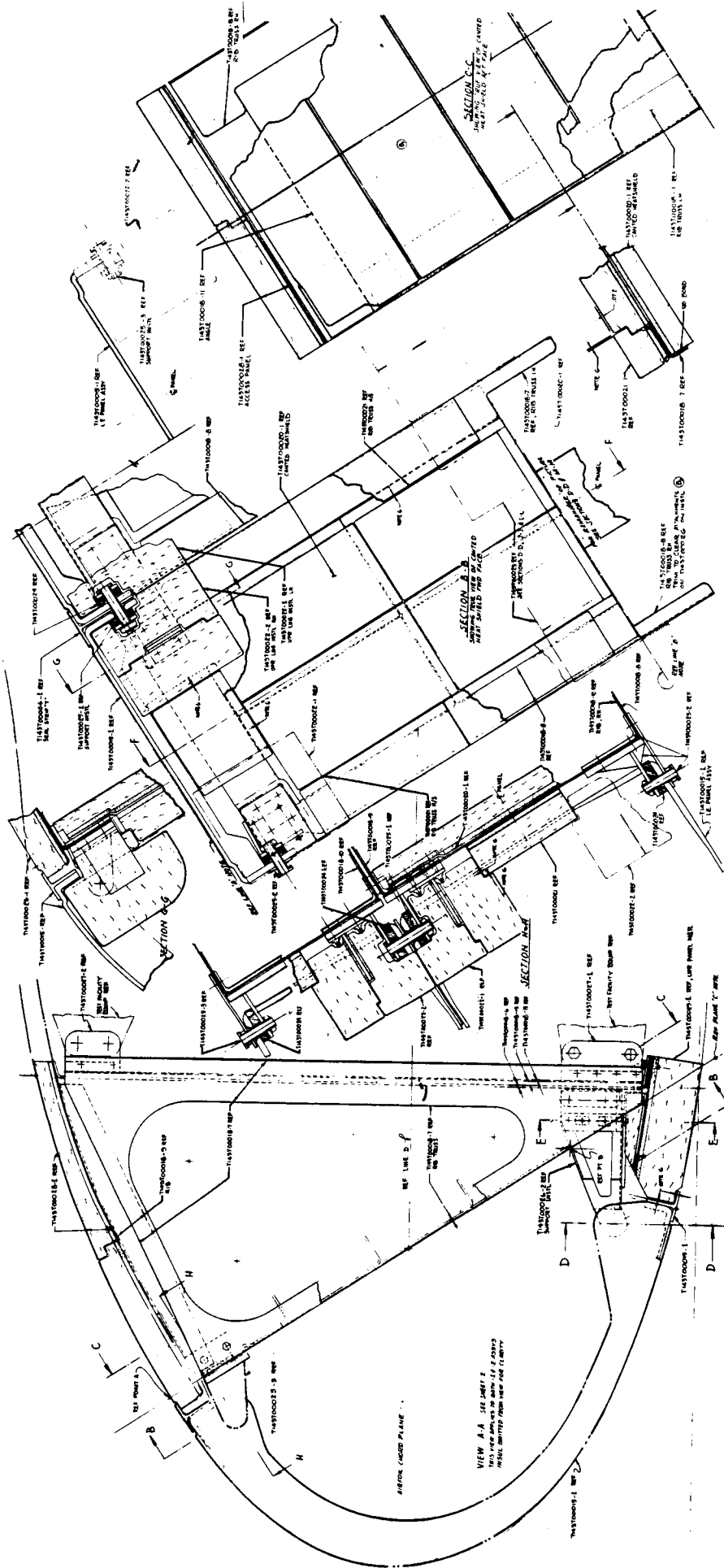


FIGURE 6 TEST ARTICLE FINAL ASSY - WING LEADING EDGE (Cont)

stress between the insulation and the titanium and attenuates bondline stresses from dynamic loadings; RTV-560 silicone rubber bonding material; and, finally, the insulation. The strain isolator was sized primarily to limit dynamic stress levels. Calculations showed that 0.10 inch thick RL1973 would maintain 3-sigma stresses at 2.55 psi for a 32 g-rms response. This is well below the failure stress for this material, which is in the 15 psi range for interlaminar tension.

The bond area is limited because bondline temperature cannot exceed 600°F for the RTV560/RL1973 materials. Therefore, a border of unbonded insulation is required. The insulation tiles are shiplapped to prevent direct radiation to the bondline.

The insulation support structure is tied directly into the brackets that support the leading edge. Temperature effect on the aluminum front beam from this technique was analyzed for the lower lug and was found to increase aluminum peak temperature by only 3°F.

The canted heatshield (Figure 6) consists of a 9-ply polyimide fiberglass structural panel, stiffened with 9 ply polyimide fiberglass ribs on the aft side; and 10 lb/ft³ Dynaquartz insulation front and rear bonded with RTV560 to 0.25 inch thick RL1973 foam strain isolator.

Polyimide fiberglass was selected because it could be made lightweight; provide a flat surface for bonding insulation tiles; produce good stiffness between stiffeners, because, due to its low density, it could be made thick without weight penalty; and the stiffeners would not become a heat short on the aft side. Polyimide parts were used in the support brackets noted above and VSD was producing parts from polyimide fiberglass for a missile program so that existing specifications could be used.

Although parametric analysis indicated that it would be more efficient, weightwise, if the insulation were all applied to the forward side of the heatshield support structure, insulation tiles could not be procured with sufficient thickness to permit this approach. Therefore, weight penalties from additional bondlines and strain isolation were incurred by splitting the insulation front and rear of the canted support structure.

Dynaquartz has high thermal efficiency and, although there are a number of other candidates for the lower temperature ($< 600^{\circ}\text{F}$) aft side insulation, it was also employed on the aft side to reduce program costs through design and handling of only one type material. Tiles were ship-lapped on the front surface to block direct radiation to the bondline. On the aft side, the temperature is sufficiently low ($< 600^{\circ}\text{F}$) that radiation is not severe, so butt joints are used.

Strain isolator thickness and tile size were established from dynamic analyses, using a 32 g-rms response limit. These analyses are discussed later (Section 1.1.1.4), but they evaluated different numbers of tiles and different strain isolator thicknesses to arrive at a suitable arrangement that would limit interlaminar tensile stresses, primarily induced from support panel flexure, within material capability. However, as will be discussed later, Dynaquartz failure in a vibration test occurred from fatigue and therefore apparently at a stress level below the 3-sigma value computed. A subsequent vibration test with several modifications (Task 2) ultimately passed the vibration test. This was a demonstration to show that a rigid insulation approach could be designed to meet design dynamic load environments.

A specific thermoeleastic analysis of the insulation design was not performed by VSD. However, the insulation is a silica, so the design was considered acceptable by similarity to the Lockheed LI-1500 material. NASA-JSC conducted analyses of LI-1500 at heating rates approximating Phase III requirements. These showed high margins, especially in the uncoated material (the Dynaquartz is likewise uncoated), which indicated acceptability of the VSD design.

The canted heatshield cannot extend full width on the front side of the canted plane because of installation limitations. Therefore separate "picture frame", rib truss insulation strips are attached on the front side. These are designed like the canted heatshield except that the insulation/

strain isolator system is bonded to a titanium "carrier" panel. This permits easy bench buildup of heatshield assemblies, which are ultimately bolted into place, and facilitates installation and removal.

Another small assembly of insulation is required between the upper support lugs. This is fabricated like the rib truss insulation in that a titanium carrier panel is employed for installation and removal.

Simulated RSI External Panels - As shown in Figures 2 and 6, an upper and lower panel were designed for the leading edge to represent RSI close-out panels. As with the internal heatshields, these were designed for 10 lb/ft³ Dynaquartz to thermally represent the RSI. Thermal analyses showed that bondline temperatures would not exceed 600°F for the designs shown, and dynamic analysis computed 3-sigma interlaminar stresses not in excess of 3.5 psi.

Each panel employs titanium support structure, 0.25 inch thick RL1973 foam strain isolator and RTV560 bond material to attach the Dyna-quartz. By virtue of panel curvature the upper panel has inherent stiffness. The lower panel by contrast is flat and therefore employs a stiffener on the front edge, while on the aft edge it is tied into the front beam along its width.

The lower panel has sculptured insulation bonded to its upper side to fill gaps, which would otherwise allow direct radiation heat shorts from the hot RPP to the cool aluminum structure. The aft end of the titanium is insulated from the aluminum front beam with laminated figerglass. This is not required on the upper panel because titanium temperature at the aft endge is sufficiently low.

Front Beam - The front beam is one piece of 0.10 inch thick 6061-T6 aluminum and is used primarily to simulate the heat sink capacity of the Shuttle wing front spar. It also serves to complete the structural box.

Ground Test Support Fittings - There are two steel lug fittings, top and bottom, that have been included to permit fastening of the two assembled to ground test frames or support structure. Each lug is equipped for two fasteners so that when load testing, bending moments from eccentric reactions are not induced into the leading edge titanium support structure.

1.1.1.2 Structures Analysis

Static structural analyses were performed on the RPP segment, brackets, and support structure to prove adequacy of design. The extent of static analyses conducted are summarized in Table 1. Dynamic load analyses are covered in Section 1.1.1.4.

Table 1. Static Structural Analyses

Condition	Element			
	RPP Panel	Support Brackets	Support Structure	Insulation
Boost Pressure	NASTRAN	Hand Calculation	Hand Calculation	-
Boost Inertia (vibration side load)	NASTRAN	Hand Calculation	Hand Calculation	Hand Calculation
Entry Thermal Stress	NASTRAN	-	Hand Calculation	By similarity to NASA-JSC analysis
Cruise Maneuver(oxidized RPP)	NASTRAN (Max stress & buckling)	-	-	-

Results of these analyses, structural design criteria employed, and design allowables used are discussed in the following paragraphs.

Design Criteria - Structural design criteria were essentially the same as those used in the Phase II program, reference 2. Significant changes from Phase II included the addition of ± 0.5 psi venting pressure lag during cruise maneuver, and a 32 g limit inertia side load condition to provide strength and stiffness against dynamic loading. Specific design pressure loads are shown in Figure 7. These load conditions incorporate the following ultimate factors of safety, which were used for design analysis:

Boost = 1.4 x Limit

Entry = 1.5 x Limit

Cruise Maneuver = 1.5 x Limit

The entry factor of safety also applies to entry thermoelastic stresses.

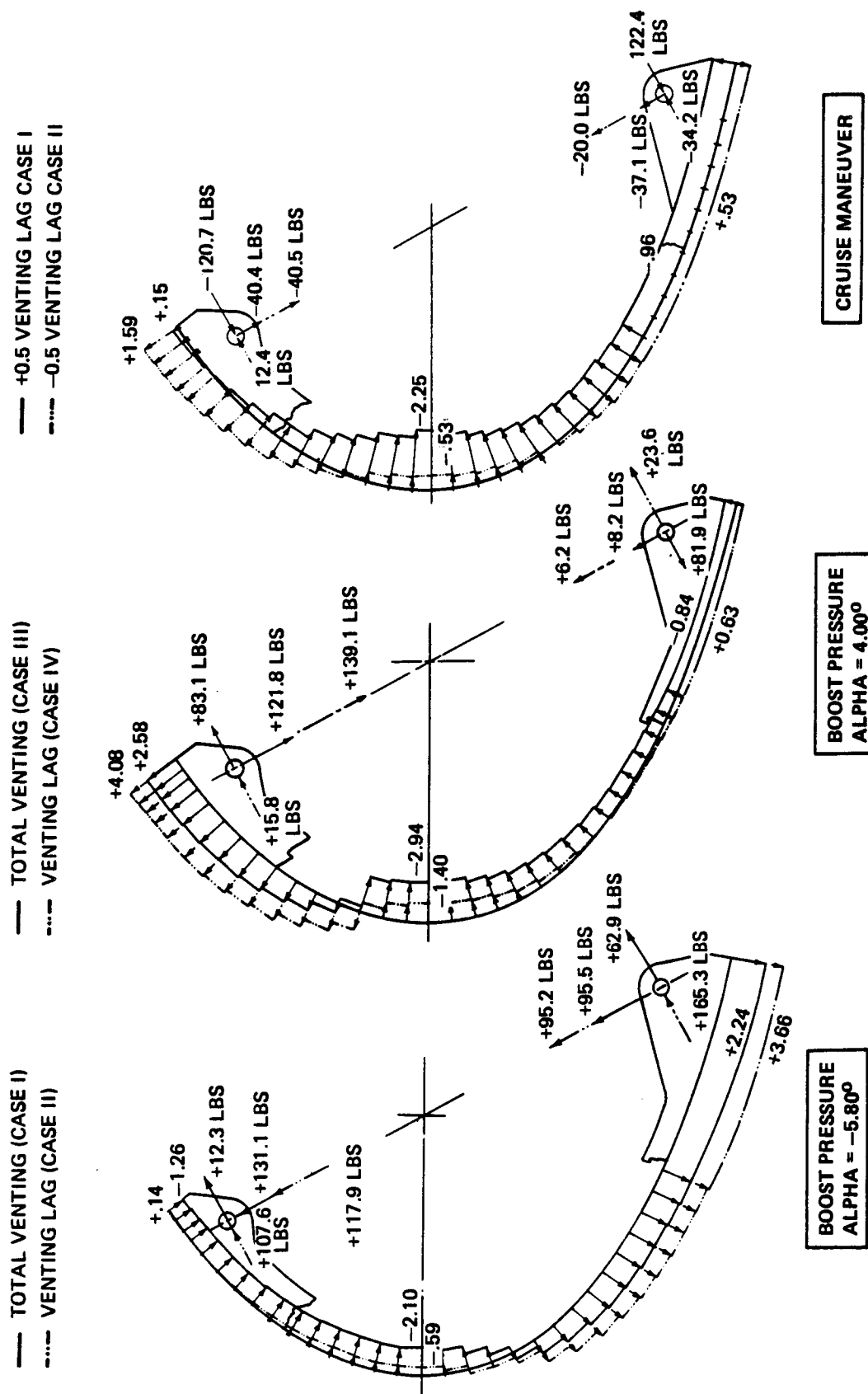


FIGURE 7 ULTIMATE DESIGN LOADS

In addition to the factors of safety employed, minimum margins of safety were established to insure conservative design in joint regions.

The following minimum margins were established:

Basic Structure	- Positive
Shear Joints	- +15%
Tension Joints	- +50%
RPP Lugs (Inplane)	- +100%

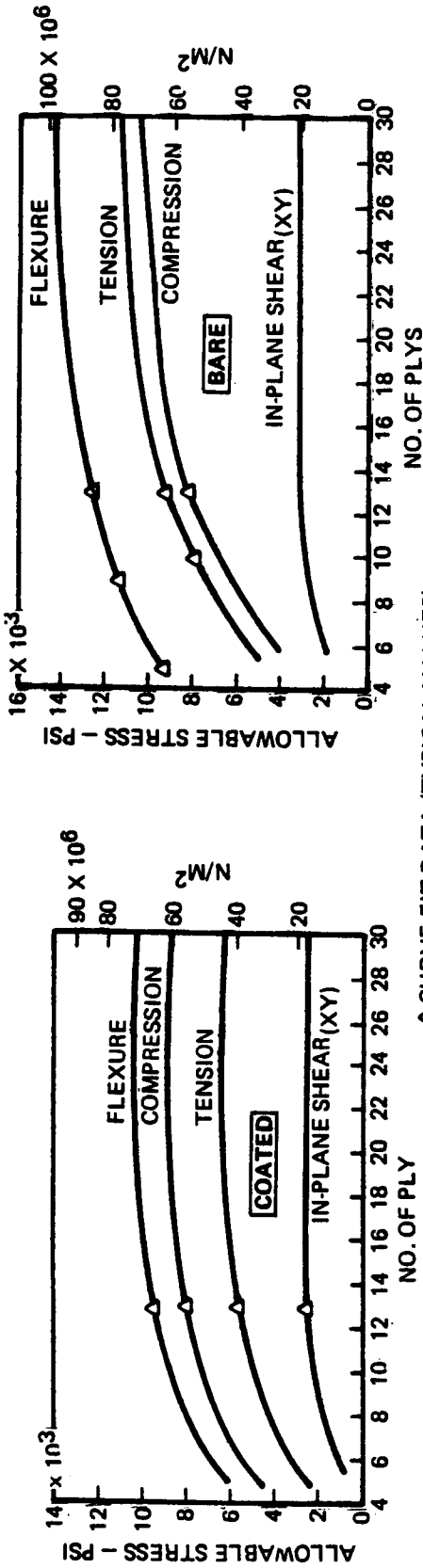
Design allowables, discussed in the next paragraph, were established to represent "A" values, and were based on data obtained in the Phase II program, reference 2. These, when combined with the noted margins of safety, were intended to provide design conservatism.

RPP Design Allowables - Structural analysis of the leading edge requires material allowables for both coated and bare RPP. Bare data is employed in analysis of the "oxidized" leading edge for cruise maneuver loads while coated data is used for all other design conditions. Since test data covering the full range of design thicknesses were not available at the time of design analysis, extrapolation of the then existing data was required to establish design allowables. Room temperature strength and elastic moduli used for analysis are shown in Figure 8. These were established from data of reference 2 and in-house tests. Strength properties show a 33% reduction from average values based on a statistical evaluation of 57 flex bars from 17 coating runs as summarized in reference 2. This produced "A" values, 99% probability, 95% confidence, approximately 33% below average values. This relationship was also applied to all other strength properties in lieu of specific statistical data.

△ CURVE FIT DATA ± 1.5

FILL = 0.60 WARP FOR FLEXURE, TENSION AND COMPRESSION

FILL = WARP FOR IN-PLANE SHEAR



△ CURVE FIT DATA (TYPICAL VALUES)

FILL = .75 WARP FOR E_c , E_t , AND E_f

FILL = WARP FOR G

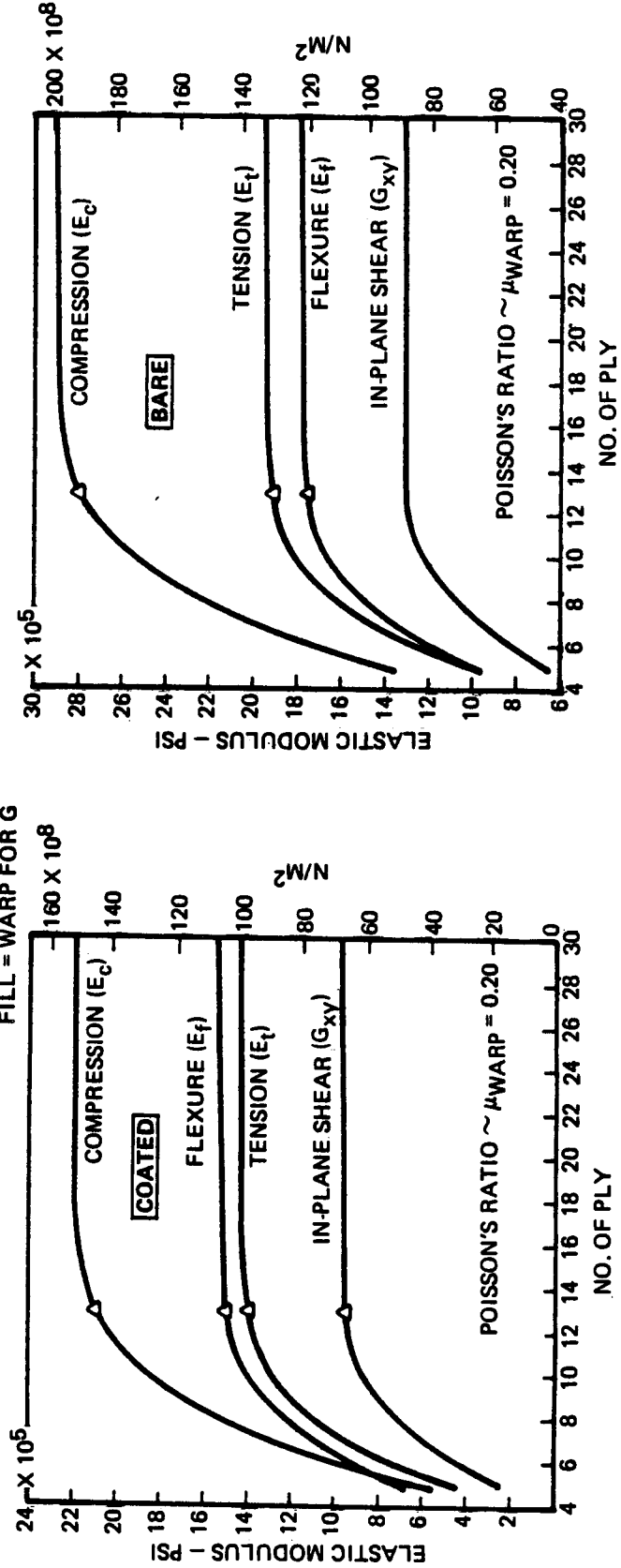


FIGURE 8 DESIGN PROPERTIES USED — RPP BARE AND COATED, ROOM TEMPERATURE, WARP DIRECTION

Temperature effects were based on the data of reference 2. The design curves are shown in Figure 9 for both strength and elastic modulus of coated RPP. The data is for 13-ply material but the trends were applied to other thicknesses as well.

Boost Loads Analysis - All structural analyses conducted on the Phase III leading edge used NASTRAN, level 11.1.4, which is a finite element computer analysis technique, employing bending and membrane elements. Because of symmetry in both loads and design only one-half of the leading edge was modeled for boost pressure loads analysis. The model, which included 3000 degrees-of-freedom, is pictured in Figure 10. This same grid pattern was also used for thermoelastic analyses and was coincident with the thermal model to avoid temperature interpolation. A summary of the critical stress conditions and margins of safety is given in Figure 11. The minimum margin for pressure loads (excluding the side load case) is 40% which occurs in the rib flange. All other margins are high, being over 100%.

Maximum panel deflection occurs at the panel centerline near the lower spar and is a reasonable value of 0.072 inch at limit load.

The 32 g-rms limit side load analysis was a special boost load case, requiring modeling of the complete leading edge segment, as opposed to half, because side loads are resisted only on one side of each segment; the other side is allowed to float. The model employed 2000 degrees-of-freedom. This loading condition was critical only for shear in the fixed side lug regions, where twist produces a relatively high inplane shear stress. The 31% margin remains substantial.

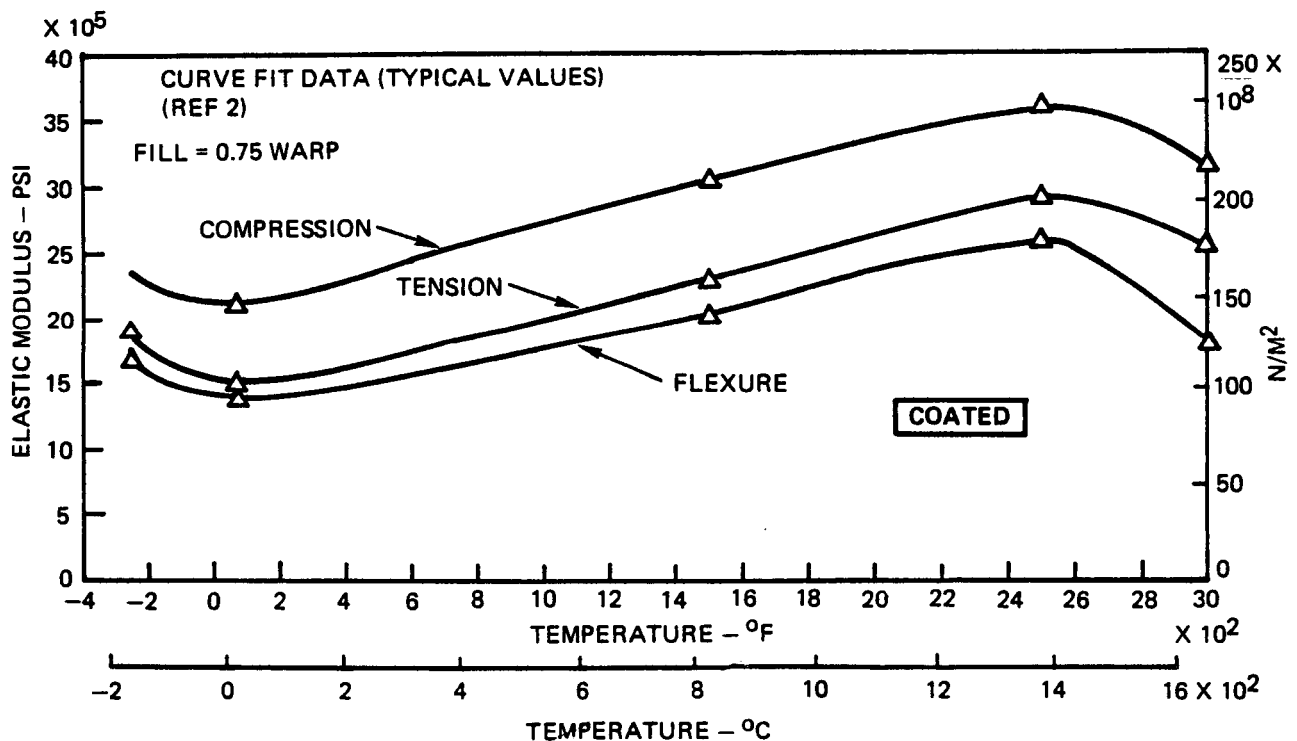
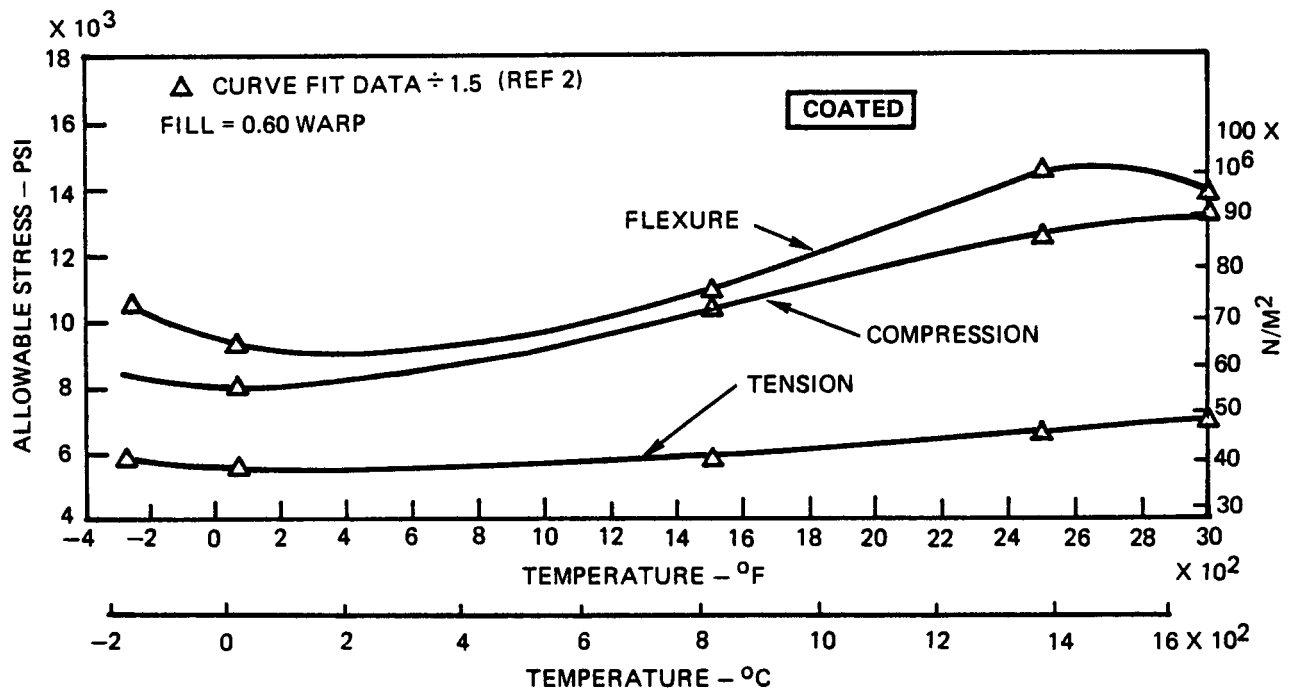


FIGURE 9 RPP PROPERTY VARIATION WITH TEMPERATURE - COATED 13-PLY MATERIAL - WARP DIRECTION

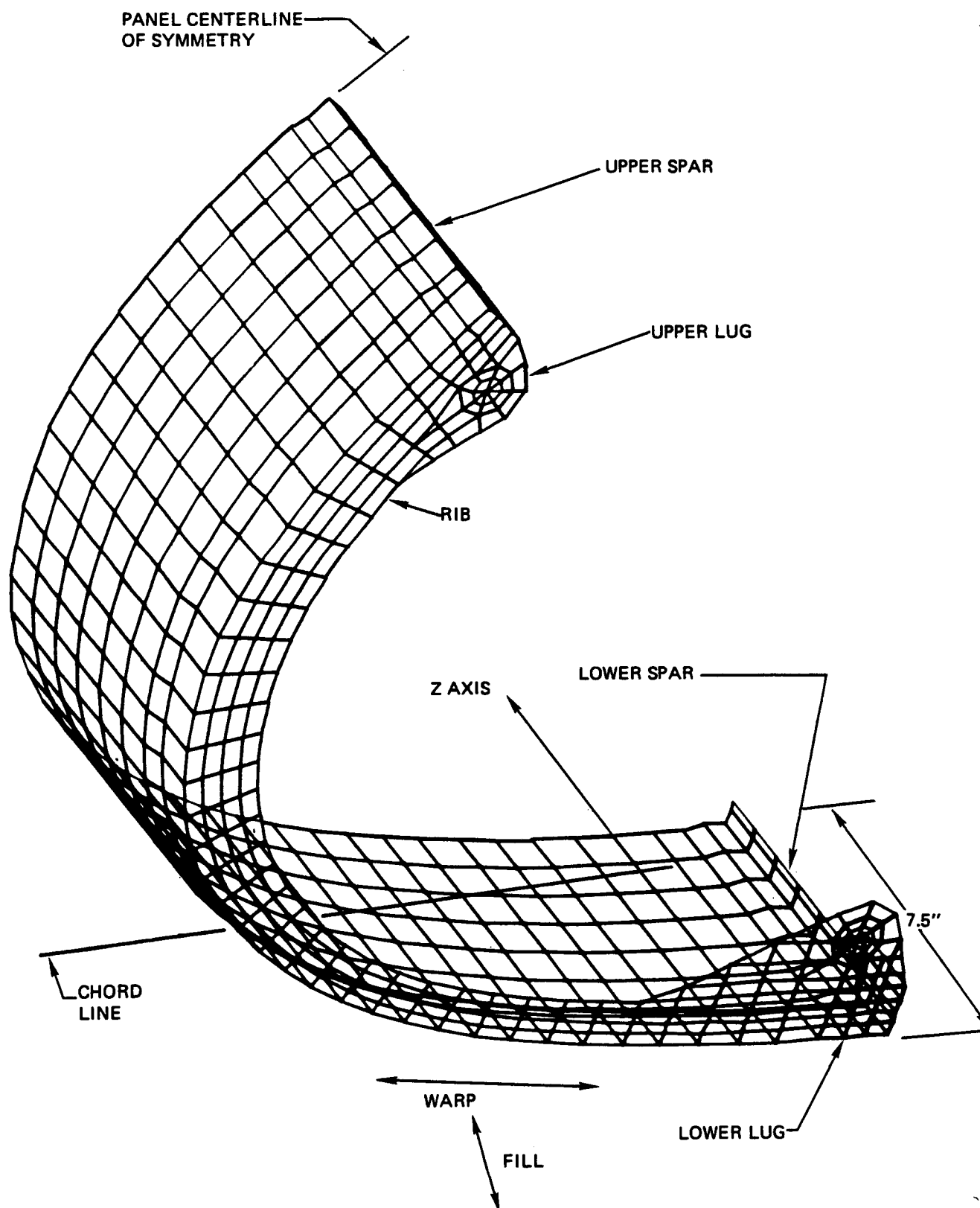
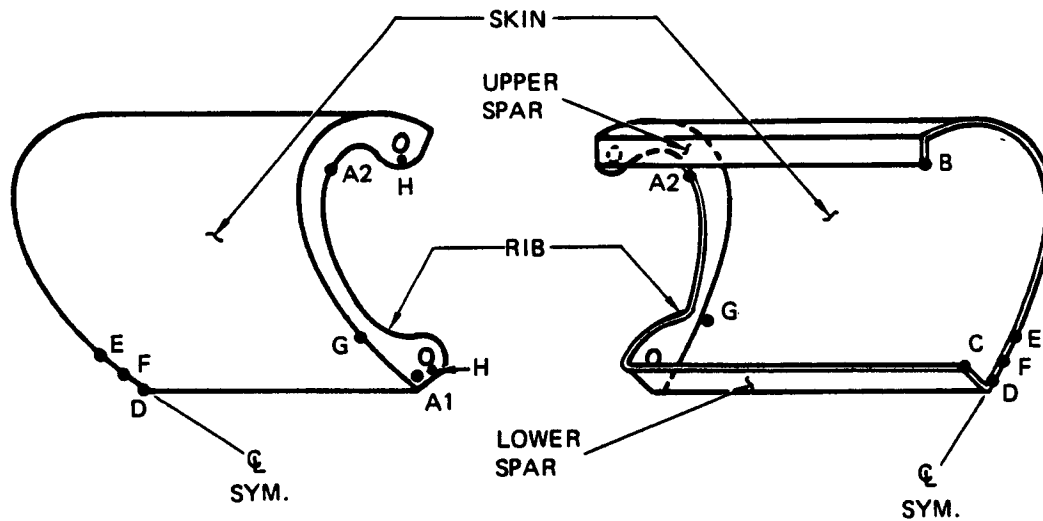


FIGURE 10 PERSPECTIVE OF NASTRAN LEADING EDGE MODEL



POSITION	STRUCTURE	MATERIAL THICKNESS	TYPE OF STRESS	MAXIMUM ULTIMATE STRESS PSI	ALLOW.* STRESS PSI	ULT. MARGIN OF SAFETY
A1	LUG	23 PLY	SHEAR	1905	2500	0.31
A2	RIB	12 PLY	TENSION	3850	5400	0.40
B	UPPER SPAR	20 PLY	COMPRESSION	-1570	-8800	4.60
C	LOWER SPAR	20 PLY	COMPRESSION	-2360	-8800	2.73
D	SKIN	20 PLY	MAXIMUM COMPRESSION	-1075	-5160 COMP. 6120 FLEXURE	+4.1
E	SKIN	22 PLY	MAXIMUM MEMBRANE TENSION	+800	6300 TENSION 10,200 FLEXURE	HIGH
F	SKIN	21 PLY	MAXIMUM FLEXURE	+800	6300 TENSION 10,200 FLEXURE	HIGH
G	SKIN	22 PLY	SHEAR	750	2500	2.33
H	UPPER LUG	23 PLY	SHEAR	800	2500	2.12
	LOWER LUG	23 PLY	FLEXURE	4250	10,200	1.40

*FROM FIGURE 8

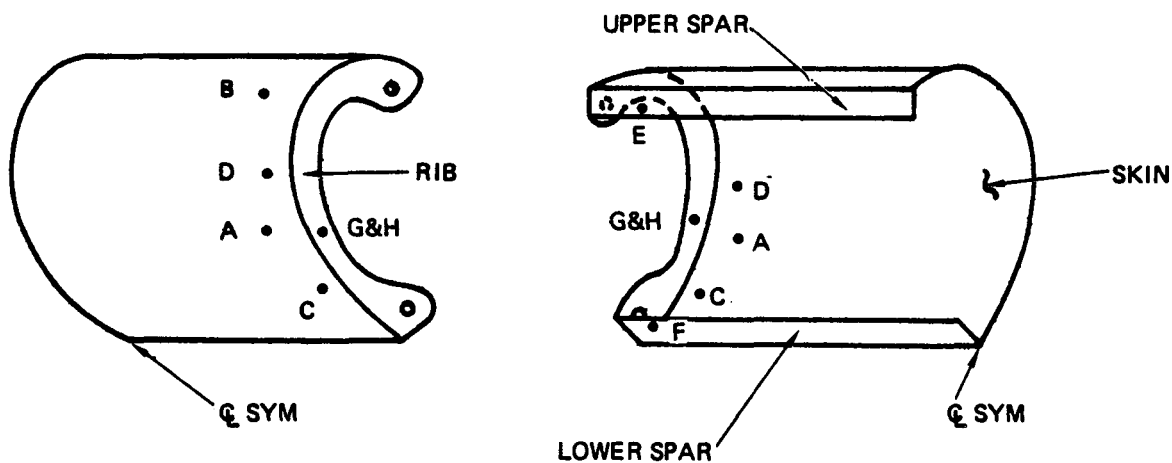
ALL STRESSES ARE FOR LOAD CASE II EXCEPT "A1" AND "H" WHICH ARE FOR 32 "g" SIDE LOAD, AND B WHICH IS FOR LOAD CASE IV. REF FIGURE 7, BOOST PRESSURE LOADS

FIGURE 11 SUMMARY MARGINS OF SAFETY BOOST PHASE

Entry Thermoelastic Analysis - Thermoelastic analyses were performed at entry times of 260, 300, and 400 seconds. These times covered conditions that produced maximum thermal gradients in ribs, through the skin, and in a circumferential direction around the leading edge. The NASTRAN model was as pictured in Figure 10 and involved 3000 degrees-of-freedom. NASTRAN handles thermoelastic problems by averaging the temperatures at the grid points defining each element, and then assumes that the temperature is constant over the whole element. Thermal elements allow the average temperature to vary through the thickness only. Free thermal strains are computed based on the input reference temperature, the element geometry and the element coefficient of thermal expansion. Then, using the input material properties, the forces necessary to return the element to its original size and shape are computed. These "equivalent static loads" are then divided equally and applied at the grid points defining the element. The anisotropic nature of the elements is retained and warp and fill properties were used. In addition, all element properties were made temperature dependent. Different from the static analysis, the compression modulus was used for the membrane element in all thermoelastic analyses, which is conservative for tensile stresses.

A summary of the margins of safety computed for the entry thermal conditions are shown in Figure 12. All margins are large with the minimum being 134% at ultimate. This results from circumferential skin gradients at 400 seconds, when temperatures are maximum. The next lowest margin is 174% on tension and occurs in the ribs due to thermal gradients through the rib flange depth.

Maximum deflections occur at 400 seconds from initiation of entry, when temperatures are maximum. The maximum spanwise growth at the stagnation line is 0.052 inch at limit conditions. This includes off-setting effects of thermal expansion and restraining stresses. Skin deflection normal to the surface was computed as 0.055 inch (bowed outward) at limit stress. This value is relatively small.



POSITION	STRUCTURE	MATERIAL THICKNESS & TEMPERATURE	TYPE OF STRESS	MAXIMUM ULTIMATE STRESS PSI	ALLOW.* STRESS PSI	ULT. MARGINS OF SAFETY	SEC. FROM ENTRY
A	SKIN	29 PLY 1960°F	TENSION	1790	6,300	+2.52	400
B	SKIN	34 PLY 2420°F	FLEXURE	1050	15,250	HIGH	400
C	SKIN JOGGLE	25 PLY 1560°F	COMPRESSION	-2900	-10,400	+2.59	400
D	SKIN	29 PLY 1560°F	SHEAR	1070	2,500	+1.34	400
E	UPPER SPAR	20 PLY 805°F	TENSION	1400	5,600	+3.00	400
F	LOWER SPAR	20 PLY 920°F	COMPRESSION	-1000	-9,000	HIGH	260
G	RIB	12 PLY 1410°F	TENSION	2050	5,600	+1.74	300
H	RIB	12 PLY 2180°F	COMPRESSION	-1560	-12,000	HIGH	400
J	SKIN	16 PLY 670°F	TENSION	1030	3,600	+2.5	400
*FROM FIGURE 8 AND 9							

FIGURE 12 SUMMARY OF MARGINS OF SAFETY – ENTRY PHASE

Oxidized Leading Edge Analysis - In the event that the coating is non-existent at initiation of entry, a substantial portion of the leading edge will be oxidized away during entry flight. The leading edge was designed such that at the conclusion of the entry phase, at least 10 plies remain, even if oxidation predictions are in error by 20%. Of the 10 plies remaining two of the plies are assumed ineffective because of back surface coating; this leaves effectively 8 plies of bare skin material structurally capable of carrying cruise maneuver and landing loads. A 2.5 g pullout cruise maneuver is the critical loading condition and is described in Figure 7.

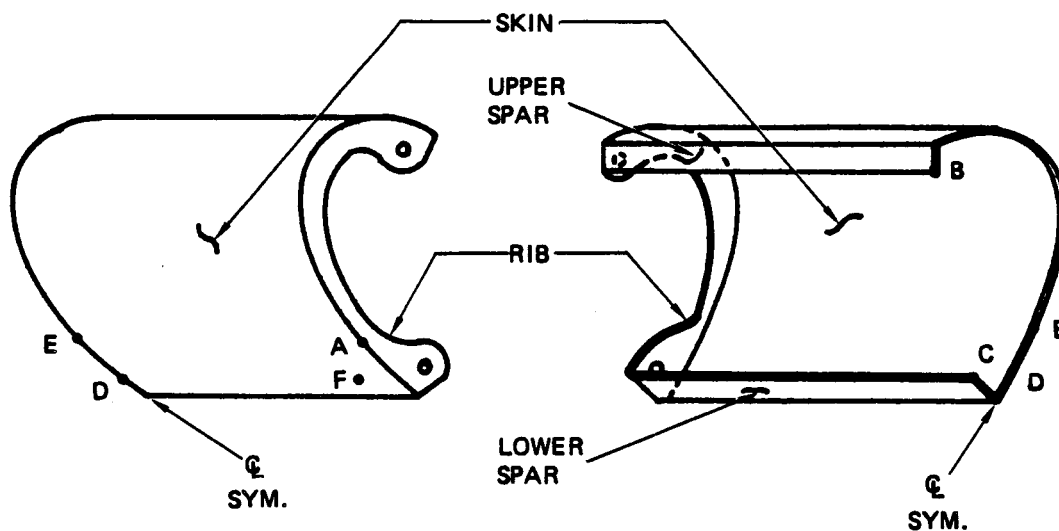
The oxidized leading edge was modeled as shown in Figure 10 to compute internal stresses. Bare material strength and elastic modulus were as defined in Figure 8. A summary of computed margins of safety is shown in Figure 13. Note that all margins are very high, with the lowest, 150%, being for shear stress in the skin.

The maximum panel deflection occurs at the panel centerline just forward of the lower spar, and is equal to 0.050 inch at limit load.

The oxidized leading edge has also been analyzed for buckling with the NASTRAN routine. The math model is shown in Figure 14 and is comprised of anisotropic membrane and bending elements. A full model is required to obtain proper buckling loads and mode shapes. The mesh size shown is larger than for the static analysis model (Figure 10) but it provides proper representation of the stiffness, which is the most important buckling parameter. Approximately 700 degrees-of-freedom were employed. Stress recovery is not needed and therefore does not dictate mesh size.

Material properties used in the buckling analysis are from Figure 8. The 8 ply bare compression and flexure moduli were used for skin membrane and bending elements respectively. The 12 ply coated tension and flexure moduli were used for the rib membrane and bending elements.

Load Case I, Figure 7, Cruise Maneuver, is the critical cruise load for buckling. This load condition occurs during a 2.5 g maneuver and includes an 0.5 psi collapse venting lag.



LOCATION	STRUCTURE	TYPE OF STRESS	MAX. ULTIMATE STRESS PSI	ALLOW.* STRESS PSI	LOAD CASE	MARGIN OF SAFETY
A	RIB	TENSION	540	5400	1	HIGH
B	UPPER SPAR	COMPRESSION	-950	-8700	2	HIGH
C	LOWER SPAR	TENSION	1190	6100	1	4.13
D	SKIN	TENSION	581	6700	1	HIGH
E	SKIN	FLEXURE + AXIAL	-840	11000	1	HIGH
F	SKIN	SHEAR	960	2400	1	1.50

*REFERENCE FIGURE 8

NOTE:

- 1) RIB ALLOWABLE STRESS BASED ON 12 PLY COATED MATERIAL
- 2) SPAR ALLOWABLE STRESS BASED ON 20 PLY COATED MATERIAL
- 3) SKIN ALLOWABLE STRESS BASED ON 8 PLY BARE MATERIAL

**FIGURE 13 SUMMARY OF MARGINS OF SAFETY
OXIDIZED LEADING EDGE – CRUISE MANEUVER**

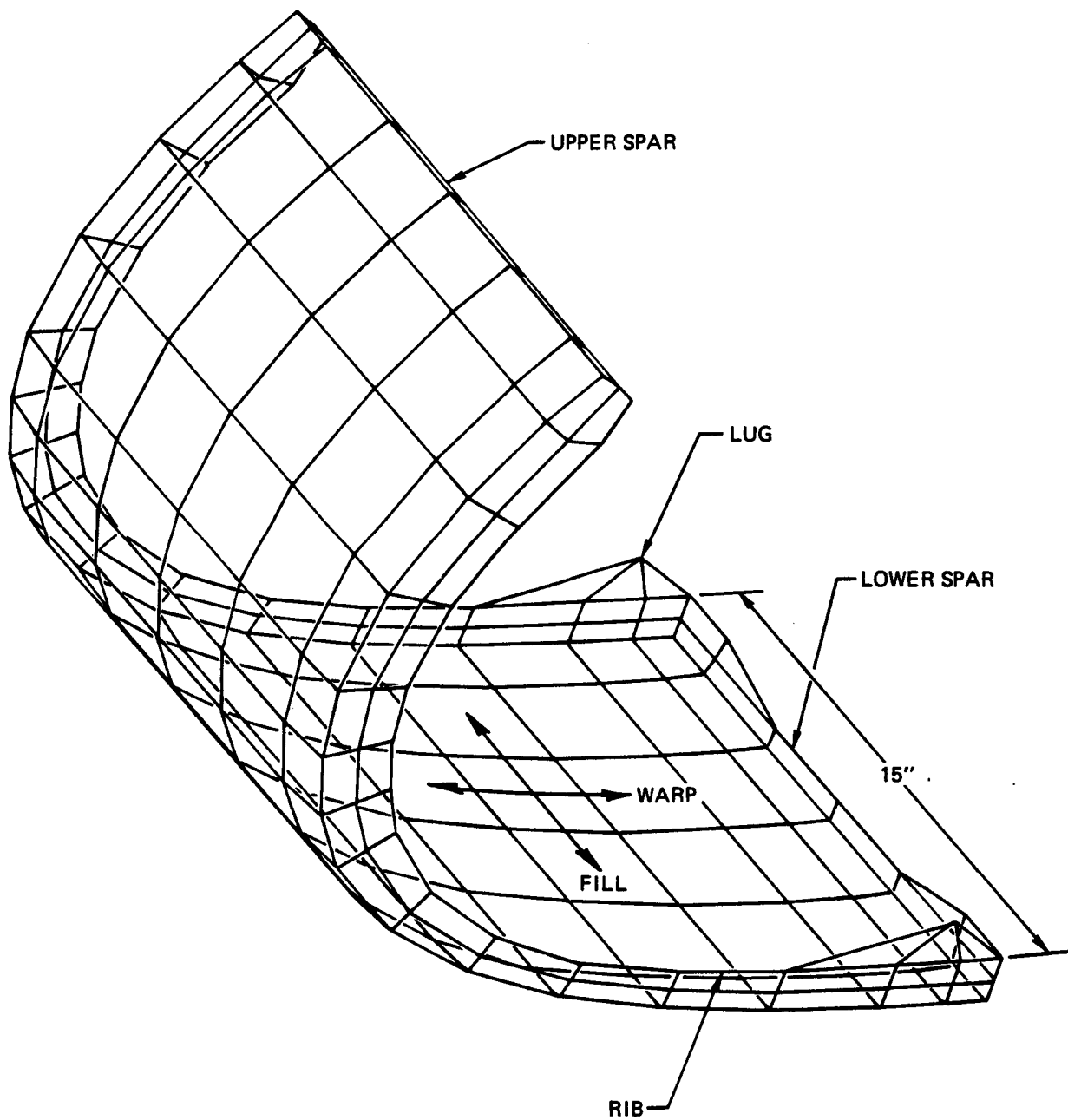


FIGURE 14 LEADING EDGE NASTRAN BUCKLING MODEL

NASTRAN performs the buckling analysis by solving for the roots or eigenvalues of a characteristic equation involving both elastic and differential stiffness matrices. Results are illustrated in Figure 15, where the eigenvalues represent the factor above ultimate load at which buckling would occur. A high margin is evident, indicating a high resistance to buckling. The minimum margin of safety is: $M.S. = (3.43 \div 1.0) - 1 = 2.43$ (243%) at ultimate.

The centerline buckle mode shapes for λ_1 and λ_2 are shown in Figure 15. The full lower panel buckle mode shape for λ_1 is presented in View A-A on Figure 15. The first mode shape is a full sine wave, which is typical of a radially loaded arch or cylinder.

A classical buckling problem was evaluated using NASTRAN and the results compared favorably. A simply supported 6" x 12" flat aluminum sheet loaded in edgewise compression was evaluated using NASTRAN and found to have a minimum eigenvalue of 0.976 and a full sine buckle mode shape. Classical theory predicts an eigenvalue of 1.05 and a full sine buckle mode shape.

A separate computer routine was written to verify external equilibrium of NASTRAN solutions. The purpose of these checks was to insure that all the applied loads are internally balanced. In all cases, equilibrium was satisfied.

Support Structure - The titanium support structure and support brackets were analyzed for the leading edge reactions from the loading conditions defined in Figure 7, the 32 g-rms limit side load condition, and for the entry condition, where the front truss member expands relative to that portion tied to the wing spar. A summary of margins is given in Figure 16.

The lowest margin, 19%, is somewhat fictitious, since this is based on crippling. For the thermal expansion condition the crippled flange will simply "get out of the way" and the remaining members will continue to support the induced loads. Other margins are considerably in excess of the 0% margin required.

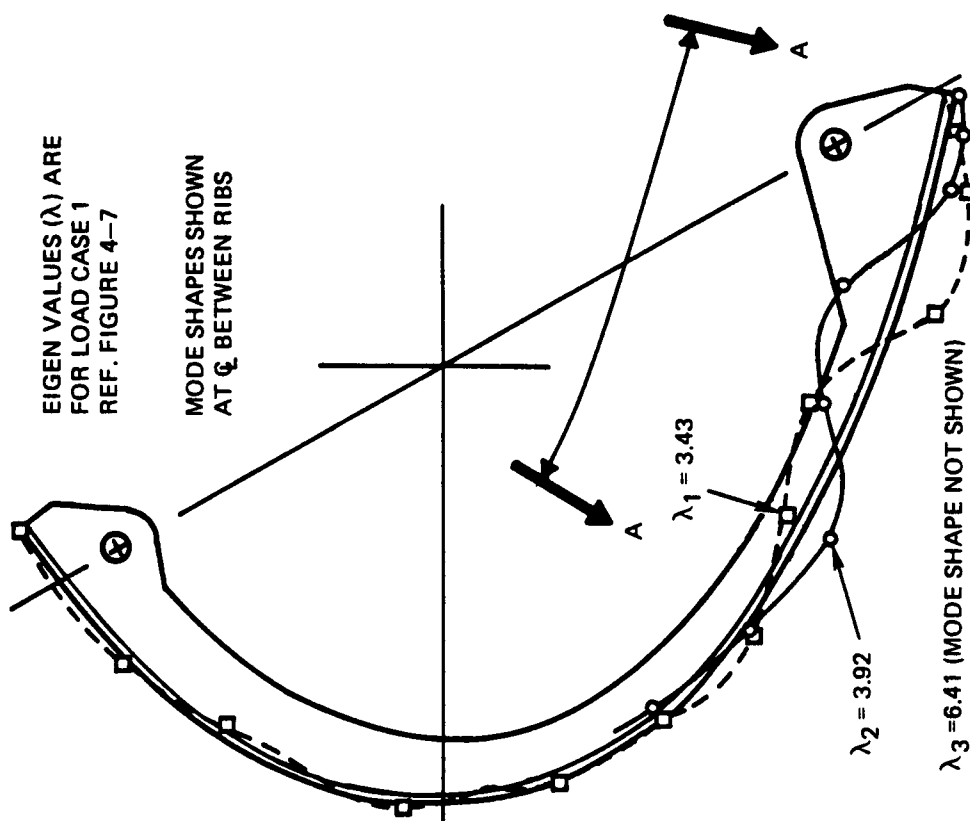
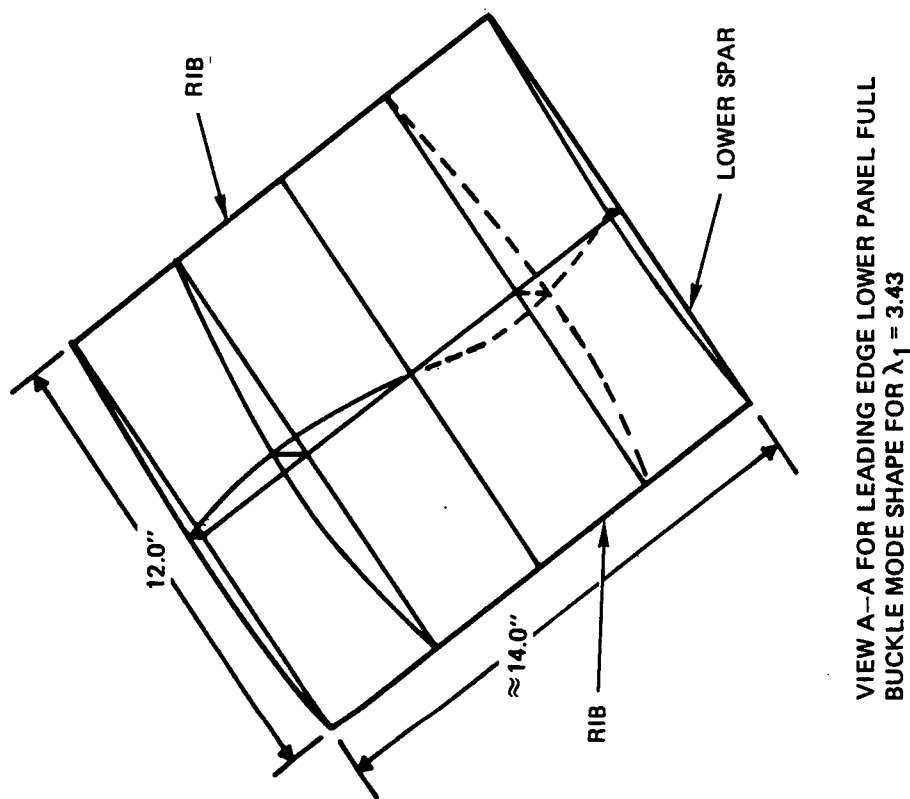
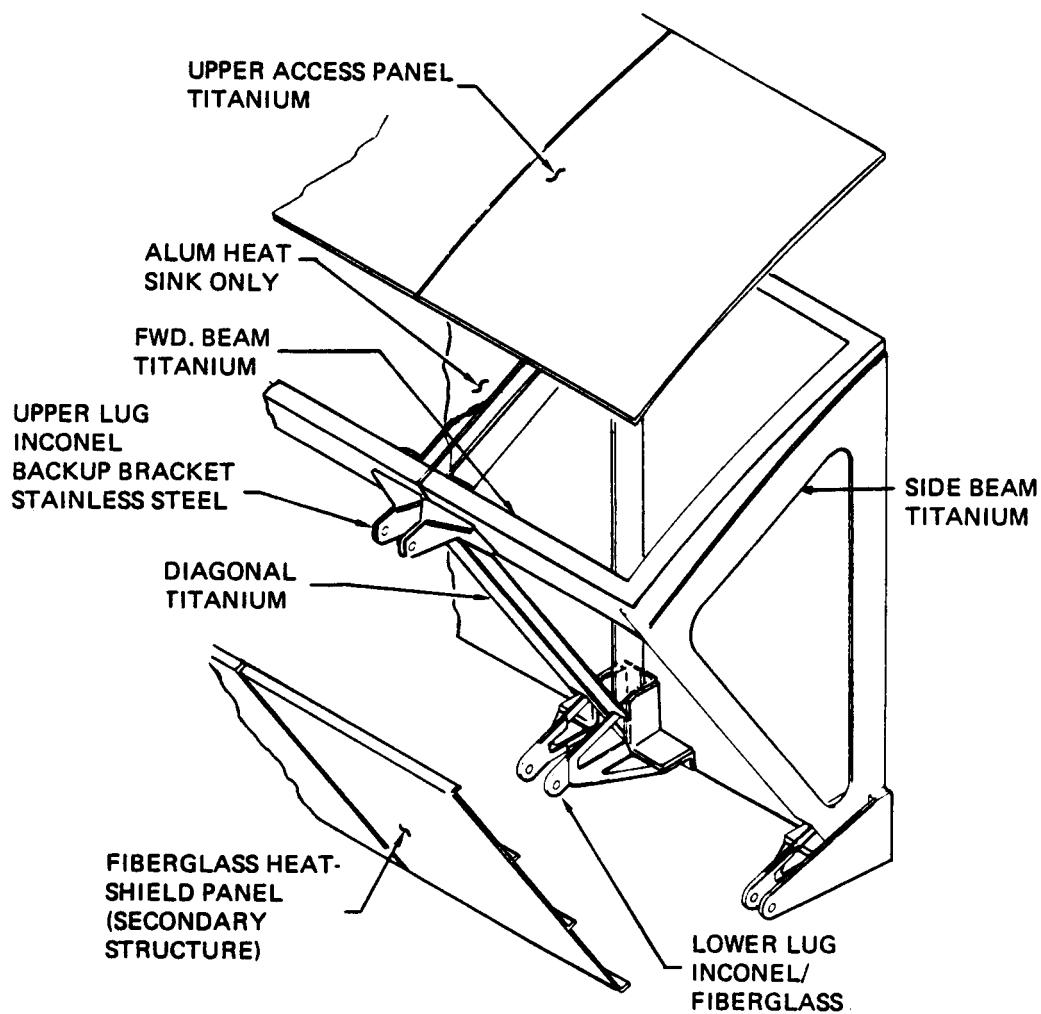


FIGURE 15 BUCKLE MODE SHAPES



ITEM	MATERIAL	CRITICAL CONDITION	ULTIMATE MARGIN OF SAFETY	MODE
UPPER ACCESS PANEL	.064 6AL-4V T1	BOOST	+1.81	BUCKLING
RIB TRUSE				
- FWD BEAM	.064-.072 6AL-4V T1	BOOST	+0.79	CRIPPLING
- SIDE BEAM	.04-.072 6AL-4V T1	BOOST	+1.00	CRIPPLING
- DIAGONAL	.04 6AL-4V T1	BOOST	+1.31	CRIPPLING
		ENTRY-THERMAL EXPANSION	+0.19	CRIPPLING
- VERTICAL	.04 6AL-4V T1	ENTRY-THERMAL EXPANSION	+1.90	CRIPPLING
UPPER LUG	.156 INCONEL 718	SIDE LOAD VIBRATION	+1.21	BENDING
BACK-UP BRACKET	.156 321 STAINLESS STEEL	SIDE LOAD VIBRATION	+0.66	BENDING
LOWER LUG	.078 INCONEL 718	SIDE LOAD VIBRATION	+0.51	CRIPPLING
- SPLICE	.25 POLYIMIDE	SIDE LOAD VIBRATION	HIGH	COMPRESSION
- ATTACH ANGLES	.125 2024-T4 ALUM	SIDE LOAD	+0.83	BENDING
LUG BOLT	INCONEL 718	BOOST ENTRY	HIGH HIGH	BENDING BENDING

FIGURE 16 SUMMARY OF MARGINS OF SAFETY – SUPPORT STRUCTURE

1.1.1.3 Thermal Analysis - Thermal analyses were conducted primarily to:

- (a) establish thickness requirements to accommodate surface recession in the event of coating loss,
- (b) define temperatures and gradients in the RPP leading edge to support the structural analyses,
- (c) define insulation thickness requirements and bondline and support structure temperatures to assure thermal integrity of the design.

Design Criteria - Thermal design criteria were the same as those employed in the Phase II program, reference (2). Only the entry trajectory is critical for thermal and thermal stress conditions. The design entry profile is given in Figure 17. No specific factors of safety were employed on heating rates or temperatures. Heating rate distribution around the leading edge, used for design, is provided in Figure 18. These data are for the Rockwell International delta winged vehicle SSV-161C, and the entry data is for trajectory No. 935.

Temperature limits for titanium and aluminum were established at 600°F and 350°F, respectively. Maximum soak temperature in orbit, based on NASA approved Rockwell International data, was +130°F.

Entry Oxidation - Entry oxidation analysis was performed using a VSD ablation routine which accounts for reaction rated control, transition, and diffusion control oxidation mechanisms. Oxidation characteristics of bare RPP were based upon plasma arc test data.

Effects of cross radiation were included in the oxidation analysis by permitting the inside surface of the skin to participate in radiant interchange with a surface of specified time variant temperature equal to the average temperature within the leading edge cavity. This cavity temperature was taken from Phase II cross radiation analysis results. Since the average cavity temperature could conceivably be different for the thick skin fail safe design than for the thin skin Phase II design, a comparison was made between peak inside skin temperatures from Phase II cross radiation analyses

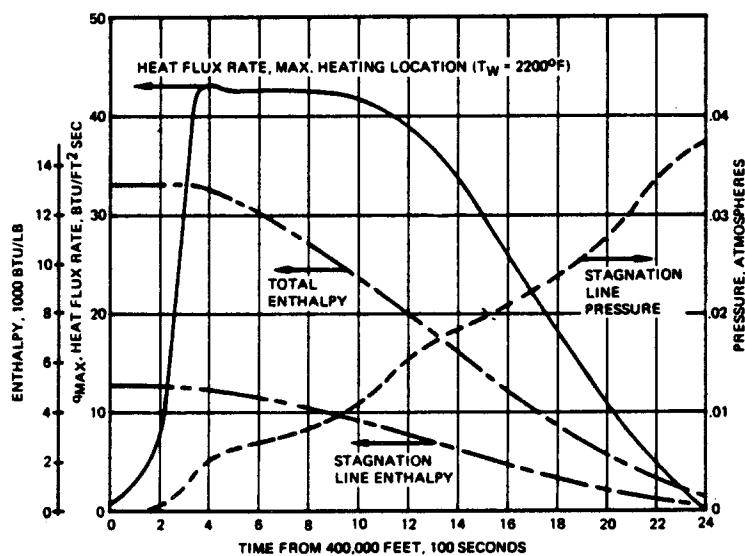
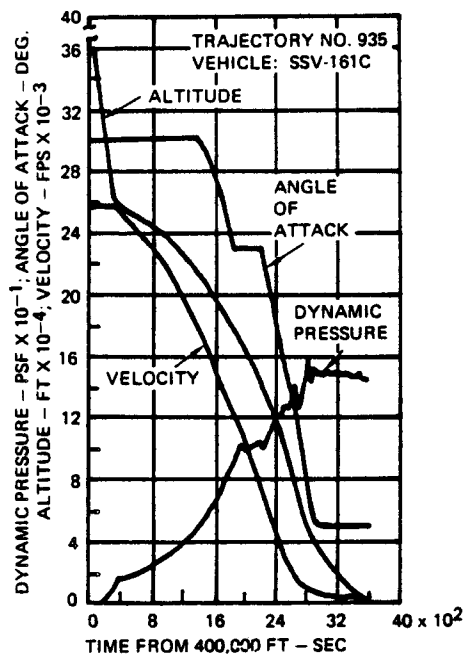


FIGURE 17 ENTRY DESIGN TRAJECTORY

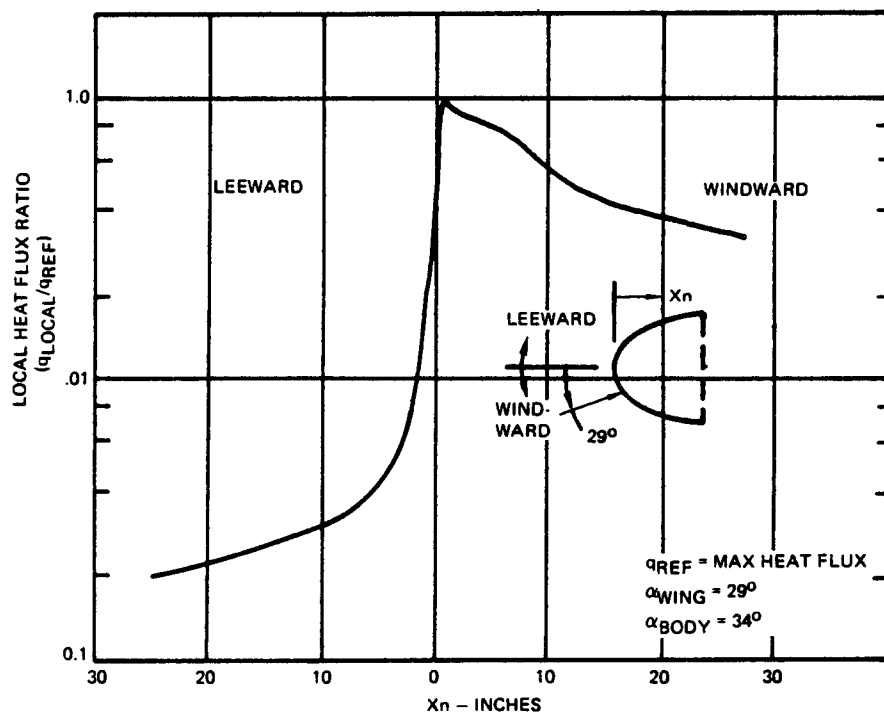


FIGURE 18 HEATING RATE DISTRIBUTION AROUND LEADING EDGE

and from the current ablation analyses. The resulting temperature distribution comparison in Figure 19 indicates that the average cavity temperature for the fail safe design with ablation is very close to that established in Phase II for the thinner skin.

Oxidation results are presented in Figure 20. Thickness losses for ten locations on the leading edge are shown as a function of wetted distance around leading edge. The maximum thickness loss from this curve is at the stagnation line and is 0.236 inch. This drops to 0.076 inch at the windward trailing edge and to essentially no recession at the leeward trailing edge.

Computed thickness losses, with an added 20% margin, were added to preliminary estimates of structural thickness requirements to establish the total skin thickness for the fail safe design analysis.

Temperature Distribution in RPP - Temperature analyses were conducted on the RPP leading edge to establish temperature distributions for thermoelastic stress analysis and to verify design conditions for the internal heatshield assemblies.

Thermal analyses were performed using a VSD computer routine which accounted for internal cross radiation, conduction and heat sink effects. Analyses extended through the periods of maximum thermal gradients and maximum temperature. For the RPP portion of the analysis an initial temperature of -170°F was used to obtain worst thermal gradients in the material.

A two dimensional thermal model was used in the analysis of leading edge skin temperatures. Internal insulation was represented by an adiabatic surface and results in slightly conservation insulation temperatures.

The temperature of the leading edge reaches a peak of 2547°F at a time of 660 seconds. Temperatures at the other locations for this time are presented on Figure 21. Comparing these results to those of the Phase II analysis shows lower maximum temperatures for the present study. The maximum temperature of the skin is 2547°F compared to 2592°F for Phase II, and the maximum temperature of the insulation is 2272°F compared

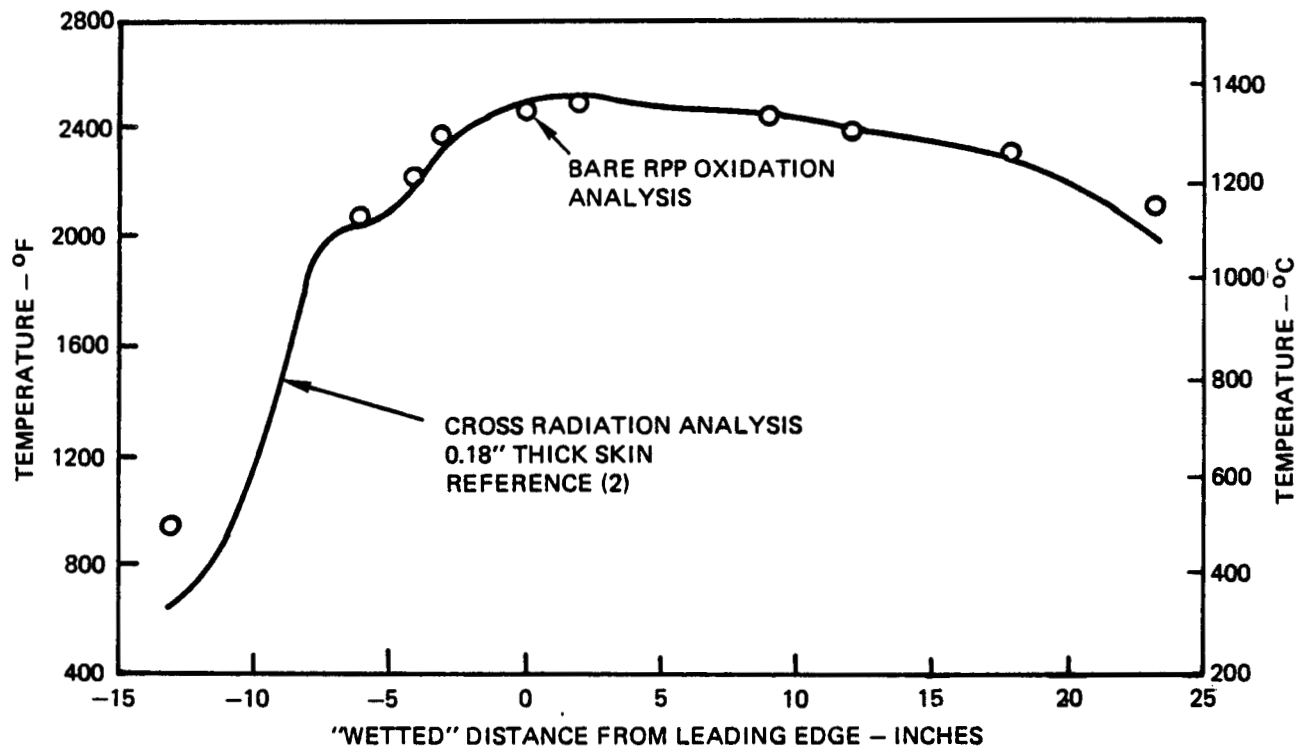


FIGURE 19 COMPARISON OF SKIN INSIDE TEMPERATURES – OXIDATION ANALYSIS

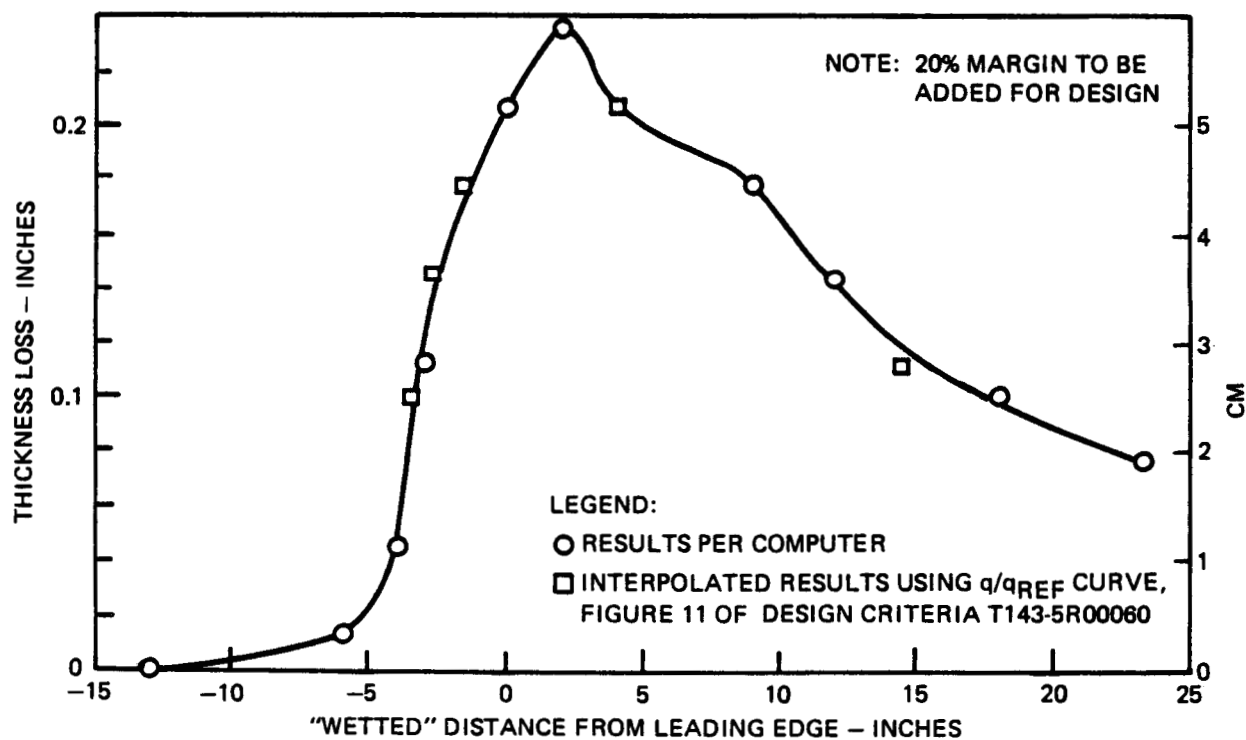


FIGURE 20 THICKNESS LOSS FOR 2400 SECONDS – RPP DENSITY = 80 LB/FT³

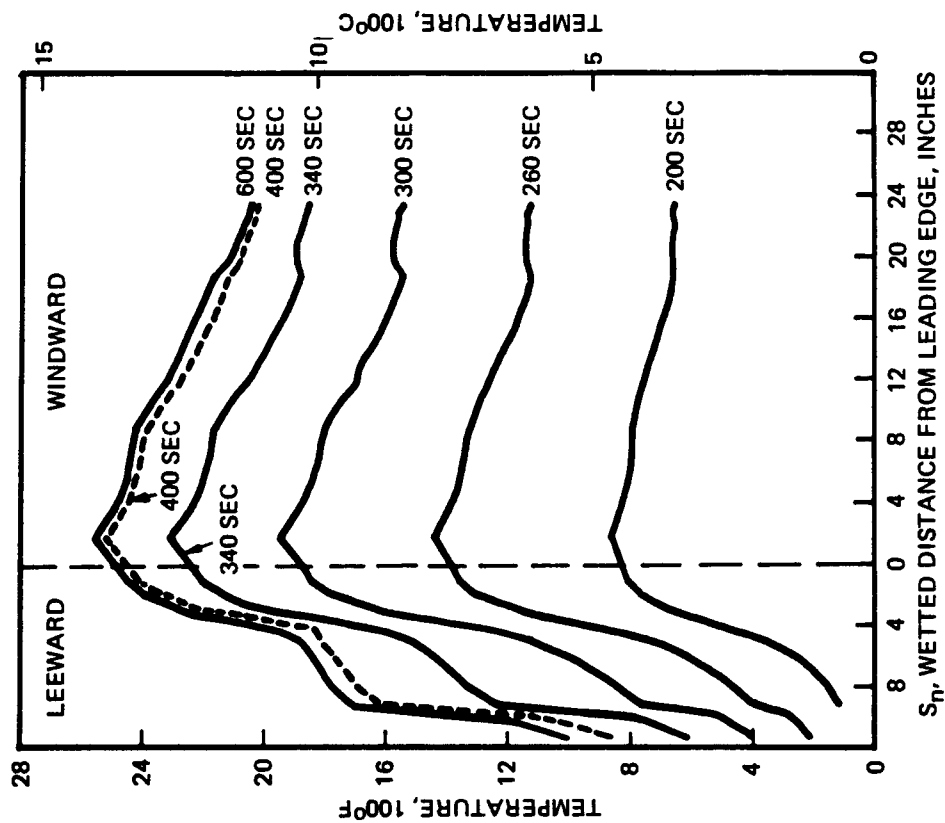


FIGURE 22 SKIN TEMPERATURE DISTRIBUTION
(OUTSIDE SURFACE)

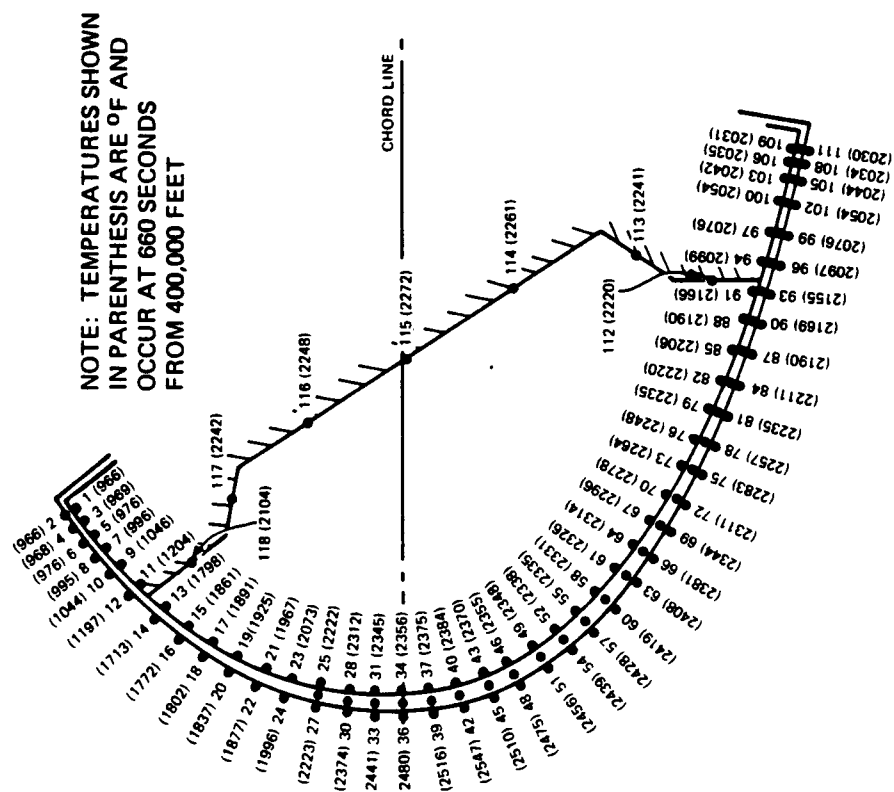


FIGURE 21 SKIN AND INSULATION MAXIMUM
TEMPERATURES

NOTE: TEMPERATURES SHOWN
IN PARENTHESIS ARE OF AND
OCCUR AT 660 SECONDS
FROM 400,000 FEET

to 2396[°]F for Phase II. The lower temperatures for this study are the result of two factors: (1) higher nominal skin emissivity (0.94 maximum versus 0.85, reference (2)), (2) higher circumferential heat conduction due to thicker skin. These two factors offset the reduction in cross radiation effect due to a thicker skin. Comparing the current temperatures with radiation equilibrium values shows that the temperature reduction due to cross radiation and heat conduction for the fail safe skin is 123[°]F, compared to 148[°]F for the thinner skin analyzed in Phase II.

One of the primary purposes of the thermal analyses was to determine the location and magnitude of the maximum thermal gradients in the leading edge. In order to determine the maximum gradient around the periphery of the leading edge, the temperatures at various times were plotted as shown on Figure 22. From this data it was determined that the maximum gradient of 541[°]F/inch occurs between nodes 12 and 14 (reference Figure 21) on the leeward side, where the wing support insulation begins, at a time of 400 seconds. This gradient is higher than the Phase II computed value of 325[°]F/inch. A finer nodal network was used in the current analysis in the vicinity of the peak gradient in order to more accurately define the magnitude of the gradient.

The maximum thermal gradient through the thickness of the leading edge is 697[°]F/inch and occurs at the maximum heating location at a time of 300 seconds.

To analyze temperature distributions in the ribs two-dimensional thermal models were constructed of the rib and seal strip at six circumferential locations in the cavity area of the leading edge; that is, the area where the skin is not internally insulated. Three-dimensional models were constructed of the two lug areas, where the skin is insulated to protect the attachment lug. Computed temperature distributions indicate that the maximum temperature drop across the rib in the cavity area is 346[°]F at the maximum heating location, compared to 300[°]F computed in Phase II. This is due to the lower thermal conductivity used in the current analysis as compared to the Phase II design value. The current conductivity is based

upon the Southern Research Institute data from Phase II (reference (2)). In the windward side lug area the maximum temperature drop across the rib is 1205°F , compared to 1100°F in Phase II.

Predicted temperatures for the rib and adjacent skin are presented on Figure 23 for a time of 660 seconds. Results of the leading edge skin analysis are included on the figure and agree very well with the predicted skin temperatures obtained in the rib analysis. Similarly, rib gradients were determined at 260, and 400 seconds. In addition, rib gradients at the maximum heating location were determined at various temperatures between 240 and 360 seconds. This confirmed that the maximum gradient occurred at 260 seconds.

The windward and leeward side support joint area rib temperatures were analyzed using 70 node three dimensional thermal models. These models included heat conduction along the skin and rib, across the insulators and into the steel bolt and support fitting. Cross radiation from the skin and surrounding structure to the portion of the rib outside of the bulk insulation was considered, as was heat conduction through the bulk insulation and into the support joint.

Computed temperatures in the windward side support joint are shown in Figure 24 for entry time of 400 seconds. This is at the time of peak skin temperature gradient. It is seen that the temperature drop across the rib for the windward side, between nodes 6 and 37 is 1191°F at 400 seconds. This temperature drop peaks at 380 seconds at a value of 1205°F . This compares to a value of 1100°F computed in Phase II. This drop is considerably higher than that in the cavity area because:

- . Heat transfer from skin to rib is by conduction only, since bulk insulation suppresses cross radiation.
- . The rib height is higher in the support joint area than in the cavity area.
- . Attachment hardware at the inboard side of the rib serves as a heat sink to maintain relatively low temperatures.

TIME FROM 400,000 FEET = 660 SECONDS

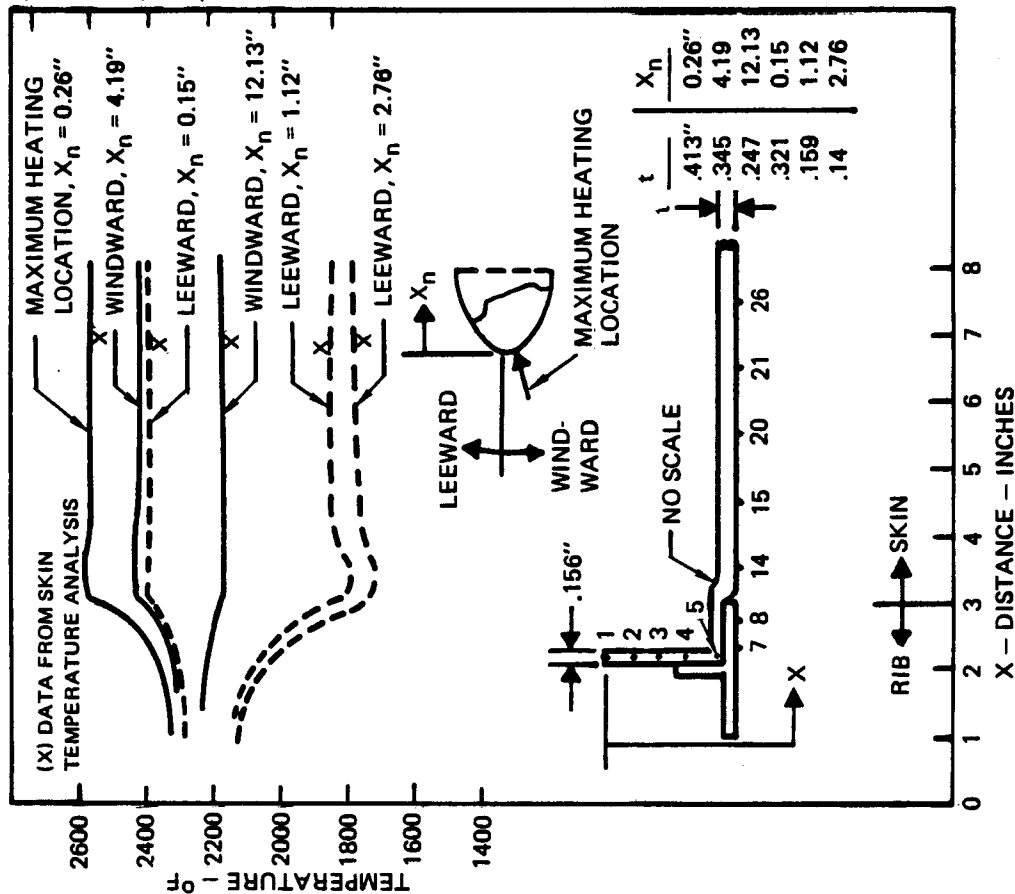


FIGURE 23 RIB TEMPERATURE DISTRIBUTION

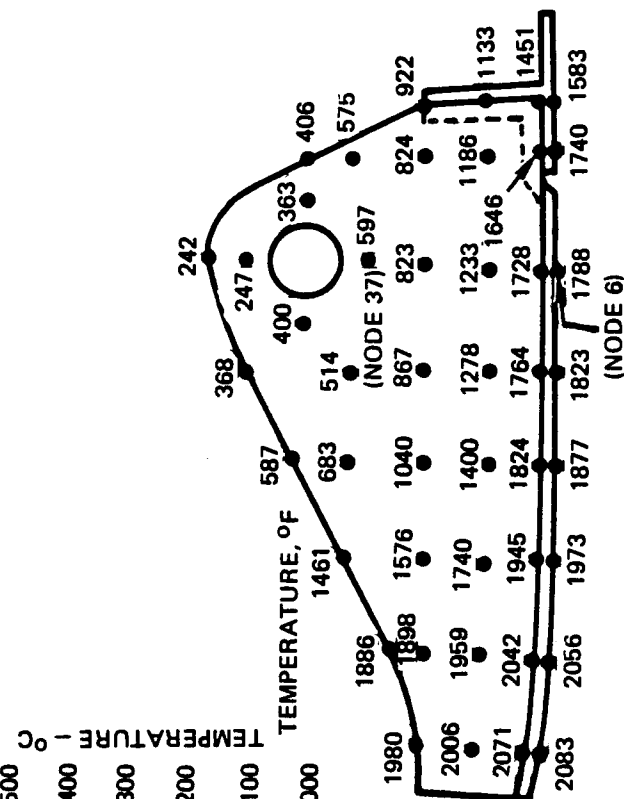


FIGURE 24 WINDWARD SIDE SUPPORT JOINT TEMPERATURES - ENTRY TIME = 400 SECONDS

Insulation Analyses - Analyses were conducted on all areas of the leading edge assembly to ensure that the insulation design was thermally acceptable and temperatures did not exceed desired limits. These analyses included the following:

- (1) Canted heatshield and front spar, combined with the interaction from the upper RSI access panel.
- (2) Titanium rib truss/aluminum front spar interface region on the windward side of the leading edge.
- (3) Lower lug support bracket insulation assembly.
- (4) Upper lug support bracket insulation assembly.
- (5) Lower panel insulation.

Each of these are discussed in the following paragraphs and temperatures of the final design configuration are presented. Parametric analyses leading to the design of the canted heatshield are covered under Task 2.

The canted heatshield was first analyzed as a one-dimensional heat transfer problem, excluding interaction effects from the upper RSI panel. The model configuration analyzed is shown in Figure 25, which shows the final selected heatshield sizing and the peak temperatures computed from the analysis. The key temperatures are the bondline temperature, which was to be limited to 600°F, and the aluminum temperature, which was not permitted to exceed 350°F. For comparison against other front face insulation thicknesses the following controlling temperatures were obtained:

<u>Forward Insulation Thickness, Inches</u>	<u>Aft Insulation Thickness, Inches</u>	<u>Bondline Temperature</u>	<u>Aluminum Temperature</u>
		<u>°F</u>	<u>°F</u>
2.5	1.0	358	275
2.0	1.0	439	297
1.5	1.0	562	346

With 1.5 inch thickness on the front side and 1.0 inch on the aft side, desired temperature limits are met. The design was based on this analysis.

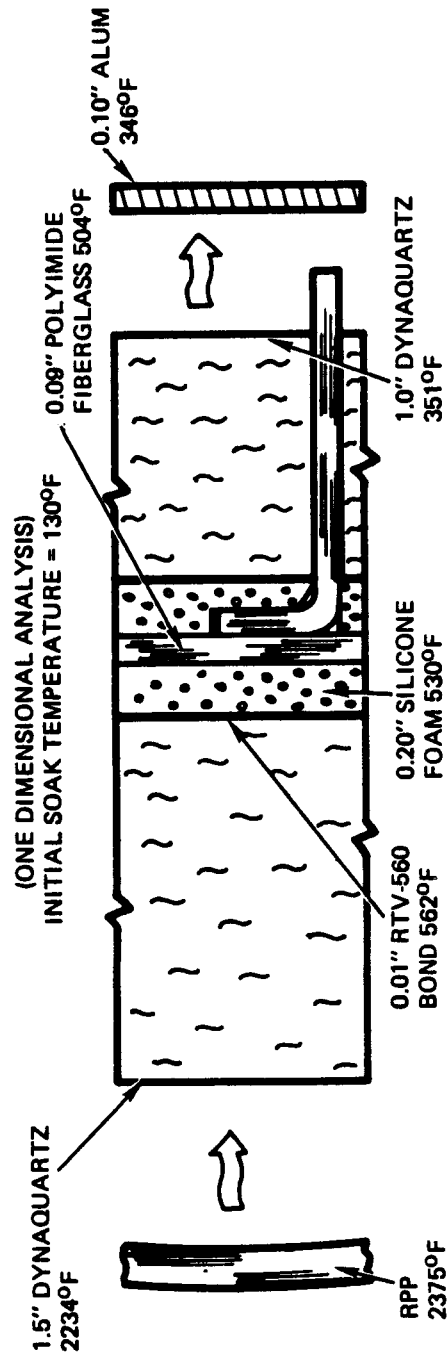


FIGURE 25 HEATSHIELD ANALYSIS MAXIMUM TEMPERATURES

*OUTSIDE SKIN TEMPS.
FOR REFERENCE, NOT
PART OF THERMAL MODEL.

**INPUT TEMPS., FROM CROSS
RADIATION ANALYSIS

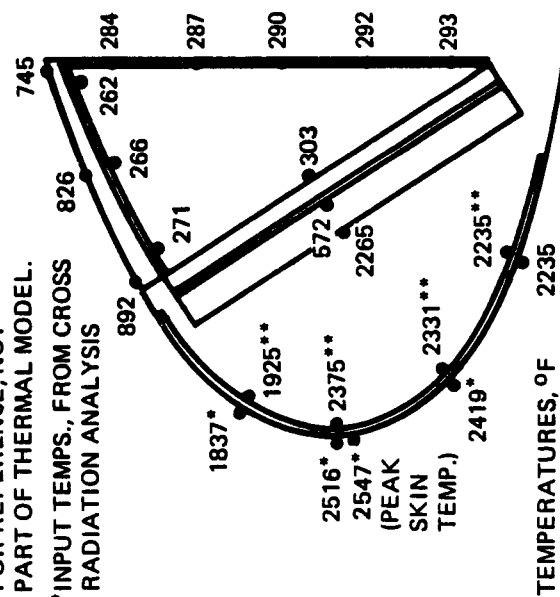


FIGURE 26 MAXIMUM TEMPERATURES
FROM HEATSHIELD ANALYSIS

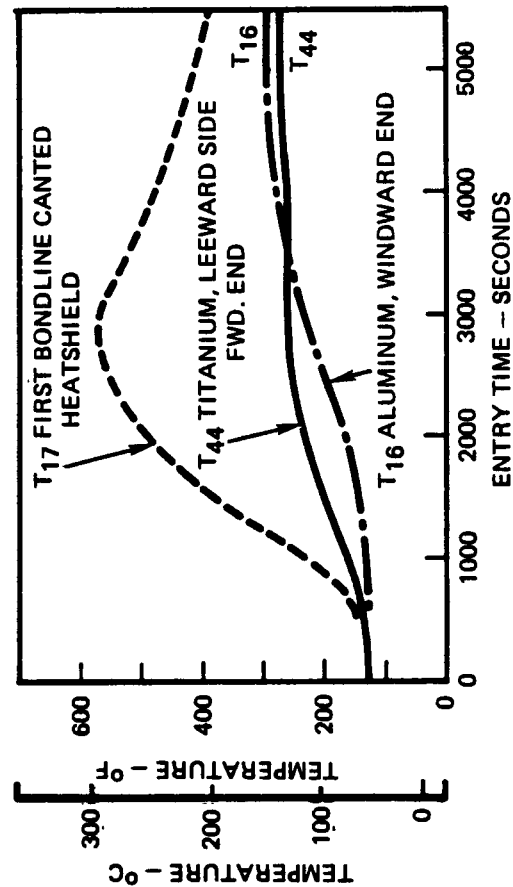


FIGURE 27 TEMPERATURE RESPONSE
HEATSHIELD ANALYSIS

In Figure 25 the RPP temperature reflects an average inner surface temperature for the stagnation region calculated from the cross radiation analysis (reference Figure 21). The insulation surface temperature is lower than that shown in Figure 21 because of heat sink and conduction influences.

Because temperatures of the upper access panel and canted heatshield peak at different times, thermal analyses were performed to determine the effect of coupling between the thermal response of the upper panel and the canted heatshield, upon titanium and aluminum structural temperatures and insulation bondline temperatures. The model included effects of cross radiation between the back surface of the canted heatshield aft insulation, the titanium structure for the upper panel, and the aluminum spar. Heat conduction between the titanium and aluminum were also included.

Maximum computed temperatures are summarized in Figure 26. It is seen that the maximum bondline temperature on the heatshield is 572°F , which is 10°F higher than was computed with the previous thermal model which did not include the upper panel. However, this temperature is still within the acceptable 600°F limit. The peak aluminum temperature is 293°F compared to 346°F with the previous model. The peak titanium temperature is 271°F forward and 262°F aft compared to 345°F and 382°F , respectively, computed with one-dimensional models. These reductions are due to heat interchange between the titanium and aluminum, whose temperatures tend to peak at different times.

Analyses which did not include heat transfer between the titanium and aluminum, indicated that the titanium forward end would peak at 345°F at 3000 seconds, at which time the aluminum would be at 165°F . The temperature-time curves in Figure 27 for the coupling analysis show that heat transfer from the titanium to the aluminum reduces the titanium temperature at this time to 260°F and increases the aluminum to 232°F . Conversely, previous analyses indicated the aluminum would peak at 346°F at 7700 seconds, when the titanium was only at 170°F . As shown in Figure 27, heat transfer from the aluminum to the titanium causes the aluminum temperature

to peak earlier at 5400 seconds, and reduces the peak aluminum temperature to 293°F, while increasing the titanium to 271°F. The reason for the tendency of the titanium temperature to peak earlier than the aluminum is that the upper panel is much thinner than the canted heatshield. An additional reason for the lower temperature in the coupling analysis is that the aluminum spar is 12% longer than the canted heatshield, providing additional heat sink which was not included in the previous analyses.

In summary, results of the final analysis indicate a substantial improvement in temperature margin for the structural panels and only a slight increase in bondline temperature, as compared with initial analyses.

A 94 node, three-dimensional thermal model was developed for the titanium rib truss-aluminum spar interface region on the windward side of the heatshield. The purpose of this model was to evaluate the potential heat short across the lower portion of the rib truss into the aluminum. The model included not only the heat short itself, but also radiation from the aft side of the aft insulation to the aluminum and conduction across the polyimide support bracket. Maximum computed temperature in the aluminum was 358°F.

The analysis was based on an early version of the heatshield and leading edge support brackets. Subsequently, potential heat shorts to the aluminum spar were reduced by revising the heatshield and support bracket designs. Further, the coupling analysis between the heatshield and upper panel showed that the aluminum spar would operate at a much reduced temperature (by 53°F) than the one-dimensional analysis would indicate. With these factors it was judged that the 358°F aluminum temperature calculated for the truss heat short would readily reduce to below 350°F for the final design, and a reanalysis was not performed.

The lower lug support bracket insulation was initially sized for 10 lb/ft³ Dynaquartz insulation, based on the heatshield analysis, since surface temperatures were equivalent. However, the lug insulation is heated from the front, sides, and bottom. This three directional heating has a significant effect upon the insulation requirements in this area. The final

lug insulation design was limited by the maximum density (15 lb/ft³) and thickness (3.0 inch) of Dynaquartz that could be obtained. This necessitated using the titanium insulation support bracket as heat sink to maintain temperature within acceptable limits for the RTV560 bondline. Details of the analyses are discussed below.

Three-dimensional thermal analyses were performed on the Dynaquartz insulation around the lower support lugs, including the titanium support brackets. The objectives of these analyses were to predict the insulation bondline temperatures and to evaluate the potential heat short down the titanium support bracket to the cool end of the Inconel support lug bracket.

A 157 node thermal model, used for analysis of the lower lug insulation assembly, was based on three inch insulation thickness, as indicated in Figures 28, 29, and 30. Analyses were performed for a two inch thickness of 15 lb/ft³ density Dynaquartz, as well as various thicknesses of the titanium bracket. Results are summarized as follows:

Insulation Thickness, Inches	Titanium Thickness, Inches	Peak Bondline Temperature, °F
2	.05	898
3	.08	647
3	.16	590

It is seen that the final design combination maintains the bondline below its temperature limit of 600°F.

Peak computed temperatures for the final configuration are presented in Figures 28, 29, and 30. Maximum temperature of the polyimide insulator in Figure 30 is 397°F, which is well within tolerance limits. The aluminum substructure temperature had not peaked at the end of the computer run at 5300 seconds. However, the temperature rise of the aluminum at this time was only 113°F as compared to a temperature rise

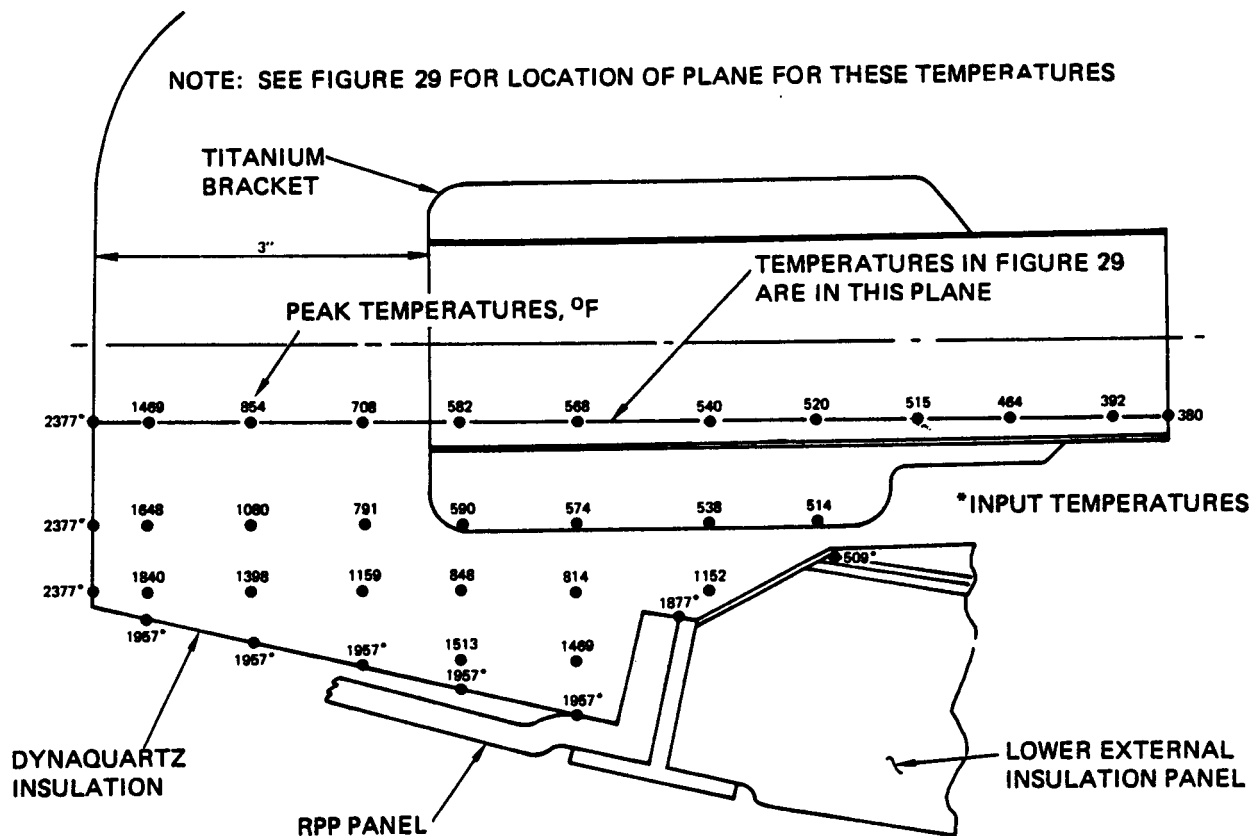


FIGURE 28 PEAK TEMPERATURES IN LOWER LUG INSULATION AND SUPPORT BRACKET – SIDE VIEW

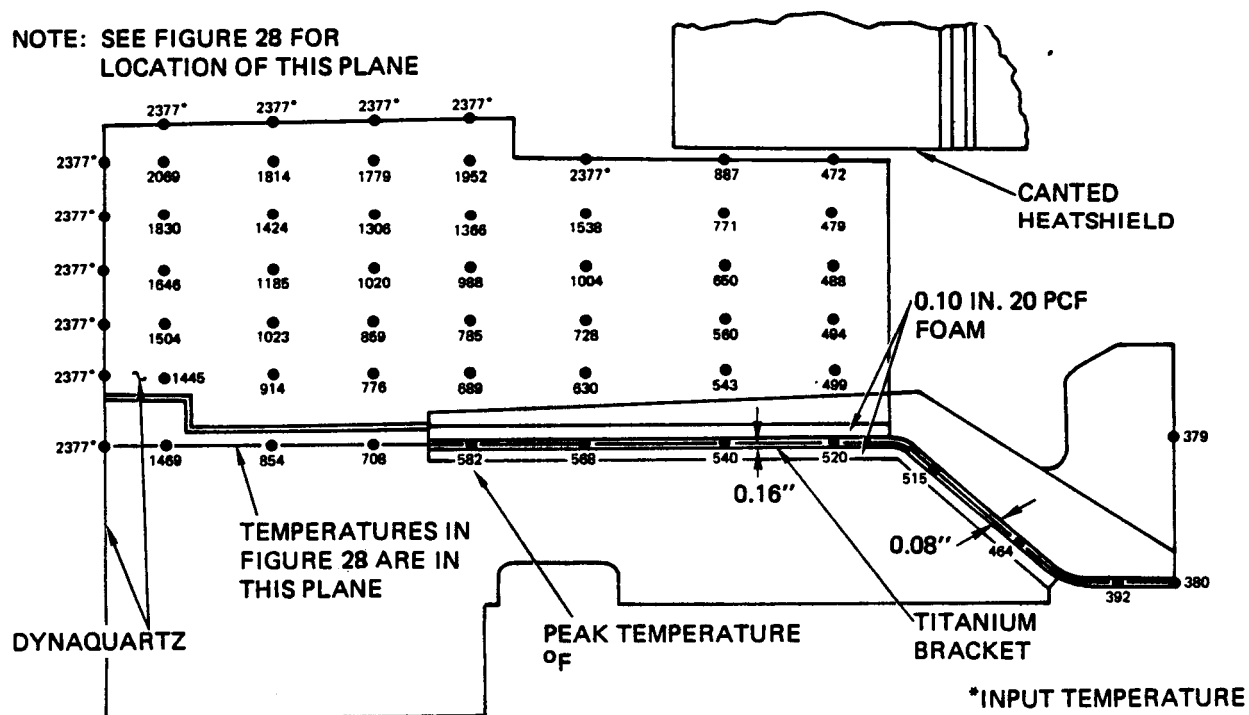


FIGURE 29 PEAK TEMPERATURES IN LOWER LUG INSULATION AND SUPPORT BRACKET – TOP VIEW

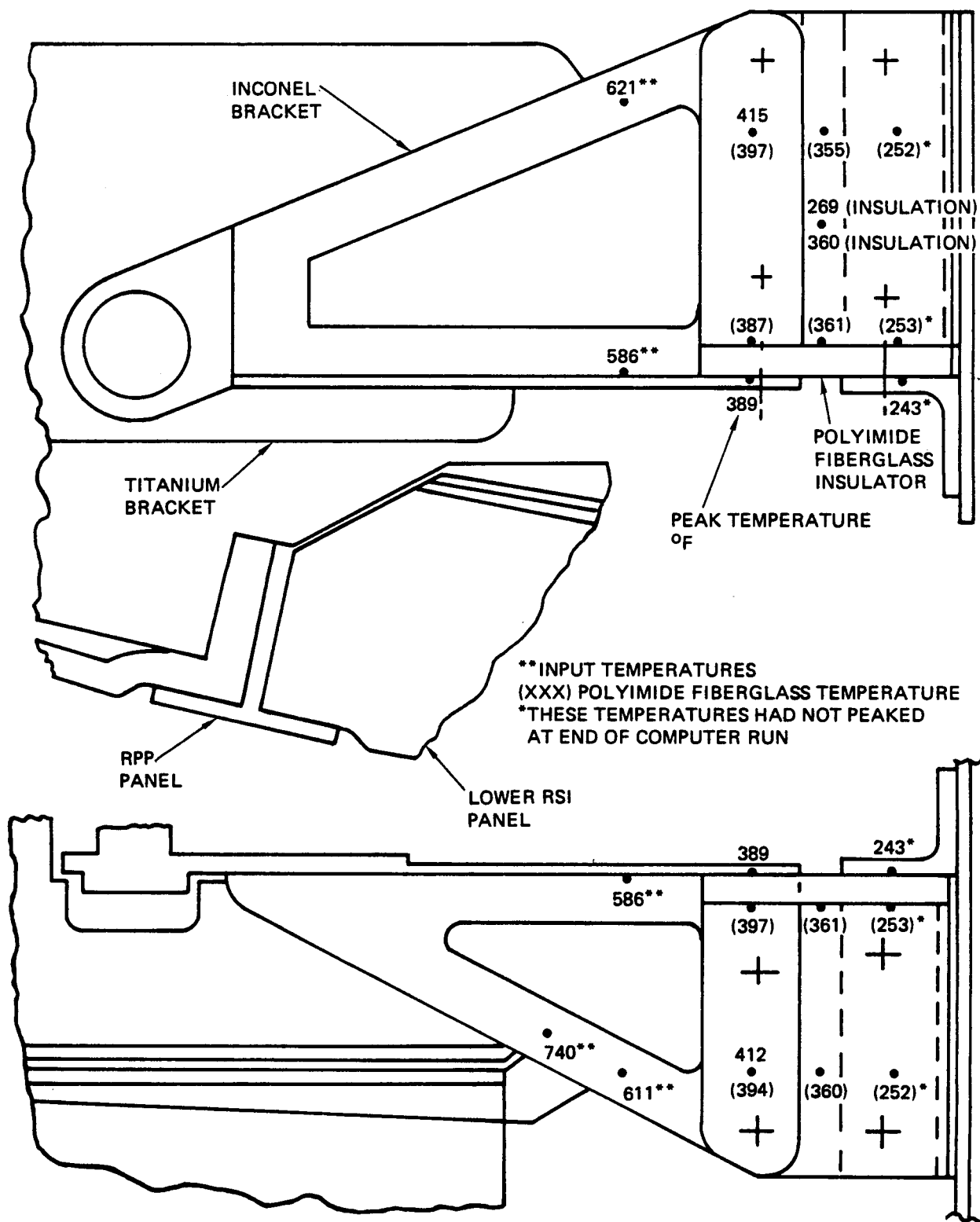


FIGURE 30 PEAK TEMPERATURES IN LOWER LUG SUPPORT

of 110°F for the previous support joint analysis which did not include heat conduction from the titanium bracket. Hence, the heat short from the titanium bracket is not considered excessive.

A 152 node thermal model was used for the analysis of the upper lug insulation assembly as indicated by Figures 31 and 32. The model was based on 2.5 inch insulation thickness on one side of the insulation block and 2.0 inch on the other side, as shown in the figures. Analyses were also performed for a 2.0 inch thickness on all sides. The insulation was 15 lb/ft³ density Dynaquartz. Various thicknesses were analyzed for the titanium bracket.

The first analysis of the insulation assembly was based on two inch insulation thickness on all sides of the insulation block, and a 0.10 inch thick titanium bracket. Results indicated that the insulation bondline would overheat; therefore, three additional analyses were made with various thicknesses of insulation on one side (dimension A of Figure 32), a constant two inch insulation thickness on the other two sides (dimension B and C of Figure 31) and various titanium bracket thicknesses. The results are summarized below:

Insulation Thickness (Dimension A) Inches	Titanium Thickness Inch	Peak Bondline Temperature °F
2	0.15	610
2.5	0.10	610
2.5	0.16	556

It is seen that the final design combination maintains the bondline below its temperature limit of 600°F. Peak computed temperatures for the final configuration are presented in Figures 31 and 32.

The lower insulation panel was designed to represent a RSI assembly, but used 10 lb/ft³ Dynaquartz as a ground test alternate to the RSI. The insulation is bonded through the strain isolator to a titanium

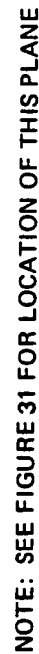


FIGURE 32 PEAK TEMPERATURES IN UPPER LUG INSULATION AND SUPPORT BRACKET, TOP VIEW

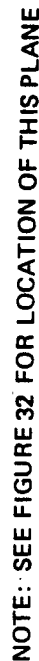


FIGURE 31 PEAK TEMPERATURES IN UPPER LUG INSULATION AND SUPPORT BRACKET, SIDE VIEW

support panel. This, in turn, attaches to aluminum structure (the front spar), which requires temperature to be limited to 350°F maximum.

A two-dimensional model of the panel was constructed for computer analysis. The particular analyses conducted used LI-1500 insulation, 0.09 inch of foam, and 0.040 inch titanium. Results are estimated to be conservative for the final configuration which consisted of 10 lb/ft³ Dynaquartz, 0.20 inch foam, and 0.064 titanium panel with additional Dynaquartz insulation on the inside of the panel.

Predicted temperatures are shown in Figure 33 for the configuration with a 0.25 inch thick strip of polyimide fiberglass insulation between the aluminum and the titanium panel. Temperatures of all the critical locations are below the maximum allowed. Peak temperature at the bondline between the insulation and the foam is about 550°F, 50°F below the 600°F maximum allowed. Peak temperature at the interface between the polyimide and the titanium is less than 510°F which is well below the 700°F maximum allowed. Also the peak aluminum temperature, extrapolated to be 333°F, is below the allowed 350°F.

An additional run was made with the thickness of the polyimide insulation strip reduced from 0.25 inch to 0.125 inch. Peak aluminum temperature increased from 333°F to 381°F which is above the allowed 350°F. Interpolation between the two thicknesses indicates that a 0.2 inch thickness of polyimide fiberglass insulator is adequate to prevent the aluminum temperature from exceeding 350°F. Due to the small margin in this area, additional analysis and tests would be required for a flight design.

Support Joint Bracket Analysis - Analyses and configurational variations leading to the final design of the support brackets are covered under the Task 3 discussion. This section presents only the analysis of the final configuration. Two elements of the design are worth reiteration and accounts for the performance and practicality of the design for flight conditions. The first is the elimination of fragile, hard, ceramic insulators in the lug bolt joint and the employment of an all-metal design. This enhances reliability and confidence that the design will work in static and dynamic load environments.

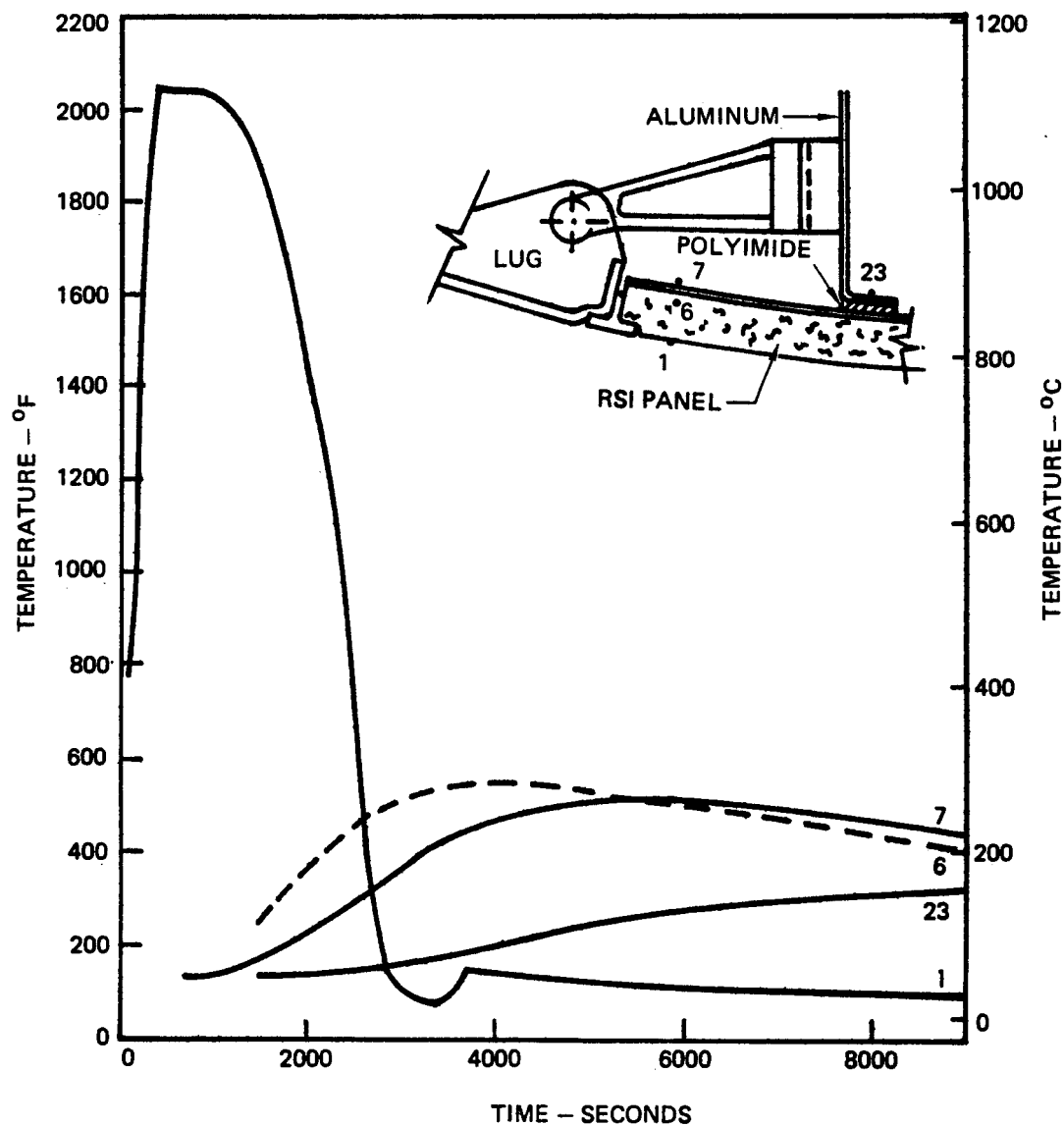


FIGURE 33 PREDICTED TEMPERATURES WINDWARD SIDE RSI PANEL

Secondly, to make the all-metal joint work for the more critical lower support bracket, a fiberglass insulator is used in series with the metallic structure to provide a low conduction area - long path thermal resistance into the aluminum. Reliability is gained by operating the fiberglass to low stress levels through the use of thick laminates. The design is probably overly conservative in this respect so that even greater thermal resistance is potentially available from the concept.

Thermal analyses were performed for the lower support bracket using a three-dimensional thermal model and a VSD computer routine which accounted for heat conduction along the skin and RPP rib, across the contact surfaces at the support joint, through the steel bolt and the bracket, and across the insulation into the aluminum wing structure. Cross radiation from the skin to the portion of the RPP rib outside the bulk insulation and radiation along the expansion gap between the rib and sealing strip were considered, as was the heat conduction through the bulk insulation and into the support joint.

From an analytical standpoint the lower bracket design is highly complex, including several joints, various materials, and gaps, where radiation could be a factor. As a result of analysis correlation with test data (reference Task 3), it was found that temperature predictions were sensitive to joint heat transfer coefficient and that a variable coefficient was required for best agreement. Furthermore, an increase in the conductivity of the Inconel material over nominal values originally used were required. This was reasonable because the literature on conductivity of nickel alloys showed this degree of scatter. One other indication from the analysis/test comparison was that an increase in conductivity for the RPP would more closely match test performance. However, there was no real justification for doing this on the basis of available conductivity data and the analysis to examine such an approach was not performed.

A summary of analysis and test data for the lower support bracket is given in Figures 34 and 35. Final analytical predictions using a

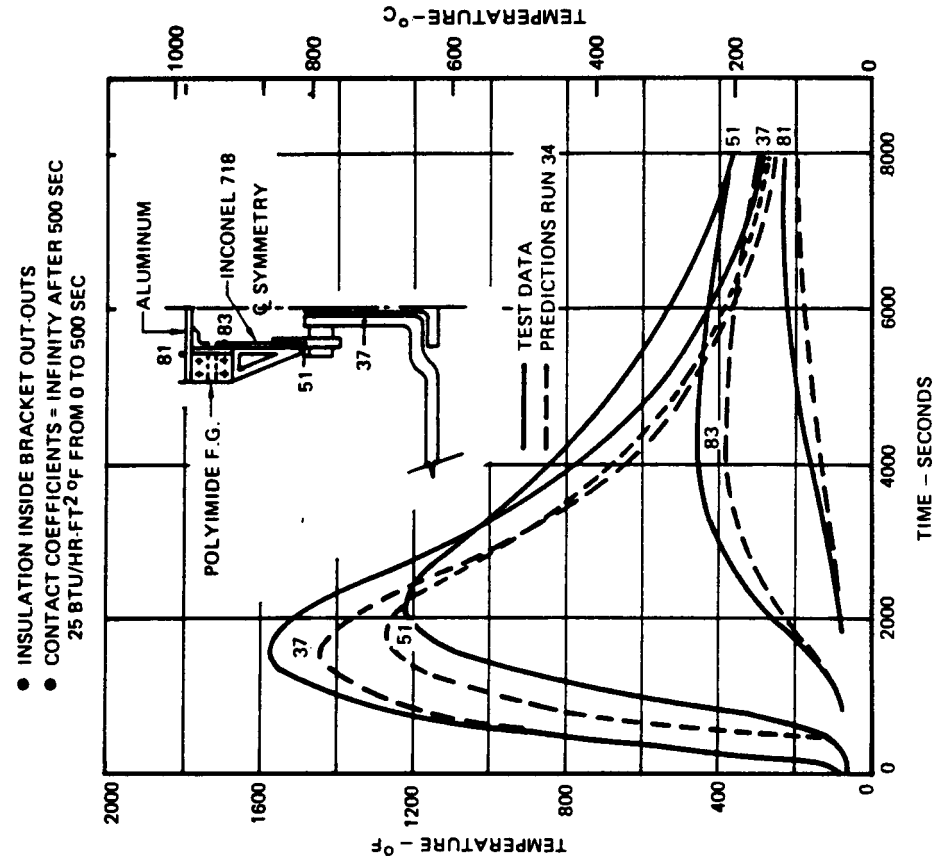


FIGURE 34 RPP LUG TEST FINAL PREDICTIONS VS TEST DATA

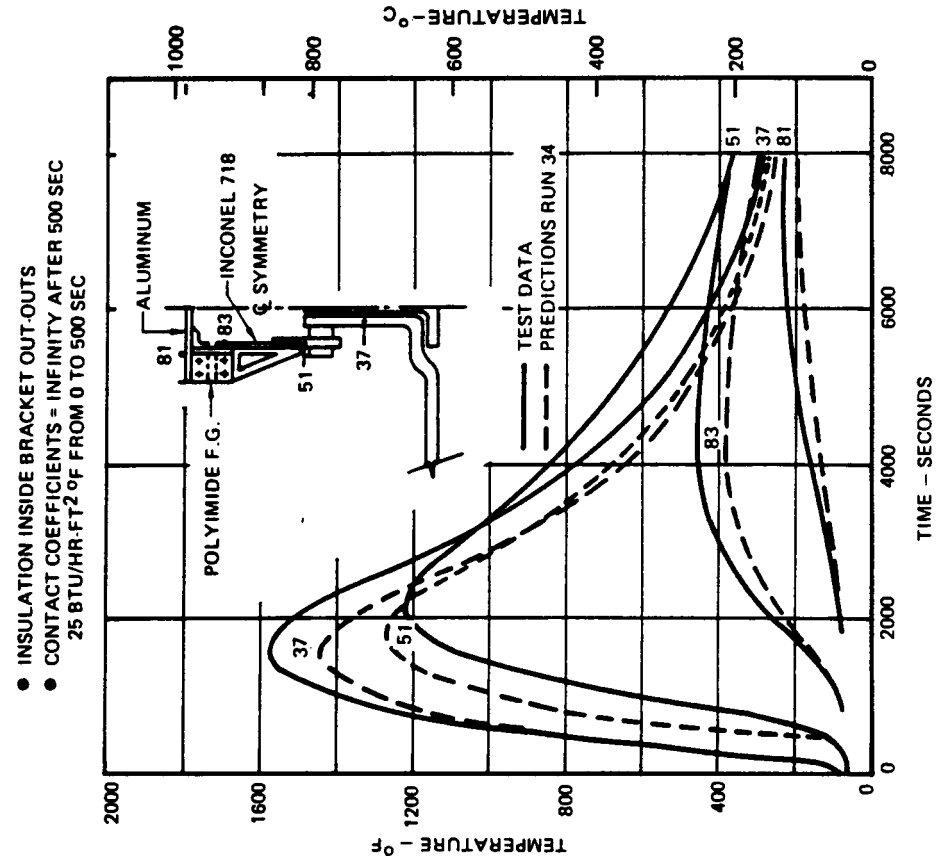


FIGURE 35 POST-TEST PREDICTIONS - EFFECT OF CHANGE IN CONTACT COEFFICIENT

variable joint heat transfer coefficient are provided in Figure 34. In this analysis joint coefficient was varied from $25 \text{ Btu/hr ft}^2 \text{ }^\circ\text{F}$ at 180°F to $40,000 \text{ Btu/hr ft}^2 \text{ }^\circ\text{F}$ at 2000°F . Temperature predictions are not exact, but the deviation from test doesn't exceed 150°F on the Inconel and is only 40°F for the polyimide fiberglass.

If a low joint coefficient ($25 \text{ Btu/ft}^2 \text{ hr } ^\circ\text{F}$) is used initially through 500 seconds and then an infinite coefficient is used throughout the remainder of the trajectory, the results shown in Figure 35 are obtained. Note that in some cases they provide higher temperatures, while in others the results are lower than achieved with the variable joint coefficient. In design analysis for flight hardware it will be necessary to examine a reasonable range of joint coefficients to establish rational temperature bounds on the problem.

The significance of both the analyses and test data is that the design of the support bracket is adequate. Aluminum temperature is well below the 350°F allowed, and the polyimide fiberglass temperature of 460°F is well within the $650 - 700^\circ\text{F}$ allowable for this material.

A three-dimensional thermal model of the leeward side support joint area was also constructed and computer analyses were performed to define peak temperatures using infinite joint heat transfer coefficients. The analysis accounted for heat conduction along the skin, the RPP rib, across the support joint and the bracket into the titanium wing structure. Cross radiation from the skin to the portion of the RPP rib outside the bulk insulation was also considered, as was the heat conduction through the bulk insulation into the support joint and bracket.

Predicted temperatures for the final bracket design are shown in Figure 36. Peak temperature of the titanium is 438°F , which is well below the allowed 600°F . This temperature should prove to be conservative since a joint coefficient of infinity (perfect contact at the joint bushings) was used.

FINAL DESIGN OF BRACKET
JOINT COEFFICIENT = INFINITY

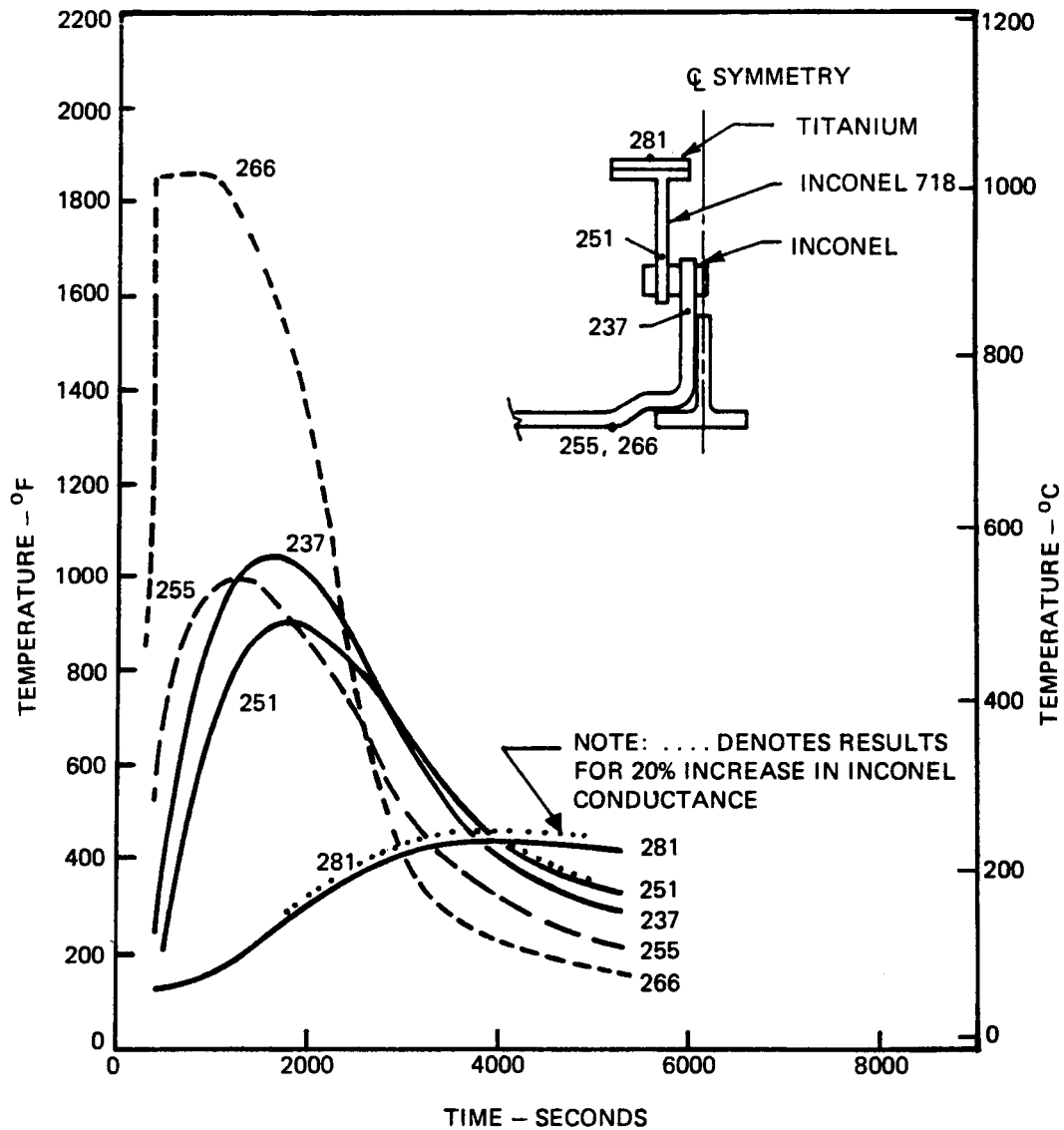


FIGURE 36 PREDICTED TEMPERATURES LEEWARD SIDE LUG AREA

1.1.1.4 Dynamics

Dynamics load analysis was conducted on the canted heatshield, support lug insulation assemblies and upper access panels to determine structural integrity of the insulation for vibration load responses. Analysis of the RPP leading edge was conducted during Phase II (reference (2)) for a 32 g-rms input and since this analysis showed the Phase II RPP design to be structurally acceptable for this condition, the analysis was not repeated for the Phase III design. This was because the Phase III design is much stronger in the critical support lug regions and considerably stiffer overall, due to the thicker skin. As part of an evaluation of the structural integrity of the RPP leading edge, particularly the attachment holes, under a dynamic loading condition, an acoustic test of the Task 12 leading edge was conducted. This section reports the findings of both the dynamic analysis of insulation components and the acoustic test of the leading edge. Additional heatshield parametric analyses and heatshield component tests are covered under Task 2.

Design Criteria - At the outset of the program, two sets of dynamics design conditions were established for design. These were a 32 g-rms vibration environment shown on Figure 37 and a 163 db overall sound pressure level illustrated in Figure 38. These are the same design requirements employed in the Phase II program.

The random vibration environment was considered as a maximum response as opposed to an input level, in accordance with agreements reached with NASA-JSC. Analyses were based on this approach; however, in the Task 2 vibration test program of the heatshield component, revised test criteria were established as discussed under Task 2.

Heatshield Dynamic Analysis - A review of the complete leading edge segment design concept indicated that only three components of the insulation system were critical relative to the flight dynamic environments. These three components are the canted heatshield, the upper access panel and the lower support lug insulation. A description of the analyses and supporting tests conducted to verify the design of these three components is presented below.

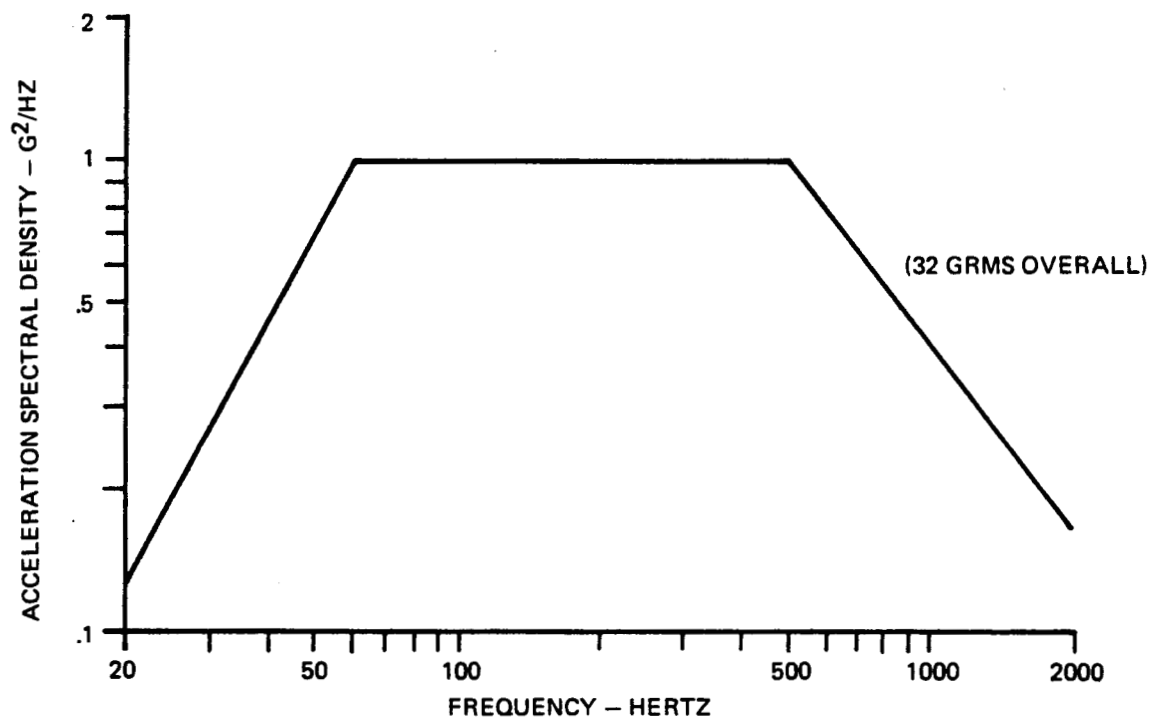


FIGURE 37 RANDOM VIBRATION ENVIRONMENT – BOOST PHASE

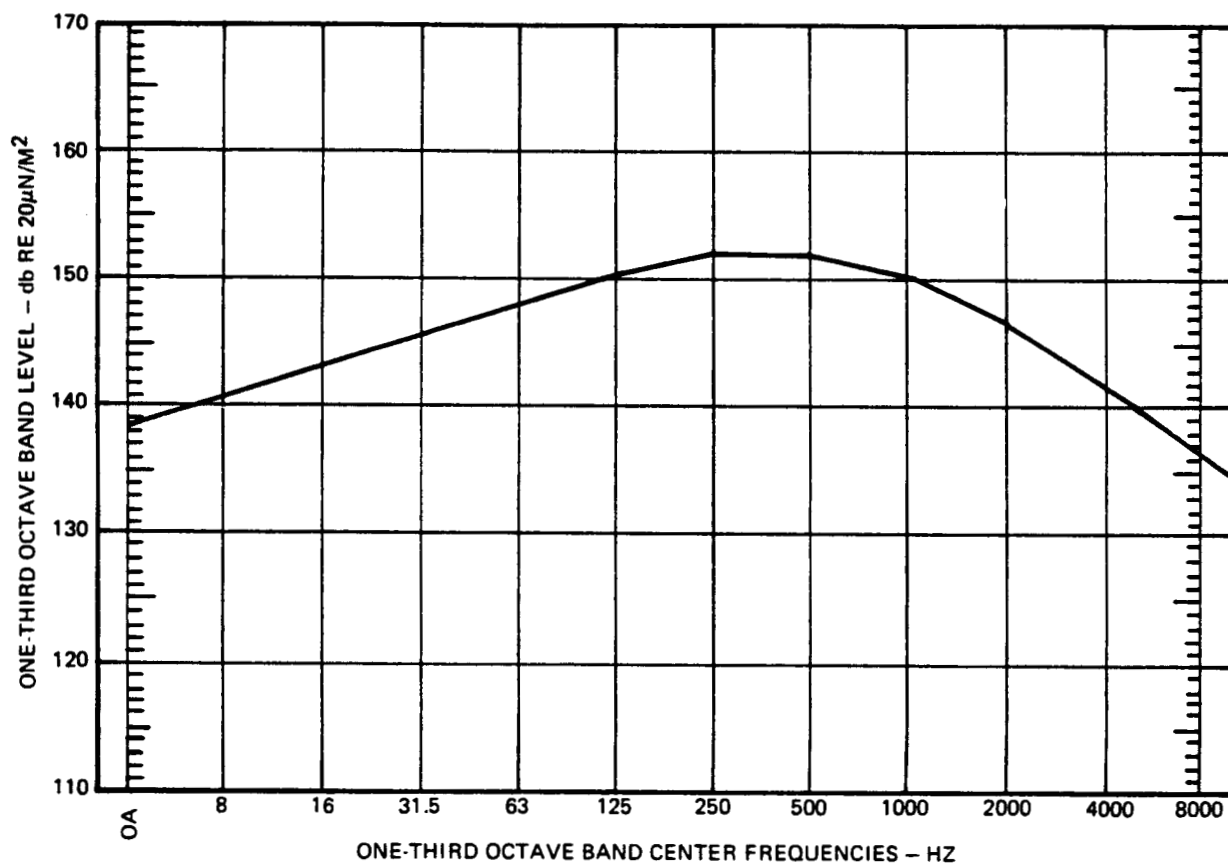


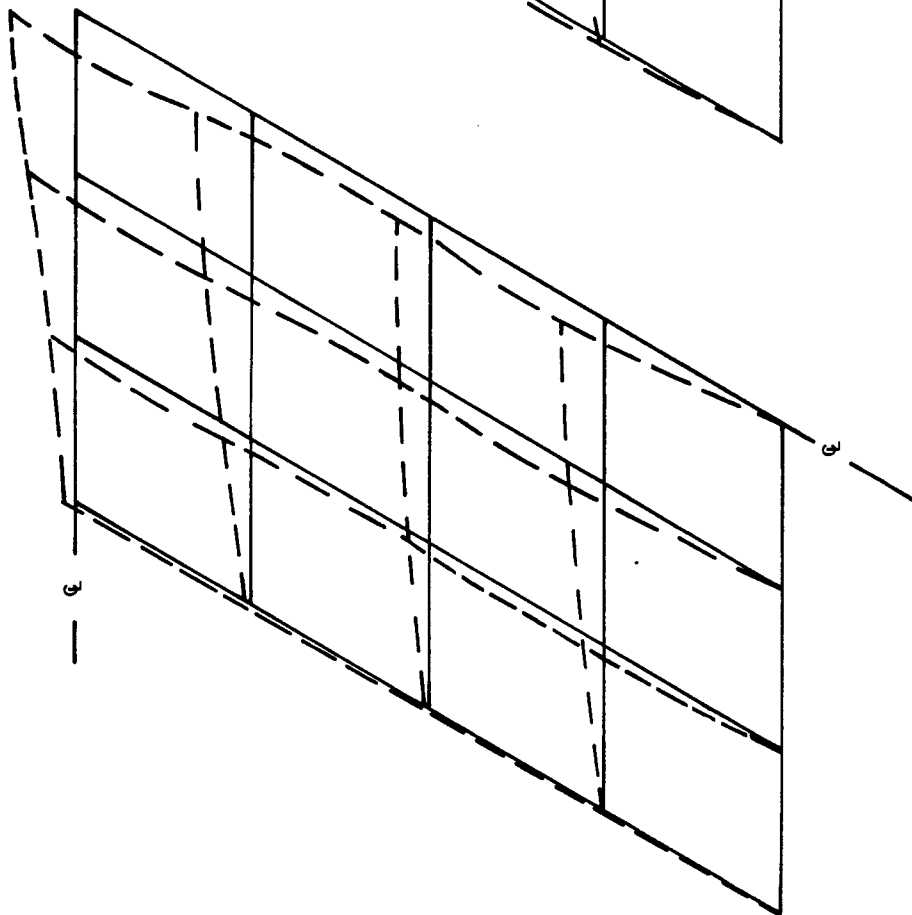
FIGURE 38 ACOUSTIC ENVIRONMENT

The canted heatshield is completely enclosed by the basic leading edge structure and hence is isolated from the external acoustic field. On this basis, the internal acoustic levels should be significantly attenuated relative to the external field, typically on the order of 20 to 30 db. These considerations indicate that the critical environment for the heatshield should be the random vibration environment and hence this environment was the only one considered in detail in the design of the heatshield.

The baseline heatshield design configuration is defined in Figure 6. This configuration was mathematically modeled by the finite element technique. Forty nodes were used to describe one-quarter of the panel, twenty on the basic polyimide fiberglass panel and twenty additional nodes located immediately above the panel nodes at the centerline of the Dynaquartz insulation on the front side. The polyimide panel and the Dynaquartz insulation were modeled using orthotropic plate bending elements. The stiffeners were represented by general beam elements to include the effect of the beam elastic axes being offset from the centerline of the polyimide panel. The strain isolator was modeled by a rectangular solid element whose formulation assumes a linear variation in displacement between the eight nodes bounding the element.

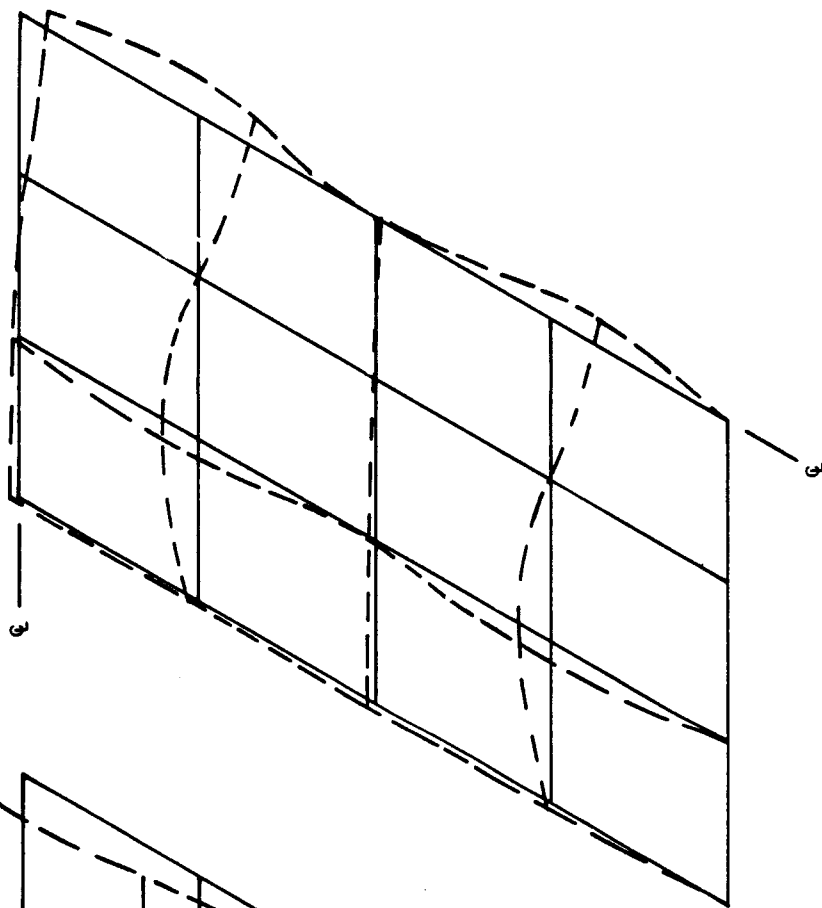
The random vibration response analysis was conducted using the first ten modes of the heatshield. Since the first two modes are the primary contributors to the induced stresses, these modes are also shown graphically in Figures 39 and 40 in terms of the displacements of the basic polyimide panel. In the response analysis, a modal equivalent damping factor of 0.02 was used for each of the modes to insure a conservative estimate of the response.

A large number of variations in the major heatshield design parameters were considered in the response analyses in an attempt to arrive at a viable design. These parameter studies showed that the number of insulation tiles and the thickness of the strain isolator were the controlling variables in defining the critical stress in the insulation weak (thickness) direction. The influence of these two parameters is shown in Figure 41



ONE-QUARTER OF PANEL SHOWN

FIGURE 39 FIRST HEATSHIELD MODE SHAPE
 $f = 144 \text{ HZ}$



ONE-QUARTER OF PANEL SHOWN

FIGURE 40 SECOND HEATSHIELD MODE SHAPE
 $f = 290 \text{ HZ}$

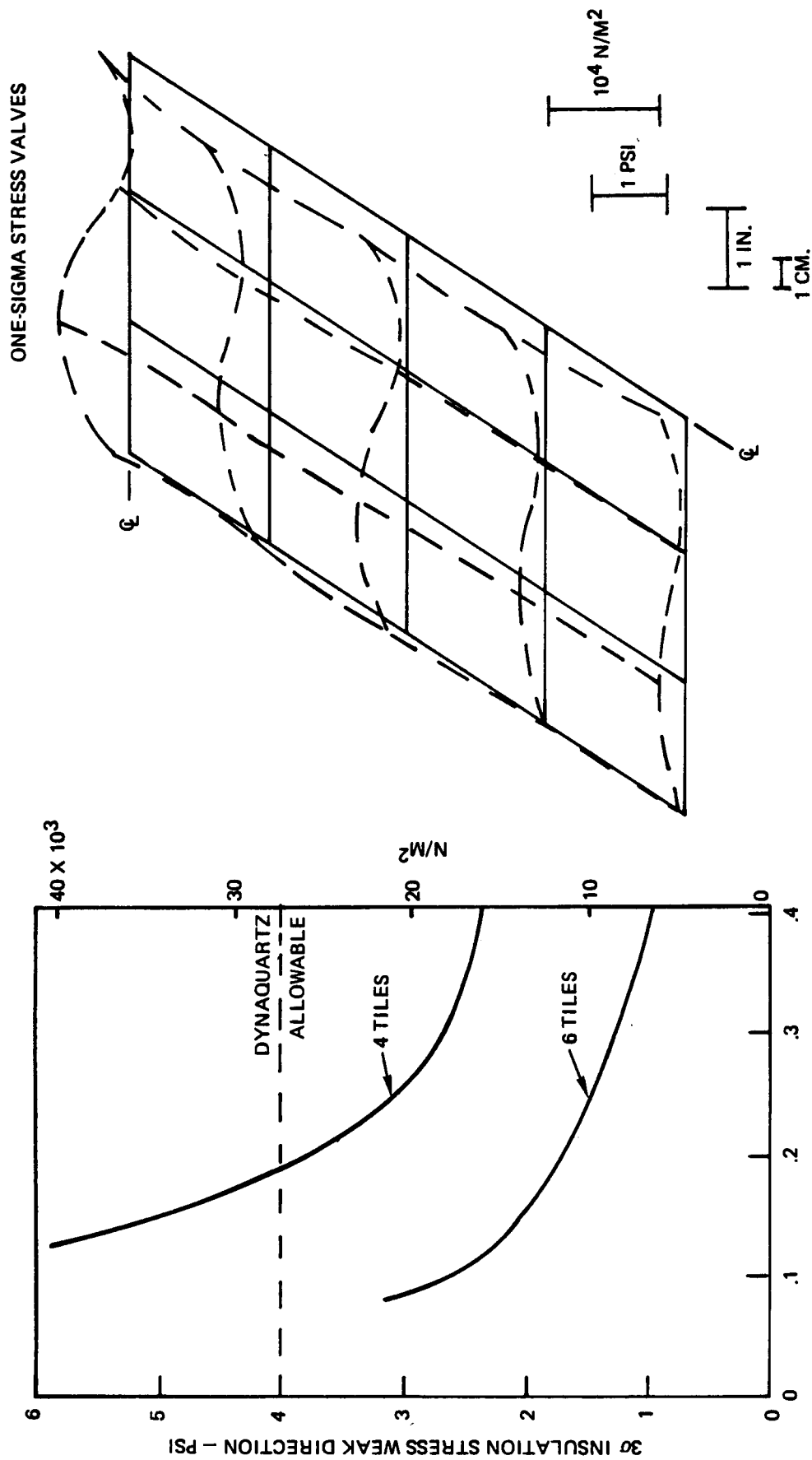


FIGURE 41 EFFECTS OF ISOLATOR THICKNESS AND NO. OF TILES ON INSULATION PEAK STRESS - CANTED HEATSHIELD

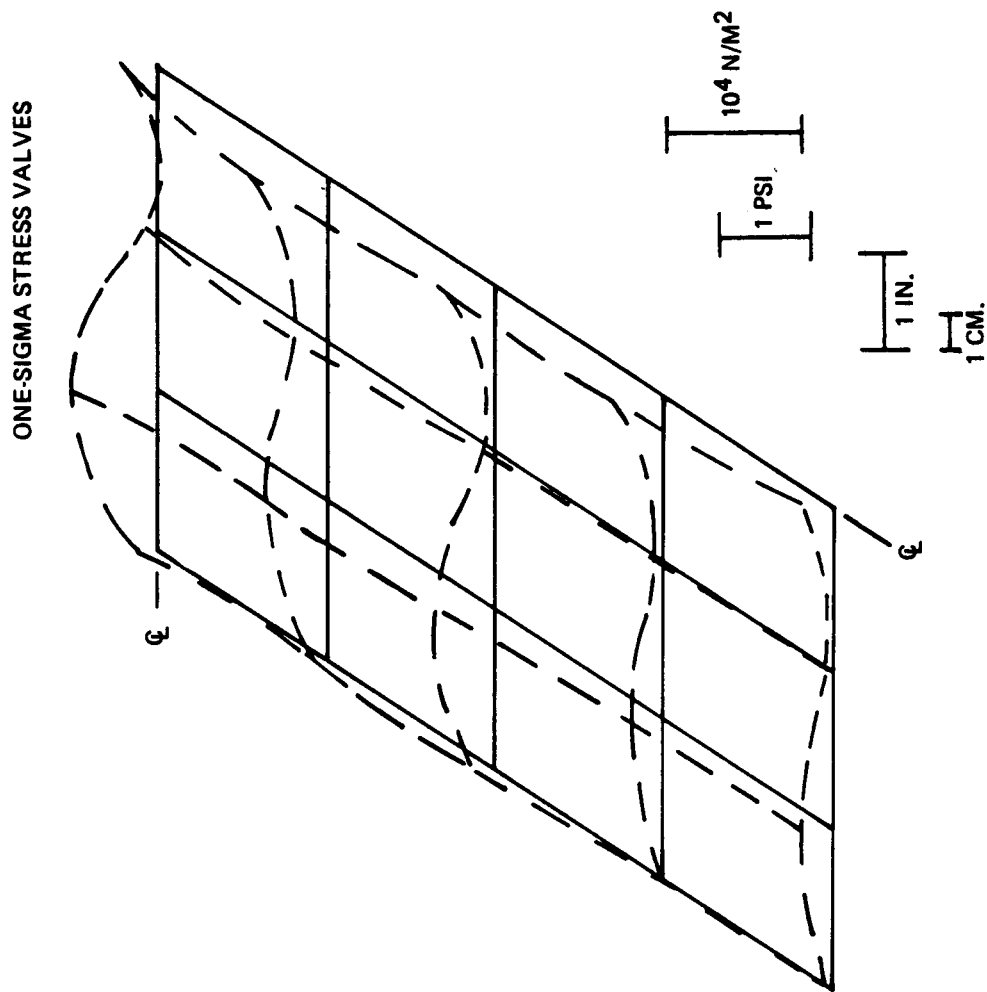


FIGURE 42 INSULATION STRESS DISTRIBUTION - CANTED HEATSHIELD - WEAK DIRECTION

for a 4-tile and a 6-tile (front side) heatshield configuration. On the basis of these results, the 4-tile configuration with an isolator thickness of 0.20 inches was chosen as the final design configuration, based on the static allowable for Dynaquartz and a 3-sigma stress level.

The calculated distribution of RMS stresses in the insulation critical weak direction is shown in Figure 42 for the final design configuration. As can be seen, the maximum stress occurs in the center of the panel near the edge of a tile. The stress level at all other points in the tile are significantly below this level. Other elements of the assembly (panel and stiffeners) are not critical.

The upper access panel, reference Figure 2, is directly exposed to the external acoustic environment. Due to this fact, the acoustic environment for this panel is more critical than the random vibration environment and, hence, was the only one considered in the design.

For purposes of analysis, the component was assumed to consist of a 16 x 15 inch titanium panel with a thickness of 0.063 inch and an 0.20 inch thickness of strain isolator supporting four tiles of Dynaquartz insulation varying in thickness from 1.30 inches at the forward edge to 0.70 inch at the aft edge. In addition, 0.63 inch thick titanium stiffeners were considered to support the two edges of the panel. These stiffeners varied in depth from a minimum of 1.0 inch to a maximum of 1.70 inches.

A 25-node finite element model of the panel was analyzed. The panel is symmetric about the centerline and hence only half of the panel was modeled with appropriate symmetry constraints along this centerline. The element types used in the model and the method of representing the strain isolator and insulation tiles were identical to that used in modeling the canted heatshield. The acoustic response analysis was conducted using the first ten modes of the access panel, and modal equivalent damping factors of 0.02 were assumed in the analysis.

The calculated distribution of RMS stresses in the insulation weak direction is illustrated in Figure 43. As can be seen, the maximum

ONE-SIGMA STRESS VALUES

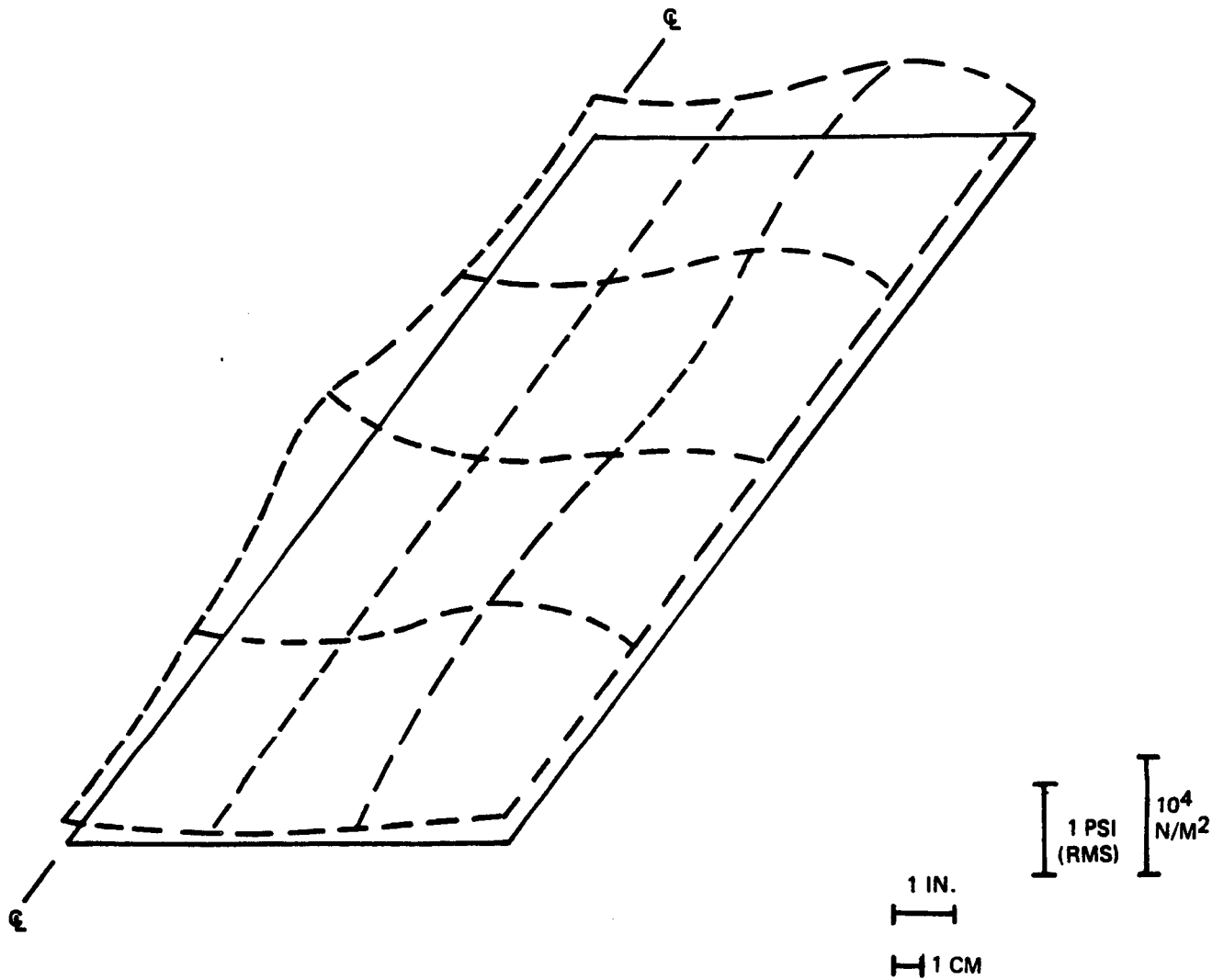


FIGURE 43 UPPER ACCESS PANEL DISTRIBUTION OF STRESSES IN DYNAQUARTZ (WEAK DIRECTION)

stress occurs in the center of the panel along the edge of a tile. The 3-sigma value of the maximum Dynaquartz stress is 3.45 psi and compares with an allowable of 4 psi used for design. Stress levels in the titanium were low and insignificant.

Due to its internal location and small frontal area, the lower support lug and the insulation surrounding it are shielded from the acoustic field and are critical relative to the random vibration environment. On this basis, only this environment was considered in the lug response analysis. The design is shown in Figure 6. Insulation material is attached to the titanium bracket through a 0.10 inch thickness of strain isolator.

A simple, one-mode analysis was performed to determine the RMS displacement response of the lug to the design random vibration environment. This displacement was then used to calculate the stresses induced in the insulation through the strain isolator. The insulation support bracket was approximated by a simple, straight beam whose bending rigidity was adjusted to account for the tapered cross sections. The frequency of the first mode was calculated to 470 Hertz.

Using the criteria of a 32 g-rms peak response in this mode, the resulting deflection was determined to be 0.0014 inch (RMS), which gives a resultant stress level in the insulation material of 0.85 PSI (RMS). The 3 stress is then 2.55 psi, which is well below the weak direction 4 psi allowable for 10 lb/ft³ Dynaquartz. Ultimately, the Dynaquartz density was raised to 15 lb/ft³. While the increased mass increased stress level proportionately, the allowable strength rose to the 15 psi range, thereby creating a net gain in margin of safety.

The above analyses for the canted heatshield, upper panel, and lower lug insulation were based on the assumption that the critical condition would result from static failure of the insulation in the weak direction (i. e., a delamination) and allowable stress was compared against 3-sigma (99.7% probability of non-exceedence) computed stress levels. A fatigue analysis could not be performed, since fatigue data for the material was not available nor was it within the scope of the program to determine for this interim

Dynaquartz material. However, on the basis of the test conducted on a heatshield component in Task 2, it appears that fatigue will be the dominant failure mode. It remains to be seen how the Dynaquartz will respond in acoustic test of the delivered leading edge assemblies.

RPP Component Acoustic Test - VSD conducted an acoustic test on the wing tip panel, fabricated in Phase II (reference (2)), to determine coating adherence, intercostal bond adherence, and coating integrity at attachment holes. The specimen, which had previously been subjected to 2.7 hours of plasma arc testing prior to 163 db OA acoustic noise exposure, suffered no failures or coating degradation. However, the small component size and means of support did not produce representative loads at the attachment holes so that further testing was indicated.

One of the leading edges fabricated in Phase III (S/N #2 - Task 12) was selected for additional acoustic testing. The primary objective of this test was to determine the structure integrity of the lug support holes under the action of dynamic loads. A secondary objective was to verify general integrity of a large panel in the acoustic field. The leading edge panel was mounted in the VSD progressive wave acoustic chamber in such a way that the noise was applied to the exterior surface, as in the flight case, while back and sides were insulated to prevent direct introduction of acoustic pressure into the leading edge cavity. Assembly on the support fixture and installation in the test facility are illustrated in Figures 44 and 45, respectively. Control microphones are seen hanging near the leading edge.

In the first test, which was applied for a total of 50 minutes to simulate 100 missions at the 163 db OA level, the support holes were damaged. Enlargement of the chamfered holes was observed and minor chipping, not exposing bare RPP, was in evidence on the fixed side of the leading edge. A countersunk hole is shown in Figure 46 after test to indicate the type of damage. The countersunk holes are located on the left side of the leading edge (looking forward) and are free to float to accommodate thermal expansion (reference Figures 1 and 4). The countersunk holes enlarged during test from an initial diameter of 0.60 inch to a final

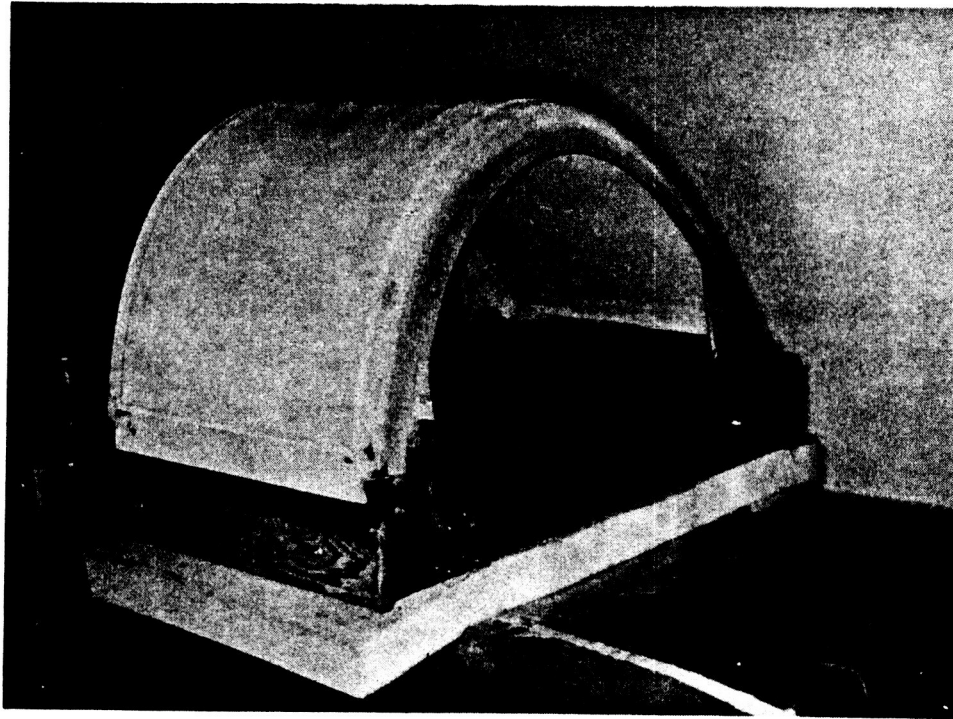


FIGURE 44 ACOUSTIC TEST LEADING EDGE AND TEST FIXTURE

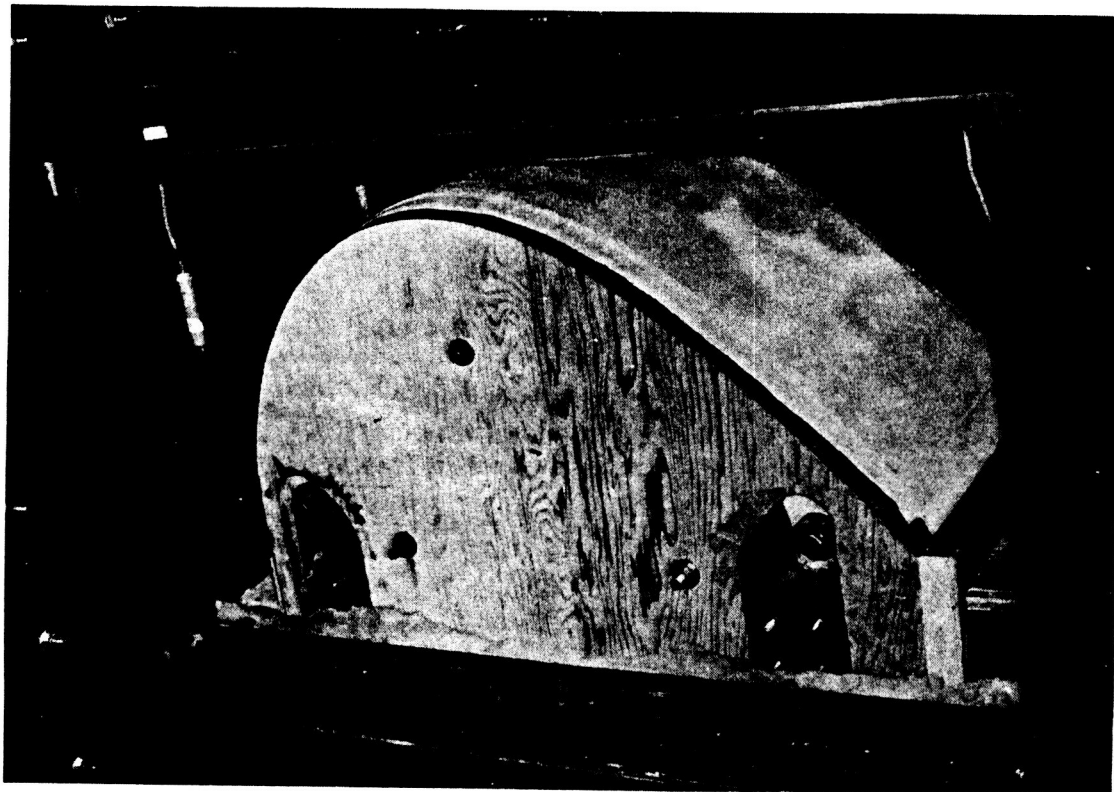
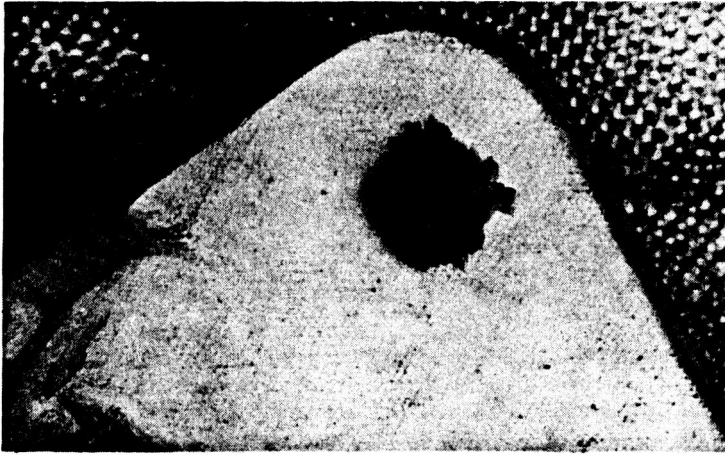


FIGURE 45 ACOUSTIC TEST LEADING EDGE INSTALLED IN PROGRESSIVE WAVE FACILITY

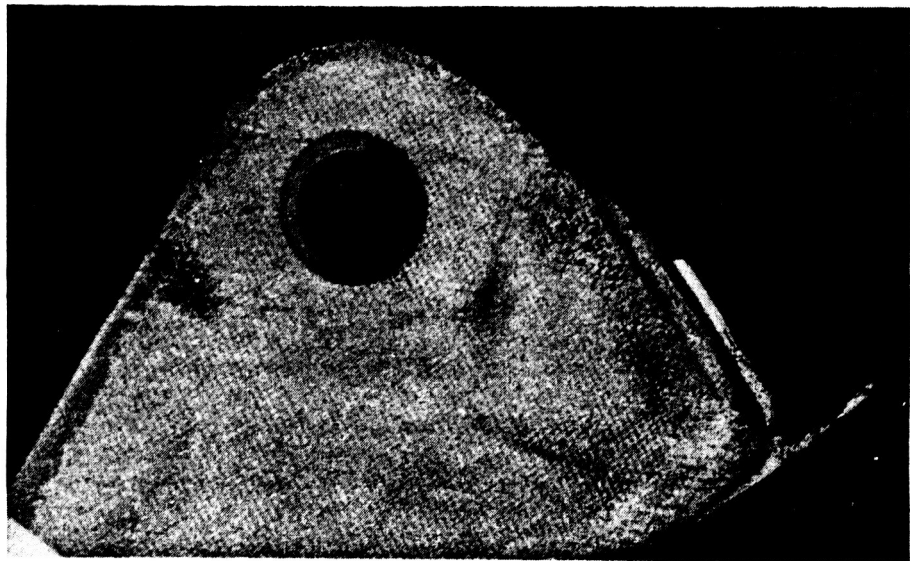
size of roughly 0.75 inch. In the process significant chipping was encountered as shown by Figure 46. Apparently, local dynamic loads were an order of magnitude higher than static loads to cause the failure. On the fixed side of the leading edge, the washers anchoring the part against side movement wore away a portion of the coating to a depth of about 10-15 mils for the 100-mission test. It is significant to note, however, that even with the severe pounding that must have been experienced at each lug, only local failure was incurred and general support lug integrity remained. No other damage to the leading edge was evident.

A successful retest was conducted with beefed-up lug holes. Thicker coated RPP lug sections were bonded and bolted onto the leading edge (Figure 47). A thickness of 0.5 inch was used for the upper lugs and 0.4 inch thick material was used for the lower. Edge radii of 0.09 inch upper and 0.06 inch lower were employed to "soften" the coated edges of the holes in an attempt to reduce the tendency for chipping. This proved effective. As an alternate to having the RPP interface directly with the attachment bolt and washers and to attenuate dynamic loads on the RPP, a separate bushing was installed in the holes on one side of the leading edge. The bushing, which was sprung into place, was split along its length to provide a gap for thermal expansion between the RPP hole and the metal bolt. Retention of the bushing was accomplished by simply bending the castled ends to a flush position on the lug. This is shown in Figure 48.

Another 50 minutes of testing at 163 db OA on the reworked assembly produced no failures, no coating chipping, and no other types of damage. NDE examination by x-ray and ultrasonic test showed no defective areas. It was concluded that with thickened lug regions the leading edge support concept is workable with or without bushings; and the bushed hole design and approach is practical and offers another level of conservatism in the design. It is also important to note that in 100-minutes of testing the leading edge skins, ribs, spars, and bonded trailing edge T-seals remained intact with no evidence of failure.



A. INNER SURFACE



B. OUTER SURFACE

FIGURE 46 HOLE DAMAGE AFTER ACOUSTIC TEST – COUNTERSUNK “FLOATING” SIDE

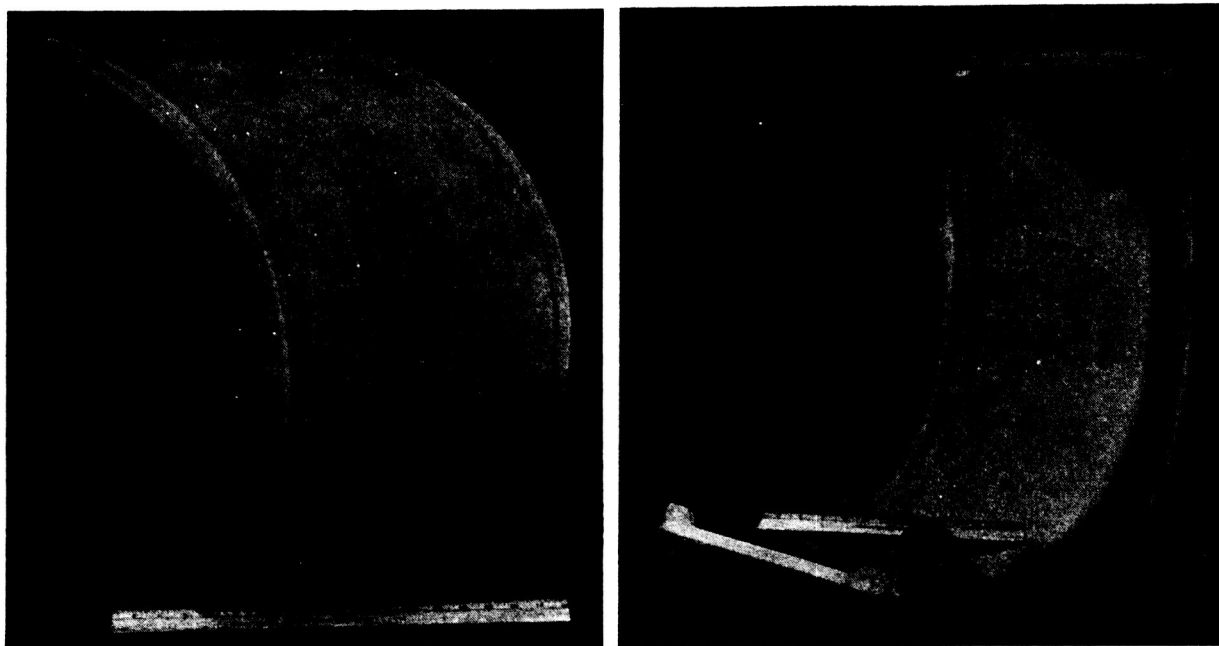


FIGURE 47 ACOUSTIC TEST LEADING EDGE SUPPORT LUG BEEF-UP

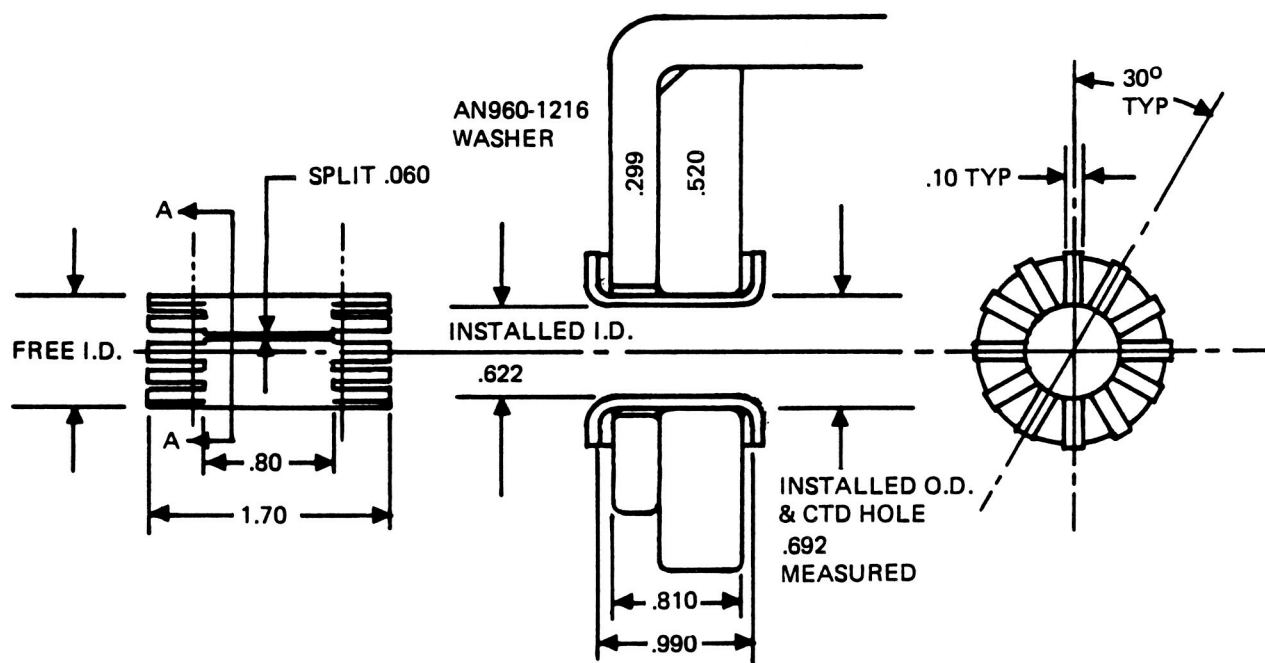


FIGURE 48 BUSHING DETAILS ACOUSTIC TEST LEADING EDGE

1.1.2 FABRICATION

This section of the report describes the efforts involved in fabricating the failsafe leading edge assemblies, discusses approaches and rationale employed, and indicates areas for possible improvement.

In the Phase II program (Reference 2), the ability to fabricate full-scale RPP leading edges of satisfactory quality was demonstrated. These were, however, limited to 12 and 14 ply layups, except in localized lug regions where a 17-ply buildup was used. Phase III presented a greater challenge, however, in that the leading edge was built up to 34 plies in the stagnation region, 20 plies at the windward trailing edge, 16 plies at the leeward trailing edge and 23 plies in the lug regions. This presented a more difficult task of layup, debulking, and pyrolyzation processing to assure sound structure.

In addition the Phase III assemblies included titanium support structure, inconel and polyimide fiberglass support brackets, and dyna-quartz insulation. The fabrication of each of these elements of the leading edge assembly are discussed in sequence.

1.1.2.1 RPP Fabrication - Processing of RPP

Processing of RPP follows the steps illustrated in Figure 49. This process shown represents refinements developed in Phase III to permit fabrication of thick RPP laminates without danger of delamination. Significant improvement from the previous (Phase II) baseline process results from separating post cure from the pyrolysis cycle and post curing in slow stepwise temperature increments to avoid generation of excessive internal gas pressure that would cause delamination. The gentle post cure is employed after initial cure and after each reimpregnation. This proved highly effective. Development of the process is covered under Section 1.14. Each step in Figure 49 is self-explanatory and is not covered in detail.

The entire fabrication process in Phase III from layup through coating was handled by the Manufacturing department with support from Engineering as required for indoctrination and troubleshooting. This was

to demonstrate that RPP fabrication was not limited to the laboratory, and to reveal possible fabrication problems with techniques or equipment operation that would require resolution for production.

Layup Tool - One of the constraints of the Phase III program was that the external configuration of the part be identical to the Phase II configuration so that existing tooling could be employed. However, as part of in-house development, an alternate approach was also employed which utilized plastic tooling. The first deliverable leading edge was layed up on the Phase II layup tool, but the next two units were layed up on plastic tooling, Figure 50, which lends itself to reproducible parts and is therefore applicable to production hardware.

The plastic tooling approach utilizes a fiberglass mold layed up on a male die, which in production would be a part of the master model of the leading edge. This should be a less expensive approach for variable contour parts, and was proved to be an acceptable approach for Phase III.

Fiberglass Break-in Part - It is standard procedure to lay up a fiberglass part as a final check of the layup mold for assurance of satisfactory part fabrication and ability to remove the part from the mold without damage. The fiberglass part proved the acceptability of the tool. Another aspect of this particular layup was that it was intended to use silicone molds to aid in the debulking of rib-skin corners and particularly rib/spar/skin corners. The fiberglass part, at its various stages of buildup, provided the mold for fabrication of a series of silicone debulking tools. These tools were then used in the fabrication of the trial leading edge, and with modification were used for all leading edges.

Trial Leading Edge - A trial RPP leading edge was fabricated to develop the techniques for laying up a 34-ply leading edge and to verify debulking and curing operations on such an item. The unit was fabricated from preliminary design information, and although final thickness variations were changed, the article was fully representative of the problems and fabrication techniques of deliverable assemblies. This trial part was fabricated as a VSD in-house effort and was not a deliverable item.

LAYUP AND CURE CYCLE

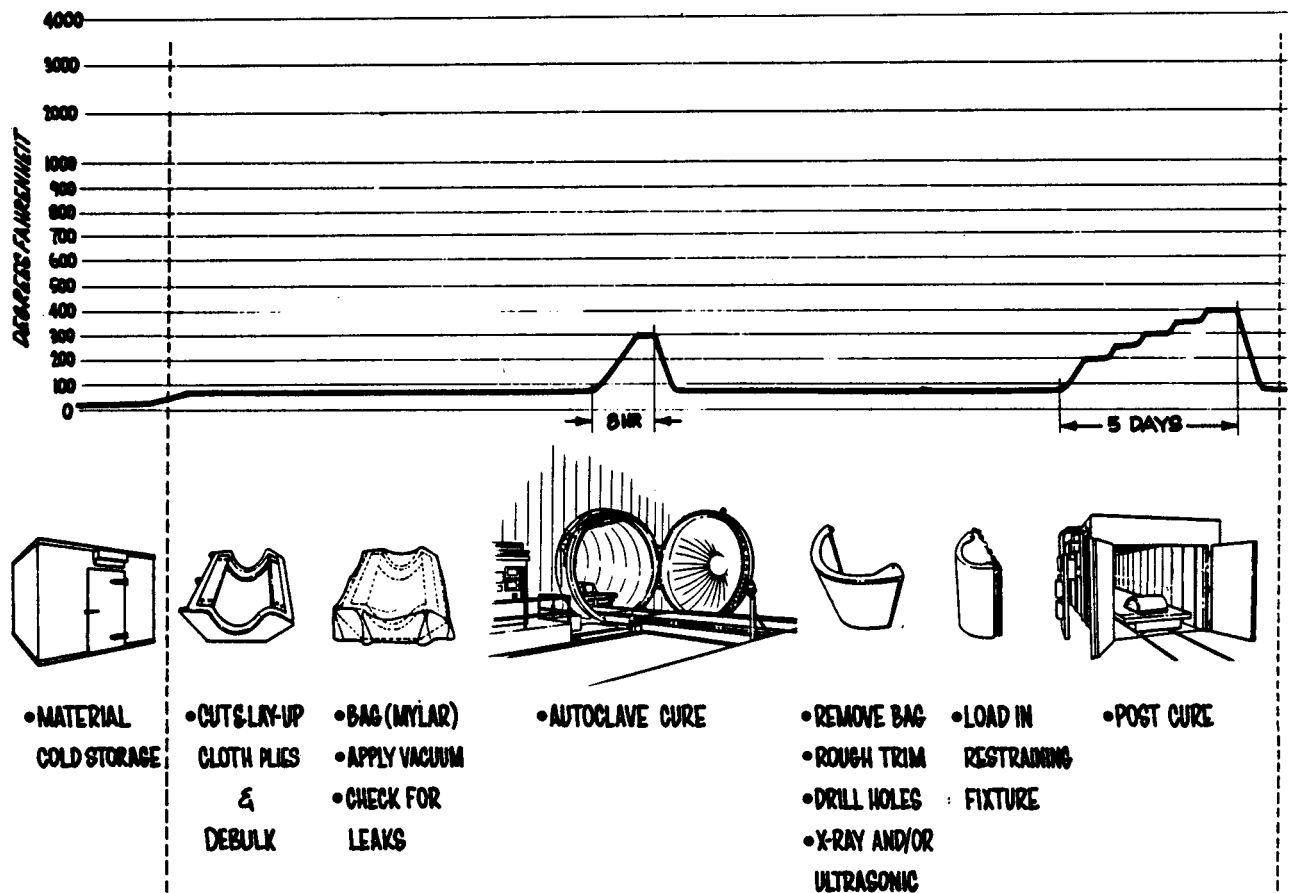


FIGURE 49 PROCESS SEQUENCE FOR COATED RPP

PYROLYSIS & IMPREGNATION CYCLES **COATING CYCLE**

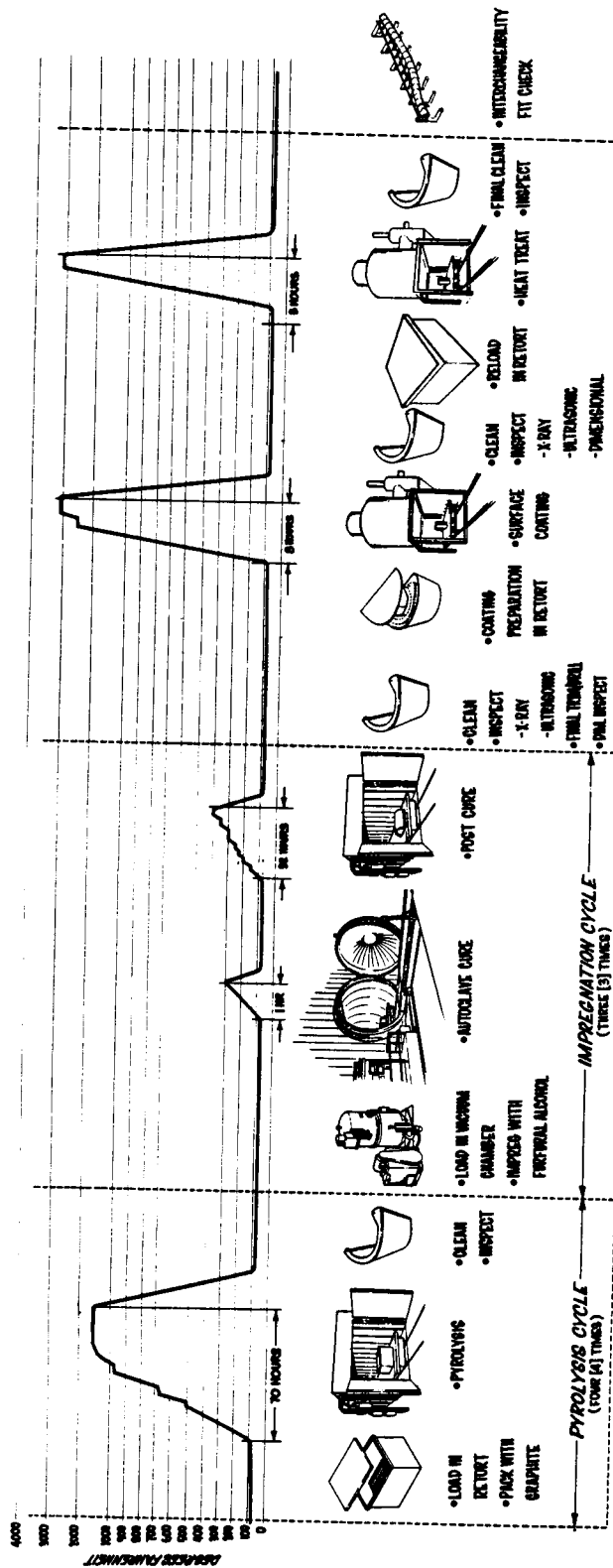
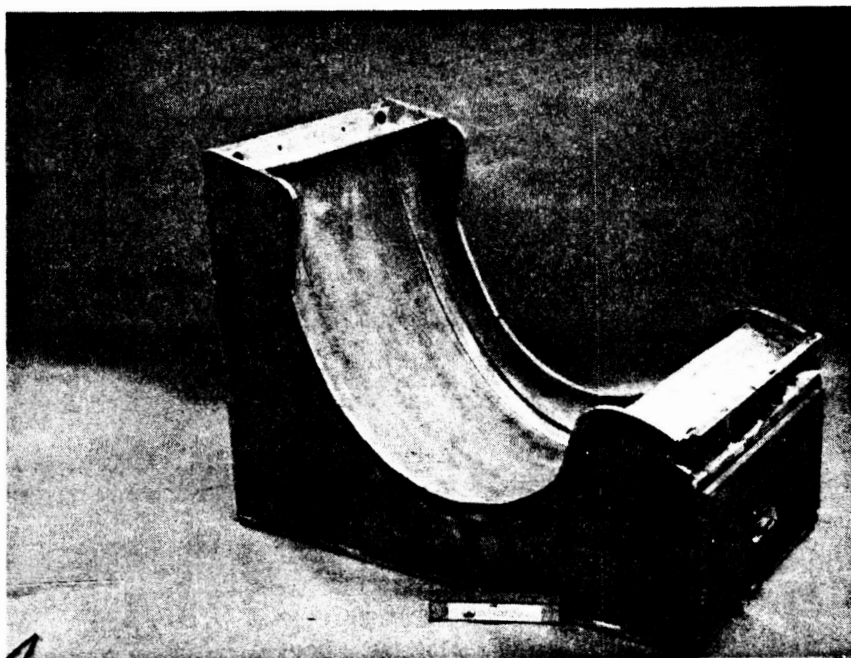


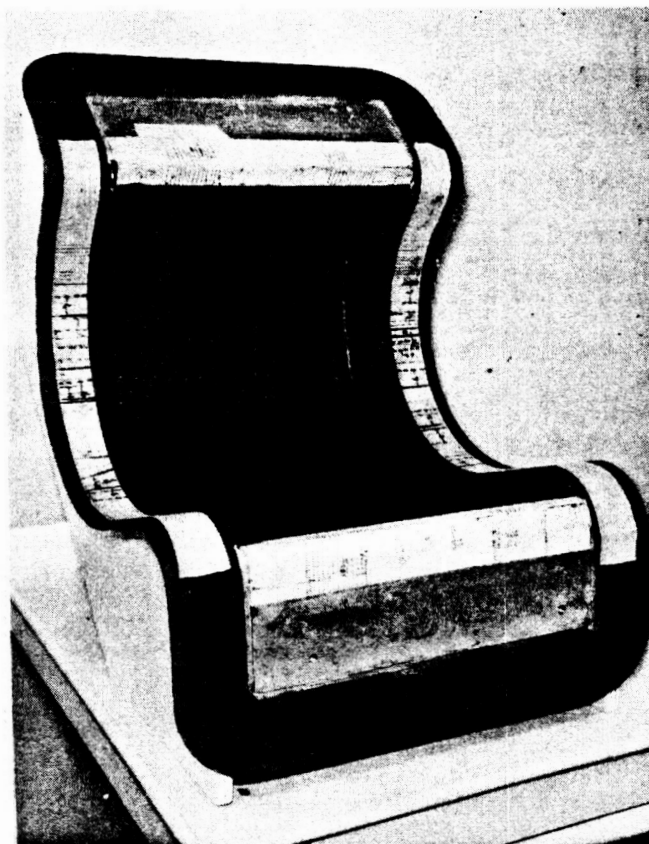
FIGURE 49 (CONTINUED)

78a

78b



ALUMINUM MOLD FOR N-1 LEADING EDGE



PLASTIC MOLD FOR N-2 AND N-3 LEADING EDGES

FIGURE 50 LAYUP MOLDS

The layup consisted of an initial eight full layers of cloth, 18 intermediate layers with various trim lengths, and eight full closeout layers. Debulking was performed at various stages of the layup process using the silicone molds and autoclave pressure debulking. Removal of excess resin during debulking was accomplished with canvas or fiberglass cloth. In general the appearance was good and the part was sound. These results and the lessons learned provided confidence for proceeding into the fabrication of the deliverable hardware assemblies.

Of particular importance was the solution of a material handling difficulty experienced when low humidity conditions caused a dry "boardy" condition of the pre-preg material. Tests proved that an increase in tack and drape occurred as humidity was increased. An acceptable level of tack and drape occurs after exposure of the material to a relative humidity of 70 to 75% for 16 hours. A separate humidity controlled area was established and all subsequent RPP layup work was performed in this area. A humidity control requirement was incorporated into material process specification 308.

Ultimately, the trial leading edge was processed through RPP-3. During this processing it was used for x-ray technique development and as a check of RPP processing records.

Deliverable Leading Edges - The first leading edge fabricated was layed up on the Phase II aluminum mold (Figure 50) while the second and third units were layed up on the experimental plastic mold. One other leading edge, a backup unit, was layed up and cured on the plastic tool but was not processed further, because of the acceptability of the first three assemblies. The first and third leading edges were ultimately selected to be delivered with the total leading edge assembly, while the second leading edge (Task 12) was assigned to the acoustic test and to be cut up and tested under Task 13.

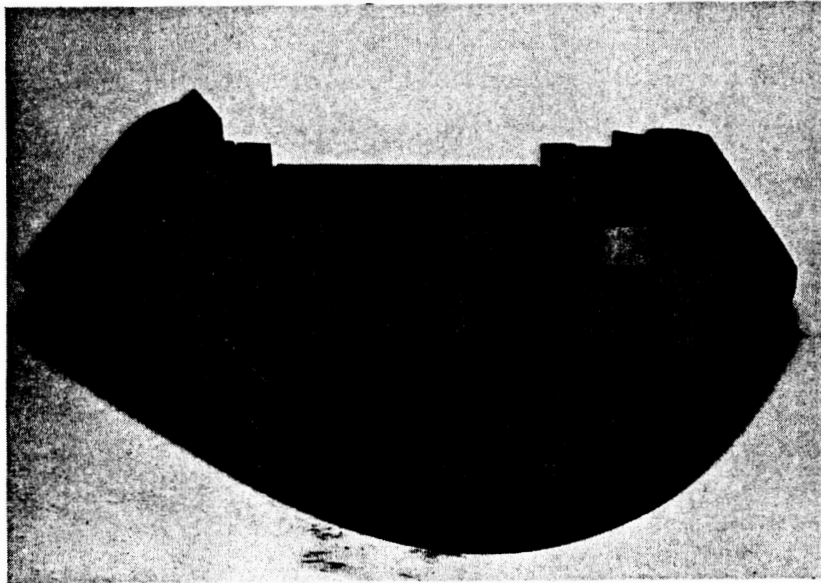
Layup of the first leading edge was rather slow due to the time involved in translating drawing details into the tailoring of plies and the need for more precise control of ply terminations than was necessary for the trial leading edge. Layup time for the following units was considerably

improved because of learning skills and the use of inspection tool aids developed during first article layup. Close attention was given to improving debulking during all layup operations. Formed metal debulking tools were used in the corners at the lug areas to aid in the debulking, where the silicone molds could not perform completely satisfactorily. Improved tooling was employed to ensure more uniform pressure during bonding of the trailing edge "T" seals. This produced bonds which were defect free.

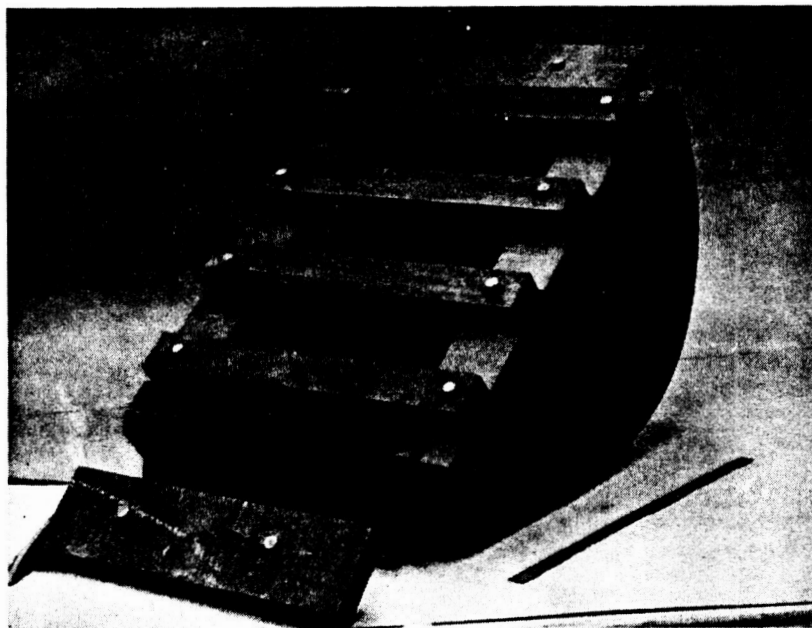
Restraint tooling variations for pyrolysis included the Phase II tooling, Reference (2), with full restraint inside and out; a modified approach, Figure 51, used on the second leading edge, which utilized only internal restraint; and a further modification for simplification of installation and removal, illustrated in Figure 52, and used on N-3 leading edge. Difficulties were experienced with each of the restraint tools and further improvement is indicated to avoid induced warpage of parts.

The various wedges used in the tooling of Figure 51, which is similar to the Phase II internal tooling, did not permit accurate control of preload on the RPP panel and resulted in spreading the lug areas and forcing a depression in the flatter regions of the panel. This was experienced on both N-1 and N-2 units. The tooling shown in Figure 52 did much to improve this situation but it produced a different problem. Not seen in the photo are a number of screws on the inner flange of the graphite that bear up against the RPP flange to provide restraint against closure. In processing the third leading edge through RPP-2, these screws were incorrectly torqued, which resulted in wavy rib flanges. This is believed correctable by designing the tooling to permit better visual and feeler gage inspection of proper application.

The maximum peak to valley waviness measured was 0.038 inch over a peak to peak length of about 4 inches. Analysis and laboratory tests showed that the flanges could be flattened without danger of failure. The flange was straightened by clamping and held during post cure and pyrolysis. This resulted in a reduction to 0.020 inch maximum waviness.

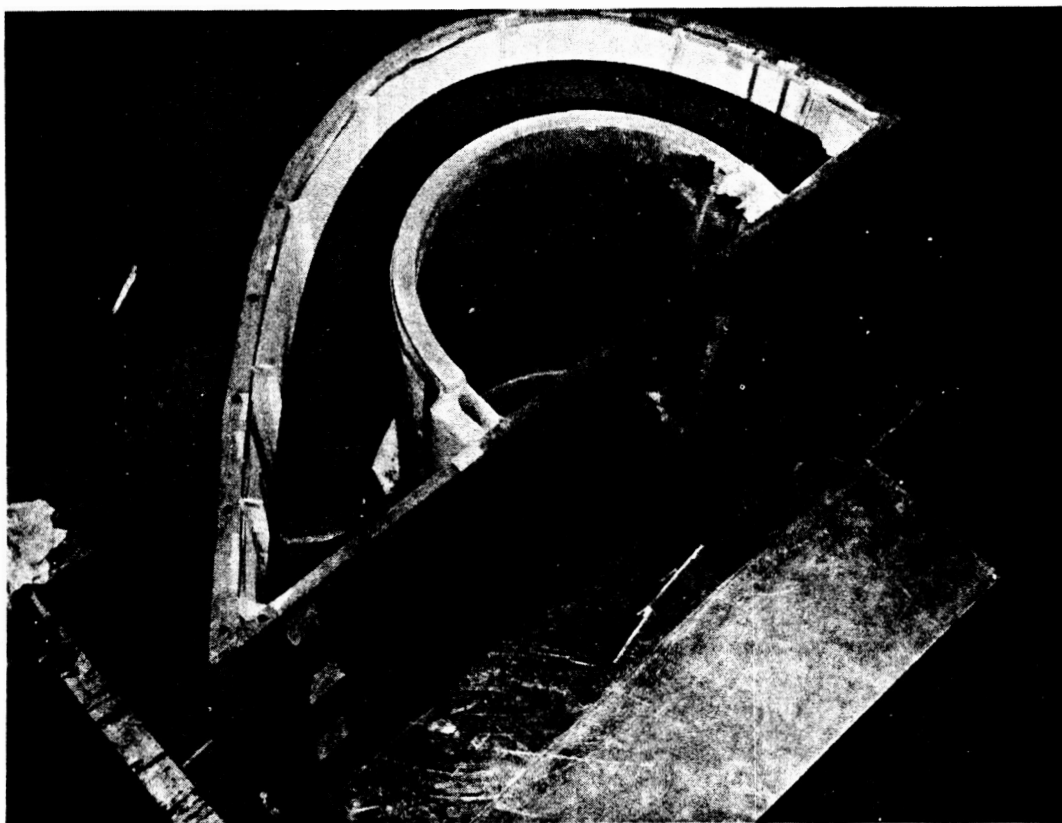


USED WITH N-2 LEADING EDGE

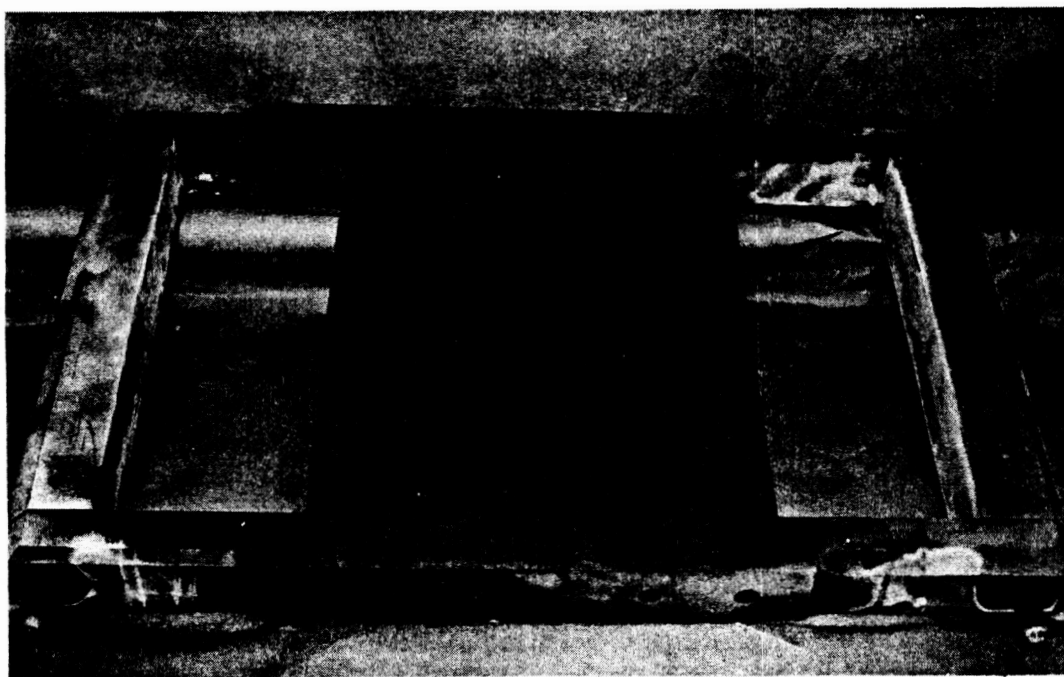


USED WITH N-3 LEADING EDGE

FIGURE 51 RESTRAINT TOOLING



RETORT FOR COATING



RESTRAINT TOOL FOR HEAT TREATING

FIGURE 52 GRAPHITE TOOLING

All of this reduction was accomplished during post cure with little change during subsequent pyrolysis. It is believed that greater reductions could be obtained in pyrolysis with different tooling. This experience indicates that, should warpage inadvertently be introduced into an RPP component during early stages of fabrication, it can subsequently be removed or substantially alleviated during final processing steps.

Leading edges were coated in the Phase II graphite retort illustrated in Figure 51. The first leading edge coating weight gain was lower than anticipated, possibly due to the thicker material, which takes longer to heat up and develops larger temperature gradients. The coating thickness (as measured by the eddy current technique) on ribs and front surface of the skin were generally equal to or greater than the 0.020 inch desired. However, thickness on the inner surface of the skin was roughly half the thickness of the front side. On the second and third leading edges steps were taken to direct more heat to the backside of the leading edge. Better thickness consistency resulted. This is discussed further in Section 1.1.3.

Coating crazing on all units was not readily apparent in the thicker or denser regions of the leading edge. However, the thin trailing edges of the trailing edge "T"s were noticeably crazed and slight delaminations in this area were evident. This could be corrected for production by thickening the "T" section. (It is noted that existing Phase II tools were employed to fabricate the non-structural "T"s, hence, a thickness increase was not incorporated.)

No separate restraint is afforded the RPP part during coating, since the retort (Figure 51) and coating powders offer sufficient restraint to avoid warpage. However, during the subsequent heat treat operation, a restraint fixture (Figure 52) was employed on units N-1 and N-3 to ensure dimensional control for the delivered leading edge assemblies. This restraint was a simple internal graphite frame which prevented panel twist or movement of the attachment points.

1.1.2.2 Leading Edge Assembly

This task included the fabrication of a two-unit leading edge assembly for NASA-JSC test. Peculiarities of the fabrication of each major component are discussed. The leading edge assemblies are shown in Figures 2-1, 2-2, and 2-3 contained in Vol. I.

Support Structure - The structural elements were fabricated from titanium, aluminum, Inconel, and steel. These are standards with the industry and presented no new or novel problems. The support structure is shown in Figure 53.

An assembly fixture was fabricated to assemble the structure and to assure interchangeability at the RPP component attachment points. Standard positioning pins were used to locate parts for drilling and riveting or bolting. The fixture is shown in Figure 54 during buildup of the support structure.

Polyimide Fiberglass Parts - Polyimide fiberglass was used for the canted heatshield structure, various insulators, and the aft end of the lower support brackets. Difficulties were encountered in two areas: (1) thicknesses varied too widely, which was corrected by machining over-thick pieces (but could also have been corrected by using matched molds), and (2) angles tended to close by as much as 3° during cure/heat treat cycles, even when restrained. In some cases this was corrected by machining and in others it was found acceptable. This could be corrected in the future by building slightly open angles in the tooling to anticipate the degree of closure measured.

The flat canted heatshield panel was fabricated using matched molds. Warpage resulted on the thin (0.09 inch thick) flat panel as expected but this was acceptable, since little force was required to return it to a flat condition.

Heatshield Assemblies - Heatshields consisted of Dynaquartz bonded to a silicone sponge, which in turn was bonded either to titanium or polyimide fiberglass. The shaping and fitting of Dynaquartz proved to be simple, once the technique was developed. Dynaquartz can be machined,

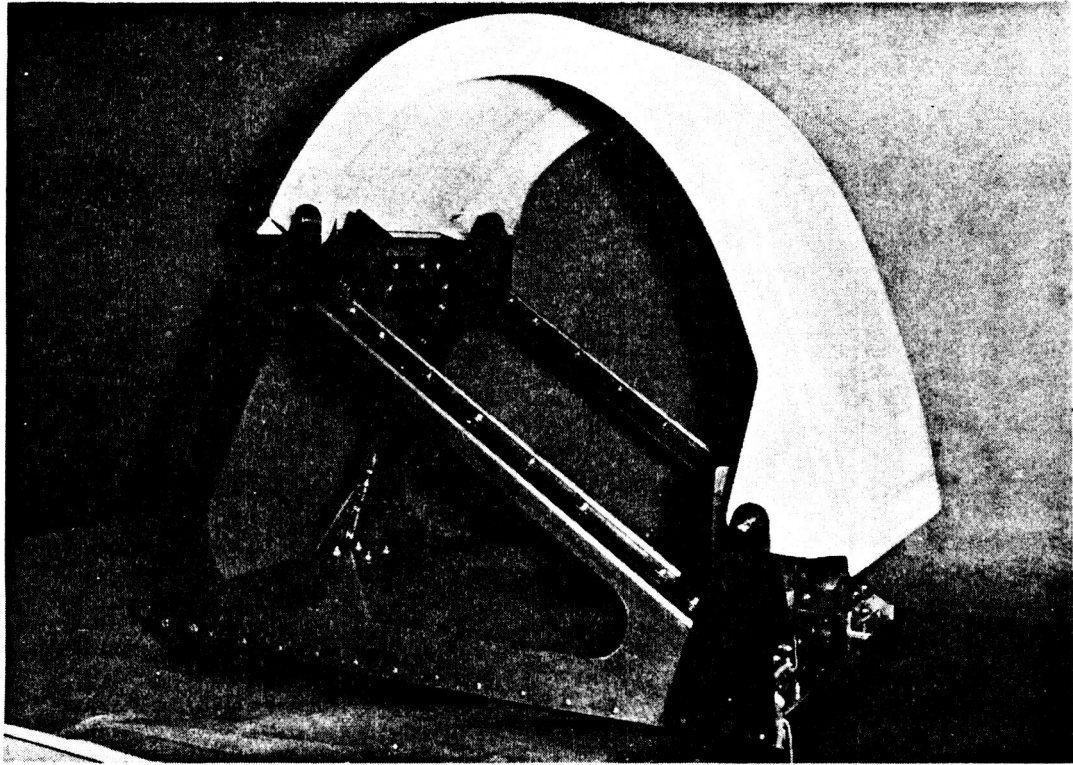


FIGURE 53 SUPPORT STRUCTURE AND RPP PAN

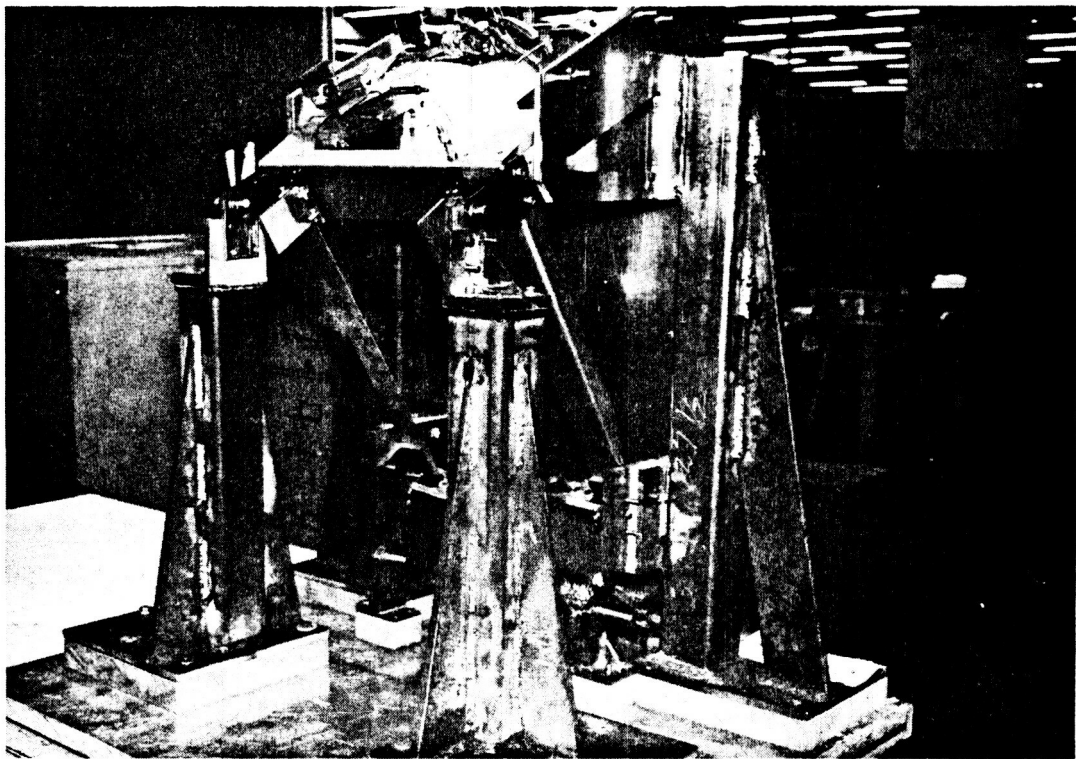


FIGURE 54 ASSEMBLY FIXTURE WITH SUPPORT STRUCTURE IN BUILD-UP STAGE

drilled, and hand carved. Slow machine speeds, and light pressure are best in the machining operations. A basic problem with the material furnished for this program was inconsistency, with random voids of varying sizes, internal delamination and hidden cracks in evidence. These features sometimes caused in-process or finished parts to be rejected after final machining. The handling of Dynaquartz required care as it is very fragile and easily subject to damage.

Because of the limited quantity of Dynaquartz details, most parts were "prefabbed" to net dimensions with selected areas left oversize for final assembly fit. This procedure worked well.

Final Assembly - Mating of structural and heatshield assemblies was conducted in an assembly fixture designed for this purpose (similar to Figure 54. In isolated cases radiation gaps between individual insulation assemblies exceeded desirable limits, but these were readily filled with Dynaflex (12 lb/ft³) insulation. This could be a feasible approach for production, although if more elaborate tooling were employed, the need for filling gaps would be diminished considerably. Overall, the assembly of the deliverable hardware went rather well and it appears that with suitable tooling, the use of rigid insulation for internal heatshields is feasible. The fabrication and assembly of the leading edge assemblies required no particular artistry, but merely careful and patient workmanship.

1.1.3 QUALITY ASSURANCE

The Quality Assurance Department participated in the fabrication of the leading edge hardware in the following major capacities:

- (1) Monitoring processing steps to ensure compliance with released Engineering instructions.
- (2) Certification that all process equipment was certified and operating properly.
- (3) Inspection of incoming raw materials.
- (4) Dimensional inspection of hardware to assure tolerance requirements were met.

- (5) Perform x-ray, ultrasonic, and eddy current NDE inspection of hardware as appropriate.

The Phase III program was conducted in a similar fashion to a production program in that quality control rigors were invoked. However, since this was a development program and tolerance control capability was not fully defined at the outset, deviations from initial goals were treated more informally between Engineering, Quality, and Manufacturing, rather than resorting to a formal Material Review Board.

Logbooks - Logbooks were established for each RPP leading edge assembly to record compliance with detailed processing requirements. Notation of compliance was provided by the appropriate inspector, and was in the form of a stamp indicating: an operation was performed and was in tolerance; by noting specific values measured; or by referencing time history recordings of processes, which are retained on file.

The logbooks contained: general operating instructions for Quality engineers and inspectors; all squawk sheets and the disposition; manufacturing operation sheets with inspection verification stamps; actual measurements taken at various processing stages, such as weights, dimensions, ply termination locations; strength data on control panels taken at various process stages; and reference to NDE records.

NDE Inspection - X-ray radiography, ultrasonic-through-transmission (C-scan), and eddy current NDE inspection techniques were employed at appropriate stages to check the integrity of the leading edge. The usefulness and application of the NDE examinations are as follows:

- (1) X-ray without an attenuator - used after autoclave cure to check for inclusions, voids, and delaminations and after coating to check for crazing and coating thickness uniformity in certain regions, such as flanges, holes and edges.
- (2) X-ray with carbon tetrachloride attenuator - applicable in the RPP-2 and RPP-3 stages to determine voids, porosity, and delaminations.

- (3) Ultrasonic - through-transmission with water couplant - determination of porosity, voids, and delaminations at the autoclave cure, RPP-2, RPP-3 and after coating stages.
- (4) Eddy current - used for coating thickness measurement over the surfaces of the part.

Standards for x-ray and ultrasonic test have been obtained to compare against response of the part. These standards were selected from panels processed in both the Phase II and Phase III programs.

No delaminations as a result of processing were found on any of the leading edges except for local edge delamination on the trailing edge "T"s. These were Phase II configured parts and relatively thin (10 ply). This situation would be improved in production by increasing the thickness of the "T"-seal. One other delamination was the result of removing a thermocouple inserted too deeply in the lower right-hand of N-1 leading edge. A hole (0.16" x 0.48" x 0.25" deep) and local ply separation was incurred but this was filled with chopped WCA cloth and R-120 resin, cured, and impregnated with furfuryl alcohol before final pyrolysis. Structural integrity to the design load levels was not believed compromised. This thermocouple was used for process control during cure. The defect incurred is not considered acceptable for a production part.

Voids were a normal occurrence in the very thick region at the corner intersection of the skin, ribs and spars. This is attributed to the reduced effectiveness of debulking in this difficult region. This is a lightly loaded area so that structural integrity is not the problem, but it represents an area requiring correction so that the region is more inspectable. Two avenues are open to improvement: (1) increase the local radius in the corner to enhance debulking, and (2) add filler material in the corner to fill the expected void. The selection of approach is a function of the local design geometry permitted.

Dimensional Control - As noted, dimensions of leading edge assemblies were measured at various stages of the process. These measurements consisted primarily of width dimensions at 38 locations around the circumference, thickness dimensions on the skin and ribs, flange waviness,

skin waviness, and coating thickness measurements on skin, ribs and spars. A detailed discussion of the findings follows.

Panel width dimensional variations, more than any other tolerance contributor, determine the joint fit and expansion gap size variation between panels after assembly. It is necessary because of in-process size variations to build allowances into the layup tool for shrinkage/expansion behavior which determines the size of the finished product. Consequently, steps were taken to characterize the size variations resulting from each operation along the manufacturing sequence and establish realistic tolerance bands so that dimensional adjustments could be made available for the fabrication of future RPP layup molds.

Three panels were completed in the Phase III program; the first was fabricated in the Phase II mold while the second and third panels were fabricated in a mold produced in the Phase III manufacturing development effort. Figure 55 presents a measurement history of the layup mold used and of the part at three of its stages along the process sequence. The figure also compares dimensional measurements of the Phase II and Phase III molds and their resulting influence on RPP panel dimensions. The Phase II mold was larger than the drawing dimension callout of $15.00 \pm \begin{smallmatrix} .00 \\ .03 \end{smallmatrix}$ (Figure 4, but the Phase III mold was fabricated close to the nominal 15.00 dimension.

Figure 55 shows that after layup, the panel shrinks until it has been carried through the final pyrolyzation stage, then enlarges during the coating process to a size larger than the layup mold and grows even larger during the final heat treatment. Note the regularity and consistency of all curves at all process stages. The figure demonstrates that, although leading edge panels number two and three were fabricated in the new Phase III mold, the dimensional variances between the part and the mold are in the same sense, of the same magnitude and reflect, with true regularity, the mold shape. Based on the width tolerance data plotted in Figure 55, conclusions may be drawn as follows:

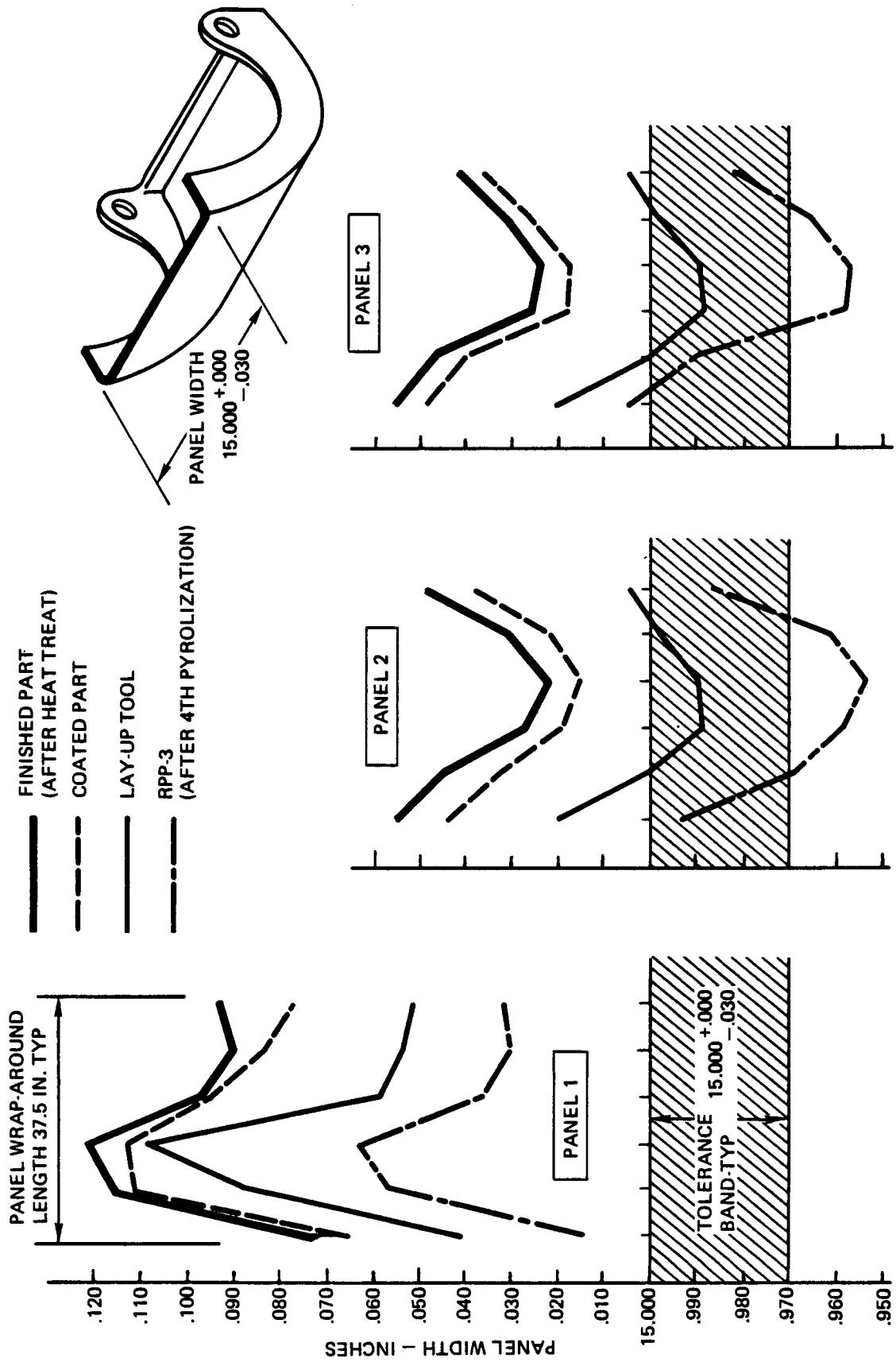


FIGURE 55 PANEL WIDTH TOLERANCE AND MEASUREMENTS

- (1) In-process shrinkage and expansion allowance may be confidently built into the initial layup mold.
- (2) The finished part shape will be identical to the mold shape.
- (3) An in-tolerance mold (i. e. , straight) will produce an in-tolerance part.
- (4) In-process size variations are known and are repeatable.

Thickness dimension allowances and tolerances for design were based on the 13-ply flat panels produced in Phase II. A single ply dimension and tolerance was defined as 0.013 ± 0.004 inch per ply on the finished part. Tolerances were believed to be accumulated in a compensating fashion so that a total thickness tolerance of ± 0.010 inches was considered realistic for the Phase II parts. It was not clear at the outset of Phase III, however, which nominal ply dimension nor which total thickness tolerance to use since the failsafe panel design was made up of various ply combinations, ranging from 16 to 34 plies. Consequently, the same 0.013 inch per ply was established as the nominal single ply dimensional allowance and the ± 0.010 inch tolerance band, carried over from Phase II, was arbitrarily used on the drawing for all thickness build-ups as an initial manufacturing goal and as a baseline for quality control measurements.

Upon completion of fabrication, measurements were made of all three panel thicknesses taken at six surface element lines described in Figure 56. Thickness measurements were plotted to highlight deviations from a nominal thickness dimension computed on the basis of a nominal 0.013 inch per ply allowance. Examination of the data in Figure 56 shows that it is unrealistic to assume an 0.013 inch per ply dimension for calculating build-up over such a large range of thicknesses making up the Phase III failsafe design. A cross-plot of the measurement data in Figure 56 defines the total thickness dimensional deviation from a nominal (based on the 0.013 in/ply) versus the number of plies in the buildup. The plot suggests a sliding scale for the "per ply" thickness allowance as a function of

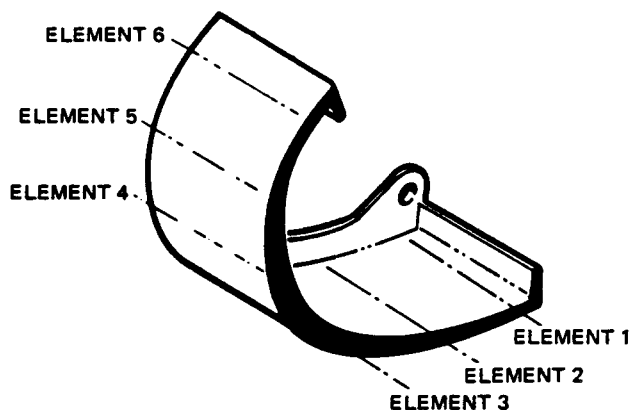
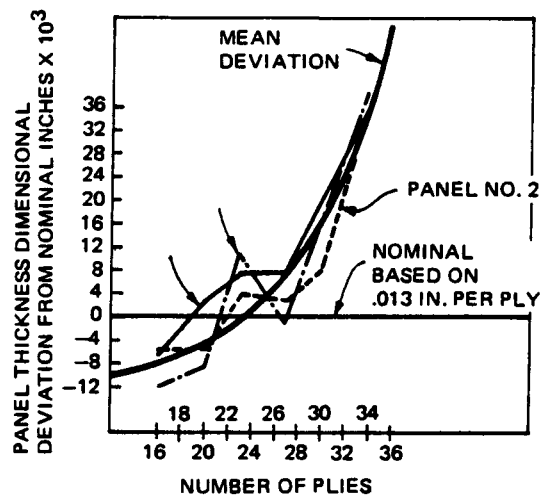
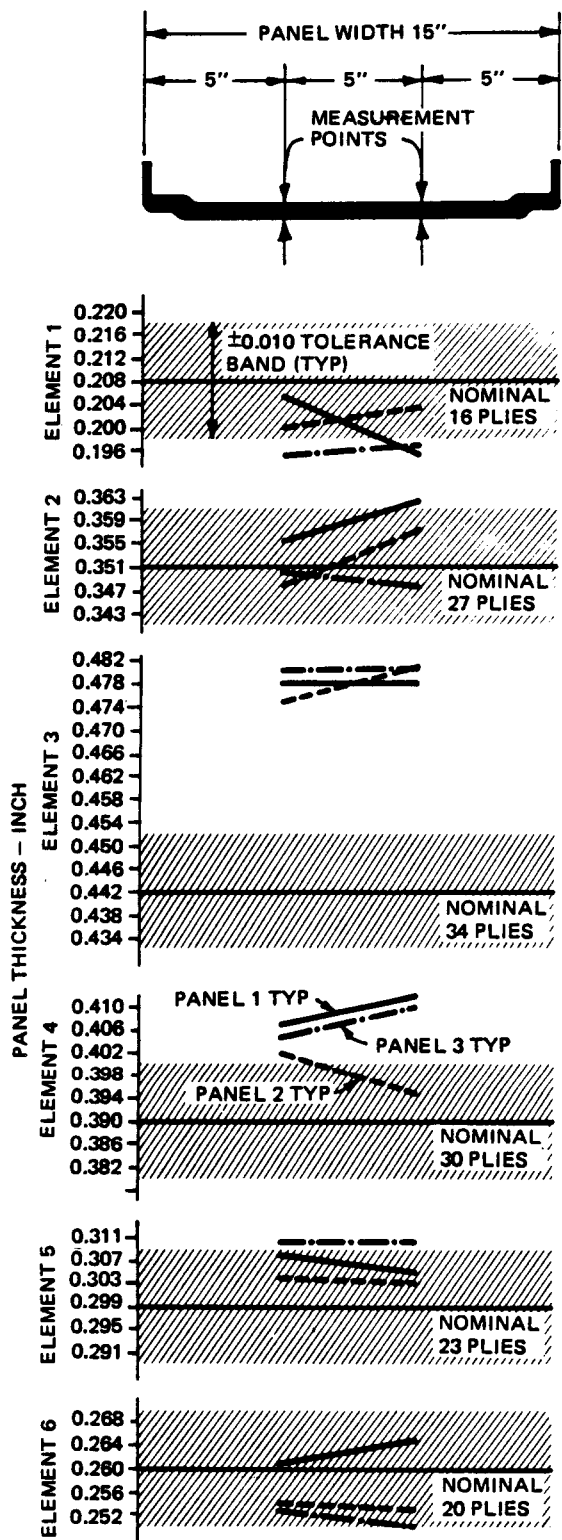


FIGURE 56 PANEL THICKNESS TOLERANCE AND MEASUREMENTS - COATED CONDITION

number of plies in the buildup. The resulting scale produces the following sample thickness dimensions:

- 0.0125 in/ply for 16 plies (minimum used on Phase III design).
- 0.0130 in/ply for 26 plies (nominal previously used).
- 0.0140 in/ply for 34 plies (maximum used on Phase III design).

With the nominal thickness thus computed, a tolerance of ± 0.020 on any thickness buildup falling within the 16-34 ply range may then be considered a realistically achievable tolerance band. This can be observed in Figure 56 where for all three panels and for all six element lines the measurement data scatter falls within a 0.020 inch band.

The need for a sliding scale thickness allowance is made necessary by the use of the pressure bag debulking and molding process, which is an economical molding technique. A fixed scale thickness allowance may be employed where the more expensive "matched mold" tooling is employed, as for T-seals or integrally stiffened panels.

The measurement data for the chordal rib and lug thicknesses are presented in Figure 57. Again, these values are plotted against the nominal thickness dimensions based on the 0.013 in/ply value and a thickness tolerance of ± 0.010 in. The data shows that the lugs are within or close to being within tolerance. The ribs are also within tolerance except for an additional ply thickness on the high side where overlap ply splices are permitted to relieve the bunching or pleating effect as laminates are draped around the leading edge curvature.

Coating thickness measurements were made on panels no. 1 and 3 (the first two panels coated in Phase III) within an accuracy of $\pm .005$ inches and a 95% confidence using a calibrated non-destructive eddy current inspection machine. A minimum coating thickness of 0.020 inches is desired for the entire inner and outer surface of all panels. Figure 58 presents a comparison of the coating measurements made on the fail-safe panels.

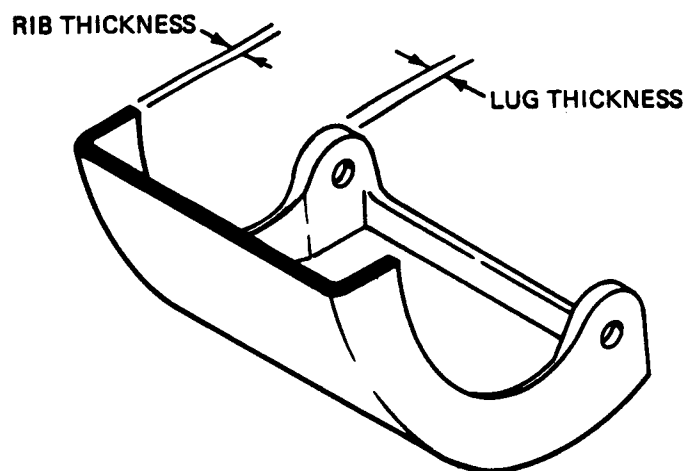
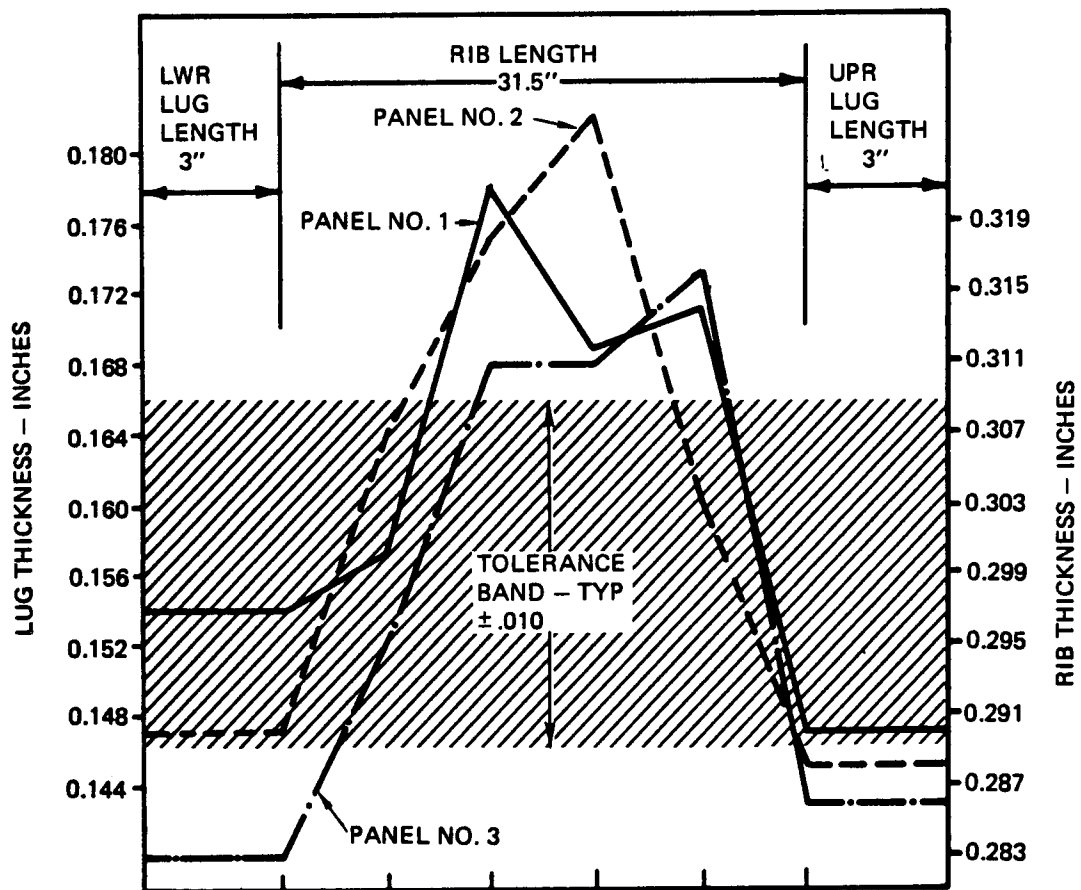


FIGURE 57 LUG AND RIB TOLERANCE AND MEASUREMENTS – COMPARISON OF L.H. RIBS OF COATED PANELS

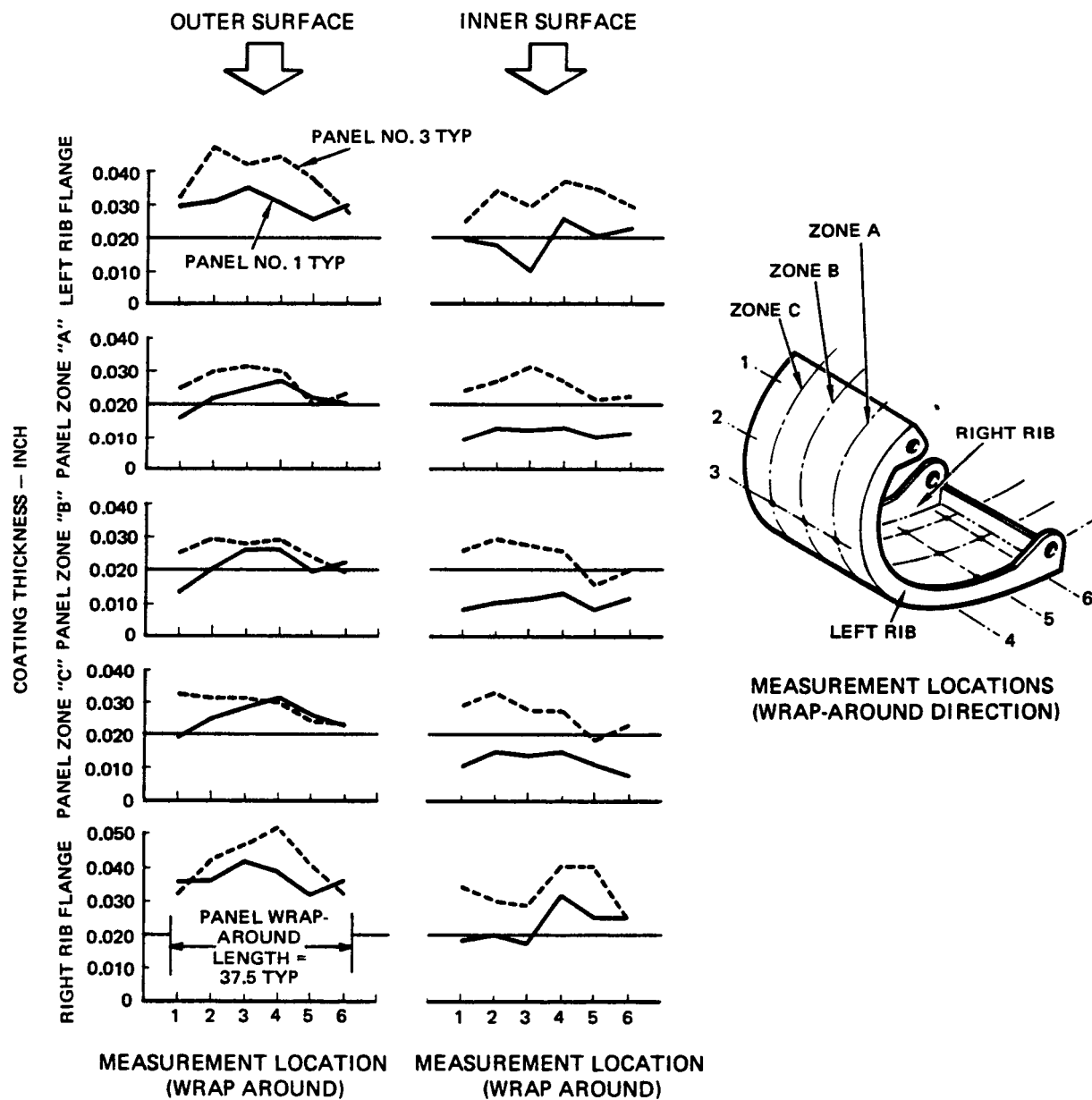


FIGURE 58 COATING THICKNESS MEASUREMENTS

Twenty-five of the sixty thickness measurements made on panel number one were below the desired 0.020 inch dimension, predominantly on the less critical inner surface, but after adjustments were made in the processing procedure, coating thickness on panel number three was produced, where only two of the 60 measurements fell below the 0.020 inch requirement. Further, because of improved packing techniques, the spread between the internal and external coating thicknesses was reduced in panel number 3. Coating thickness is primarily controlled by such parameters as the time-temperature profile, heat distribution through the packing material, and the packing material pressure against the part surface. By varying these and other parameters the desired coating thickness may be achieved and the data in Figure 58 shows excellent convergence after only one processing adjustment.

Surface straightness measurements were taken along six element lines of the cylindrical surface of each of three panels as shown in Figure 59. The measurements were made by first establishing a datum line at each of the six element locations; the datum line passes through two datum points of contact located 1.25 inches inside the left and right hand edges. Deviations of the panel surface along the element line measured from the datum line were then recorded for each location on all three panels as shown in Figure 59.

Three processing factors play a part in the straightness or waviness of a surface, viz: the restraint tooling design used in the pyrolyzation cycles; the shrinkage and expansion of the RPP material itself throughout the process; and, the relationship of the fit and grain orientation of the ATJ graphite restraint fixture with the RPP part during the heat treatment operation. The latter can be significant because of differences in the graphite coefficients of thermal expansion between the parallel and perpendicular grain orientation, which is about 50%.

The data in Figure 59 illustrates the degree of improvement that may be expected as improvements are made in the restraint tooling

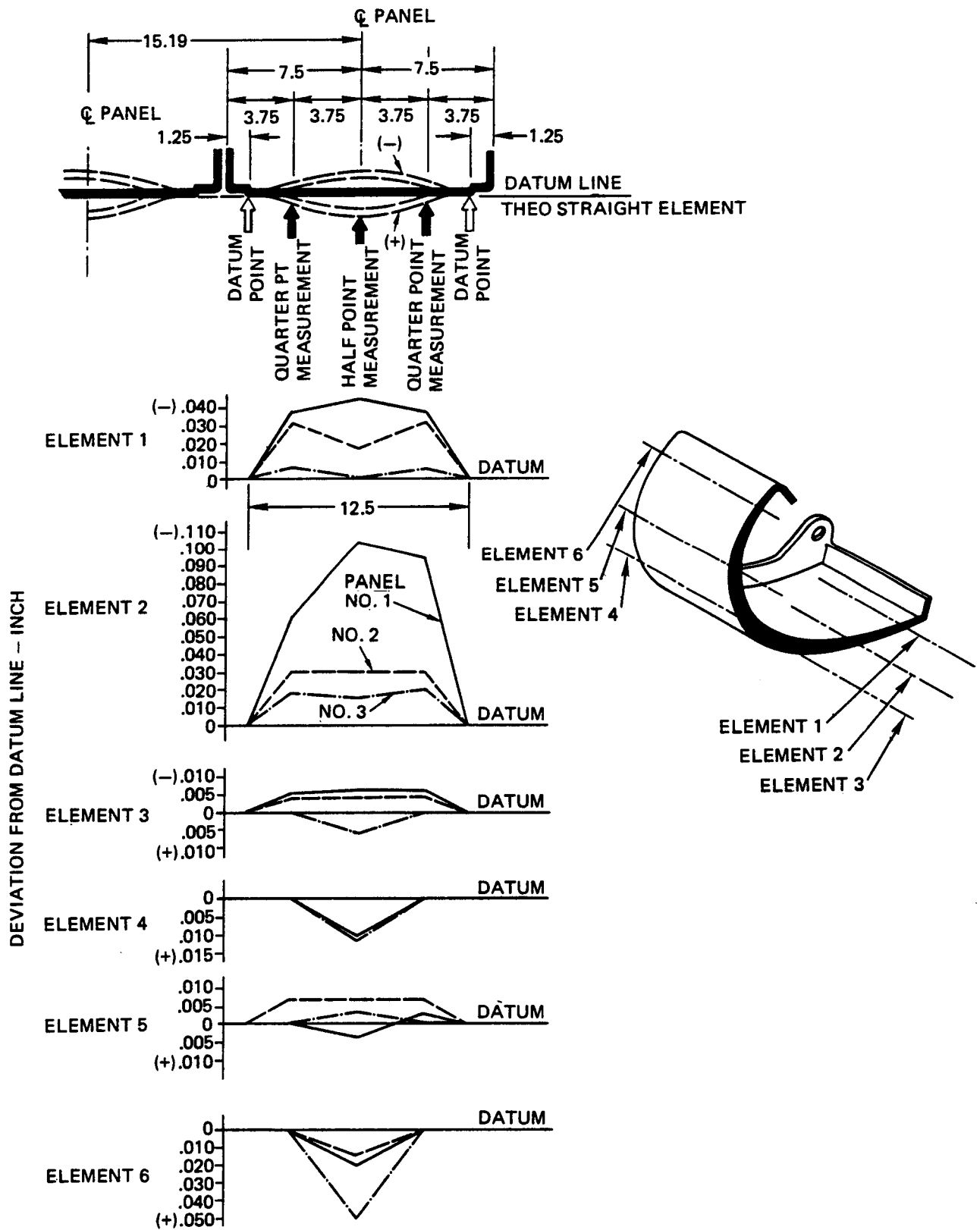


FIGURE 59 PANEL SURFACE STRAIGHTNESS MEASURED ALONG ELEMENT LINES

employed during the pyrolyzation and heat treatment process cycles (Section 1.1.2).

It is evident from the data that the greatest problem lies in the flatter regions of the panels, element lines 1, 2, and 6 of Figure 59. This data suggests that future tooling must be designed so as not to force warpage into the part from a combination of RPP shrinkage and differential expansion between RPP and graphite restraint fixtures; and, flatter regions must be restrained inside and out if closer tolerance control on bowing is required.

1.1.4 THICK LAMINATE DEVELOPMENT

In order to make a failsafe leading edge feasible, a process for fabricating thick laminates (up to 0.5 inch) had to be developed. Previous work on the leading edge concentrated on material less than 0.25 inch thick. In in-house studies it was found that delaminations were prevalent, when thicker laminates were attempted. It was necessary, therefore, to modify the process technique from the previous standard to be able to reliably fabricate thicker laminates.

At the outset of the program, it was not clear what process modifications were required to produce sound laminates or indeed if thick laminates from WCA cloth could be processed through RPP-3 and coating without delamination. Therefore, a number of different approaches were undertaken simultaneously to better ensure one or more successes in a timely fashion.

The major problem to the production of sound laminates is the control of decomposition gases. If gas buildup is too rapid or if passages for the escape of gases are closed, delamination will occur. This can happen during initial pyrolysis or at some later stage (predominantly during RPP-3 processing).

A series of twenty panels, 38-ply thick, measuring 10" x 12", were initiated to cover a range of possible processing approaches. Variations introduced were categorized as follows:

- (1) Standard processing
- (2) Modified debulking, cure, post cure, and/or pyrolysis
- (3) Lower resin fraction
- (4) Alternate resin to the R-120 phenolic
- (5) The use of graphite and carbon powder fillers
- (6) Manufactured gas escape paths (#40 holes on 1.0 in. centers)
- (7) A composite assembly in which a central core was pyrolyzed first and then additional virgin layers were to be added that required a second pyrolysis.

To support the selection of specific process profiles thermogravimetric analyses (TGA) and oven tests were conducted to determine temperature levels at which significant gas generation occurred. These were performed on both the R-120 resin and the furfuryl alcohol, used for reimpregnation. As a result of the data obtained, which indicated significant gas generation (3% weight loss) at a temperature of only 360°F, the post cure cycle was separated from the pyrolysis cycle, where it had been previously integrated for thin laminate fabrication, and was lengthened. Ultimately, a 5-day oven post cure was employed for initial pyrolysis and 32 hour oven post cure was found effective for furfuryl alcohol.

A summary of the results of the investigation are given in Table 2. Eight panel variations were successfully processed through coating without failure, one panel (#21) was deleted after layup, one panel (#19) was a duplicate of another and was not layed up, and eight panels suffered delamination during processing.

A review of the table shows the following:

- (1) The previous standard process, panel #5, results in delamination.
- (2) Drilled gas passages (panel #20) overcomes the deficiencies of the previous standard process but this is an undesirable solution.

TABLE 2 PROCESS HISTORY OF THICK RPP LAMINATES

Panel No.	Starting Material WCA Graphite Cloth Reinforcement	Debulk Condition	Cure Method	Post Cure	RPP-0	Pyrolysis RPP-1	RPP-2	RPP-3	Coating
1	307-7-7 (Resin Level A(High))	20 psi, room temp	Standard ⁽¹⁾	5 day oven	Standard	Standard	Standard	Standard	Standard ⁽⁸⁾
2	307-7-7	20 psi, room temp	Standard	5 day 50 psi	Modified	Standard ⁽⁶⁾	Standard	Modified ⁽⁶⁾	Standard ⁽⁸⁾
3	307-7-7	20 psi, room temp	Standard	24 hour 50 psi	Standard	Standard	Standard	Standard	Standard ⁽⁸⁾
4	307-7-7	20 psi, room temp	Standard	24 hour 50 psi	Modified	Modified ⁽⁶⁾	Modified	Modified ⁽⁷⁾	--
5	307-7-7	80 psi, 180°F	Standard	Standard	Standard ⁽³⁾	--	--	--	--
6	307-7-7	80 psi, 180°F	Standard	24 hour oven ⁽³⁾	--	--	--	--	--
7	307-7-7	80 psi, 180°F	Standard	24 hour oven ⁽³⁾	--	--	--	--	--
8	307-7-7	80 psi, 180°F	Standard	24 hour 50 psi	Modified	Standard ⁽⁶⁾	Standard	Modified ⁽⁶⁾	--
9	307-7-7	20 psi, room temp	Vacuum Bag ⁽³⁾	--	--	--	--	--	--
10	Resin Level B (Moderate)	20 psi, room temp	Standard	Standard	Standard	Standard	Standard	Standard ⁽³⁾	--
11	Resin Level B (Moderate)	20 psi, room temp	Standard	5 day oven	Standard	Modified ⁽⁶⁾	Modified	Modified ⁽⁶⁾	Standard ⁽⁸⁾
12	Resin Level C (Lower)	20 psi, room temp	Standard	Standard	Standard	Standard	Standard ⁽³⁾	--	--
13	Resin Level C (Lower)	20 psi, room temp	Standard	5 day oven	Standard	Modified ⁽⁶⁾	Modified	Modified ⁽⁶⁾	Standard ⁽⁸⁾
14	Resin with Carbon Filler	20 psi, room temp	Standard	5 day oven	Standard	Standard	Standard	Modified ⁽⁶⁾	Standard ⁽⁸⁾
15	Resin with Graphite Filler	20 psi, room temp	Standard	5 day oven	Standard	Standard	Standard	Modified ⁽³⁾ ⁽⁴⁾	--
16	US Polymeric FM5014	20 psi, room temp	Standard	Standard	Standard	Standard	Standard	Standard ⁽³⁾	--
17	US Polymeric FM5441	20 psi, room temp	US Polymeric	Standard	Standard	Standard	Standard	Modified ⁽⁶⁾	Standard ⁽⁸⁾
18	Resin with Thermax Filler	20 psi, room temp	Standard	Standard	Standard	Standard	Standard	Modified ⁽³⁾ ⁽⁴⁾	--
19	Resin with Thermax Filler	(5)	--	--	--	--	--	--	--
20	307-7-7 with Drilled Holes	20 psi, room temp	Standard	Standard	Standard	Standard	Standard	Standard	Standard ⁽⁸⁾
21	307-7 Composite Assembly	(5)	--	--	--	--	--	--	--

(1) Standard = 308-7-10 Specification

(3) Delaminated at this process step

(4) Modified Pyrolysis without Modified Post Cure

(5) Deleted

(6) Modified Furfuryl Post Cure

(7) Successful through RPP-3 but not coated

(8) Successful through coating

- (3) It is necessary that a gentle post cure cycle be used, particularly during processing to RPP-3, where gas passages are reduced, thus providing a greater chance for gas entrapment.
- (4) Reduced resin levels of 45% (level B) and 40% (level C) are practical and provide sufficient strength to prevent delamination with the proper processing cycle. One of these levels might have been chosen as the standard for the Phase III program had material commitments not been required before completion of processing of these panels. A lower resin content would ease debulking of complex parts.
- (5) Fillers can also be employed (with separate post cure process) although it isn't clear that they offer an advantage over other approaches.
- (6) U.S. Polymeric resin could be employed if necessary but there is no apparent advantage over the R-120 currently in use.
- (7) Autoclave pressure cure is required to prevent delamination, since vacuum bagging alone is unsatisfactory.
- (8) Various post cures may be employed, varying from long time/no pressure to short time/autoclave pressure. VSD elected to use the long time (5 day) post cure in an oven to avoid tying up an autoclave for a 24 hour post cure. The long time post cure is considered appropriate for production parts.

Strength data was obtained on successful panels and is provided in Table 3. The panel numbers can be correlated with the processing data in Table 2. Note that strengths are uniformly high and generally exceed those for thinner ply material (reference (2)). Only the U.S. Polymeric panel has strength levels falling outside of the general trend. This may be because processing was not necessarily optimized for this resin system.

TABLE 3 PHYSICAL PROPERTIES OF THICK RPP LAMINATES

Panel No.	Interlaminar Tensile Strength, Bare, psi	Flexure Strength, psi x 10 ³	
		Bare	Coated
1	576	19.3	22.1
	540	18.9	20.3
	549	18.7	22.5
	555 Avg.	19.0 Avg.	21.6 Avg.
2	574	19.2	16.7
	645	18.7	18.8
	575	18.8	20.7
	598	18.9	18.7
3	581	19.4	23.0
	665	19.3	23.1
	575	19.4	23.1
	663	19.4	23.4
11	483	20.3	19.9
	533	20.6	20.3
	483	20.5	18.3
	500	20.5	19.5
13	620	20.7	22.6
	668	21.2	23.0
	543	18.4	20.6
	610	20.0	22.1
14	435	19.3	22.0
	556	19.9	18.6
	537	19.4	20.8
	509	19.5	20.5
17	590	16.8	15.4
	645	16.0	17.1
	565	16.4	16.0
	600	16.4	16.2
20	598	19.7	22.5
	577	19.5	23.8
	568	18.9	21.1
	575	19.4	22.5

Interlaminar tension stress is satisfactorily high and indicates good reimpregnation penetration so that the center of the panel is not weak. In general, coated flexure strength exceeds bare flexure strength. This is the reverse of the trend for thinner, 13-ply material, and is not fully understood.

Another observation of significance is that, even with the variations represented by the eight successful panels, properties are very consistent. This tends to indicate that with the proper processing, strength and laminate integrity are not highly sensitive to starting material resin variations.

Ultrasonic and x-ray investigations of these panels were made during processing. Density variations observed were examined for effect on strength but no correlation was found. Portions of these panels were therefore taken to be used as standards to define acceptable levels of density variation.

Coating of these panels was essentially craze-free up to 10 x magnification. However, x-ray examination revealed the normal crazing pattern on all panels.

Based on the results of this investigation, process selection was made using the 307-7-7 WCA graphite cloth phenolic pre-preg. The process includes a standard specification 308-7-10A autoclave cure, a 5 day post cure and a 70 hour modified pyrolysis cycle. Impregnated furfuryl alcohol receives a standard cure plus a 32 hour post cure prior to the modified 70 hour pyrolysis cycle.

As noted previously, other processes or materials could also be employed. In particular, the use of reduced resin fraction is attractive to ease fabrication and should be pursued further.

1.2 TASK 2 - INSULATION DEVELOPMENT

An insulation system is a necessary element of the leading edge system to block heat from the 2500°F RPP leading edge to the aluminum wing front spar, which is not permitted to exceed 350°F. The objective of this task was to investigate and evaluate various material candidates that could potentially be used in insulation capacities in the leading edge design and select those particular materials to be employed in the deliverable hardware.

The term "insulation system" implies that not only the insulation, but the method of attachment, its installation, and its thermal and structural integrity must be examined as part of the selection process.

The insulation system must be capable of withstanding the imposed temperatures for 100-missions without significant degradation. It will be subjected to moisture from humid conditions at the launch site and perhaps from rain seeping through gaps during launch or cruise flight after entry. Vibration and acoustic environments are the most significant loads to be imposed on the insulation and attachment system. And, of course, for use in Phase III the insulation had to be available in quantities, forms or sizes that the design required, and had to be within a reasonable cost.

This section of the report summarizes the work leading to the selection of materials for, and the design of, the insulation system. Materials studies are covered first, followed by parametric analysis results which directed the design of the heatshield. Finally, vibration tests that confirmed the validity of the heatshield concept are discussed.

1.2.1 MATERIALS EVALUATION

Insulation Screening - The approach taken in this study was to collect data and samples of candidate insulations with a potential application in the 2300-2500°F temperature range. The temperature limit was based on anticipated requirements for flight hardware. The computed temperature of the insulation based on Phase III criteria was 2272°F

(Fig. 21.). Preliminary screening tests were conducted by cycling material samples in a furnace, each cycle consisting of 15 minutes in the furnace and then sufficient time outside for cool down to room temperature. Weight, dimensional stability, and brittleness or change in appearance were monitored. A listing of the materials evaluated in this manner are given in Table 4.

Other screening tests conducted included chemical compatibility with RPP, and nickel alloys with which the insulation could come in contact at high temperature. Another significant test was the response to water and temperature cycling. As a final test of acceptability, thermal cycle testing of larger segments of the insulation was conducted and vibration tests of a heatshield component were performed. These investigations are discussed in the following paragraphs.

The insulations tested consisted of rigid and non-rigid varieties, RSI's, existing product lines, experimental varieties, and even new fibers not yet formed into an insulation blanket. Notes on specimen performance are provided in Table 4. Further comments are as follows:

- (1) Non-rigid varieties tended to slump when soaked with water and did not return to shape. Since a suitable moisture barrier had not been developed, it appeared that the extensive use of a non-rigid insulation would be risky for flight hardware. However, non-rigid insulation could be used in small or thin pieces where the moisture effect on their dimensional stability is not significant. Dynaflex (12 lb/ft³ density) was used in localized areas of the deliverable hardware in small quantities. Applications included gap filler material between insulation assemblies and insulation around the lug bolt between the RPP and Inconel flanges, where it was trapped by the rigid insulation.

TABLE 4 PHYSICAL CHANGES IN INSULATION
AFTER 15 MINUTE - 2500°F CYCLES

Material	Type	No. Cycles	Weight Loss, Percent	Condition of Specimen
REI Mullite (uncoated)	Al ₂ O ₃ -SiO ₂	98	6.22	No change; includes 4 soak, freeze, thaw, heat cycles.
REI Mullite (coated)	Al ₂ O ₃ -SiO ₂	25	0.96	Coating cracks, primarily on sides.
HCF (coated)	Al ₂ O ₃ -SiO ₂	20	1.23	Crawling of coating; 2 soak, freeze, thaw, heat cycles causes cracking of coating; insulation intact.
LI-1500 (coated)	SiO ₂	3	0.71	Shrinkage: 5.1% on hot face, 17.9% on back face; orange peel of coating.
CPI	Al ₂ O ₃ -SiO ₃	3	(gain) 0.0045	Reacts/coated RPP thermal shock sensitive.
Dynaquartz	SiO ₂	102	1.18	No change, crack opening along as-received defect, includes 3 soak, freeze, thaw, heat cycles.
Zirconia board	ZrO ₂	99	4.42	No change; reacts Irish Refrasil, gives green tint; reacts cera-form.
Dynaflex 12 pcf	Al ₂ O ₃ -SiO ₂	23	2.03	Adherence/coated RPP; moisture promotes slumping, adherence; includes 3 soak, freeze, thaw, heat cycles.
Microquartz	SiO ₂	17	1.14	No change.
Zirconia felt	ZrO ₂	21	6.97	Friable.
Zirconia cloth	ZrO ₂	15	2.43	Losing cohesion
Cera-Mat	Al ₂ O ₃ -SiO ₂	60	5.4	Stiffening.
HPHA	Aluminate glass	82	3.91	Slight reaction/coated RPP; includes 2 soak, freeze, thaw, heat cycles; fibers only.
MSDF	Al ₂ O ₃ - SiO ₂	16	8.04	Slight reaction/coated RPP; fibers only.
3 M Alumina	Al ₂ O ₃ - SiO ₂	3 41	6.88 11.84	Long fibers, woven into cloth
Astroquartz	SiO ₂	10	0.538	Brittle.
Irish Refrasil B-1576	SiO ₂ -Cr ₂ O ₃	21	3.09	Reacts/coated RPP stiffening.
Irish Refrasil SS-1986	SiO ₂ -Cr ₂ O ₃	3	2.84	Reacts/coated RPP; 3.8 micron fibers.
Fiberfrax-H 6 pcf	Al ₂ O ₃ -SiO ₂	16	2.17	Slumps; stiffening.
3M-alumina	Al ₂ O ₃ -SiO ₂ -Cr ₂ O ₃	14 3	15.8 3.73	Losing color, long fibers only.
Cera-Form	Al ₂ O ₃ -SiO ₂	10	1.24	Slight reaction/coated RPP
SIX	Al ₂ O ₃ -SiO ₂	96	5.52	Slight reaction/coated RPP
Cera-Blanket	Al ₂ O ₃ -SiO ₂	44	1.98	Stiffening
Irish Refrasil B-1573	SiO ₂ -Cr ₂ O ₃	6	3.89	Reacts/coated RPP; stiffening
Irish Refrasil C-1554-48	SiO ₂ -Cr ₂ O ₃	6	4.2	Reacts/coated RPP; stiffening
Refrasil A-100	SiO ₂	6	1.39	Heavy shrinkage
Refrasil B-100	SiO ₂	6	2.77	Slight stiffening
Superface Board	Al ₂ O ₃ SiO ₂	8	1.67	Cracking, shrinkage
MAR-SI (uncoated)	Al ₂ O ₃ SiO ₂	16	0.203	No change
MAR-SI (coated)	Al ₂ O ₃ SiO ₂	8	-	Coating cracks, coating reacts/ Fiberfrax-H

- (2) Only one zirconia product, zirconia board, remained stable during the cycle testing. However, it is relatively heavy at 30 lb/ft³ and therefore of lower efficiency than the silicas or mullites.
- (3) The mullite materials were stable at the temperatures involved and looked very promising within limited testing done. However, there were apparently other problems with these materials as determined by NASA, including radiation shine-through, which lowers thermal efficiency, and thermoelastic stresses to produce cracking.
- (4) Two silica materials were evaluated, LI-1500 with no coating and Dynaquartz. In VSD tests, which required a 15 minute hold at maximum temperature in accordance with Phase III design criteria, the LI-1500 material produced excessive shrinkage. However, Dynaquartz (10 lb/ft³) by contrast was relatively stable, even when subjected to watersoak, freeze, thaw, and heat cycles.
- (5) Some fibers, particularly the HPHA variety, showed potential for high temperature application if constructed into a cloth or blanket. It was beyond the scope of this program to pursue these product further.

On the basis of the screening tests and design studies it was apparent that an RSI material would offer the best solution to the RPP heat-shield requirements for a number of reasons. First, the RSI's were being designed for at least 2300°F operation and by proper design, the RPP heat-shield requirements could be reduced to this level. Second, the RPP program could reap the benefits of RSI development and another insulation would not have to be developed specifically for the leading edges. Finally, leading edge internal environmental requirements are less severe than RSI requirements, which makes this a feasible approach.

Three RSI materials were given serious consideration: GE's MOD-1A, Martin's MAR-SI, and Lockheed's LI-1500 and LI-0900. An evaluation of these are given below.

Uncoated MOD-1A remained stable in mission cycling tests but the coated material suffered coating cracks. However, the internal installation does not necessarily require a coating (except possibly for handling) so this was not a factor in the selection of material. G.E. also reported that their material had been tested to 2500°F and 163db OA acoustic level for 25 simulated missions. With the exception of coating cracks the material successfully withstood the environments. VSD also tested a small sample (a 1 in. cube) to a 163 db OA acoustic level for 50 minutes without failure, after having previously been subjected to 2500°F for 4 hours.

NASA-JSC tests and analyses, however, indicated some problems with the mullites. First, the fiber diameter used permitted radiation shine-through in component tests, which lowered their efficiency significantly. Second, in thermoelastic analyses, conducted for VSD, failure was predicted at design temperature gradients. The computed margin of safety was - 41%, occurring at 1500°F during heatup. This analysis was based on 6" x 6" tile size and a completely unrestrained back face.

On the basis of the NASA information the MOD-1A was not selected for Phase III fabrication

MAR-SI data provided by Martin indicated a lower elastic modulus than G.E.'s mullite so that lower thermal stresses were estimated. Both coated and uncoated MAR-SI were tested by thermal cycling to 2500°F for 15 minutes duration. A weight loss of 0.203% after 16 cycles was noted on an uncoated specimen and dimensional changes were nil after the 16 cycles. Cracking of the coating on the hot face was noted after the third cycle to 2500°F. Cycling of coated specimens was discontinued after 8 cycles.

MAR-SI was rather friable and would require a coating for protection during handling. This would have to be developed, although it did not appear to be a problem. One of the major disadvantages of MAR-SI was the fact that it was relatively new and was not well characterized. Therefore, VSD decided not to pursue it further. Tests performed by NASA JSC on MAR-SI did not give promising results.

The LI-1500 silica insulation was not subject to significant thermal stress, because of its low thermal expansion, and it offered good thermal efficiency. In VSD tests, however, it exhibited high shrinkage. Thermal cycling tests were conducted at 2300°F and 2400°F for a duration of 22 minutes. Insulation to limit heating to only the front face was accomplished by using Irish Refrasil around the sides and back face of the LI-1500 block. The LI-1500 was placed on a thin sheet of coated RPP, also buried within the Irish Refrasil blanket. Three cycles to 2300°F produced shrinkages of 1.75% to 2.72% in length/width and 1.44% in thickness. Two cycles to 2300°F followed by a single cycle to 2400°F resulted in shrinkage of 6.19% to 9.83% in the length/width dimensions; thickness changed by 5.46%. Tests consisting of a 10 minute cycle to 2300°F were also run on LI-1500, insulated with Irish Refrasil. Shrinkage in the length/width directions varied between 0.197% and 0.51%; thickness shrinkage was 0.59%.

It is clear that resultant shrinkage was time sensitive for a given cycle. Lockheed reports that the coating will help stabilize the material in the hot surface layer, which is relatively thin, because of the high thermal gradient near the heated surface. Lockheed plasma arc data, conducted up to 2500°F with 8 minutes above 2300°F per cycle, suggested that the material could meet the leading edge requirements without excessive shrinkage.

On the basis of VSD tests, NASA-JSC data, and vendor tests it was believed that LI-1500 would provide the safest choice with the data available at the time of selection, since LI-1500 at least had structural integrity and thermal efficiency for the leading edge application. Further,

coating cracking if incurred was acceptable for the internal application because its prime function would be for material handling and shrinkage resistance. In addition, analysis of wing leading edge temperatures showed that with a vertically oriented heatshield, as opposed to the canted design employed in this Phase III program, insulation temperature could be maintained below 2250°F , and could even be held below 2100°F for the inboard 60% of the wing.

It was expected therefore that LI-1500 could meet the Shuttle requirements with perhaps limited areas, such as the interference heating region, requiring periodic replacement during the 100-mission life of the Orbiter. On this basis LI-1500 was the prime selection for the Phase III leading edge assembly. However, due to a number of factors, an alternate material had to be selected for the Phase III test article. Among the reasons were: (1) the high cost of LI-1500 for the Phase III program, (2) the unavailability of the material for the Phase III program, because all production was being taken for NASA tests, and (3) the RSI selection decision had not been made for the Shuttle so that any selection made by VSD would be premature.

VSD elected, therefore, to pursue an alternate route and utilize Dynaquartz to thermally represent an RSI system. Dynaquartz of 10 lb/ft^3 density in VSD tests had demonstrated thermal stability to 2500°F and had a potential for even higher limits. Free standing acoustic tests to 163 db OA for 50 minutes showed no failure on a block $4\frac{3}{8}\text{ in. square} \times 1\text{ in.}$, thus indicating a degree of structural integrity to dynamic load environments. It was relatively inexpensive, available, thermally efficient, and was chemically compatible with coated RPP and Inconel structure. Like LI-1500 the thermal expansion is low because it is 99% pure silica, thus offering a high degree of resistance to a thermal stress failure mode. Its' prime weakness was low strength in the thickness direction, which is about 4 psi.

In recognition of the low strength, VSD requested that Johns-Manville attempt to fabricate a higher density material (15 lb/ft^3) in an effort to enhance the strength. This was accomplished on an experimental basis with the new material exhibiting a potential fourfold increase of strength in the weak direction. Ultimately, the 15 lb/ft^3 material was used to insulate the leading edge support brackets, even though the material was experimental and subject to many flaws.

Bonding Studies - A study of possible attachment techniques, which included various mechanical approaches and bonding, resulted in selecting bonding as the best approach, since it was less developmental, provided for more uniform support of the insulation and was tested extensively by RSI contractors and found acceptable. Since Dynaquartz was the selected insulation, all bonding had to be conducted inhouse; therefore, materials had to be selected and techniques developed for fabricating insulation assemblies.

The insulation is bonded to either 6Al-4 V titanium or polyimide fiberglass with desired operation temperature extremes of -250°F to $+600^\circ\text{F}$ for 100-mission life. Total time at maximum temperature for the 100-missions is approximately 40 hours.

Bonding studies of 6Al-4V titanium were initiated using RTV 560 and RTV 140 as bonding agents. Thermogravimetric analysis on RTV 560 showed a major weight loss beginning at 850°F that was complete by 1200°F . RTV 140 had a weight loss beginning at 750°F , completing by 1120°F . RTV 560 with 4004 primer was tested at various temperatures after a 64 hour cure. Results are given in Table 5. The strengths indicated that RTV-560 could be employed in the temperature range of interest (up to 600°F), since the weakest link in the insulation system was the insulation itself, which has a strength of 4 psi for the 10 lb/ft^3 variety. In view of the performance achieved with the RTV-560 no further effort was devoted to RTV-140.

TABLE 5 TENSILE STRENGTH of RTV-560
64-HOUR CURE

ENVIRONMENT	STRENGTH RANGE PSI
-250°F, 30 min. Test at -250°F	2580
Ambient Temperature	395 - 417
600°F, 20 min., Test at R. T.	314 - 326
600°F, 64 Hr, Test at R. T.	117 - 132
650°F, 40 Hr, Test at R. T.	60 - 89

Refinement of the bonding/cure process was made (primarily 7 day cure rather than 3) and additional evaluation was conducted. Tensile strengths of RTV-560 bonded to titanium and using 4004 primer produced cohesive failures at all conditions. Results are summarized in Table 6. Improvement with the longer cure time is apparent (ref. Table 5). Indications were that the bond would meet the 600°F temperature requirement

TABLE 6 TENSILE STRENGTH OF RTV 560
7-DAY CURE

Environment (Test at Ambient Unless Noted)	FTU, psi (Average of 3)
-250°F, 20 min; test at -250°F	3283
-250°F, 20 min.	505
Ambient Temperature	510
Vacuum, 10 days/ambient temp.	578
500°F, 20 min.	500
550°F, 20 min.	502
600°F, 20 min.	456 (av. of 2)
650°F, 20 min.	354 (av. of 2)

and far exceed the strength of the insulation it was to hold in place. Therefore, RTV-560 was deemed acceptable.

Strain Isolator Studies - A strain isolator material located between the insulation and the titanium or fiberglass structure serves two functions: (1) it absorbs the differential thermal and load strains between the insulation and support panel to prevent failure of the insulation or insulation/bond interface, and (2) it absorbs differential deflections between insulation and support panel under dynamic loadings to reduce insulation/bondline tensile stresses to an acceptable level. For the Dynaquartz insulation dynamic conditions govern strain isolator design.

Drawing on the experience of the RSI contractors, a foam material in the 20 lb/ft³ density range was sought to provide the best compromise between elastic properties and retention of strength at elevated temperature. Three materials were examined: RTV-560, and TBS 757 from G.E., and RL 1973 from Raybestos Manhatten. The G.E. products had to be foamed inhouse, while the RL 1973 could be bought as foam sheet, slit to desired thicknesses.

Foamed RTV-560 tension strengths varied between 27 and 187 psi through the density range, 16 to 24.5 lb/ft³. Strength on a 21 lb/ft³ variety was 155 psi at room temperature, which reduced to 58 psi after 20 minute exposure at 600°F. In comparison to the 4 psi Dynaquartz strength the RTV-560 foam strength appeared acceptable and could be varied as desired by density modification. However, it was found that process control for densities less than 20 lb/ft³ was difficult and reproducibility would suffer.

Foamed TBS 757 was examined at densities in the 27-30 lb/ft³ range. Thermal cycling to 600°F for 20 minutes resulted in an average strength of 102 psi. Testing at -250°F after a 20 minute soak gave strength values averaging 1185 psi. Primer 4155 was used with titanium alloy fixtures in the TBS 757 testing; failures were cohesive in each

environment. This material had merit if the density could be lowered, but further work was terminated in favor of the RL 1973 material discussed below.

RL 1973 is a methyl phenyl silicone sponge which, had been under evaluation by General Dynamics for NASA and showed attractive properties. VSD tested 20 lb/ft³, 0.25 in. thick material, bonded with RTV-560, and found strengths more than adequate for bonding Dynaquartz for a simulated 100-mission time span (40 hours). Results are given below. Even at 600°F where applied stresses are nearly zero, the RL 1973 retains some strength (10.9 psi average) and recovers to 47 psi average at room temperature, when critical vibration loads are encountered.

TENSILE STRENGTH OF RL 1973

(Bonded to 6 Al - 4 V Titanium Tension Fixtures)	
Environment (Test at Ambient Unless Noted)	FTU, psi (Average of 3)
-250°F, 20 min; test at -250°F (2 specimens)	516
Ambient Temperature (1 specimen)	47.5
600°F, 40 Hrs.	47
550°F, 40 Hrs.; test at 550°F	10.0
600°F, 40 Hrs.; test at 600°F	10.9

On the basis of these tests and the availability of a supplier for RL 1973 foam sheets (as opposed to in-house fabrication of RTV-560 foam with its attendant control and learning difficulties) the RL 1973 foam was selected for the Phase III test articles.

The RL 1973 is a closed pore foam and as such will expand or contract slightly as pressure varies until pressure equalization is

re-established. To minimize the response time for pressure equilibrium, the foam was "diced" at about 1 inch increments. In addition, the insulation designs were configured to permit both load and pressure deflections of the foam without endangering the insulation and bond. Further investigation of the effects of a closed pore foam must be made before committing to a flight design. Open pore foamed RTV-560 remains a suitable backup.

Thermal test assemblies, consisting of 10 lb/ft³ Dynaquartz bonded with RTV 560 to RL 1973 strain isolator, which were in turn bonded to 6 Al - 4V titanium alloy stiffening panels, were prepared. The test assembly with a typical Dynaquartz tile size of 6" x 2 4/5" x 1" was placed within a Fiberfrax H "coffin" to thermally protect the bottom and sides while permitting front face heating to be simulated. This insulation component package was cycled to 2300°F with the hot face and Dynaquartz/RL 1973 bond line instrumented. The hot face temperature reached 2270°F in 6 minutes. Continued thermal cycling to 2300°F produced no change in physical appearance or thermal response of the Dynaquartz after twenty cycles.

In summary the use of RL 1973 foam in combination with Dynaquartz insulation and RTV-560 bond were found acceptable for the Phase III articles.

1.2.2 PARAMETRIC ANALYSES

At the outset of the program it wasn't clear exactly what the basic concept of the insulation system should be. Questions were raised concerning such factors as the type of insulation, method of attachment, location (e.g. all on front side of canted support, split front and rear, or apply a portion to the aluminum spar), effect of reflectance on heat transfer, and requirements for strain isolation. Thermal parametric analyses were conducted to indicate best approaches, which had to be tempered somewhat with practical design constraints (such as insulation material size limits). Dynamic analyses were performed to evaluate the significance

of dynamic environments on the design. Thermal and dynamic analysis findings are discussed in the following paragraphs.

1.2.2.1 Thermal Analyses

Parametric analyses were conducted to guide concept selection using a one-dimensional math model that included both radiation and natural convection between the RPP and the forward face of the heatshield, and between the 2 ft. face of the heatshield and the aluminum front beam. For these analyses two different insulation systems were examined: (1) Dynaflex, 12 lb/ft³, forward and aft, and (2) LI-1500 forward and MIN-K (20 lb/ft³) aft. (Foreward and aft is relative to the canted heatshield support structure). These insulations were selected early in the program and were believed to provide representative results for the final insulation used (Dynaquartz).

The basic geometry analyzed was as provided by Figure 1, except that titanium was assumed for the canted heatshield support structure, rather than the polyimide fiberglass ultimately selected. RTV-560 silicone was assumed for bonding insulation to a foam strain isolator and to the structure. The strain isolator had properties like the G. E. PD-200 material.

Analyses conducted include:

- (1) Effect of forward face emittance variations
- (2) Effect of aft face emittance variations
- (3) Effect of insulation location
- (4) Effect of RTV-560 bond thickness and support structure thickness

Significant findings from these studies are as follows:

- (1) An emittance of 0.2 at elevated temperature compared to 0.9 reduces front face insulation temperature by only 70° F and titanium support structure temperature by 40° F. Normally, without emittance enhancement the insulation

materials would not approach an emittance of 0.9 and would probably be closer to 0.5. Therefore, a more realistic improvement by striving for a low emittance compared to that normally obtained would be about 35°F for the support structure. The equivalent weight savings for a 70°F front face temperature reduction is 0.2 lb/ft^2 in a 5 lb/ft^2 insulation system. Development of a low emittance surface was, therefore, not deemed sufficiently beneficial to pursue on this program.

- (2) Gold plating of one surface in the aft cavity reduces the aluminum temperature 15°F compared to a high emittance surface. Plating both surfaces with gold reduces the aluminum another 1°F . The 15°F reduction is also equivalent to only 0.2 lb/ft^2 weight savings in a 5 lb/ft^2 system. Therefore, no special radiation shield was included.
- (3) The most desirable location of the aft insulation is on the titanium canted panel rather than on the aluminum front beam. This produces minimum aluminum temperature for a given insulation system weight.
- (4) If only one type or density of insulation is employed, it is more efficient to place all of it on the forward side of the support structure with none aft. However, thicknesses required (approximately 3.5 in.) exceeded material availability and this approach could not be employed. Further, if a more efficient insulation can be used at lower temperatures, then splitting the insulation fore and aft could be more efficient.
- (5) Insulation is more efficient on a weight basis than utilizing bond material in a heatsink capacity; therefore, bondlines should be maintained as thin as practicable.

- (6) Similarly, utilizing titanium support structure as heat-sink is less efficient than adding insulation. Therefore, support structure should be the minimum thickness consistent with structural/dynamic requirements.
- (7) RPP or beryllium are more weight effective than Titanium. Not only can a lower temperature be obtained but also a lighter weight and thicker, stiffer panel. At 600°F RPP would not have to be coated. Polyimide fiberglass also provides an efficient heatshield support. Cost and weight considerations ultimately led to the selection of polyimide fiberglass for the support structure. Both RPP and beryllium would have been too expensive.
- (8) Natural convection and air pressure changes during entry significantly affect the calculated temperatures. Ignoring these effects can result in calculating temperatures 30°F lower in the Titanium and 15°F lower in the aluminum than would actually be experienced in flight.

Concept optimization and sizing analyses were conducted with the same one-dimensional model used in the parametric analyses. Six different forward insulations and three different aft insulations were analyzed to obtain a "feel" for the relative efficiencies of various approaches and their sensitivity to final design. Typical results are presented in Table 7, where all concepts were sized to produce a maximum titanium temperature of 600°F and a maximum aluminum temperature of 350°F. In some cases, where insulation thickness was limited, heat sink material was added to bring temperature within acceptable limits. Properties of the insulation materials were based on vendor data at the time of analysis and could be optimistic in some cases. Non-rigid insulations were assumed packaged in a container of mullite cloth or titanium foil as appropriate.

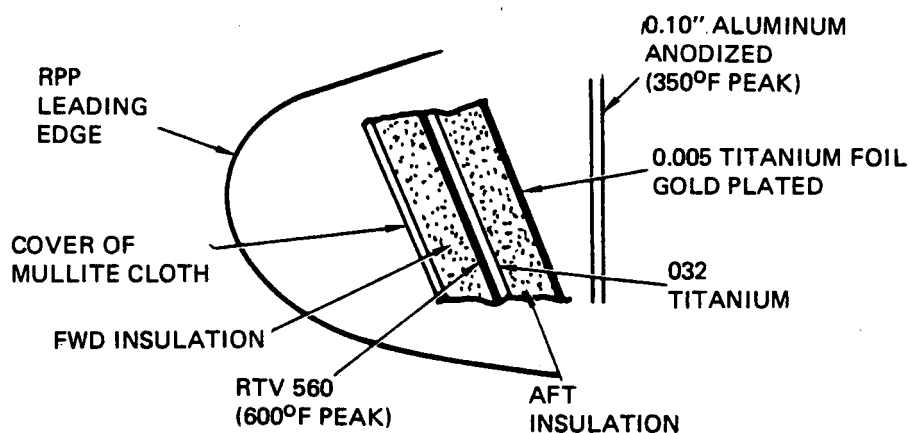


TABLE 7 COMPARISON OF FAIL-SAFE LEADING EDGE HEATSHIELD CONCEPTS

FWD INS.			AFT INS.					TI FOIL LB/FT ²	TOTAL
TYPE	QUANTITY	M/A LB/FT ²	TYPE	QUANTITY	M/A LB/FT ²	X	M/A LB/FT ²		M/A LB/FT ²
G.E. MOD I 15 PCF	2.5"	3.12	GHF 4. OPCF	2.36"	0.787	0.079"	.612	.851	4.9
G.E. MOD IA 12 PCF LOW "K" HIGH "K" (AS MDC MUL) MAX. 2.0" 12 PCF LOW "K" HIGH "K"	2.36"	2.36	GHF 4. OPCF	1.68"	0.560	0.03"	.235	.851	4.0
	2.40"	2.40	GHF 4. OPCF	1.905"	0.634	0.03"	.235	.851	4.1
	2.0"	2.0	GHF 4. OPCF	1.80"	0.600	.109"	.853	.857	4.3
	2.0"	2.0	GHF 4. OPCF	1.83"	0.610	.117"	.916	.851	4.4
MDC-HCF MUL. 15 PCF	2.452"	3.06	GHF 4. OPCF	1.26"	0.430	.03"	.235	.851	4.6
DYNAFLEX 12 PCF	3.62"	3.62	-	-	-	.03"	.235	.730 (0.30 COVER)	4.6
DYNAQUARTZ 10 PCF	3.30"	2.75	-	-	-	.03"	.235	.736 (+.3 COVER)	3.7 + COVER 4.0
LI-1500 15 PCF	2.0"	2.50	MIN-K 20 PCF	0.87"	1.45	.03"	.235	.851	5.0
DYNAQUARTZ 10 PCF	2.42"	2.01	DYNAQUARTZ 10 PCF	1.0"	0.833	.03"	.235 (+.0.3	.851 COVER)	4.2
LI-1500 15 PCF	2.0"	2.5	GHF 4 PCF	2.36"	0.787	.03"	.235	.851	4.4
G.E. MOD IA 12 PCF HIGH "K"	2.40"	2.40	MIN-K 20 PCF	0.87"	1.45	.03"	.235	.851	4.9
G.E. MOD IA 12 PCF HIGH "K"	2.40"	2.40	DYNAQUARTZ 10 PCF	1.0"	0.833	.03"	.235	.851	4.3
G.E. MOD IA 12 PCF 2" LIMIT HIGH "K"	2.0"	2.0	DYNAQUARTZ 10 PCF	1.0	0.833	.117	.916	.851	4.6
DYNAQUARTZ 10 PCF	2.42"	2.01	GHF 4 PCF	2.36"	0.787	.03"	.235 (+.3	.851 COVER)	4.2

FOR: 600°F RTV-TEMP.
350°F ALUMINUM TEMP.
M/A IN LBM/FT²

The G.E. MOD-1A RSI and Dynaquartz look most attractive weight wise for the front face primarily because of their lower density.

Backface insulation covered the extremes from MIN-K to Glass Heat Felt (GHF). The higher density of MIN-K made it inefficient for this application. GHF and Dynaquartz were comparable and since Dynaquartz was ultimately selected for the front face, it was likewise chosen for the aft face. This simplified design, analysis, and fabrication of heatshield components without loss of thermal efficiency.

The full range of unit weights computed varied between 4.0 and 4.9 lb/ft², but the most reasonable designs showed a variation between 4.2 and 4.6 lb/ft². The design concept chosen for Phase III is at the lower bound, 4.2 lb/ft².

A typical temperature response analysis is plotted in Figure 60. This example uses MOD-1A RSI on the frontside and Dynaquartz aft. It shows that maximum bond and support structure temperature occurs at about the time the Shuttle lands but the aluminum front spar does not peak for 1.75 hours after touchdown. The final design configuration, employing Dynaquartz front and rear, would behave similarly.

1.2.2.2 Vibration Analyses

Preliminary sizing of the canted heatshield was accomplished by first estimating the natural frequency of the support panel required to prevent failure, then checking the integrated design for structural integrity. Support structure was examined for a natural frequency of 120 Hz. Required panel thickness and stiffener spacing for a polyimide fiberglass panel are shown in Figure 61.

Examination of heatshield support structure weight as a function of stiffener spacing for the 120 Hz requirement reveals weights varying from 1.85 lbs for 5 bays with nominal stiffener spacing of 4 in. to 5.20 lb. with no stiffeners. A compromise design was selected that has four bays (5 in. nominal stiffener spacing) and a computed weight of 2.00 lb. to compare with the above. This produces a relatively simple design

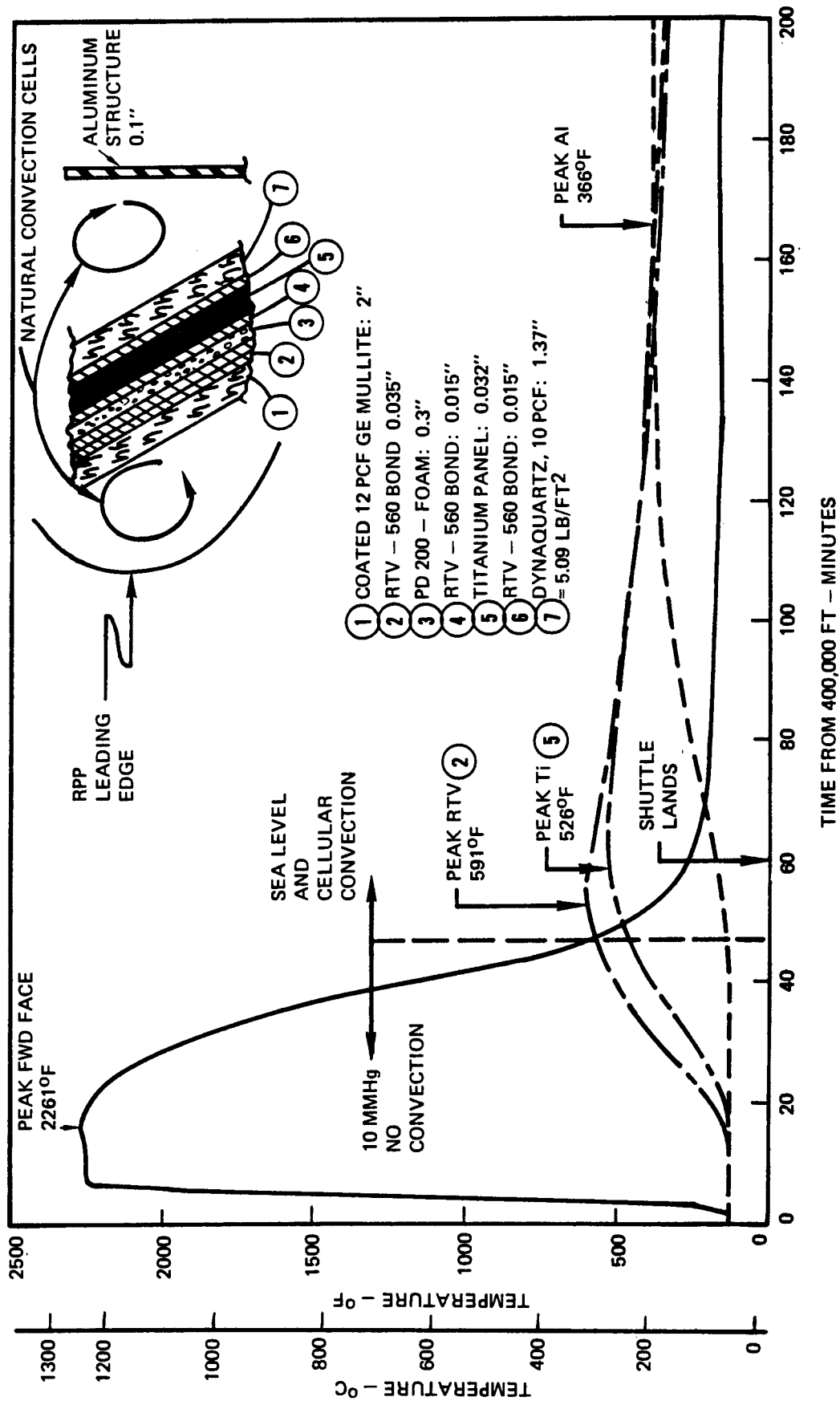


FIGURE 60 TYPICAL TEMPERATURE RESPONSE

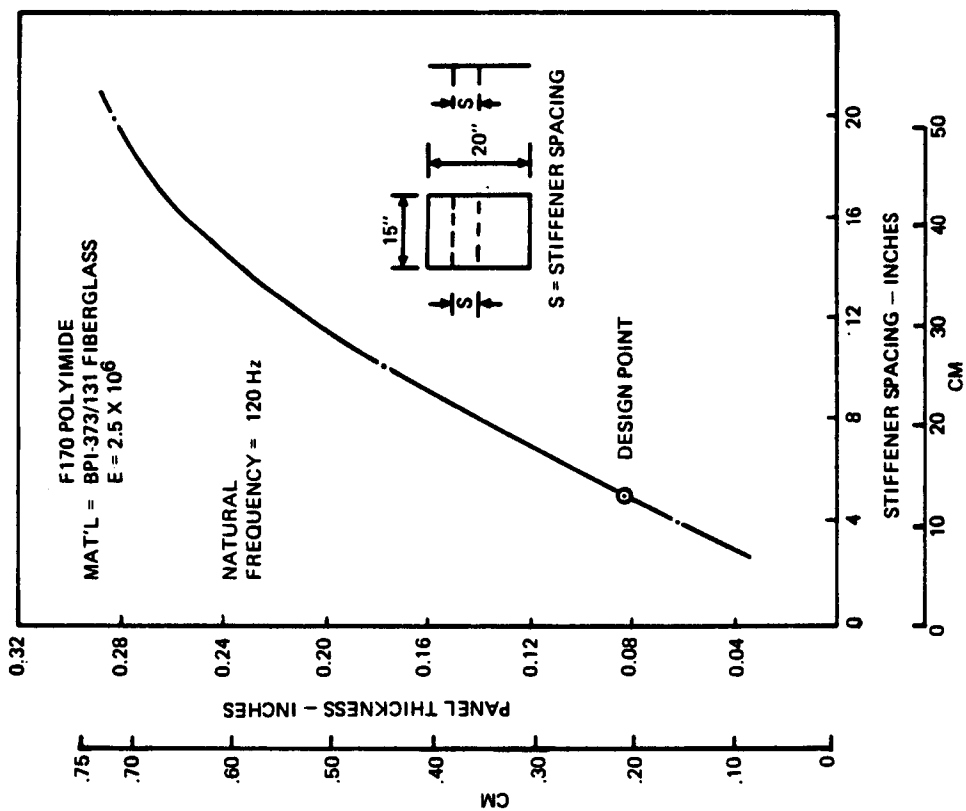


FIGURE 61 HEATSHIELD PANEL THICKNESS

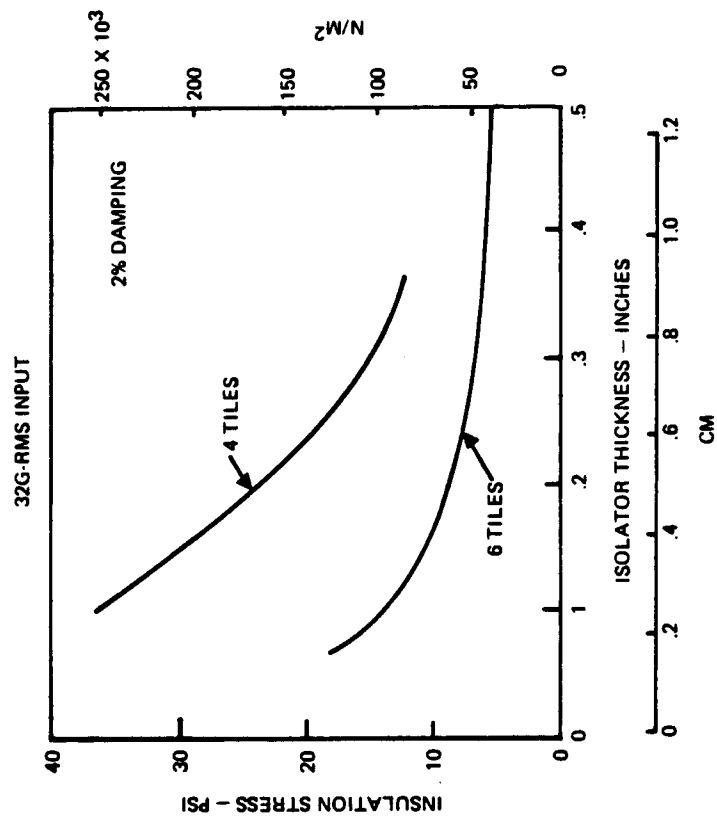


FIGURE 62 HEATSHIELD VIBRATION RESPONSE

and one in which, because of their size, aft face insulation tiles should not be critical for the dynamic load environment.

Preliminary analyses were conducted on the response of the canted heatshield to acoustic and random vibration inputs. Due to the difficulty in determining the attenuation of the acoustic levels through the leading edge and the effects of reverberations within the leading edge cavity, the predicted external acoustic levels (Figure 38, 163 db OA) were used to establish a conservative estimate of the baseline heatshield acoustic response. The random vibration input was the 32 g-rms overall level (Figure 37) applied at the basic heatshield attach points. On the basis of these analyses, it was determined that the random vibration environment was more critical than the acoustic environment, even with the assumption of noise levels of 163 db. Therefore, the random vibration environment was used in subsequent analyses.

Parametric analyses were conducted to determine the influence of insulation tile size (i.e., number of tiles used on the heatshield) and strain isolator thickness on the magnitude of stresses imposed on the tiles from the vibration response. Results are shown in Figure 62 where the critical stress in the weak (thickness) direction is plotted. The stresses shown are one-sigma values, but for design purposes, three-sigma stresses need to be compared against static strength allowables and two-sigma values should be tested against the insulation material fatigue allowables. For example, with this approach the maximum applied insulation stress for six tiles and 0.3 in. thick strain isolator would be three times the 6.5 psi, one-sigma stress value or 19.5 psi. None of the RSI materials (much less the Dynaquartz) can meet this requirement, because this is in the region of average to maximum failing strength for these materials in the critical thickness direction so that a design allowable would be substantially lower, perhaps in the 10 psi range. The alternative would be to increase the number of tiles, which amounts to decreasing tile size.

However, discussions with NASA-JSC personnel resulted in agreement that the design requirement was too conservative and the 32 g-rms design level should be treated as a maximum acceleration response, rather than as an input. With this interpretation, heatshield stresses were reduced by a significant factor. For example, the calculated stresses for a 4 tile insulation configuration with 0.20 inch thickness strain isolator are presented below. These stresses are within the allowable for all component materials. Specifically the three-sigma insulation stress of 3.15 psi compares with 4 psi allowable used for static analysis. This configuration was chosen for the Task 1 design.

<u>Component</u>	<u>Stress (psi)</u> one-sigma	<u>32-g-rms Output</u> three-sigma
Insulation (weak direction)	1.05	3.15
Insulation (strong direction)	1.80	5.40
Polyimide fiberglass (stiffener)	14,500	43,500
Polyimide fiberglass (panel)	186	558

1.2.3 VIBRATION TESTS

Vibration tests of two heatshield components were conducted to determine the ability of Dynaquartz to withstand the flight dynamic load environment, particularly from a fatigue standpoint for which no test data was available, and to demonstrate the ability of a rigid insulation design to meet Shuttle dynamic environments. Two components were tested, which approximated the dynamic characteristics of the actual heatshield. However, the first natural mode of each of the test articles had a higher natural frequency and greater deflection curvature at the center of the article than the actual heatshield. This additional curvature should result in greater induced stresses in the test article insulation than in the complete heatshield.

The first of the test components shown on Figures 63, employed a fiberglass panel and stiffeners to which was bonded two 1 3/8 in. thick tiles of 10 lb/ft³ Dynaquartz through a 1/4" thick RL 1973 foam strain isolator. This component was configured to represent a section of the

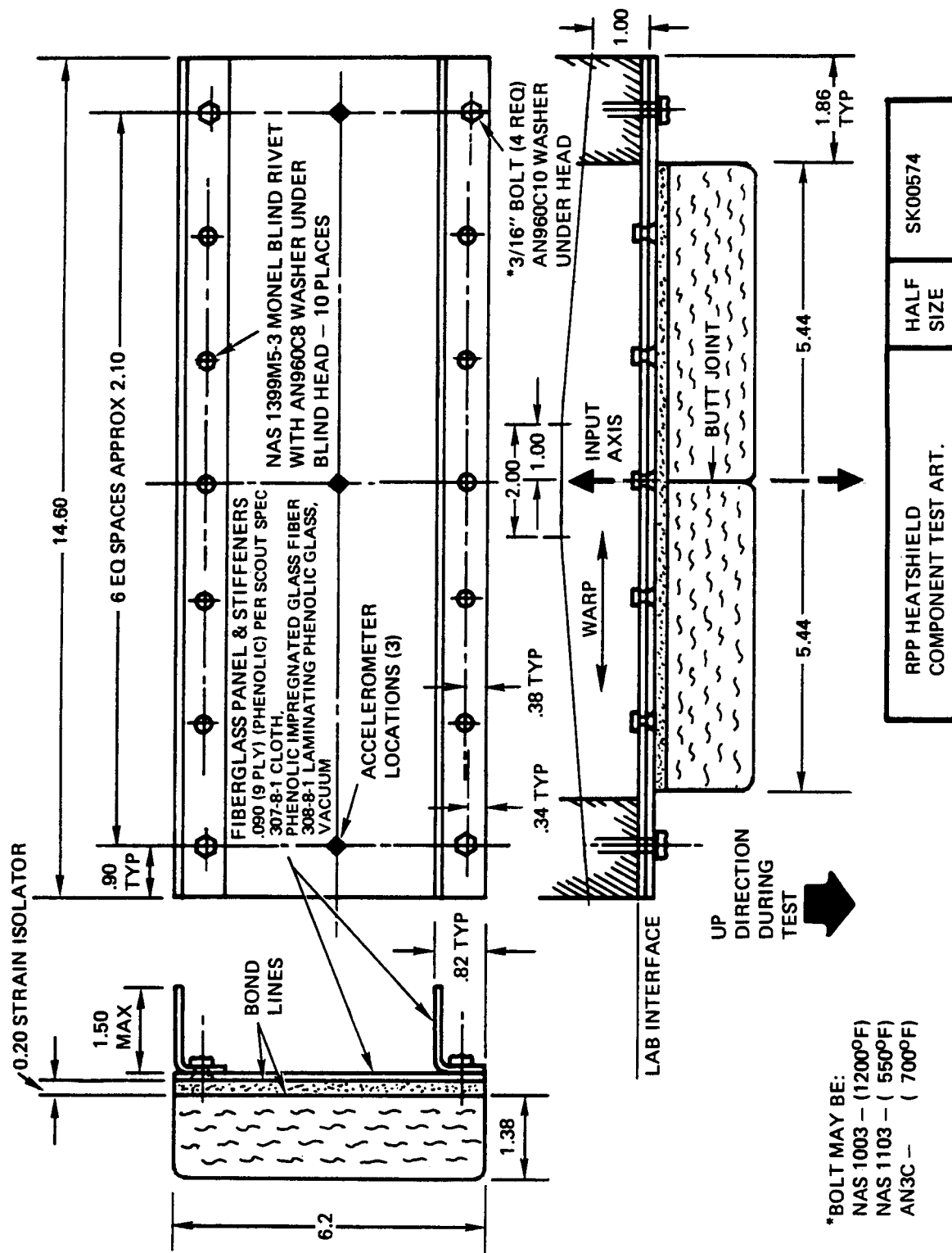


FIGURE 63 INITIAL HEATSHIELD TEST COMPONENT

canted heatshield. It was full span (14.6 in.), but trimmed to produce only one of the four bays of the heatshield.

The vibration input was normal to the plane of the panel, which produces critical loads on the insulation. In accordance with agreements reached with NASA-JSC the maximum response was limited to 32 g-rms. Actual test conditions resulted in the center accelerometer (SK00574) reaching 26 g-rms and one end of the panel responding at 31 g-rms. Power spectral density (PSD), however, which is the most important consideration, peaked at a whopping $10.2 \text{ g}^2/\text{Hz}$ at the first resonance (170 Hz) and showed a second peak of $1.6 \text{ g}^2/\text{Hz}$ at 500 Hz. This is an order of magnitude higher than the design spectrum, reference Figure 38. These levels resulted in failure of one tile at the bondline within two minutes and failure of the second tile in three minutes. This is equivalent to 7 to 10 missions at the frequencies involved, but this is not adequate. Failure occurred at the center of the panel in the Dynaquartz adjacent to the bondline. This is exactly where analysis predicts maximum stresses. It appears that these were fatigue failures because of the time required to produce failure. A static stress overload should have produced failure almost immediately.

In an effort to prove that a feasible design and attachment technique can be produced for the Shuttle, the test component was redesigned with major changes as follows:

- (1) tiles were reduced in size
- (2) strain isolator thickness was doubled
- (3) the density (and therefore strength) of the insulation was increased from 10 lb/ft^3 to 15 lb/ft^3 (an experimental Dynaquartz)

The redesigned component is shown in Figure 64.

Further discussions on the test environment with NASA-JSC resulted in a revision to remove much of the remaining conservatism. It was agreed to limit the PSD response of the two dominant resonances to

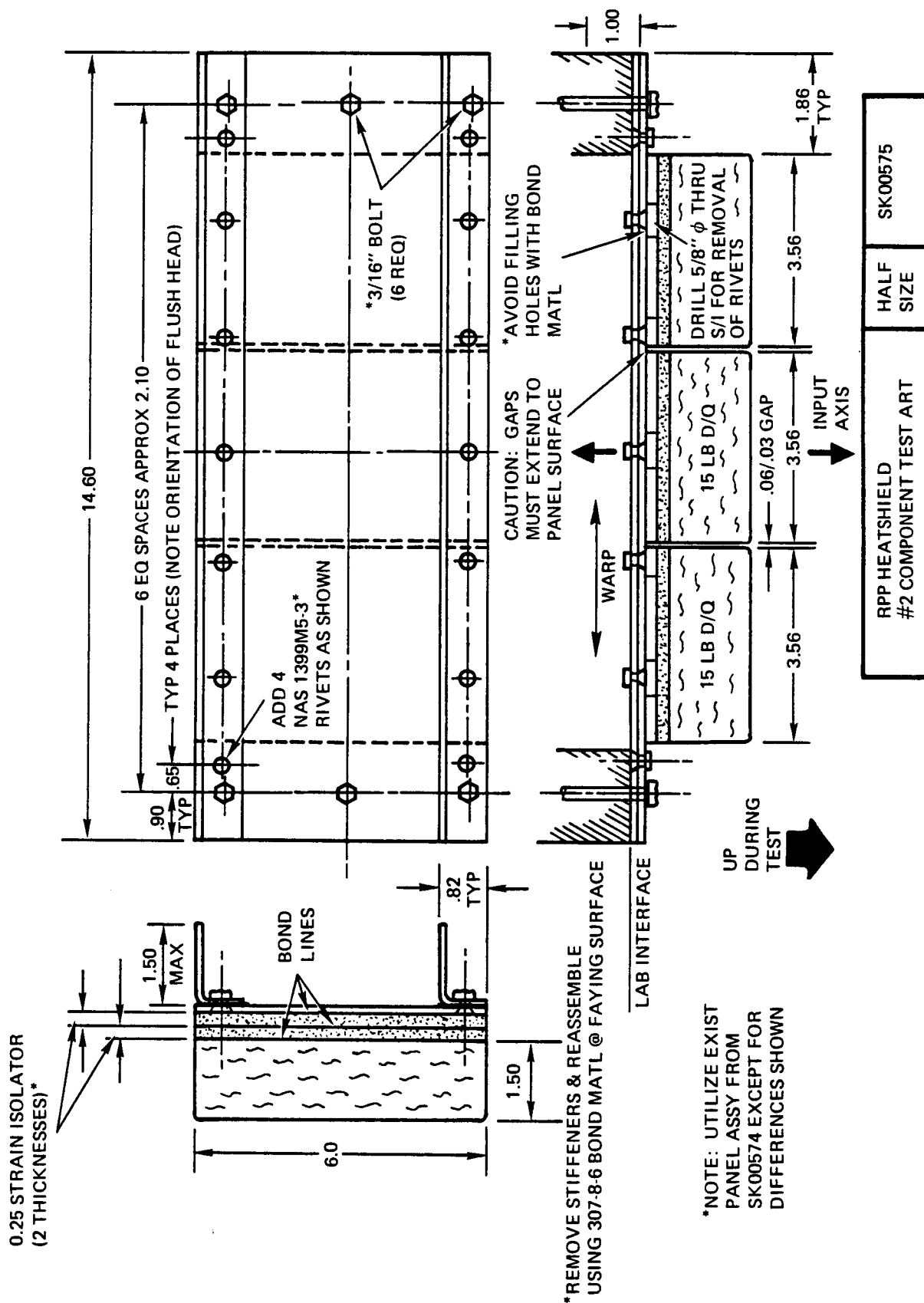


FIGURE 64 SECOND HEATSHIELD TEST COMPONENT

2.25 g^2/Hz , which includes a 1.5 factor of safety for current unknowns.

Using these new ground rules, the second article was tested.

The component was exposed at two levels. For the first exposure, the PSD was limited to 1 g^2/Hz and the g-rms value was 18.5. Test duration was 36 minutes to simulate 100 missions. This time was arrived at by the ratio of heatshield component resonant frequency to test article resonant frequency and assuming 30 second exposure per flight in the actual flight environment.

The second exposure was conducted to a PSD of about 2.5 g^2/Hz at resonant frequencies of 143 and 486 Hz. A third resonance at 175 Hz peaked at 1 g^2/Hz . During the 36 minute test run, the g-rms value rose from 25.8 to 29.7 with the average being 27 g-rms. Also, the PSD peaked at 4 g^2/Hz during a one to two minute period before a correction could be made.

No failures were observed at any location on the component, even though one of the tiles used in the component had known gross flaws. This suggests that all of the modifications employed on this redesigned component were not necessarily required, and a reduction in the number of tiles or a reduction in strain isolator thickness may prove reasonable. The test component following test is shown in Figure 65.

The significance of this test is that it demonstrates feasibility of a heatshield design in the Shuttle dynamic loads environment.

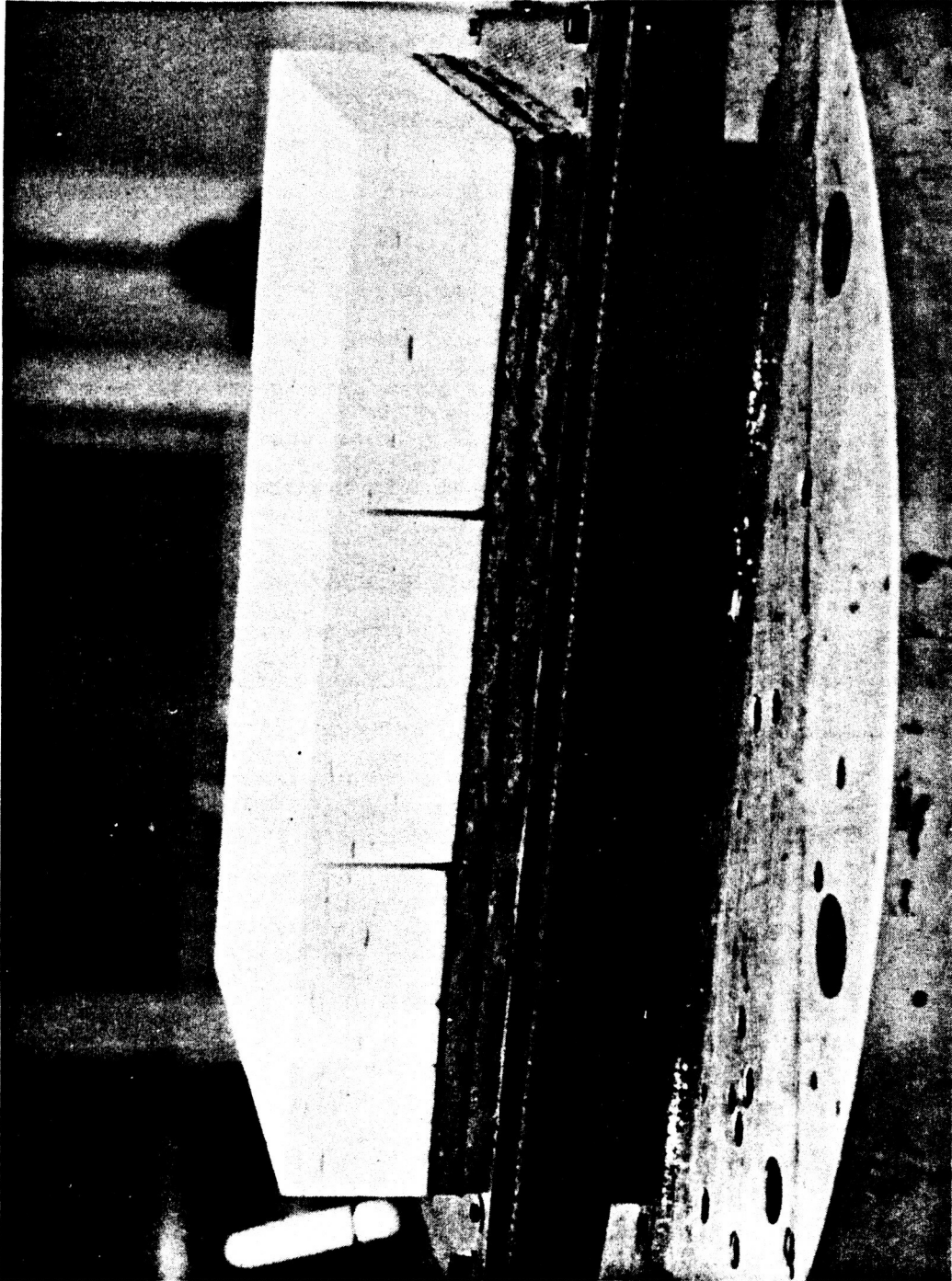


FIGURE 65 SECOND HEATSHIELD TEST COMPONENT AFTER SUCCESSFUL TEST

1.3 TASK 3 - SUPPORT LUG THERMAL TEST

The lower support bracket, which attaches the lower end of the RPP leading edge to the aluminum front spar (Figures 2 and 5) must serve as both a structural element and as an insulator to protect the aluminum spar from overheating. The support bracket, therefore, bridges the gap between the 2100°F RPP surface temperature in the lug region and the 350°F maximum allowance at the aluminum.

The purpose of this task was to determine and verify a satisfactory lug joint design and to establish design and analysis capability through thermal test of a joint component.

At the outset of the Phase III program, the support bracket concept was like that of Phase II, Reference 2, in that ceramic insulators were used at the lug bolt attachment and an Inconel bracket was used for structural support. In Phase II, however, the leading edge tied to titanium with a 600°F temperature allowable rather than to 350°F limited aluminum like Phase III. The Phase III requirement made the design task more difficult and forced the design concept to be more sophisticated.

The controlling aspects of the design were:

- (1) Temperature of the metal portions of the fitting must be maintained below acceptable limits, e. g., 1700°F for Inconel 718.
- (2) The aluminum must not exceed 350°F with an initial temperature of 130°F.
- (3) Temperature of intermediate insulators must be maintained to acceptable levels.

To achieve this, long conduction paths were employed in the design, and conduction area was reduced as required.

The final design evolved in an iterative fashion with thermal analyses guiding the design evolution. The planned approach was to perform design analyses studies to arrive at a preliminary design configuration, which was built and tested. The test data was intended to confirm analysis

techniques or provide data for modification of analysis so that predictions of performance of the final configuration could be made with confidence. However, the initial test component met with disaster in a severely overheated and, consequently, non-representative test. In a retest the test component was of the final design configuration so that analysis and test were directly applicable to the Task 1 design.

This section summarizes analyses leading to the selected design concept, discusses the tests of the two support lug components and covers analysis results of the test data in support of the final design.

1.3.1 PARAMETRIC ANALYSIS

There are two basic elements of the support lug design: (1) the details of the lug bolt joint and (2) the bracket configuration. Early design of the lug bolt employed ceramic insulators like that shown in Figure 66. The philosophy was that in order to reduce the temperature of the metal lug bolt and metal bracket to acceptable levels, an insulator (ceramic) must be employed between the RPP and the metal. Much of the initial analyses were based on this approach. Ultimately, an all-metal design was found acceptable as discussed later.

Support bracket design followed two basic themes as illustrated in Figure 67. Configuration 1 uses a metal support fitting which is insulated at the aft end by a material like fiberglass. This is a rather conventional approach but has certain drawbacks, among them being: (1) the large contact area between metal bracket and insulator, and between insulator and the aluminum front beam produces a large conduction area through the insulator, (2) attachment bolts through the insulator provide direct heat shorts into the aluminum, and (3) the insulator must be thick and therefore heavy if a substantial temperature drop is desired. Typical results using this approach indicated that it would take slightly in excess of 0.6 in. thick silicon fiberglass laminate at the aft end of the fitting to maintain aluminum temperature below 350° F if fused silica insulators were used at the lug bolt. Greater than 0.8 in. thickness of silicone fiberglass would be required

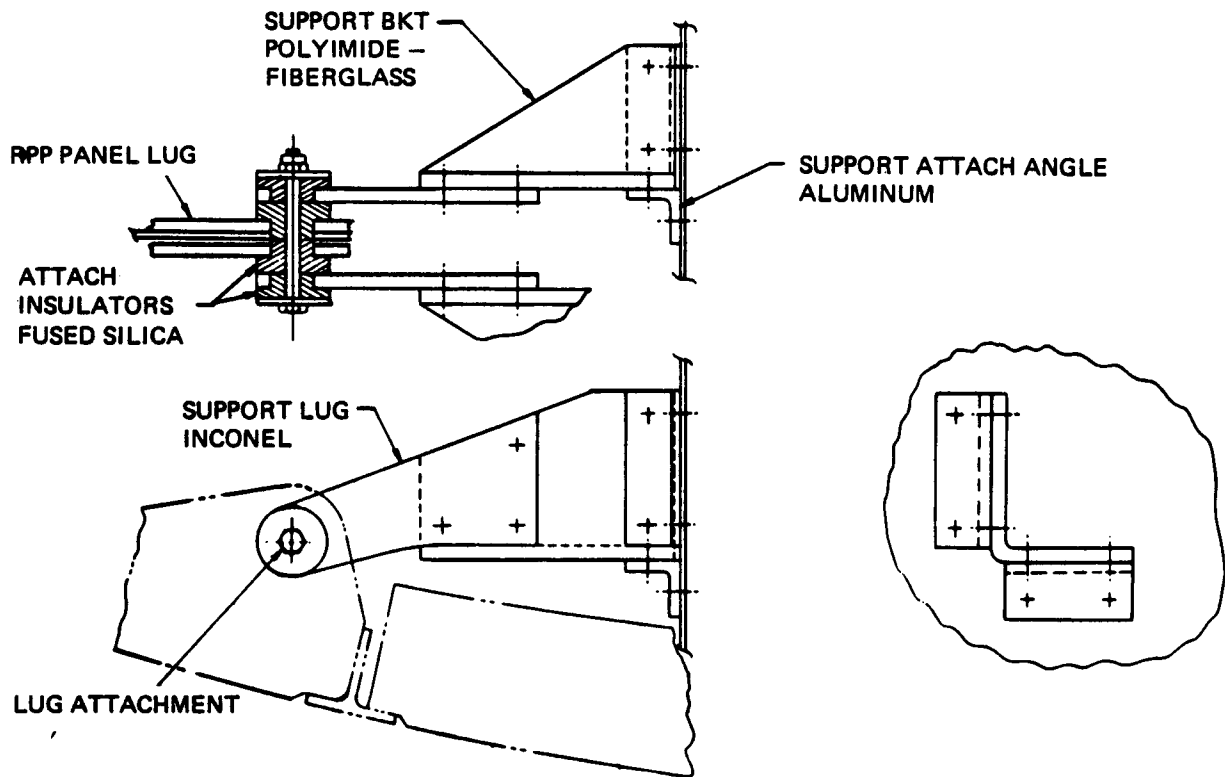


FIGURE 66 EARLY SUPPORT JOINT DESIGN

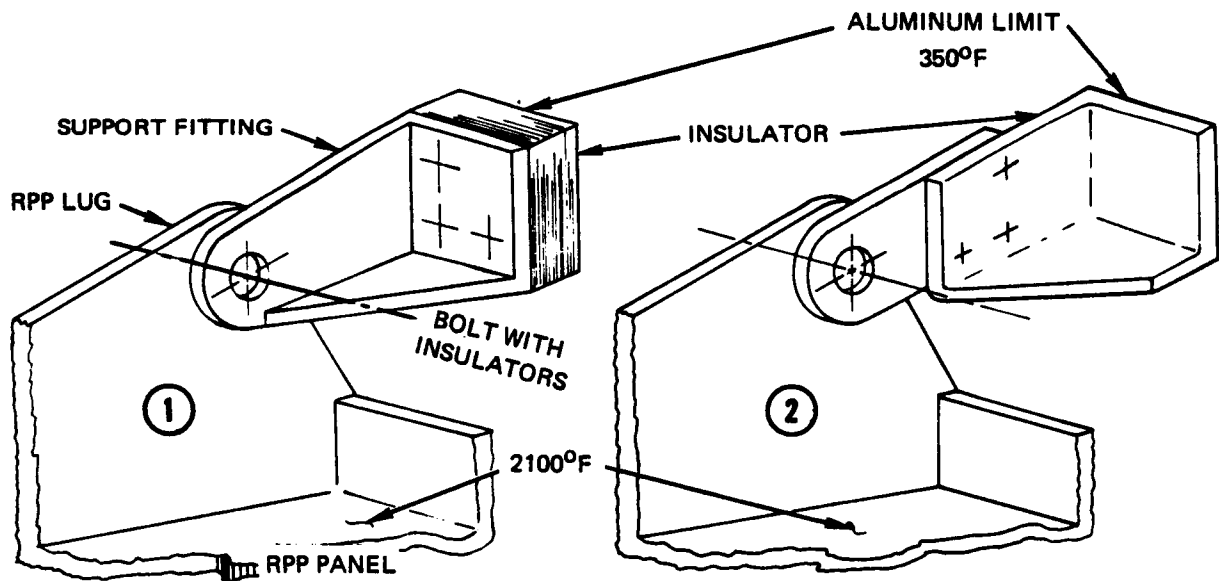


FIGURE 67 SUPPORT BRACKET CONCEPTS

if zirconia insulators were used at the lug bolt.

Configuration 2 of Figure 67 utilizes a technique wherein the aft insulator is in series with the metal bracket and also functions as structure. The design shown indicates that the insulator is built as a bath tub fitting and ties into the aluminum front spar. The alternative to this arrangement is to employ separate aluminum attach angles between the insulator and front spar, thus relieving the insulator from the difficult task of carrying the structural loads around a corner and into the tie-down bolts. Typical results, using 0.2 in. thick silicone fiberglass laminate for the aft end of the bracket and fused silica insulators at the lug bolt, produced 292°F aluminum temperature and 645°F fiberglass temperature. This indicated performance was attractive and, therefore, this basic approach was pursued further, while Configuration 1 was dropped from further consideration.

Once the concept for the aft end of the bracket was selected, effort was concentrated on the lug bolt/insulation design. Analysis had shown that with ceramic insulators bolt temperature was only 1200°F and could be permitted to operate at least 500°F or more higher, depending upon the metal selected. Furthermore, the aluminum temperature had a safe margin with the metal/fiberglass bracket design, and indicated that perhaps an all metal lug bolt design could be employed to eliminate the brittle and potentially unreliable ceramic insulators.

Analysis showed that a tubular Inconel lug bolt had the potential for limiting Inconel temperature to 1350°F and polyimide fiberglass temperature to 620°F, both within design temperature allowables. On this basis the initial test article was configured to employ a metal lug bolt design.

1.3.2 INITIAL TEST

The initial test component is pictured in Figure 68 as installed for test, while the lug bolt design is illustrated in Figure 69. The component was insulated with Dynaflex (12 lb/ft³) insulation^s to simulate flight insulation around the support bracket and lug joint, but Figure 68 does not show this for clarity. In Figure 68 the configuration of the test article is readily seen. It is like that of

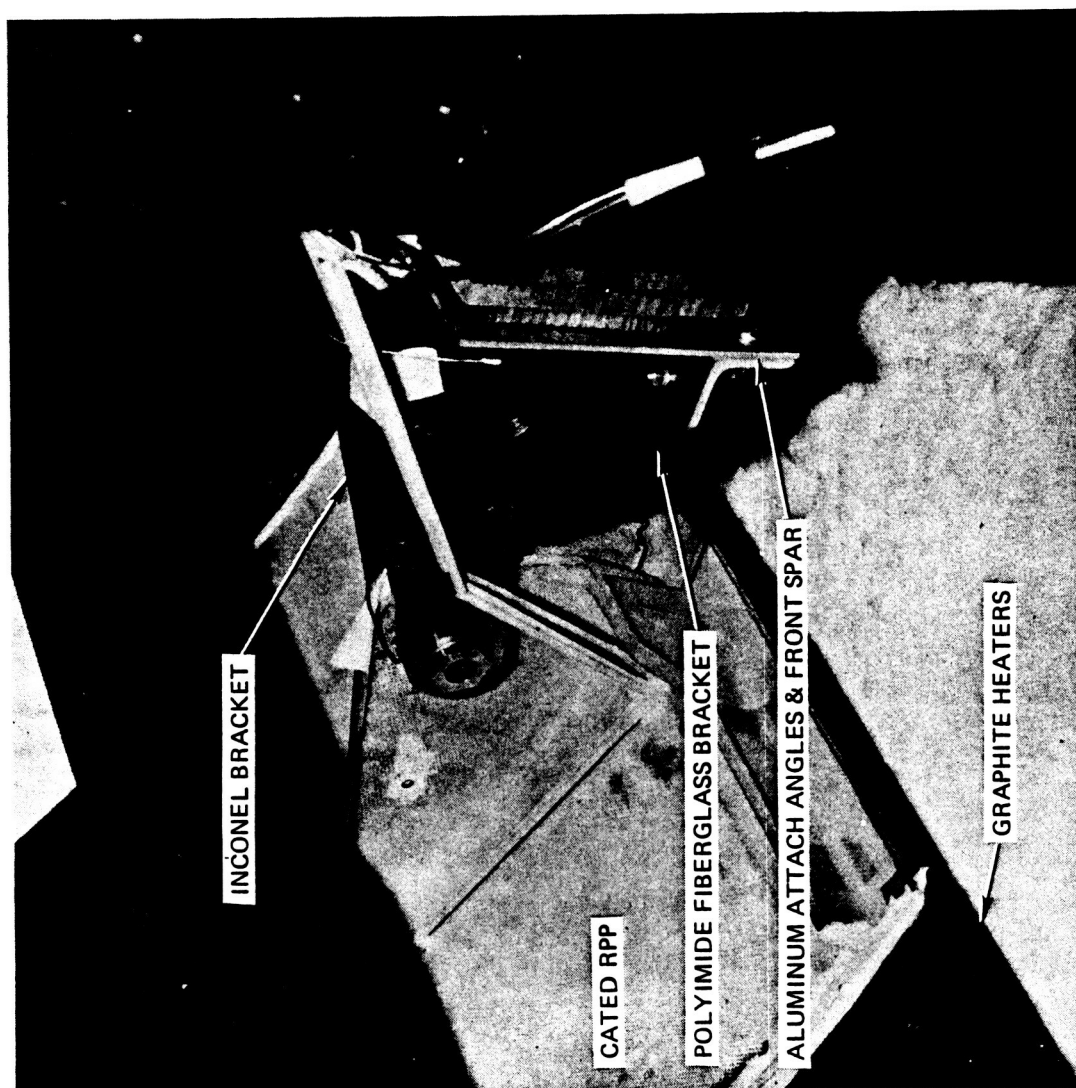
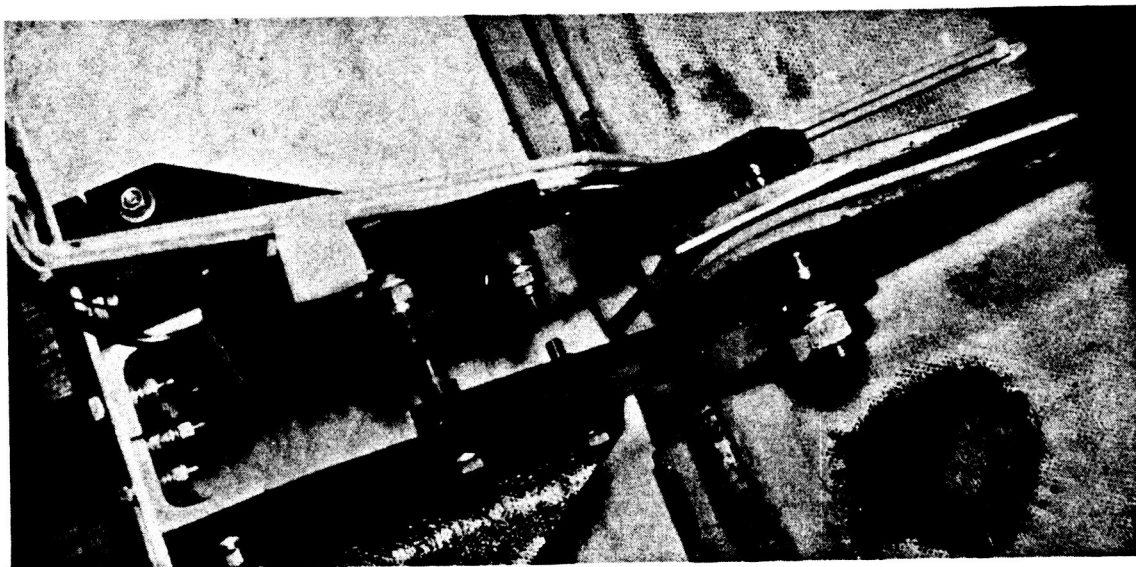
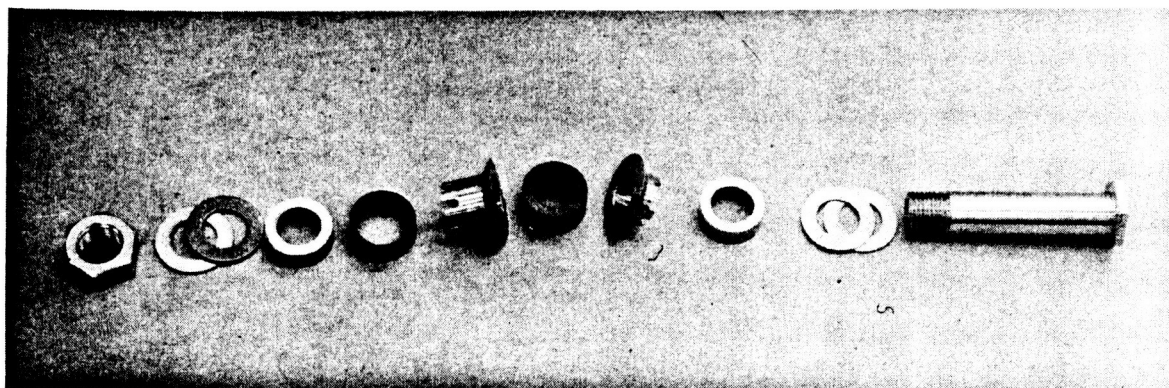
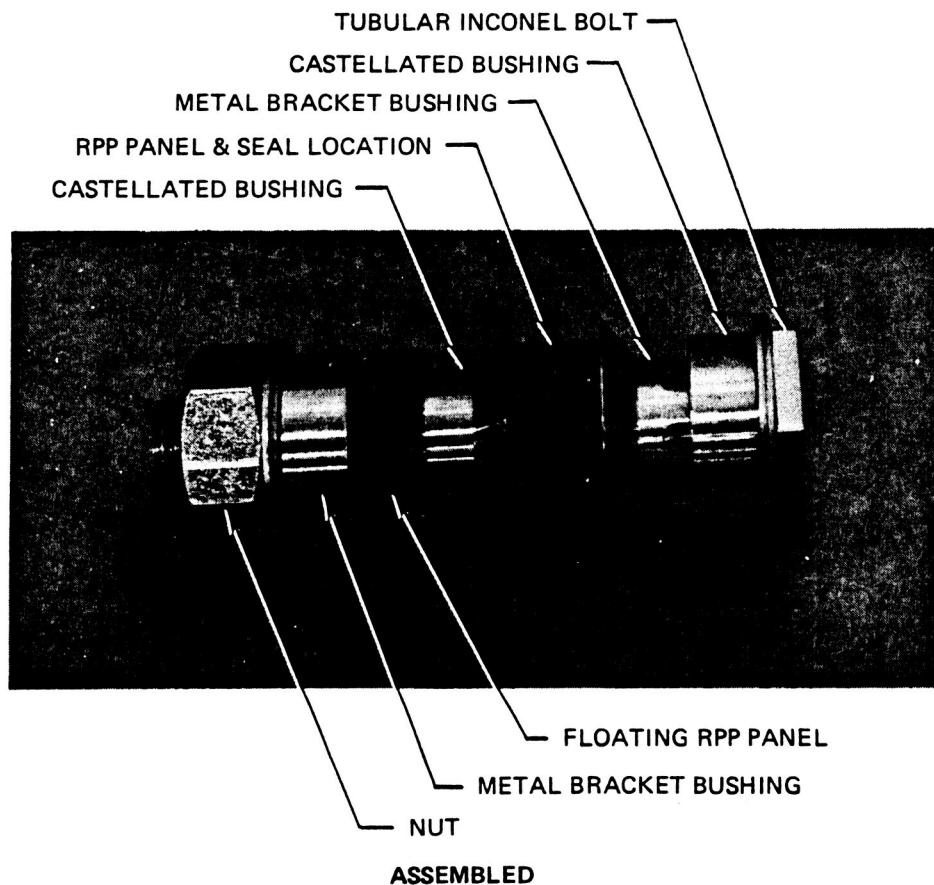


FIGURE 68 INITIAL SUPPORT LUG — COMPONENT TEST



COMPONENT PARTS

FIGURE 69 LUG BOLT FOR COMPONENT TEST

Figure 66, except that the fused silica insulator system was replaced by the bolt assembly of Figure 69. This assembly is like that used in the final design (Figures 1, 5, and 6). However, since Phase II RPP parts were used in the test, the existing 3/4 inch diameter lug holes had to be bushed with graphite to fit the lug bolt assembly. Similarly, the Inconel bracket holes, which were initially configured for the fused silica insulators, were bushed as indicated in Figure 69.

The lug bolt was an 0.5 inch diameter tubular bolt sized to provide high bending stiffness and low RPP bearing stresses. Two castellated bushings secure one leading edge panel and seal strip, while the other leading edge panel is permitted to slide on the longer of the castellated bushings to accommodate thermal expansion requirements. Castellated ends are employed to reduce conduction contact area to the metal brackets.

Graphite resistant heater rods were used to heat the RPP and insulation around the joint. The component was tested at one atmosphere conditions, because heat transfer effects at reduced atmosphere were considered insignificant for this test. However, this turned out to be the prime factor that destroyed the test article and invalidated results. Flames were observed during test, possibly from outgassed products from the surrounding insulation or graphite. These produced convective heating currents that flowed through various cracks or gaps in the insulation and thoroughly overheated certain areas of the test component.

A time-temperature profile was followed that approximated the design entry profile, except that cooldown rate could not be achieved, which aggravated the overheat situation. The temperatures measured were 1640°F on the bolt, 1426°F at the polyimide fiberglass, and 450°F on the aluminum.

Post-test analysis indicated that the only explanation believed valid for the high temperatures achieved is that convection and/or combustion effects were responsible for the results. Since the results are meaningless in terms of design/analysis influence, they are not shown.

A retest was required to develop the data required from this task, but a number of significant changes were made to ensure representative testing. This is discussed below.

1.3.3 DESIGN CONFIGURATION LUG SUPPORT TEST

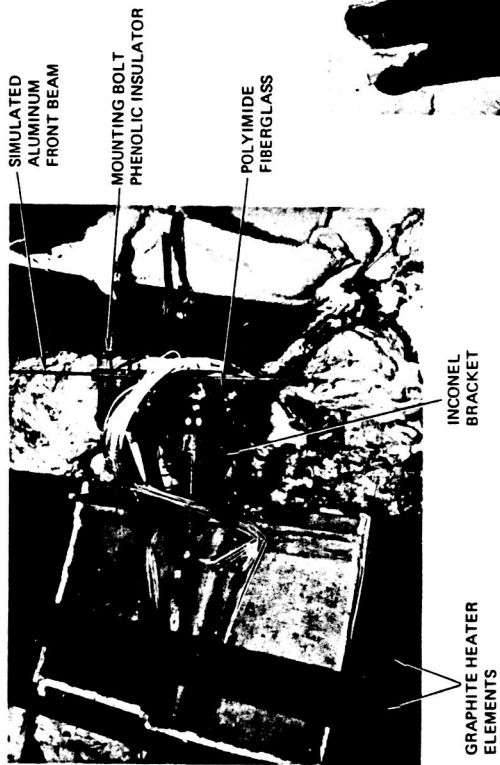
Since a retest was required, new test hardware, duplicating the Task 1 design (Figure 6) was used. The retest was conducted in an inert atmosphere at 10 mm Hg pressure to simulate the average entry pressure during the high temperature period of the trajectory. Cooldown control was improved by removing insulation immediately behind the graphite heaters. Calibration runs indicated that close control could be achieved for 40 minutes or to a point where heater temperature was down to 1200°F. Beyond that slight conservatism in total heat input existed, but was acceptable.

In addition to the support bracket design change from the initial test configuration, the mass of the simulated aluminum front beam was increased to be more representative and include that portion behind the lug support insulation. The lug insulation was changed to 10 lb/ft³ Dynaquartz and replaced the Dynaflex in the initial test.

The objectives for the retest were slightly different from the initial test. Since the test configuration represented the final Task 1 design, the results of this test would verify design adequacy. The other objective of confirming analysis techniques remained as before.

Pretest predictions were that the aluminum temperature would peak at 235°F while the polyimide fiberglass would reach 345°F. Thus, high thermal margins were indicated by the new design.

The test article is shown in Figure 70 after test. Significant elements are indicated. Two thermal tests were performed in the vacuum chamber with the modified support lug design. All temperatures were well below the allowed maximums for both tests. Test data for the first and second tests are shown in Figure 71.



139 a

FIGURE 70 DESIGN CONFIGURATION SUPPORT LUG THERMAL TEST

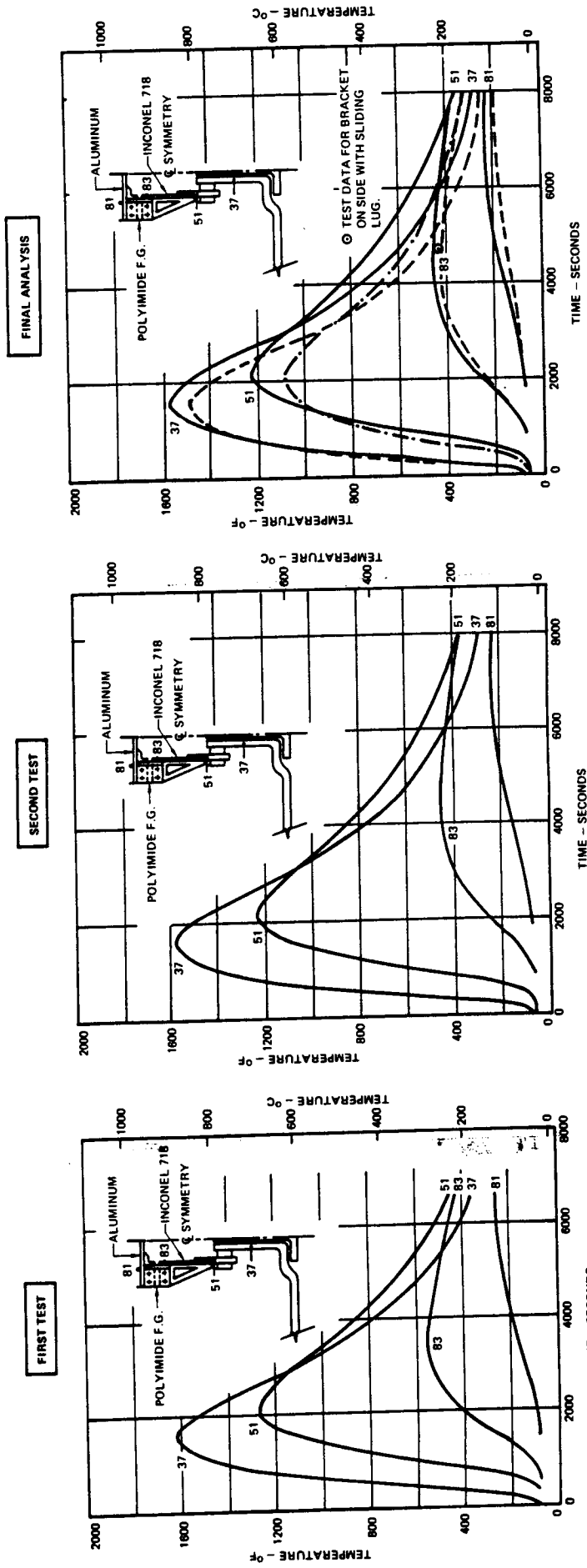


FIGURE 71 TEST RESULTS DESIGN SUPPORT LUG THERMAL TEST

FIGURE 72 RPP LUG TEST FINAL PREDICTIONS VS TEST DATA

The first test produced maximum temperature of the polyimide fiberglass and the aluminum of 550°F and 255°F , respectively. Maximum temperatures of the polyimide fiberglass and aluminum were 450°F and 231°F , respectively, for the second test. These temperatures contrast to an allowable of $650 - 700^{\circ}\text{F}$ for the polyimide fiberglass and 350°F for the aluminum, and the above noted pretest predictions.

In the first test, insulation was not installed in the cut-out areas of the brackets, but in the second test, insulation was included to better represent the flight configuration. However, post-test analysis showed that this would not affect polyimide fiberglass temperature by more than 13°F . Also, for the first test, the maximum temperature of the RPP skin in the vicinity of the lug was too high (2360°F compared to a desired value of 2050°F); and the input temperature of the insulation around the support bracket peaked 300°F higher than planned. For these reasons the second test was conducted and achieved closer control of applied temperatures. Resultant temperatures of the Inconel, fiberglass, and aluminum were therefore closer to predictions. Because the second test was more representative of the desired test conditions, only that test is discussed.

The peak temperature of the polyimide fiberglass was 450°F and the aluminum reached only 231°F . Maximum Inconel lug bolt temperature was 1320°F . All temperatures were well within the allowable for the materials involved (see Section 1.3.5 for polyimide fiberglass test data).

However, maximum temperature of the polyimide fiberglass for the second test was 100°F above the predicted value of 345°F . Post-test analysis was performed to determine required changes to the thermal model of the test configuration so that it yields better predictions. These analyses are discussed below.

1.3.4 TEST ANALYSIS

Two major areas of disagreement between analysis and test were found. First, polyimide temperature calculations were 100°F low, and second, predictions indicated that temperatures in the Inconel should peak

earlier. Pretest predictions were based on infinite joint heat transfer coefficient to conservatively estimate the aluminum temperature. In fact, however, joint coefficient during test was a variable so that part of the test evaluation analysis was concerned with estimating joint coefficient actually achieved.

Post test thermal analyses were performed using a three-dimensional thermal model and a VSD computer routine which accounted for heat conduction along the skin and RPP rib, across the contact surfaces at the support joint, through the steel bolt and the bracket, and across the fiberglass insulation into the aluminum wing structure. Cross radiation from the skin to the portion of the RPP rib outside the bulk insulation and radiation along the expansion gap between the rib and sealing strip was considered, as was heat conduction through the bulk insulation and into the support joint. Input temperatures were those measured in test for the RPP skin and Dynaquartz insulation around the support bracket and bolt. A number of thermal model variables were changed independently to determine their temperature sensitivity and ascertain significant model changes for best predictive capability. Results of these analyses are summarized in Table 8. Results showed that much better agreement could be achieved by making two changes to the model: (1) thermal conductivity values used for the Inconel needs to be increased by 20%, and (2) contact coefficient at the support joint needs to be made a function of the temperature of the joint. The joint coefficient should be low (starting at about 25 BTU/hr ft² °F) for low temperatures and high (approaching infinity) for high temperatures. This predicts the temperature response delay as well as the maximum temperature for the Inconel.

A comparison of measured temperatures from the final thermal test and computed temperatures from the final thermal model as a function of time is shown in Figure 72. Joint coefficients was varied from 25 BTU/hr ft² °F at 180°F to 40,000 BTU/hr ft² °F at 2000°F. Reasonable agreement was obtained between the test and analysis results. The main

TABLE 8 PREDICTED TEMPERATURES - EFFECTS OF SYSTEM VARIABLES

VARIABLE	EFFECTS OF CHANGE
Contact Coefficient at Joint	Increasing the contact coefficient from a constant value of 100 BTU/hr ft ² °F to a constant value of 400 BTU/hr ft ² °F increased the maximum polyimide temperature by 63° F. Further increase in the coefficient yields smaller increases; changing from 400 to infinity (perfect contact between the parts of the joint) increased the maximum polyimide temperature by only 33° F. Reducing the contact coefficient from infinity to a value of 25 BTU/hr ft ² °F (loose fitting parts) greatly improves the computer predictions for the hot end of the Inconel during the first 700 seconds of test time.
Thermal Radiation in Gap Between T-Seal Strip and Panel Lug	Accounting for radiation in the 0.06 in. wide gap resulted in a 13° F increase in temperature at the hot end of the inconel and a 3° F increase at the polyimide.
Heat Input from the Sides of the Insulation	Predictions using the same surface temperature for the sides of the lug insulation as was used for the front of the insulation, yield approximately the same polyimide and aluminum temperatures as obtained with no heat input from the sides of the insulation.
Polyimide F. G. Conductivity	Reducing the conductivity to 1/2 the nominal value decreases the aluminum temperature slightly (5° F) but increases the polyimide/inconel interface by 43° F. Temperatures near the hot end of the bracket are not affected.
Treatment of Cut-outs in the Brackets	Prediction with insulation in the cut-outs instead of cross-radiation in the cut-outs results in a decrease in the temperature of the polyimide of 13° F and a decrease of 9° F of the aluminum.

TABLE 8 PREDICTED TEMPERATURES - EFFECTS OF SYSTEM VARIABLES (Cont'd.)

VARIABLE	EFFECTS OF CHANGE
Thermal Conductivity of Inconel 718 Bracket	Increasing the thermal conductivity by 20% results in much better agreement with the measured temperature drop in the bracket. The predicted temperature at the cold end of the bracket (at the inconel/polyimide interface) was increased from 387° F to 428° F.
Dynaquartz Insulation Thermal Conductivity	Increasing the thermal conductivity of the insulation by about 60% (using 1 atmospheric properties instead of 10 MM Hg properties) has only a small effect upon the predicted temperatures of the aluminum and the polyimide.
Conduction from Brackets to Insulation	Because of the thermocouple leads, it was difficult to have good contact between the sides of the brackets and the insulation. With the contact area reduced to approximately 20%, a 21° F higher peak temperature of the polyimide fiberglass was found.

difference is that the RPP flange near the bolt (node 37) peaked at a temperature 100°F higher during the test than the calculated value. This resulted in other temperatures on the Inconel bracket and aluminum being slightly higher than calculations. Further improvement in the agreement between test and analysis results would require either increasing RPP conductivity or increasing input RPP skin temperatures in the model. However, there is no test data to justify such changes.

Part of the reason for the difference between test data and predictions is that more than half of the total heat input to the aluminum travels through the fixed side of the RPP joint rather than the sliding side. Peak temperatures measured on the sliding side are shown in Figure 72 for reference. Peak temperature drop through the sliding side was 95°F less than for the fixed side. The thermal model, however, was based on the fixed portion of the joint and assumed symmetry about the centerline of the T-seal to maintain the problem within reasonable computational bounds.

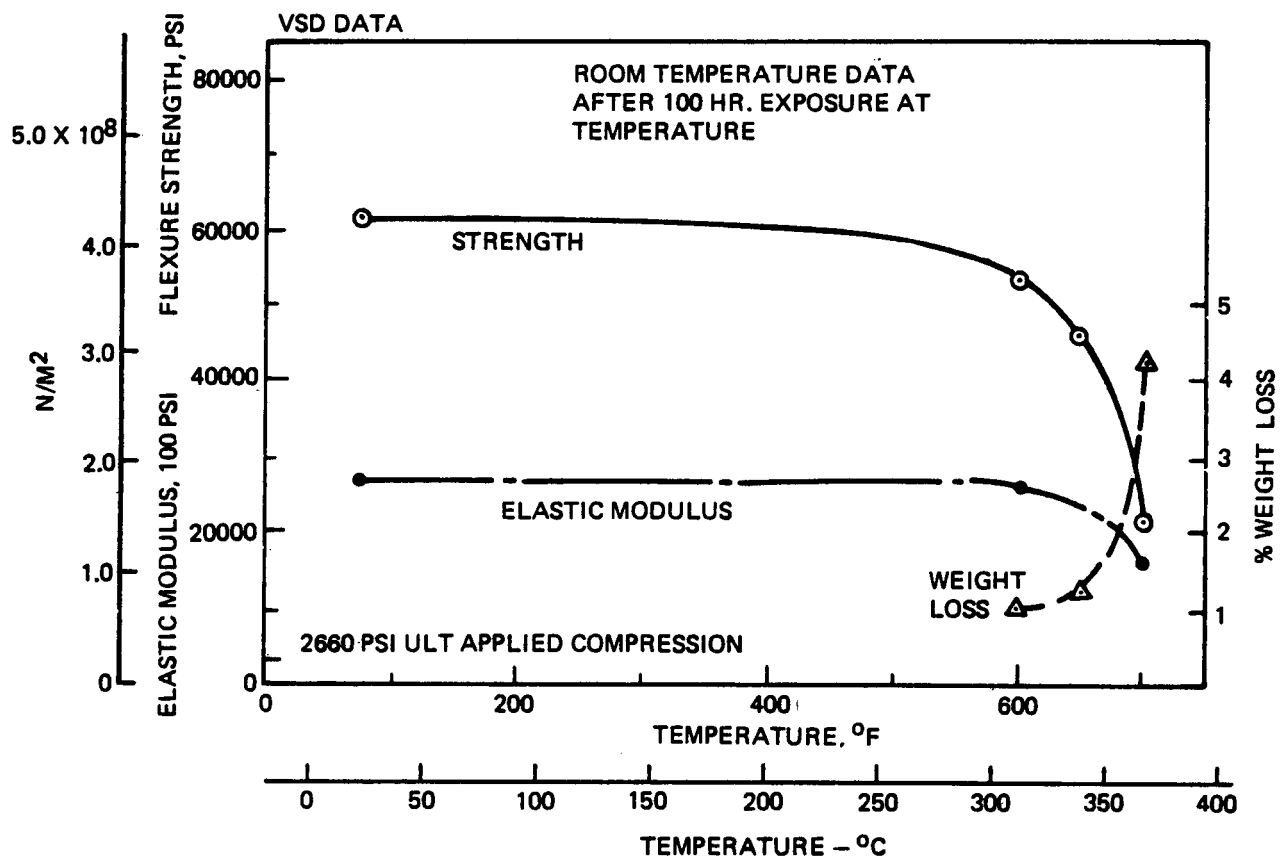
Note in Figure 72 that after a time of 1500 seconds, all the predicted temperatures are below the test data. This tends to indicate that more heat was input to the RPP than was simulated in the predictions. In order to increase the predicted temperatures to the test values one of the following methods would be required: (1) increase the thermal conductivity of the RPP so that node 37 would get hotter, or (2) increase the RPP skin temperatures to values greater than those recorded during the test. Since there is no test data to justify making either of these changes, the results of Run 44 were considered the final predictions.

In summary, the support lug thermal test demonstrated that the design is acceptable and has a good thermal margin. Also, with rational adjustments to joint heat transfer coefficients to account for temperature sensitivity and consideration of possible variations in conductivity of the materials involved, analysis can satisfactorily predict experimental results.

1.3.5 POLYIMIDE FIBERGLASS TEMPERATURE LIMIT

Fundamental to the support lug design is the capability of the polyimide fiberglass to operate reliably for 100-missions within the temperature levels required. Tests were conducted on this material to gain the confidence necessary for its selection. Data collected included both vendor and in-house test results. A summary of findings is given in Figure 73.

Based on thermal analysis of the support bracket, it was estimated that the polyimide fiberglass material would operate within 50°F of its peak temperature for 100 hours for 100 mission life. Exposure for test data was therefore limited to 100 hours. Flexure data was obtained for ease to establish data trends and tests were conducted up to 700°F. Shown for comparison on Figure 73 is the maximum ultimate applied stress level (maximum during launch) in the polyimide fiberglass for the support bracket. The stress level is only 2660 psi in compression and, even when compared against the 700°F exposure data which produces 20,000 psi flexure strength, a high margin of safety is indicated. VSD would normally like to limit the allowable temperature to 600°F for the polyimide fiberglass, but temperature exposure to at least 700°F appears feasible if required, even though significant strength reduction is experienced.



VENDOR DATA

CONDITION	FLEXURE PSI	COMPRESSION PSI	TENSION PSI
ROOM TEMP AS FAB.	64000	45000	53000
100 HR. AT 600°F TESTED AT 600°F	33900	22800	—

FIGURE 73 POLYIMIDE FIBERGLASS LAMINATE TEST DATA

The segmented construction of the VSD Leading Edge design introduces small gaps and external grooves between adjacent RPP panels, which are required to accommodate thermal expansion. The gaps are covered by RPP seals to minimize the leakage of hot boundary layer air during ascent and entry. However, small surface gaps and grooves will be unavoidable, and tests and analyses were required in Phase III to fully evaluate their effect upon local RPP temperatures in joint areas. The purpose of this task, seal strip joint gas leakage, was to establish the magnitude of external and internal heating effects due to gas leakage and to determine methods of minimizing or eliminating this leakage if found excessive in the current design.

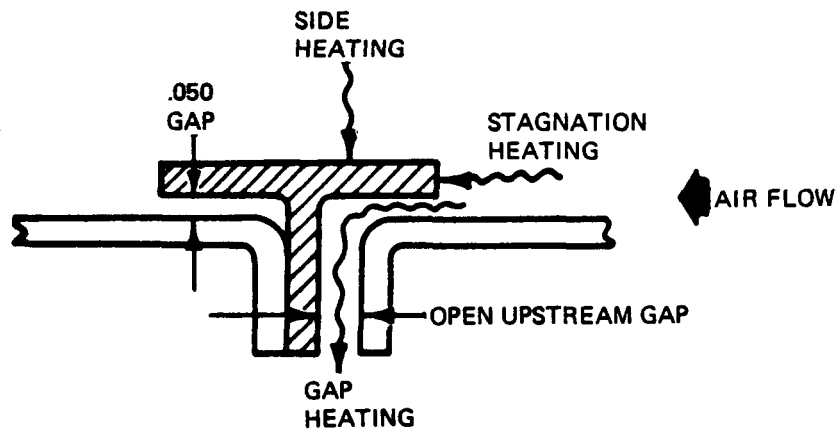
In the initial phase of Task 4, while correlation analyses were being made between plasma arc test flow conditions and entry conditions, VSD made an early analysis of entry air flow, heating rates, and seal strip temperatures resulting from the then current seal strip design having an assumed gap width of 0.050 inches. The analysis initially indicated that heating effects could be excessively severe. The importance of this development focused attention on the Task 4 program and created a corresponding increase in sophistication to the gap simulation test model. Simultaneously, an in-house effort was initiated to explore other practical joint seal design concepts prior to freezing the design for the gap test model. Despite the greater emphasis placed upon the gap heating investigation, the basic plan initially envisioned for the test program was basically followed with little perturbation other than taking expanded precautions for assuring faithful simulation of gap sizes, angles of attack, leading edge sweep angles and optimum placement of the gap test region in the plasma arc plume.

This section covers all aspects of Task 4 including thermal analyses, alternate joint design concepts, the test model design, instrumentation design and installation development, the calibration model design, test plan, the teflon test model, test program results, and the final thermal math model and analysis.

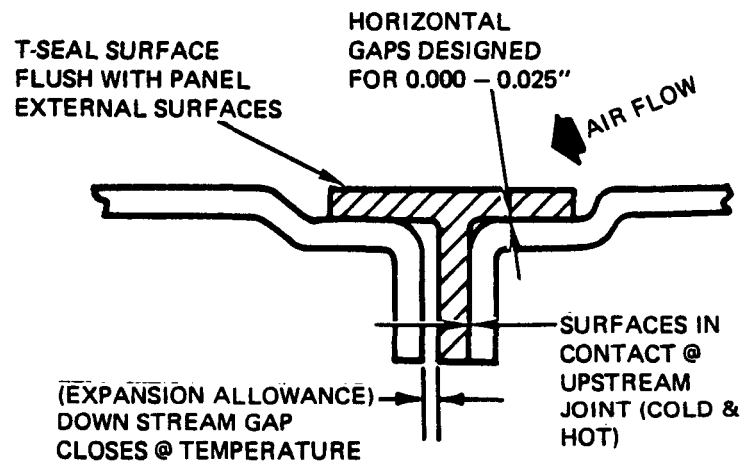
1.4.1 ALTERNATE DESIGN CONCEPTS

The early thermal analysis predicting unacceptable heat conditions mentioned above was based on certain assumptions which were not realistic and which were not pertinent to the T-seal strip design. Nevertheless, the Phase III in-house study of alternate seal designs was benefited at the outset by the thermal analysis problem statement that temperature increases due to gap leakage came from three heat sources: (1) stagnation heating on the T-seal edge, (2) gap flow heating, and (3) side heating on the exposed surface of the T-seal. The early analysis would be valid if the T-seal, as was assumed, completely protruded from the external surface with an assumed 0.050 inch gap oriented forward into the airstream. Although the actual T-seal design, in fact, does not protrude and does not include an open upstream gap as seen in the comparison of Figure 74, by highlighting possible design pitfalls the analysis made evident certain useful design criteria for use in generating new seal concepts and for refining the existing design. The design criteria included the following guidelines:

- o Seals should be made to fit perfectly flush as much as possible to minimize stagnation heating.
- o Shorten seal overlap length to reduce its conduction path back to cooler regions, thereby reducing seal leading edge temperatures.
- o Shield the exposed seal leading edges as much as possible by squaring off panel joggles adjacent to the seal lip.
- o Increase the seal thickness to provide a larger conduction cross-section for heat transfer away from seal leading edge.
- o Place the expansion allowance gap on the downstream side of the seal to avoid a possible "air scoop" effect.
- o Trim seal edges at an angle to match panel joggle angles at expansion gaps in order to reduce size of large external grooves.



ASSUMED JOINT DESIGN USED IN PRELIMINARY THERMAL ANALYSIS



JOINT DESIGN DEVELOPED IN PHASE II

FIGURE 74 COMPARISON OF PHASE II JOINT SEAL DESIGN VERSUS INITIAL THERMAL ANALYSIS MODEL

- o Eliminate or minimize external and internal gaps and provide full contact of adjacent part mating surfaces throughout the mission as much as possible.

Using this criteria, 25 joint/seal design concepts were generated which were arranged into six categories. A typical example of each category is shown in Figure 75. The tongue and groove approach of Concept A permits panel thermal expansion while at the same time inhibiting gas flow through the joint. Concept B is one of many ship-lap configurations which eliminates the upstream gap in the T-seal approach and thereby eliminates a seal leading edge in the joint system. Several approaches represented by Concept C provide a close fit condition prohibiting protrusions into the air stream by the use of a stored energy device for mounting the "T-strip" or "strap" seal. Concept D shows a typical joint gap sealed by an internal "secondary seal", i. e., a "springy" seal trapped just inside the panel external overlap seal. Concept E, a variation of Concept D, makes the internal seal feature integral with the panel structural flange and relies on the RPP material elasticity to flex as the expansion gap width changes with thermal variations. Concept F, a further variation of the internal seal, features a separately mounted internal member which keeps the adjacent panel flanges clamped, and gaps sealed. Concept F like Concept E relies on the RPP material elasticity for flexing under thermal growth.

Each of the many ideas included in the six categories presented in Figure 75 retains one or more attractive features of the Phase II T-seal design, but each introduces problems, many irreconcilable, adds costly manufacturing and operational complexities and sacrifices a significant retention redundancy feature inherent in the T-seal concept. Consequently, the Phase II T-seal approach was refined to offset any undesirable feature conflicting with the above design criteria. The result of this refinement is presented in Figure 76 which lists the desirable features not completely inherent in the alternate concepts. The design in Figure 76 was traded off against all 25 alternate concepts at VSD by knowledgeable members of several departments who were familiar with the RPP material

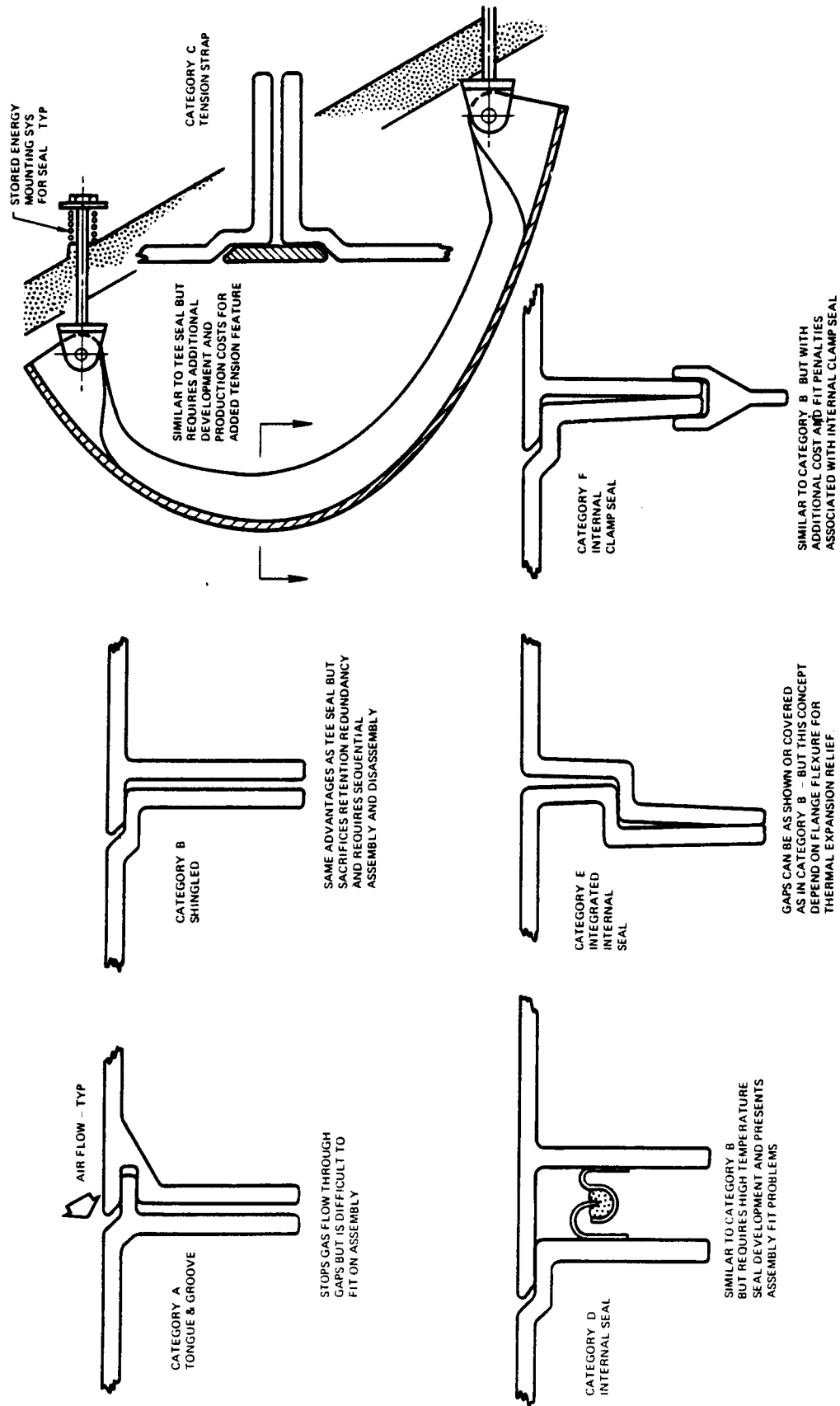


FIGURE 75 TYPICAL EXPANSION JOINT SEAL CONCEPTS

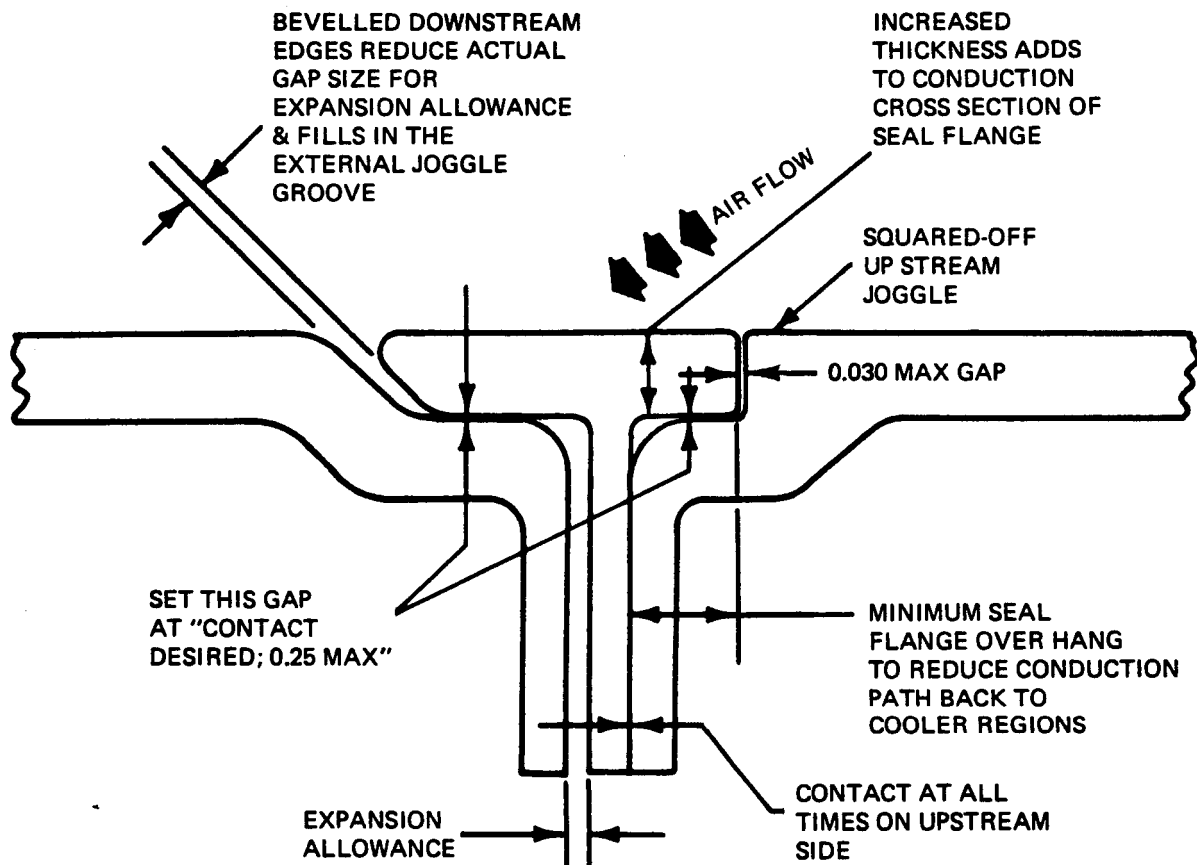


FIGURE 76 REFINEMENTS MADE TO PHASE II JOINT SEAL DESIGN

and it was determined that:

- (1) The T-seal/expansion joint concept developed in Phase II and refined in Phase III is superior to all other concepts.
- (2) The T-seal concept would not produce the undesirable features assumed in the early thermal analysis.
- (3) The Task 4 gap heating test model should incorporate a T-seal design and utilize as many of the refinement features permitted by the subscale test model.
- (4) The refined T-seal design should be incorporated in any new leading edge work done beyond Phase III (by contract, no new seal parts were to be produced in Task 1)

With the superiority of the T-seal design reconfirmed by the results of the alternate concept investigation, VSD proceeded with the gap heating test plan and with the formulation of a test model gap configuration matrix.

1.4.2 TEST PLAN AND GAP CONFIGURATIONS

The objective of the Task 4 plasma arc evaluations were to:

- (1) Determine the magnitude of the gas leakage heating through the seal strip.
- (2) Provide parametric data on effect of flow and seal design variations upon model temperatures.
- (3) Provide confirmation or correction to gas leakage analysis methods.
- (4) Evaluate potential methods of eliminating or reducing gas leakage heating.

To accomplish these objectives, a modular test model was designed and fabricated having optional arrangement capabilities to produce the required gap configurations shown in Figure 77. The model shown in Figure 78 was a full-scale section of the NASA-JSC 25K Shuttle Orbiter vehicle wing tip leading edge represented by the NACA 0010-64 air foil. This

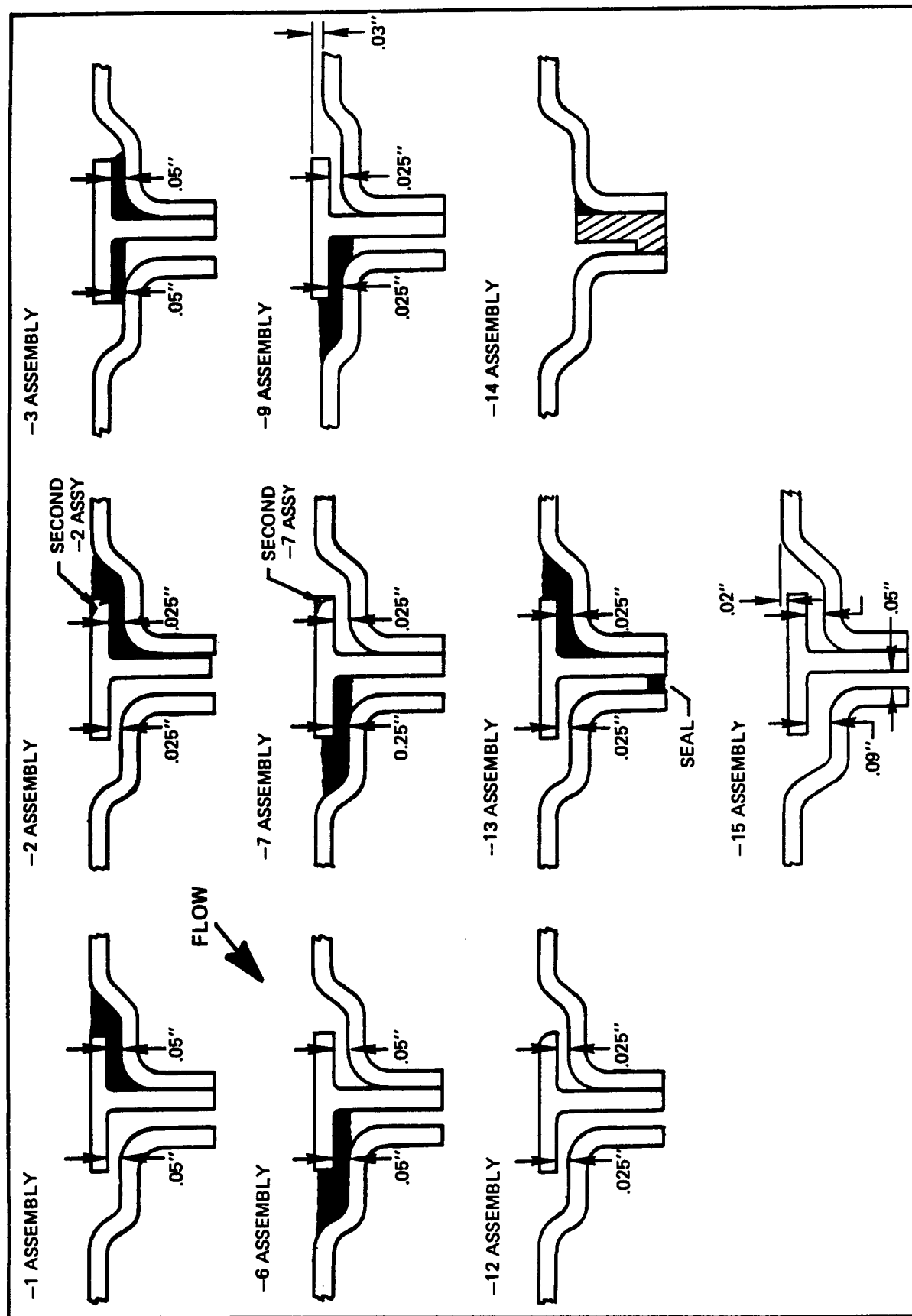


FIGURE 77 SEAL GAP TEST CONFIGURATION MATRIX

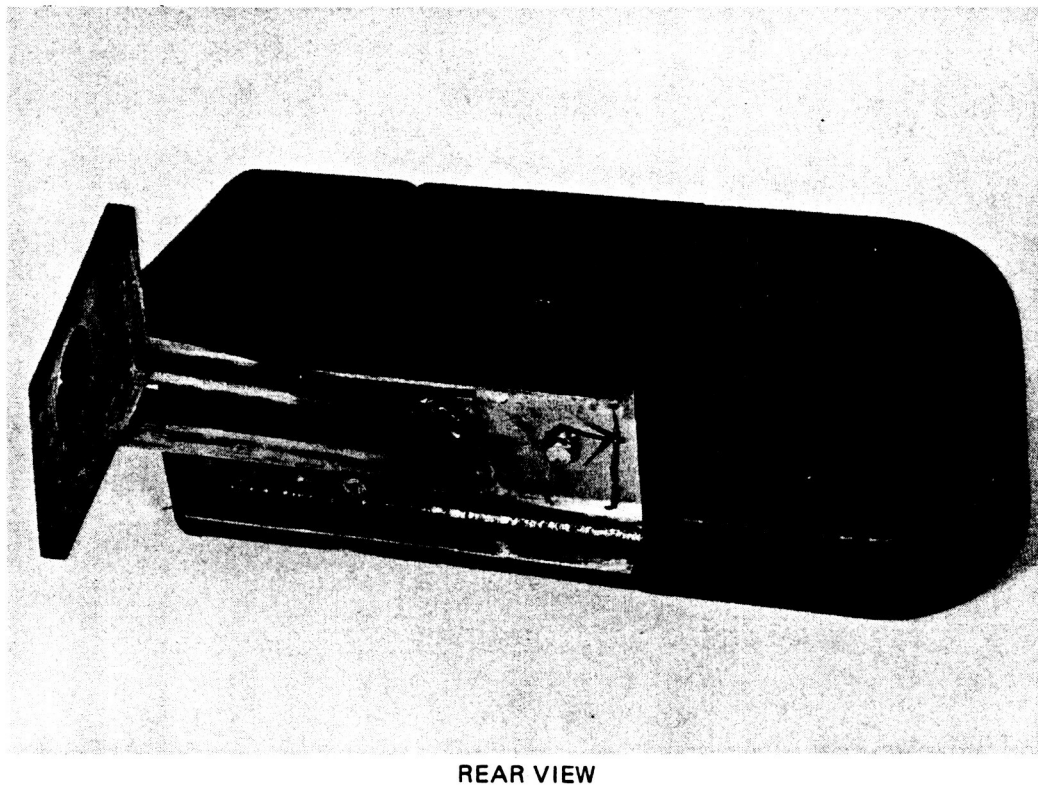
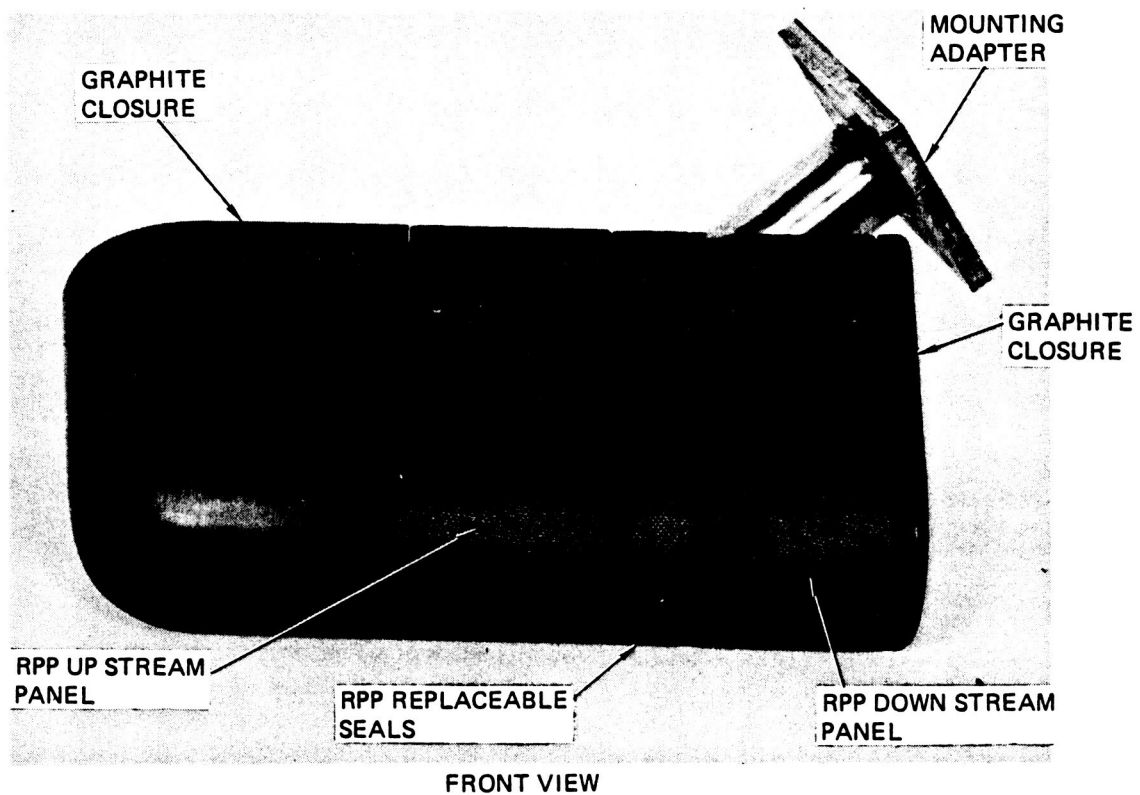


FIGURE 78 GAP HEATING TEST MODEL

configuration was selected for the following reasons:

- (1) Consistency with test facility.
- (2) Desirability of employing a model which will represent entire gas leakage flow pattern.
- (3) Pretest analyses indicated model configuration provides reasonable simulation of boundary layer flow.

The basic model size was 12.5 inches wide by 5.25 inches long with a 1.61 inch leading edge radius and model material was bare RPP-1 with graphite end closures. The width of the model was split into two sections by a seal strip which provided for adjustable seal geometry. Four seal strips were constructed to obtain the nine seal geometries in Figure 77. Model ends were closed out with graphite aerodynamic fairings and the downstream fairing included a vent to free stream. Mounting to a sting adapter assembly was accomplished with a graphite back closure. This closure was insulated with carbon felt. The model was instrumented with sixteen thermocouples, the locations of which are shown in the test results section below.

A calibration model was designed and fabricated by VSD for use in the test facility. This model having the same size and external contour as the gap test model was instrumented with nine pressure taps in line with nine calorimeters arranged as shown in Figure 79.

As an adjunct to the primary gap heating test model, an alternate model was fabricated using a build-up of Avcoat 5026-39HCG Ablator material. The center section of the model containing the gap configurations was fabricated of Teflon material. The purpose of this back-up model was to provide test data augmenting the test results of the primary model in the event test data proved erratic, inadequate or inconclusive. Although test runs were made on the back-up teflon model, shown in Figure 80, it became unnecessary under the circumstances to analyze the results since test data gathered from the principal test revealed a consistent pattern.

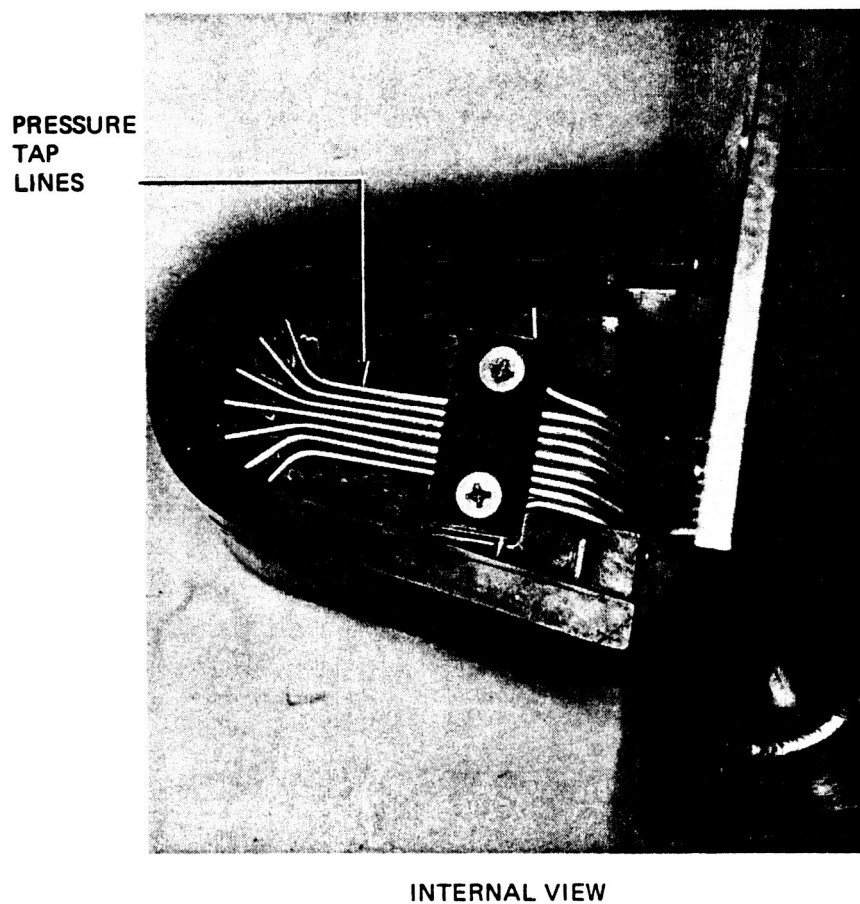
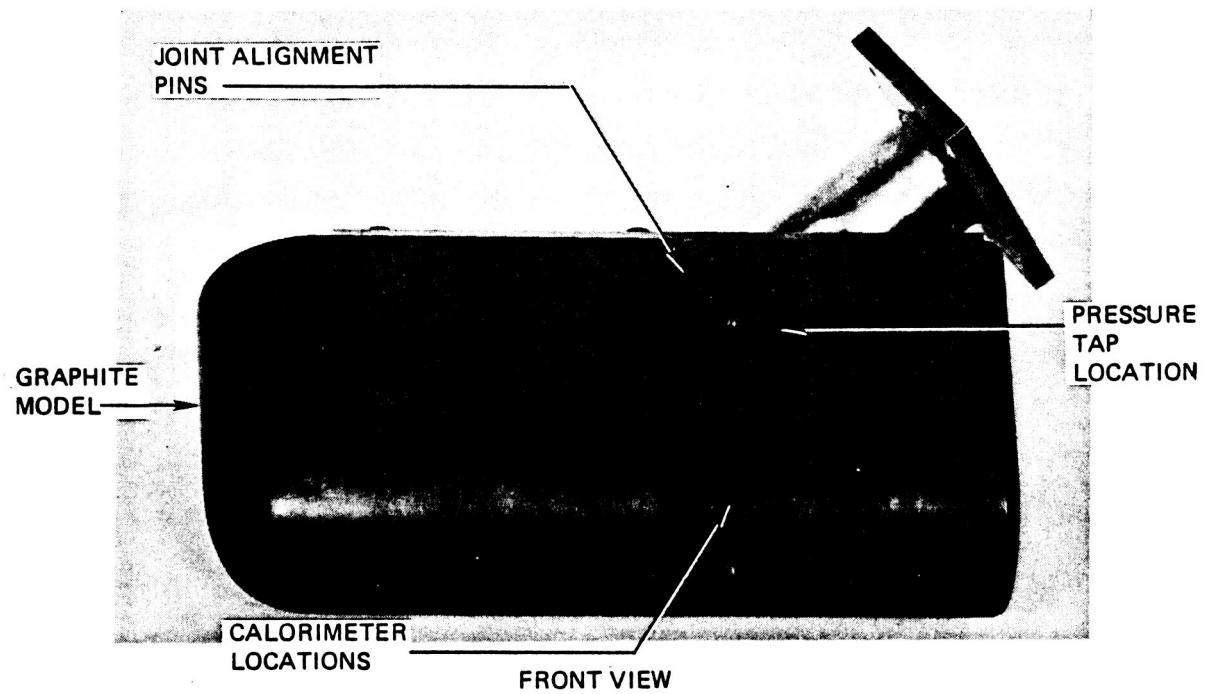


FIGURE 79 CALIBRATION MODEL FOR SEAL STRIP JOINT LEAK TEST

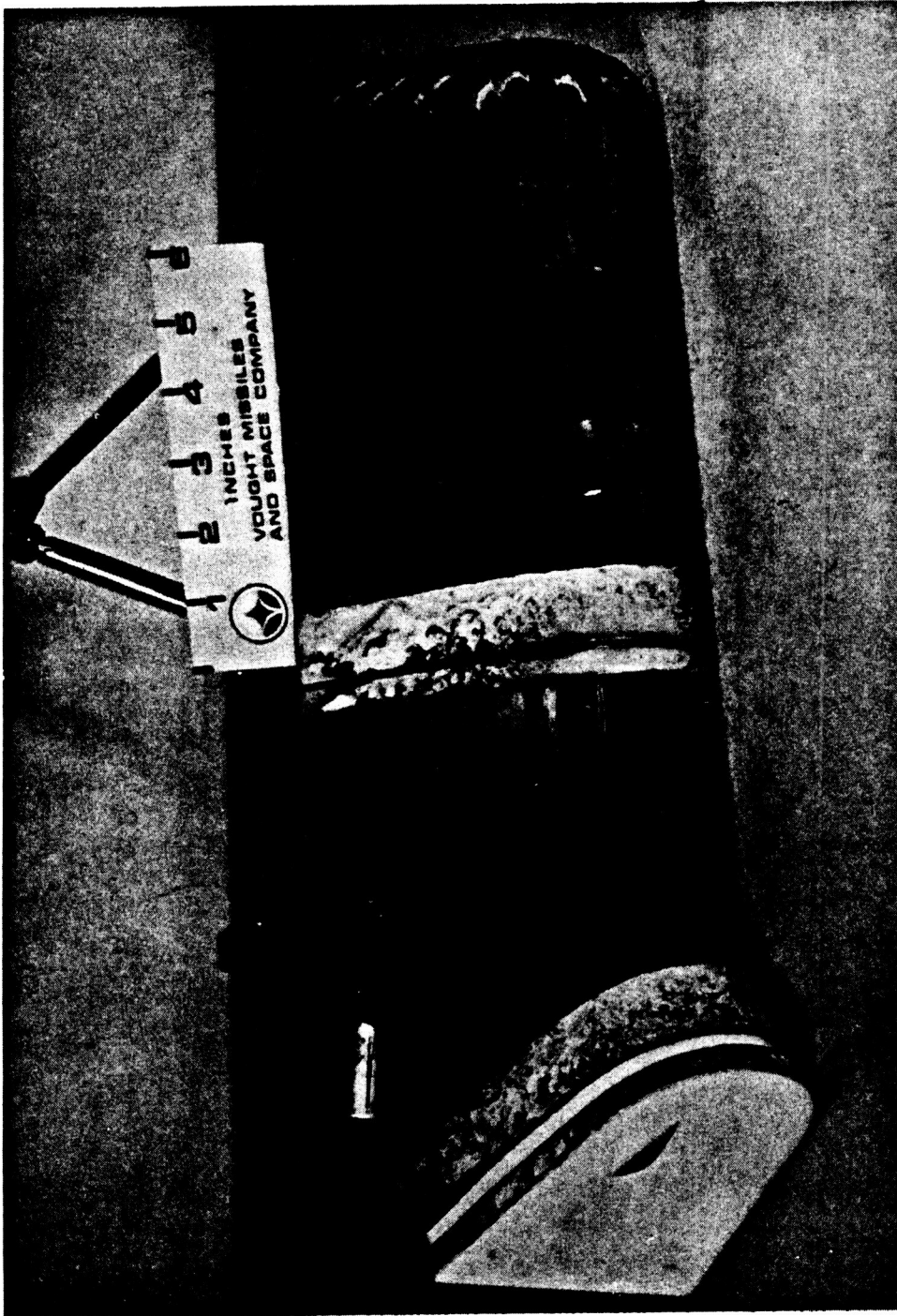


FIGURE 80 TEFLON MODEL FOR SEAL STRIP JOINT LEAK TEST — SHOWN AFTER TEST

1.4.3 INSTRUMENTATION DESIGN AND INSTALLATION DEVELOPMENT

To support the data acquisition requirements of the gap heating test operation, VSD embarked on an effort to develop a thermocouple assembly and installation technique suitable for the test environment.



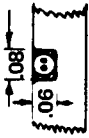






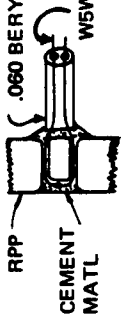
1.4.3.1 Instrumentation Attachment Technique

Beryllia sheath was selected as the thermocouple insulation material for the gap heating tests because of its compatibility with all the adjacent materials and its ability to survive the expected high temperatures. In previous model tests at various plasma arc test facilities, the attachment of thermocouple assemblies was a significant problem. In Phase III, Task 4, five candidate cements were tested to determine their efficiency in providing a thermocouple attachment to bare RPP-3 which would withstand multiple thermal exposure cycles. The five candidate materials were:

- o C-34, Union Carbide Corporation
- o Furane X-2, Furane Plastics Incorporated
- o Sauereisen 75, Sauereisen Cements Company
- o Astraceram A and B, Granite State Machine Co., Inc.

Various concepts for attaching the thermocouple sheath as shown in Table 9 were to be evaluated. Each cement was tested in configuration 1, which utilized only cement to effect a bond. All of the candidate materials, with the exception of the C-34, failed to provide a secure attachment of the sheath after only one exposure cycle, and therefore, no further testing was done on these materials. Plasma arc testing with a temperature level of 3600°F and 3 minutes per exposure was employed to screen the cements and attachment techniques. The C-34 cement applied to the thermocouple sheath per configuration 1 provided a test specimen which after 5 temperature exposure cycles still had the thermocouple sheath attached, although the C-34 cement showed some erosion. The C-34 cement applied in configuration 2 was not appreciably changed after 5 cycles and good attachment of the sheath was maintained. The test specimen using C-34 cement and fabricated in accordance with configuration 5 withstood 5 cycles with the sheath

TABLE 9 CERAMIC CEMENT ADHESION TEST MATRIX - T/C SHEATH TO BARE RPP FOR SLOT HEATING TEST MODEL

CONFIG NUMBER	CONCEPT MECHANICAL DESCRIPTION	MATERIALS (CERAMIC CEMENT AND TESTED OR RETENTION WIRE)	REMARKS
1	W5W26010 T/C WIRE JOINT IN SHEATH  CERAMIC CEMENT MATL 10-13 PLY RPP 3/4" D	C-34 GRAPHITE FILLER & FURANCE X-2 SAUERREISEN NO. 75 ASTROCERAM (A&B)	C-34 ONLY SUCCESS
2	DIRECT CONTACT BETWEEN KREHA AND RPP  SAME AS CONFIG NO. 1 BUT WRAP SHEATH WITH KREHA CARBON SPUN YARN BEFORE CEMENTING TO RPP	C-34	ACCEPTABLE FOR MULTI-CYCLING
3	 SAME AS CONFIG NO. 1 EXCEPT SUBMERGED INTO GROOVE AS SHOWN	—	NOT TESTED BECAUSE OF SUCCESS OF CONFIG. 2
4	 1/4" X 45° FILLET SLIP-FIT SHEATH INTO BORED HOLE AND CEMENT WITH FILLET	—	NOT TESTED BECAUSE OF SUCCESS OF CONFIG 5
5	 SAME AS CONFIG NO. 4 EXCEPT BUILD INTERNAL FILLET WITH KREHA THEN COVER WITH CERAMIC CEMENT	C-34	ACCEPTABLE FOR MULTI-CYCLING
6	 TIE LOOSELY WITH WIRE  CEMENT FLUSH	—	NOT TESTED BECAUSE OF SUCCESS OF CONFIG 2
7	 START END CERAMIC CEMENT SHOULDER (HARDENED) WITH 3-HOLER CHINESE FINGER LOCK - SINGLE WIRE 	—	NOT TESTED BECAUSE OF SUCCESS OF CONFIG 2
8	 RPP CEMENT MATL W5W26010 .060 BERYLLIA SHEATH	—	NOT TESTED BECAUSE OF SUCCESS OF CONFIG 2

still attached. After 3 cycles it was noted that the plasma arc had eroded away the surface of the RPP-3 button and exposed the thermocouple bead. Attachment was maintained during the following 2 cycles, however. The C-34 cement was not tested in the other configurations because of the success obtained with configurations 2 and 5, where the sheath was wrapped with the Kreha carbon yarn before application of the cement.

It should be noted that the Sauereisen and Astroceram cements require an elevated temperature cure to develop their maximum adhesive properties. This amounts to approximately 1200°F for the Sauereisen and Astroceram A and 2200°F for the Astroceram B. Test specimens using these cements were not given this elevated temperature cure because this would be impractical for attaching these particular thermocouples, which have low temperature insulation over a portion of their length.

Once attachment configurations 2 and 5 were selected, plasma arc testing was begun on operating thermocouples to compare their readings against optical pyrometer measurements.

1.4.3.2 Instrumentation Development

An experimental evaluation was performed in the VSD 180 KW plasma arc and the NASA-JSC 1.5 MW plasma arc facility to evaluate and develop thermocouple installation techniques for the gap heating model. The first installation techniques used in the evaluation were those selected in paragraph 1.4.3.1 above, and all subsequent configurations, employed ten mil diameter tungsten-5% rhenium/tungsten-26% rhenium thermocouples with an 0.06 inch diameter beryllia insulator for 1.0 inch aft of the junction. Initially, the junction was located 0.08 inch behind the heated surface, the lead wire was routed straight back from the junction and the insulator was bonded to the specimen back side with C-34 cement reinforced with Kreha fibers.

Initial tests were run on RPP-3, but after it was determined that temperature gradients through the specimen thickness were probably significant, a change was made to RPP-1, which is the gap heating model

material. Tests were run for multiple 3-5 minute cycles at nominal optical temperature levels of 3300^oF and 3700^oF.

Low thermocouple measurement compared to pyrometer reading on the initial run was corrected on subsequent runs, primarily by assuring that the two junctions of tungsten to compensation lead wire were at the same temperature. Alumina insulator also replaced fiberglass insulation aft of the beryllia insulator, and graphite felt was used behind the specimen to reduce temperature gradients across the specimen thickness.

After these changes were made, thermocouple measurements were still significantly lower than pyrometer readings by several hundred degrees fahrenheit and the magnitude of the difference was not consistent from run to run. Several runs were made to evaluate the effect of ceramic coatings on the thermocouple bead to eliminate possible carbon reactions and the effect of thermocouple lead routing to eliminate or minimize heat conduction down the wire. Results of the lead routing investigation showed that the leads should be routed parallel to the heated surface rather than straight back. Results of the ceramic coating study were not conclusive; Astroceram coating showed no improvement, while in some cases, Ceram-acast 505 coating showed improvement and in other cases it did not. Repeated exposure results tended to indicate that the thermocouple wire was not being "poisoned".

With the leads routed parallel to the surface, the thermocouple still generally read lower than the pyrometer and without consistency, the difference generally being from 0 to 200^oF. It was also observed that as the surface eroded away the thermocouple reading increased, approaching the pyrometer reading. This led to the tentative conclusion that temperature gradients across the specimen thickness were responsible for the discrepancies.

Runs were then made at NASA-JSC using a 3-inch diameter specimen of bare RPP-3 instrumented with three thermocouples installed with different techniques. For one, the leads were routed straight back, for a second and leads were routed parallel to the heated surface and for the third

the leads were routined on a 4° slant to the surface. At a pyrometer temperature of 2700°F the thermocouples read consistently 200°F lower than the pyrometer; at 3200°F the thermocouples read 40°F to 180°F low, with the parallel lead routing giving best agreement. At 3545°F the parallel lead thermocouple failed, the straight back lead agreed well with the pyrometer and the slant lead was 285°F low. Hence, the results showed continued inconsistency.

Since the evidence seemed to indicate an effect of temperature gradients on the thermocouple reading, runs were made at VSD with a relatively high conductivity material, ATJ graphite, and with RPP-1, which is the material for the gap heating model. Results for the graphite model did not indicate a reduced temperature gradient. However, with RPP-1 which has lower conductivity than RPP-3, the thermocouple did read lower in initial exposure cycles than for RPP-3 and the reading approached the pyrometer near the time of RPP burn-through to the thermocouple.

A two-dimensional thermal model was developed for the plasma arc test specimen to predict temperature gradients. This model included heat losses across the graphite felt insulation and losses from the specimen edge to the holder. Results indicated a 218°F temperature drop from the front of the specimen to the mid-plane thermocouple location at a surface temperature of 3300°F . This analysis tended to confirm that temperature gradients across the specimen can have significant effect upon the comparison between optical and thermocouple temperatures for the VSD test configuration.

In order to eliminate or minimize temperature gradient effects, subsequent runs were made with the thermocouple bead located on the surface and covered with a thin layer of either tantalum, C-34 cement, graphite foil, or RPP-3. In the test with tantalum foil, the foil overheated due to its low emittance, and this approach was abandoned.

In tests with C-34 over the thermocouple bead, the bead had to be recovered with C-34 after each 3 minute exposure cycle, except for the

first run when two cycles were attempted. Results showed the thermocouple reading consistently 100 to 120°F lower than the pyrometer at the end of single 3 minute exposure cycles at 3300°F. It should be noted that during the course of each 3300°F exposure cycle the C-34 burned off of the bead before the end of three minutes exposure, but no abrupt change in reading was noted.

At 3700°F with C-34 over the thermocouple bead, the thermocouple read higher than the pyrometer. In one test the bead was well above the surface at the end of the run, due to large accumulated surface recession of surrounding RPP-1 on previous runs of the specimen. In the other test the C-34 was lost early in the exposure cycle.

Results at 3300°F with graphite foil and RPP-3 discs over the bead were similar to those with C-34; however, the thermocouple measurements were somewhat lower. All or nearly all of the graphite foil burned away, whereas some RPP-3 remained over the bead at the end of an exposure cycle.

Since best results were obtained with the C-34 cement, and application and repair were relatively easy, this approach was taken for the model. Thermocouples were mounted either slanted into the material thickness or run parallel to the surface for a short distance as appropriate to the individual installation. This proved highly effective as judged by the remarkable consistency of thermocouple readings during model tests. This consistency prevailed from run to run and even after new thermocouples or new instrumented components were introduced into the test program. Results are given in Section 1.4.5.

1.4.4 TEST CONDITIONS AND PROCEDURE

The model was oriented at an angle-of-attack of 25° and a sweep angle of 60° to the flow as shown in Figure 81. This orientation results in a local theoretical angle of attack normal to the leading edge of 43°. Nitrogen test gas was used to avoid oxidizing the bare RPP model and thermocouples. Calibration runs were made with the graphite model to establish flow conditions required to meet three test points. Two conditions were

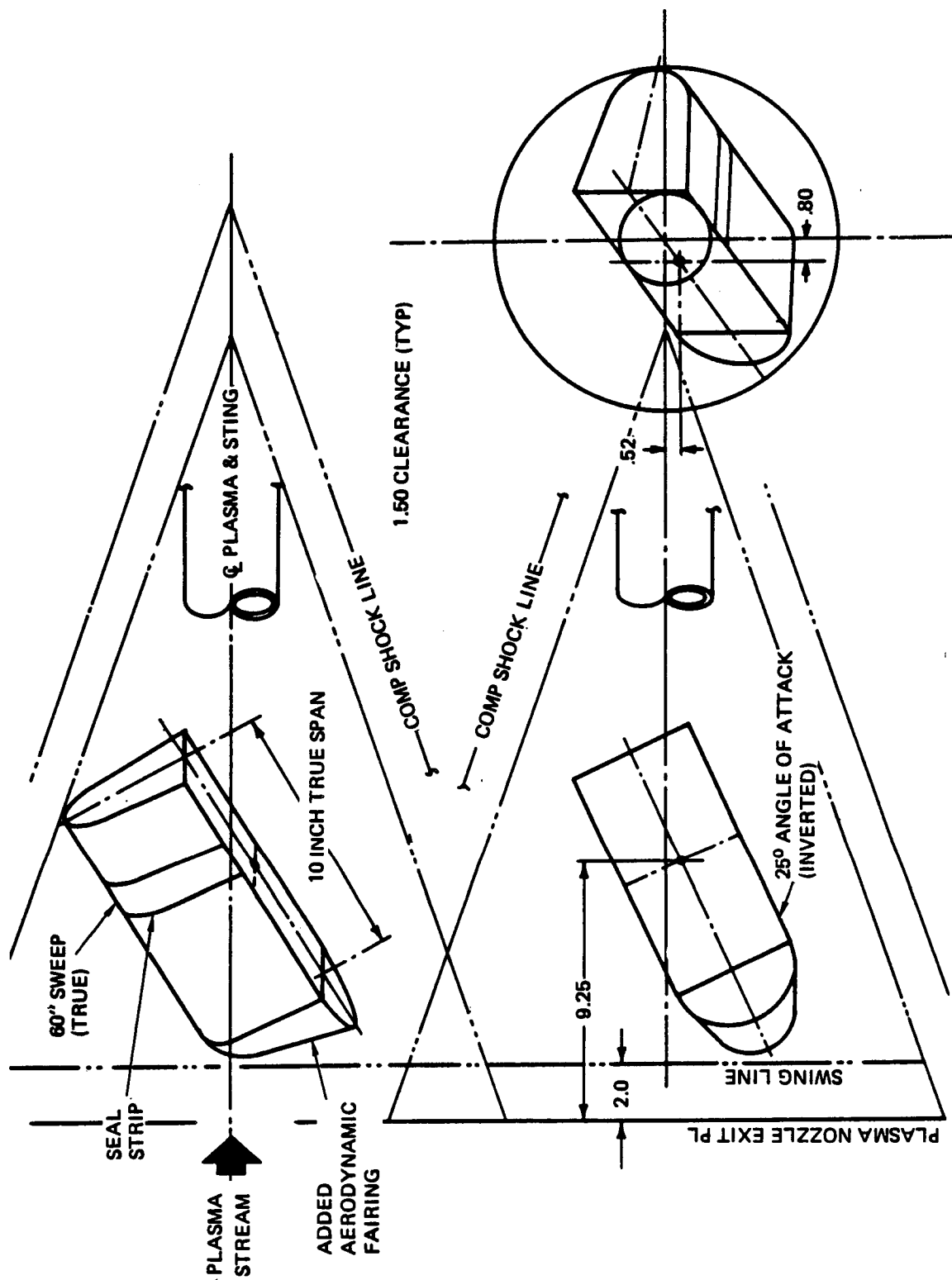


FIGURE 81 SEAL JOINT LEAK TEST MODEL -- LOCATION AND ORIENTATION IN PLASMA ARC FACILITY

achieved as defined below. A high pressure test condition (0.59 psia) could not be met.

Test Point	Enthalpy BTU/Lb	Pitot Pressure PSIA	Wing Stag. Line Press. PSIA	4" Dia. Flat Face Heating Rate BTU/Ft ² Sec	Wing Stag. Line Heating Rate* BTU/Ft ² Sec
1	16,500	0.18	0.071	102	24.8
2	11,000	0.11	0.041	55	24.0

* Measured on model stagnation calorimeter

The bulk of the testing was performed at test point 1; one test was performed at test point 2. Stagnation line heating rates, as measured by calorimeters on the calibration model, were 1/3 to 1/4 of expected values, and the reason for this is not known. The principal parameters requiring simulation are enthalpy and pressure, because of their influence on boundary layer thickness. Since the values of these parameters for the two lower pressure test points were achieved, the low heating rates were accepted. It will be seen in the discussion of post test thermal analyses that in order to obtain agreement between computed model skin temperatures and thermocouples in areas undisturbed by gap effects, it was necessary to assume a stagnation line heating rate of 42 BTU/ft² sec at test point 1, which is in somewhat better agreement with expectations than the calorimeters.

Heating rate and pressure distributions around the model for test point 1 are defined in Figure 82. When test facility operating conditions for each test point were established, a four inch diameter, flat face model with a transfer reference calorimeter was inserted to establish a correlation between heating rate on the model and that on the reference calorimeter.

It should be noted that the enthalpies for test points 1 and 2 are preliminary values. Personal communication with NASA JSC indicates that the actual enthalpy may be either higher or lower than the preliminary values, with an uncertainty range of 7200 to 35,000 BTU/lb.

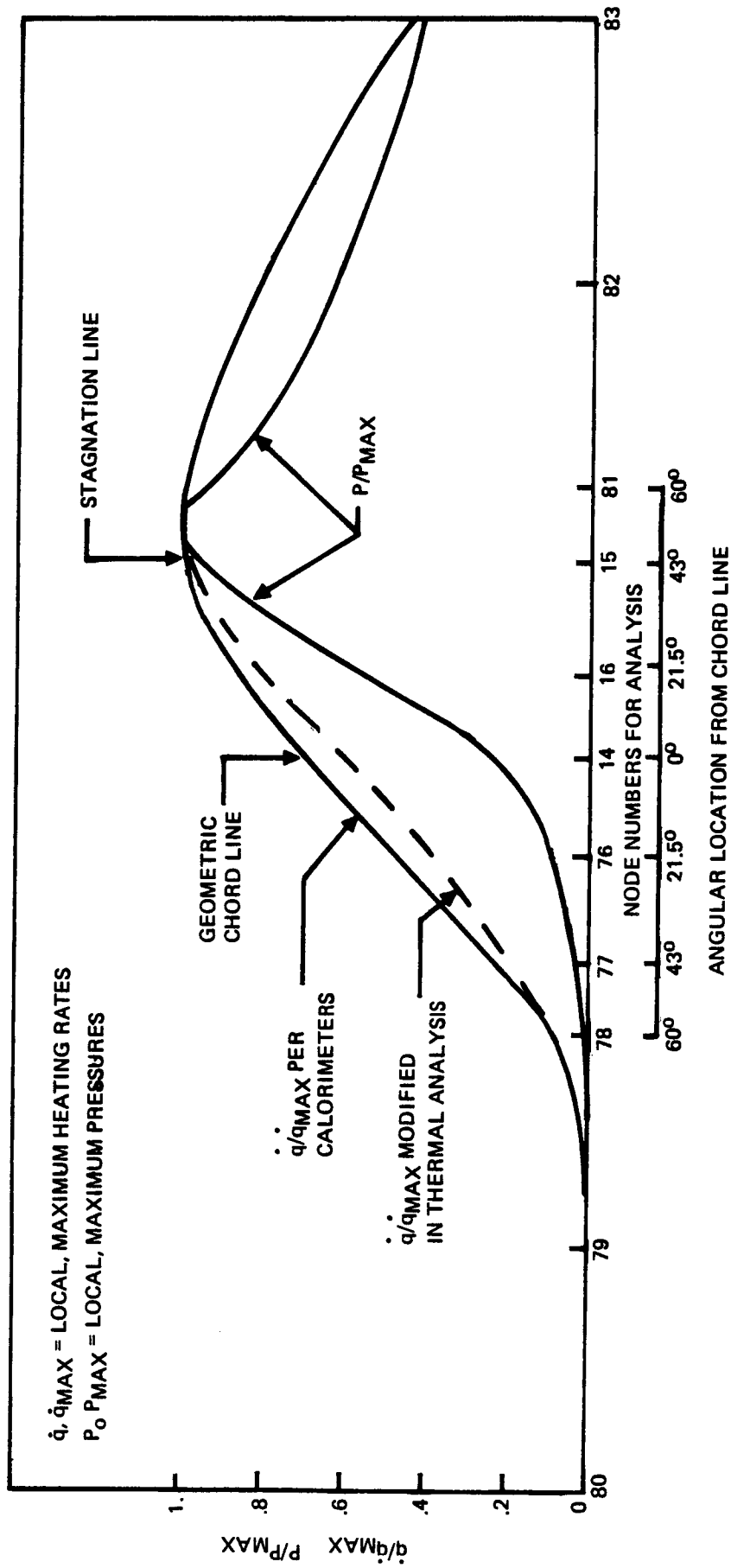


FIGURE 82 CHORDWISE HEATING AND PRESSURE DISTRIBUTIONS FROM CALIBRATION MODEL

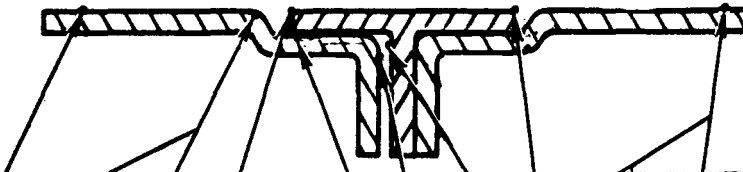
When plasma arc operating conditions for a given test point were established, the reference calorimeter was inserted to confirm the heating rate. The test model was then inserted, held for 120 seconds, and removed. This provided time for stabilization of thermocouple readings with time. In the first test run only, exposure time was 60 seconds and thermocouples did not stabilize; therefore, this run was repeated. During each test run, surface temperatures were obtained at selected points by optical pyrometer.

1.4.5 TEST RESULTS

Test results are summarized in Tables 10 and 11 for the seal configurations shown in Figure 77. Thermocouple measurements for the reference thermocouples upstream of the tee, T_{17} and T_{18} , and downstream, T_{14} and T_{15} , were quite repeatable and in reasonable agreement with pyrometer measurements. The upstream reference thermocouples read 160 to 180°F higher than the downstream thermocouples, indicating higher heating rates upstream, although another contributing factor was higher cross radiation relief on downstream thermocouples due to radiation out of the vent hole on the downstream end of the model. For a preliminary evaluation of the data, undisturbed reference temperatures at the tee leading and trailing edges were established by interpolation between measured values for T_{18} and T_{19} on the stagnation line and T_{17} and T_{14} on the chord line.

The highest temperature area in the seal region was the leading edge of the tee, which ran about 180°F higher than the undisturbed value at the stagnation line and 160°F higher at the chord line, for an 0.025 inch upstream gap between the tee and the skin. This temperature was not affected significantly by rounding the edge of the tee. On the stagnation line it was increased about 140°F over the value for an 0.025 inch gap (320°F over undisturbed value) by increasing the gap to 0.05 inch and about 70°F (250°F over undisturbed value) by protruding the tee 0.03 inch above the skin surface. Filling the gap with carbon filler material increased temperature of the seal leading edge at the stagnation line by 90°F, over the value for an 0.025 inch gap, presumably due to suppressing cross radiation cooling effects by increasing thermal resistance across the gap.

TABLE 10 STAGNATION LINE GAP HEATING TEST RESULTS



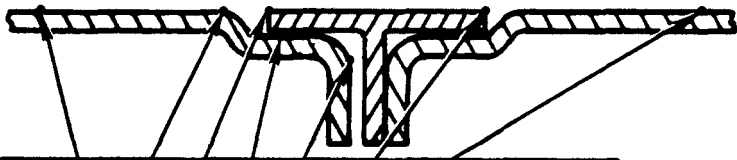
RUN	ASSY	QFF BTU/ FT ² -SEC	T ₁₅	T ₂₃ PYRO**	T ₂₃	T ₁ PYRO**	T ₁	T ₂	T ₃	T ₁₃	T ₁₀	T ₁₈ PYRO**	T ₁₈
1	-2	100	2366	-	-	2400*	2465	2034	1256*	1719*	2671	2590	2533
2	-2	55	1944	-	-	2100	2104	1710	1386	1681	2227	1980	2104
1 (REPEAT)	-2	100	2399	-	-	2700	2555	2044	1934	2160	2730	NO DATA	2499
4	-13	100	2377	2425	-	2700	2567	2094	1925	2145	2742	2500	2561
5	-7	100	2355	2300	-	2650	2578	1905	1729	2185	2647	2380	2516
6	-1	100	NO DATA	2600	2432	2700	2510	2034	1955	2165	2730	2425	2550
7	-3	100	2280	2480	2366	2650	2555	1905	1826	2135	2742	2585	2555
8	-6	100	2275	NO DATA	2323	NO DATA	2590	1876	1807	2217	2790	NO DATA	2556
9	-9	100	2323	2490	2312	2540	2567	1876	1846	2186	2718	2600	2613
10***	-14	100	2433	NO DATA	2790	-	-	2421	2377	-	-	2660	2660
10*** (REPEAT)	-14	100	2476	2900	2813	-	-	2399	2333	-	-	2630	2499
11	-12	100	2301	-	2338	2640	2366	2004	1975	2227	2648	2600	2323****
11 (REPEAT)	-12	100	2301	-	2421	2700	2410	1985	1975	2248	2648	2575	2323****
12	-2'	100	2280	-	2399	2700	2454	1965	1945	2217	2718	2560	2522
13	-7'	100	OUT	-	2312	2650	2488	1827	1807	2259	2682	2630	2533
14	-15	100	2377	-	2642	2960	2600	2135	2095	2269	2625	2540	2510

*NOT STABLE
**UNCORRECTED

***CARBON FELT FILLER LOST DURING TEST
****THERMOCOUPLE BAD

NOTE: ALL TEMP IN °F

TABLE 11 43° OFF STAG. LINE GAP HEATING TEST RESULTS



RUN	ASSY	QFF BTU/ FT ² -SEC	T ₁₄	T ₂₄ PYRO	T ₇	T ₈	T ₉	T ₁₁	T ₁₇	T ₁₇ PYRO	T ₇ PYRO
1	-2	100	2104	-	2074	1566	1089*	2290	NO DATA	-	-
2	-2	155	1734	-	1816	1509	2124	1974	1816	-	-
1 (REPEAT)	-2	100	2114	2280	2237	1885	2825	2432	2258	2215	-
4	-13	100	2084	-	2237	1905	1758	2432	2185	-	-
5	-7	100	2059	-	2237	1758	1585	2399	2135	-	-
6	-1	100	2034	-	2196	1866	1739	2095	2185	-	-
7	-3	100	2024	-	2216	1748	1652	2095	2201	-	-
8	-6	100	2024	2220	2248	1739	1633	2125	2186	2250	2240
9	-9	100	2014	-	2176	1729	1643	2344	2165	-	-
10	-14	100	2145	-	-	2217	2105	-	2186	-	-
10 (REPEAT)	-14	100	2114	-	-	2206	2135	-	2135	-	-
11	-12	100	2024	-	2054	1827	1720	2280	2206	-	-
11 (REPEAT)	-12	100	2024	-	2085	1846	1749	2196	2217	-	-
12	-2'	100	2004	-	2075	1846	1749	2344	2217	-	-
13	-7'	100	1985	-	2135	1729	1652	2301	2238	-	-
14	-15	100	2044	-	2206	1975	1895	2280	OUT	-	-

*NOT STABLE

NOTE: ALL TEMP IN °F

The next highest temperature area on the seal was the trailing edge of the tee, which ran about 110°F above the undisturbed value at the stagnation line and 100°F higher at the chord line for downstream gaps up to 0.05 inch. Note that these preliminary evaluations did not account for thermocouple or test environment variations.

Increasing the downstream gap to 0.10 inch (which is considered to be an unrealistically large gap) increased this temperature at the stagnation line by 450°F over the value for smaller gaps. The 0.10 inch gap also increased the skin temperature immediately downstream of the tee, T_{23} , by 280°F over the value for smaller gaps. The only effect of filling the downstream gap, relative to gaps of 0.025 to 0.050 inch, was in reducing temperatures on the skin and rib underneath the tee. Blocking this gap at the interior flange of the tee and rib (-13 assembly) had no effect.

Removing the tee completely and replacing it with a filler, as shown in Figure 77 for the -14 assembly, increased the skin temperature downstream of the tee, T_{23} , by 440°F over the value for tees with small downstream gaps.

1.4.6 THERMAL ANALYSIS

Results of the gap heating tests show that temperatures on the tee seal are higher than those on the undisturbed portion of the model skin. However, data trends indicate that a large part of this temperature increase may be due to suppressed cross radiation cooling in the seal area. It is important to separate such effects from heating due to gap air leakage and surface disturbances. A thermal analysis was therefore performed of the gap heating model to assess the relative importance of heat conduction and cross radiation effects as opposed to convective heating due to gaps.

A 166 node three-dimensional thermal model was developed for the gap heating model. The model includes effects of heat conduction in the RPP in spanwise, chordwise and across thickness directions. Heat transfer across gaps is by either radiation or conduction in carbon filler material, as appropriate. Cross radiation is included between the inside of the skin,

ribs, graphite felt insulation, and downstream aerodynamic fairing with vent holes. Baseline computer runs were made with external convective heating rates as determined by calorimeters on the calibration model. Adjustments were then made to these heating rates to force agreement with thermocouples in undisturbed heating areas. Heating in gaps was inferred by adjusting heating in these areas to force agreement between calculations and thermocouple readings. The thermal model included appropriate view factors for radiation out of gaps. Emittance of bare RPP was taken as 0.85.

1.4.6.1 Undisturbed Heating Distribution

Initial analyses to establish the undisturbed convective heating distribution were conducted for the -3 assembly tee configuration shown in Figure 77 with both upstream and downstream gaps sealed. Results using calorimeter heating rates with constant heating in the spanwise direction showed calculated temperatures to be below thermocouple readings by the following amounts.

	<u>Downstream</u>	<u>Upstream</u>
Stagnation Line	340°F	490°F
Chord Line	200°F	290°F

To correct these differences it was necessary to incorporate the following changes to the undisturbed heating distribution.

- (1) Increase stagnation line heating rate at tee centerline from 24.8 to 42.3 BTU/ft² sec.
- (2) Incorporate a spanwise heating distribution defined by $q \approx L^{-.316}$ where L is wetted distance from stagnation point on upstream fairing.
- (3) Modify chordwise heating distribution as shown in Figure 82.

It will be noted that the exponent in the spanwise heating distribution relation $N = -.316$ is intermediate between the values normally associated with purely stagnation line flow $n=0$ and wedge or flat plate flow, $n=-.5$. Computed temperatures using undisturbed heating distribution developed in this analysis were in reasonable agreement with measured values for the -3 assembly and for the other assemblies analyzed below.

1.4.6.2 Heating in Disturbed Flow Areas

Initial computer runs on the -3 assembly were performed with no heating in the upstream gap between the tee leading edge and skin. Results at the stagnation line gave a temperature for the tee leading edge, node 10, 73°F above that of the upstream undisturbed value, node 18. Thermocouples indicated a temperature difference of 202°F . It was concluded that part (73°F) but not all of the increased tee temperature was due to suppressed cross radiation cooling caused by the carbon filler and two thicknesses of RPP (tee and skin). Hence, additional runs were made with convective heating in the upstream gap. Likewise, in the downstream gap between the tee trailing edge and skin joggle, assuming no gap heating results in underpredicting temperatures. At the tee trailing edge suppressed cross radiation cooling accounted for 145°F out of a total of 205°F temperature increase over the downstream undisturbed value, node 15.

In order to obtain agreement between computed and measured temperatures at the tee leading and trailing edges and on the skin in the downstream joggle area, heating rates were established over the test model area using ratios of local heating rates (average over the nodal area) to the undisturbed heating rates. The convective heating rates were thus set for the -1, -2, -3 and -7 gap configurations shown in Figure 77. Comparison between calculated and measured temperatures were made at eight stagnation line locations and at 6 chord line locations as shown in Figure 83 for each of the four gap configurations.

The calculated temperatures for all 14 locations of each configuration were generally in quite good agreement and with few exceptions were within one percentage point of the measured temperatures. The exceptions were the calculations for the tee leading edge T_{11} located on the chordline and the panel rib surface T_3 under the tee inside surface at the stagnation line. The temperature comparisons between these two locations are presented in Table 12. Several comments in explanation of the few large variances are as follows:

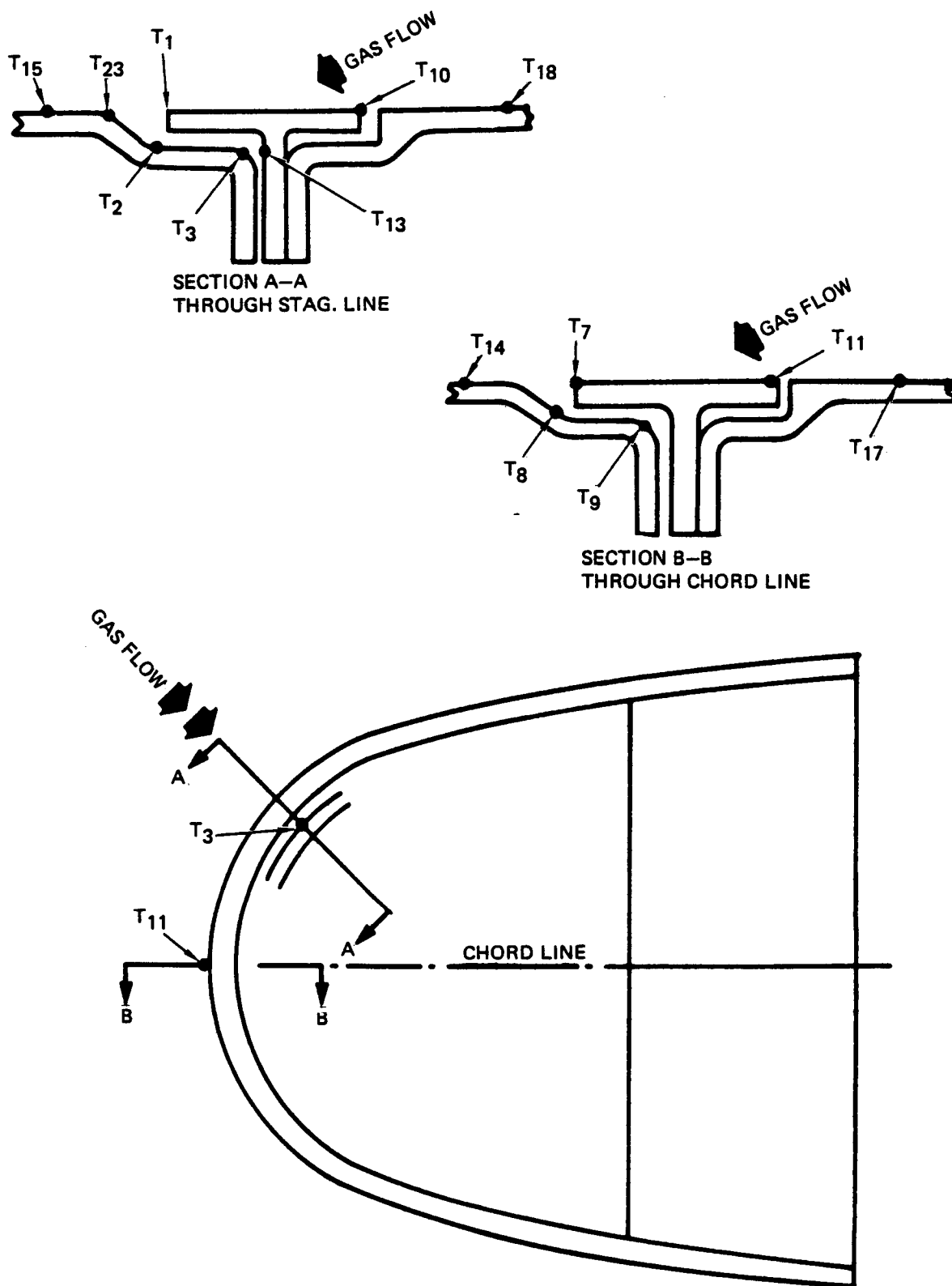
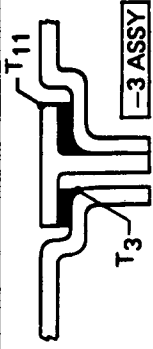
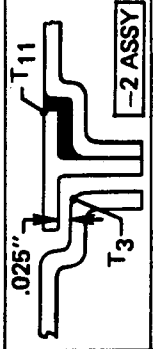
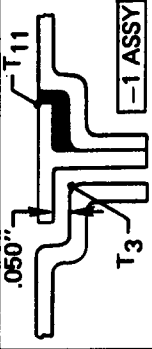
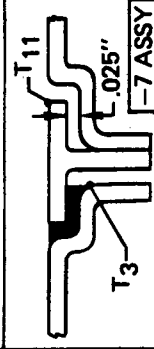
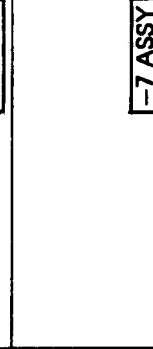
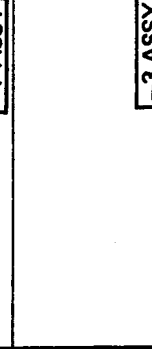


FIGURE 83 THERMAL MODEL WITH SAMPLE TEMPERATURE LOCATIONS

TABLE 12 COMPARISON BETWEEN CALCULATED AND MEASURED GAP HEATING TEMPERATURES

* (+) COMPUTED EXCEEDS MEASURED (-) MEASURED EXCEEDS COMPUTED		(°F) MEASURED TEMP'S	(°F) CALCULATED TEMP'S	(°F) DIFFERENCE +	SEE NOTES IN PARA. 3.4.7.2
	T ₁₁ AT CHORD LINE	2095	2339	+295°	1
	T ₃ AT STAG. LINE	1826	1978	+152°	2
	T ₁₁ AT CHORD LINE	2432	2417	-15°	3
	T ₃ AT STAG. LINE	1934	2032	+98°	
	T ₁₁ AT CHORD LINE	2095	2432	+337°	3 & 4
	T ₃ AT STAG. LINE	1955	2033	+78°	4
	T ₁₁ AT CHORD LINE	2399	2384	-15°	5
	T ₃ AT STAG. LINE	1729	1991	+262°	2 & 5
	T ₁₁ AT CHORD LINE	2399	2385	-14°	(RE-RUN) SEE NOTE 6
	T ₃ AT STAG. LINE	1729	1922	+193°	
	T ₁₁ AT CHORD LINE	2095	2373	+278°	(RE-RUN) SEE NOTE 7
	T ₃ AT STAG. LINE	1826	1841	+15°	

- (1) The computed temperature at T_{11} is 295°F above the measured value for the -3 assembly, but the local heating was not adjusted (reduced) to bring about better agreement because for the -2 assembly, which also had a sealed upstream gap, the measured temperature at this location was 337°F higher than for the -3 assembly.
- (2) At the T_3 chordline location there was a consistent trend for calculated temperatures to exceed measured temperatures especially for the -3 and -7 assemblies where both had downstream gaps sealed with filler material. For these two assemblies the differences are believed partly due to inaccuracies in conductivity values used for the carbon filler material.
- (3) The calculated temperature for T_3 on the -2 assembly, exceeded the measured value by 98°F , which is similar to but less than the difference for the -3 assembly. The most surprising result for the -2 assembly was that in order to match measured temperatures, it was necessary to impose increased heating on the tee leading edge exterior nodes, even though the upstream gap was completely sealed as shown in Table 12. This is not understood at this time.

- (4) The 337°F difference for T_{11} on the -1 assembly is similar to that for the -3 assembly and the heating at this location was not reduced to bring about better agreement for the same reason discussed in conjunction with the -3 assembly (note 1 above). The 78°F difference for T_3 is somewhat less than that noted previously for the -3 and -2 assemblies.
- (5) The calculated rib temperature T_3 for the -7 assembly exceeded the measured temperature by a sizable amount consistent with calculated temperatures for the other assemblies. Because it was believed that the nominal carbon felt conductivity values were too large, additional computer runs were made using reduced conductivity values. See comments below.
- (6) A final computer run was made for the -7 assembly. Heating rates were unchanged but carbon felt conductivity values were reduced to $1/3$ the nominal value. The result is an improvement in difference between computed and measured T_3 rib temperatures. The T_{11} temperature remained in good agreement.
- (7) A final computer run was made for the -3 assembly. Heating rates were changed, increasing heating on the cavity floor to the same values used in the -2 and -1 assemblies, since heating in this area should be similar for these assemblies. The calculated rib temperature T_3 was brought into good agreement with the measured value while computed external tee temperatures exceeded measurements.

1.4.6.3 Stagnation Line Temperature Profile

Temperatures at the stagnation line of the -7 assembly are detailed in Figure 84 in order to illustrate a complete profile of computed temperatures, including locations where there were no thermocouples in the test model. The calculations reveal that the temperature on the skin, T_{155} , immediately opposite the tee leading edge, T_{10} , is almost as hot as the tee leading edge, 2642 versus 2669°F. This is due to radiant heat transfer across the gap, since the convective heating imposed on node 155 was undisturbed heating. This indicates the need for close control of the gap involved and the need to instrument this area more fully on future tests to more completely evaluate this region.

1.4.6.4 Applicability of Results to Flight

An earlier analysis which was part of the seal strip gas leakage test effort made a comparison between test and entry flow parameters. This comparison indicated that boundary layer thickness in the test would be less than that in flight, and energy inflow into gaps would be comparable to the high altitude entry condition and about one-half of that for the low altitude entry condition. Test results indicate that the disturbed heating on the seal is primarily a rough body or cavity flow effect, which is sensitive to boundary layer thickness, rather than an inflow effect.

It should be noted that according to personal communication with NASA JSC, they have computed entry boundary layer thicknesses lower by a factor of 0.60 to 0.70 than those used in VSD's early analysis. The difference appears to be primarily in assumed leading edge radius which was 3 inches in the NASA JSC analysis and 9 inches in VSD's. NASA JSC boundary layer thickness calculations for the test model are comparable to those used in VSD's analysis for similar assumed enthalpy. Enthalpy for the tests, however, has been measured by various means as between 7200 and 35,000 BTU/lb, according to personal communication with NASA JSC. It is evident that this important parameter must be defined more closely in order to make a firm comparison of entry and test flow parameters.

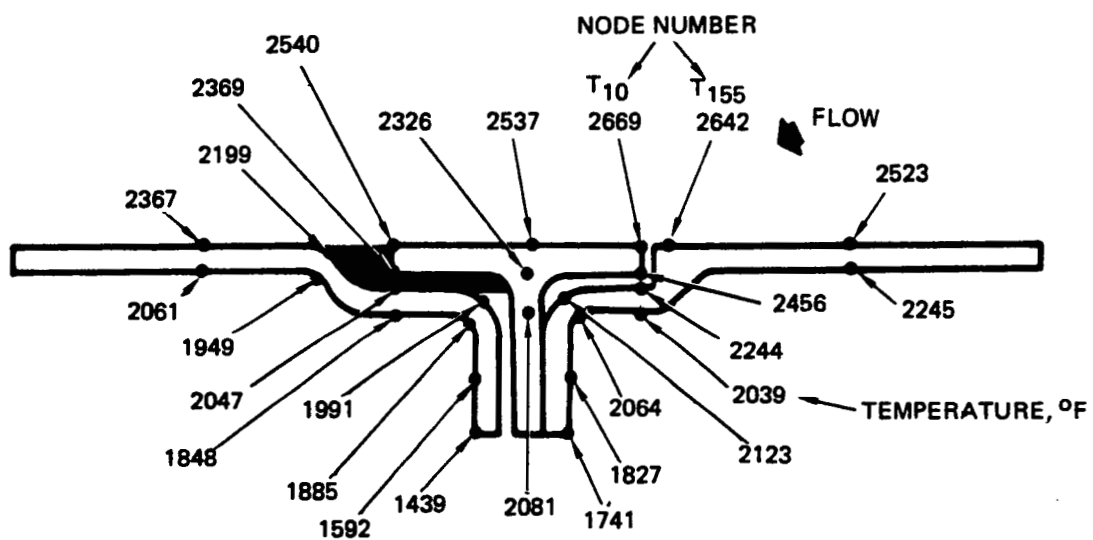


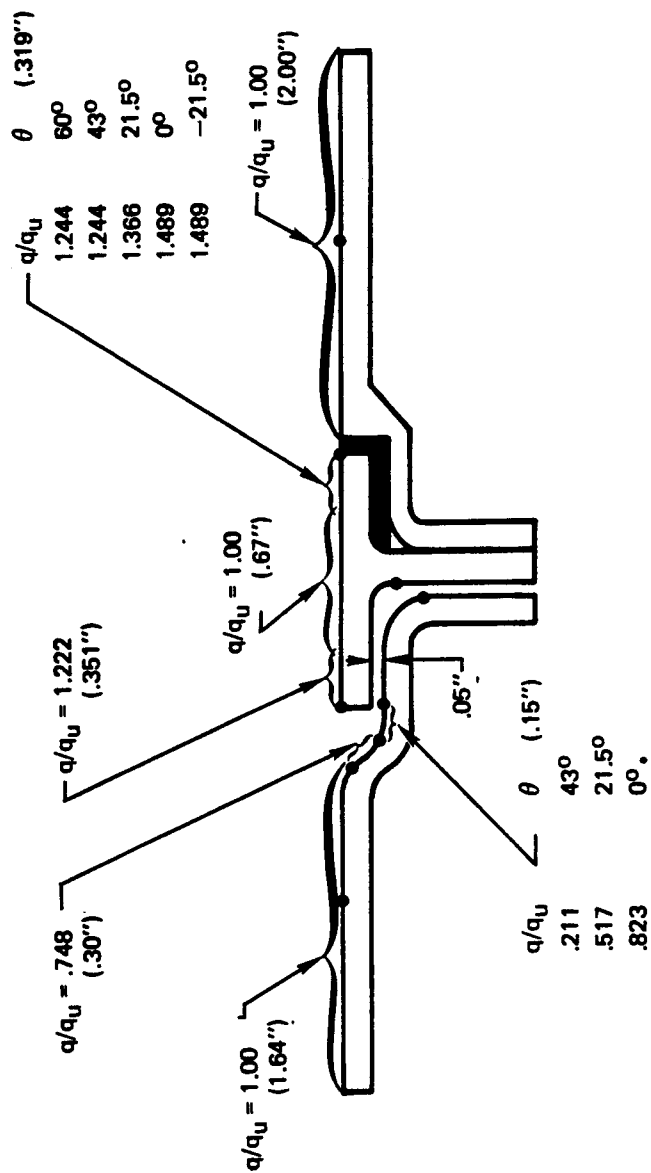
FIGURE 84 DETAILED TEMPERATURES, - 7 ASSEMBLY STAGNATION LINE

The convective heating over four of the model assemblies inferred from the measured temperatures are presented in Figures 85 to 88. These figures present the ratio of local heating rate to the undisturbed heating rate at the same location. The local heating rate presented is the average heating rate over the nodal heated area shown in the figures. Correlation of these disturbed heating rates with available analytical relations and other empirical data in the literature is a most desirable next step in the analysis in order to provide a rational basis for application to flight conditions. However, it will be necessary to define the enthalpy for the tests more closely in order to perform such analyses with confidence.

1.4.7 CONCLUSIONS

As a result of test and analysis the following conclusions relative to gap heating are offered.

- (1) Gaps should be maintained below 0.05 inch and tee protrusion should be avoided.
- (2) The magnitude of temperature increase on the tee seal compared to the unperturbed skin amounts to about 180°F for a 0.025 inch gap. Temperature increase on the skin immediately opposite the tee will be slightly less.
- (3) Alternate seal configurations represented by -13 and -14 assemblies are not beneficial.
- (4) Making the tee fully integral with the upstream panel would result in increased temperatures of about 110°F for the downstream overlap area.
- (5) Rounding of the tee leading edge is not beneficial.
- (6) Both increased convective heating and suppression of cross radiation cooling contribute significantly to the increased temperatures measured on the tee seals.
- (7) The technique of measuring temperatures, using tungsten-rhenium thermocouples mounted within approximately 0.010 inches of the outer surface and covered with C-34 cement, produced consistent and reproducible results. Replacement thermocouples and replacement parts produced little variance in temperature measured.



q = LOCAL HEATING RATE
 q_u = UNDISTURBED HEATING
 (.XXX) = DISTANCE OVER WHICH
 HEATING OCCURS

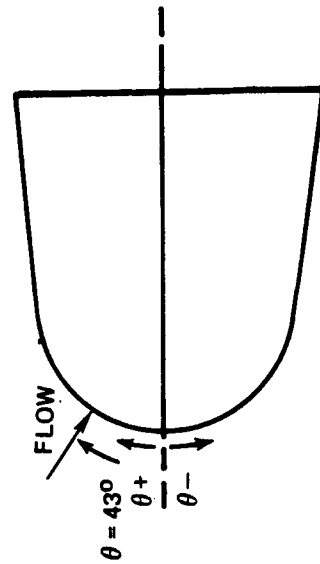
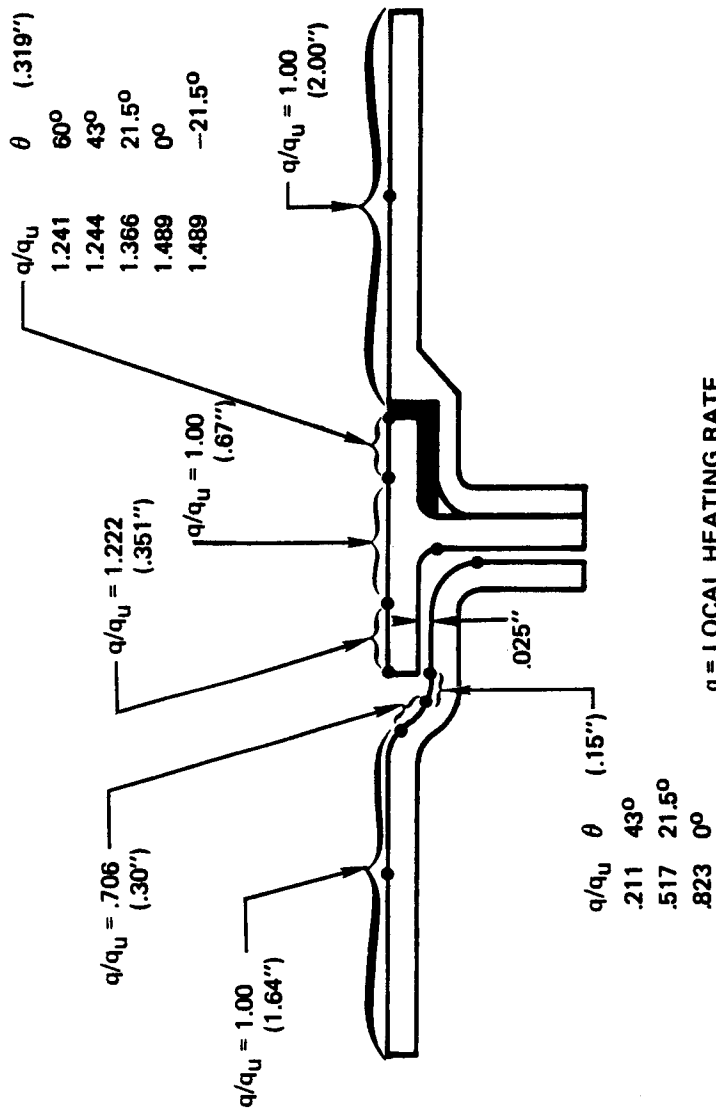


FIGURE 85 HEATING ON -1 ASSEMBLY



q = LOCAL HEATING RATE
 q_u = UNDISTURBED HEATING
 (.XXX) = DISTANCE OVER WHICH HEATING OCCURS

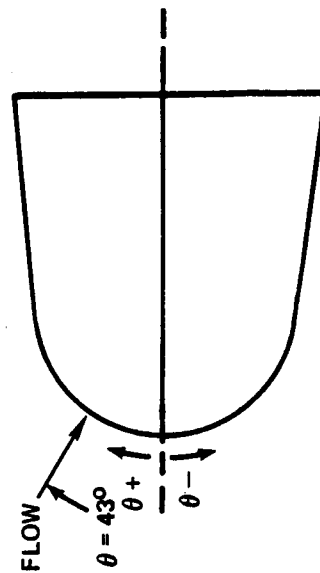
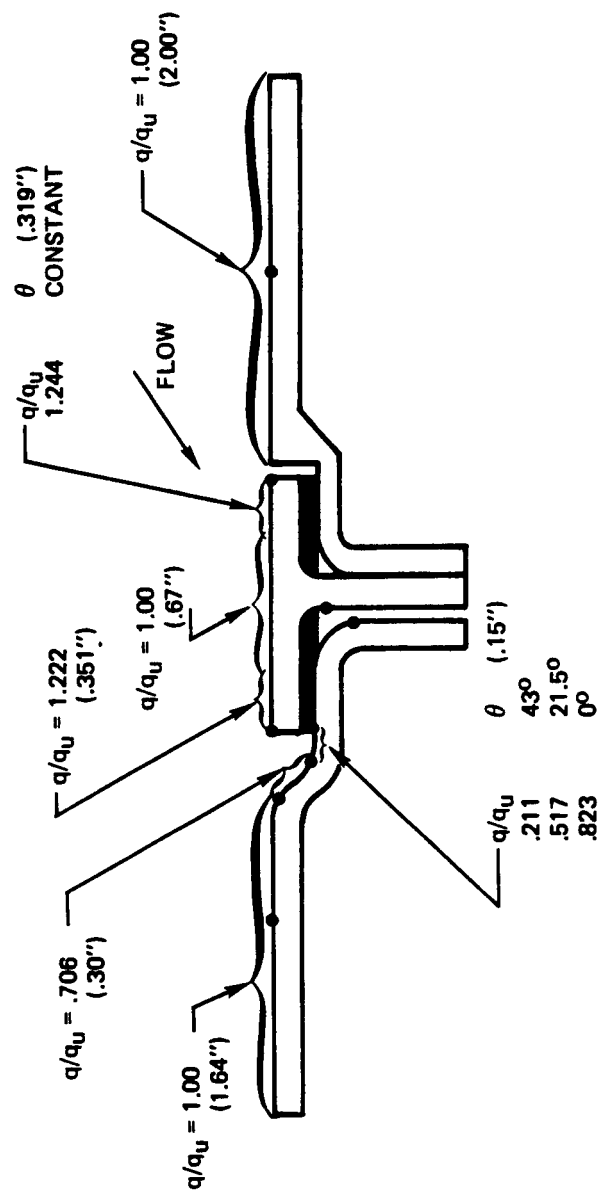


FIGURE 86 HEATING ON -2 ASSEMBLY



q = LOCAL HEATING RATE
 q_a = UNDISTURBED HEATING
 $(.XXX)$ = DISTANCE OVER WHICH HEATING OCCURS

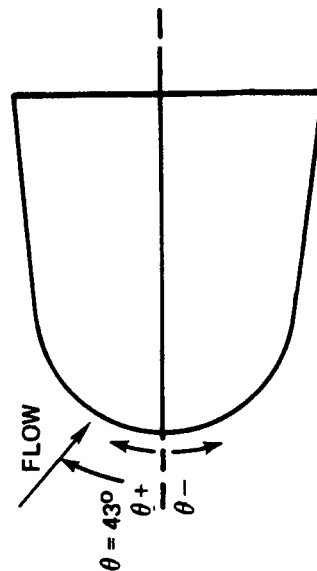
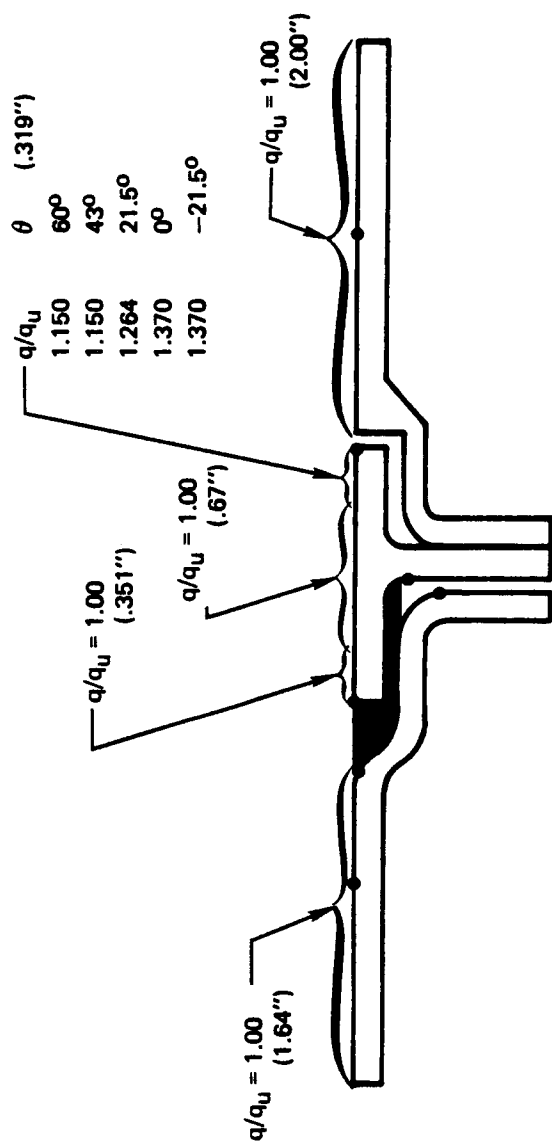


FIGURE 87 HEATING ON -3 ASSEMBLY



q = LOCAL HEATING RATE
 q_u = UNDISTURBED HEATING
 (.XXX) = DISTANCE OVER WHICH
 HEATING OCCURS

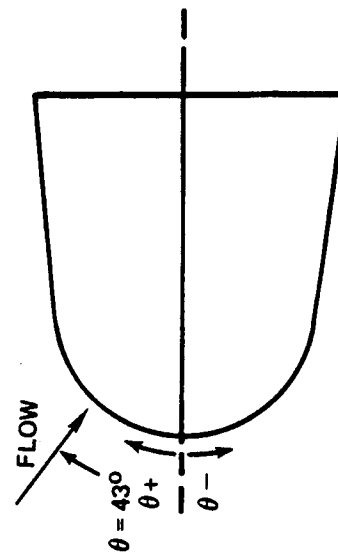


FIGURE 88 HEATING ON -7 ASSEMBLY

1.5 TASK 5 - THICK LAMINATE MATERIAL FOR NASA EVALUATION

The purpose of this task was to supply NASA-JSC with test specimens produced from 34-ply RPP material fabricated in accordance with the selected thick laminate process developed in Task 1. Material was fabricated as 10 inch x 12 inch panels from which specimens were cut.

Delivery schedules for these panels did not permit final selection of the Phase III material configuration before committing to fabrication. Therefore, three material variations were fabricated into three panels each as follows:

- (1) 3 panels, WCA/R-120 prepreg cloth to VSD specification 307-7-7. This has been the standard material used by VSD, and was ultimately selected for the Phase III program as well.
- (2) 3 panels, WCA/R-120 prepreg cloth with 43-47% resin content as opposed to the nominal 55% of the standard material.
- (3) 3 panels, WCA/R-120 prepreg cloth with 40-45% resin and 7-10% graphite powder filler.

All panels were fabricated through RPP-3 to the processing of Figure 49. At that point the decision had been made to use the standard 307-7-7 specification material for Phase III work, so most of the specimens were extracted from that material, coated and heat treated per Figure 49. Specimens in excess of panel area available were taken from the reduced resin content panel. The following specimens were supplied:

Number of Specimens	Configuration	Material System	Nominal Thickness, inch
16	3 in. dia. plasma arc specimens	Standard 307-7-7	0.50
4	3 in. dia. plasma arc arc specimens	Reduced resin %	0.40
5	3 in. dia. bare RPP plasma arc specimens	Reduced reduced %	0.40
9	3 in. I.D. coated plasma arc holders	Graphite	--

Note that graphite holders were included with the specimens. These were finish machined by VSD and coated in the same fashion as the RPP specimens. This preserves the life of the holders and provides a more uniform temperature distribution between specimen and holder.

Both Battelle and Southern Research Institute were to evaluate Phase III material for NASA-JSC and VSD, respectively. One panel of the graphite filled bare RPP was sent to each of these agencies as trial material for establishing mechanical property specimen configurations and for developing test techniques.

All material was inspected by x-ray, and ultrasonic-through-transmission NDE techniques and found free from defects. Plasma arc testing of sample specimens in the VSD 180KW unit indicated coating performance was acceptable.

1.6 TASK 6 - DOCUMENTATION

This task was devoted to documentation of data for NASA-JSC. Included were the nine monthly progress reports listed below, this technical summary report, a "Design Evaluation Test Plan", Report No. T143T-5R-30745 (MSC-06849), and three formal presentations given to NASA-JSC on 18 August, 10 October, and 17 November 1972.

MONTHLY PROGRESS REPORTS

<u>No.</u>	<u>For Month</u>	<u>Report No.</u>
1	May 1972	T143-5R-20155
2	June 1972	T143-5R-20171
3	July 1972	T143-5R-20188
4	August 1972	T143-5R-20200
5	September 1972	T143-5R-20716
6	October 1972	T143-5R-20728
7	November 1972	T143-5R-20740
8	December 1972	T143-5R-20744
9	January 1973	T143-5R-30004

The Design Evaluation Test Plan was prepared to define a test program for NASA-JSC to evaluate the structural and thermal performance of the delivered leading edge assemblies (Figures 2-1 through 2-3), ref. Vol. I. The test program includes the flight phases and test environments of most significance to the integrity of the hardware. It includes the following tests entry temperature, boost static pressure loads, orbit vacuum/temperature, boost acoustic noise, and finally, an ultimate load test of the most critical boost loading condition. The plan describes the tests to be performed, instrumentation required, test procedures, acceptance/rejection criteria, precautions to be observed, inspection requirements, and documentation of results. The plan is presented in Appendix A.3.

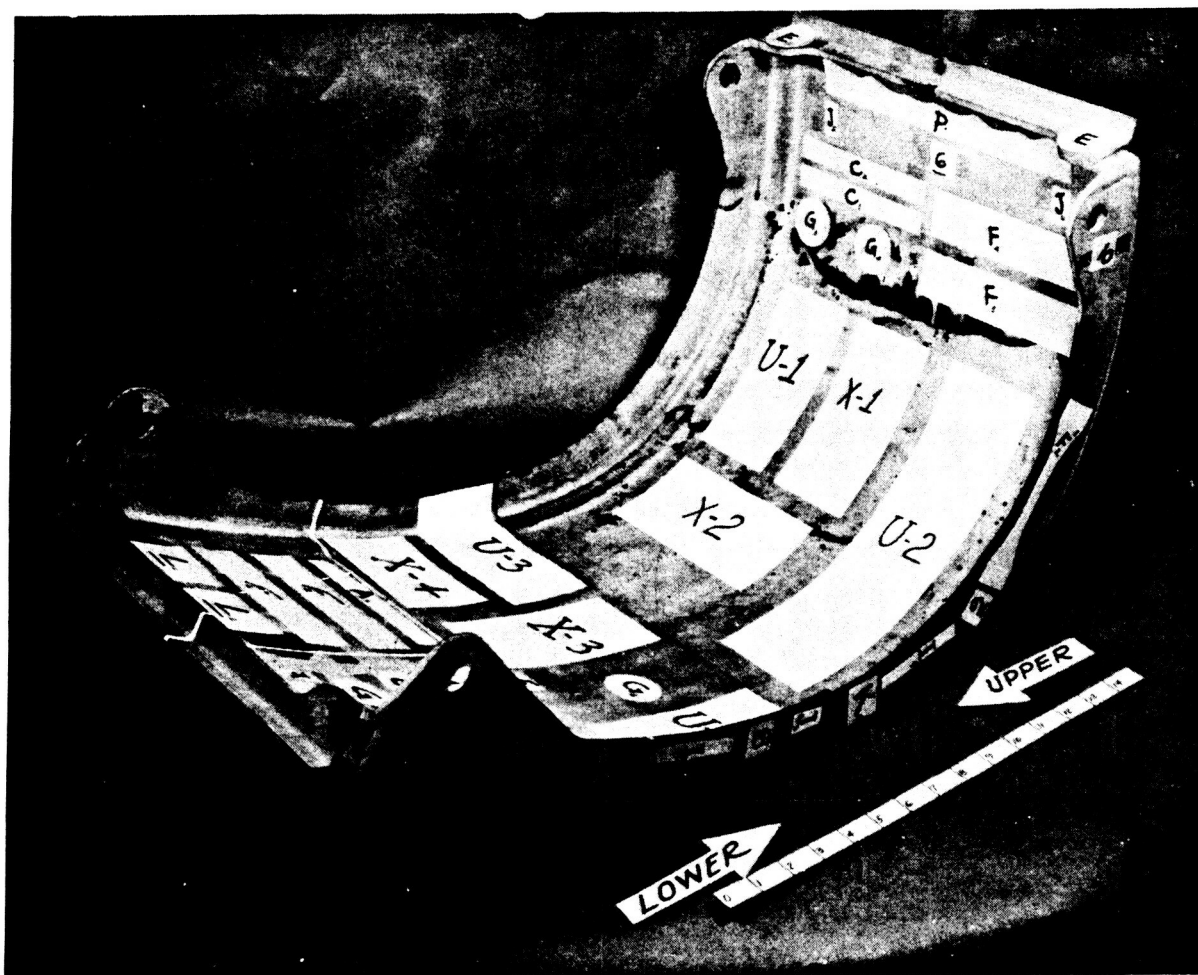
1.7 TASK 7 - DESTRUCTIVE EVALUATION OF A PHASE II
LEADING EDGE

The purpose of this task was to determine by destructive test the quality of an RPP leading edge fabricated in Phase II, and to compare the results against non-destructive evaluation techniques (NDE) and against flexure bars coated along with the selected leading edge.

Leading edge S/N 2 was chosen for this study because it appeared to have some minor imperfections (believed to be porosity as determined by NDE), had an acceptable weight gain during coating, had undergone both boost pressure and entry thermal tests, and should be more representative of the fabrication technique than the first article fabricated.

The leading edge was re-x-rayed and rechecked by ultrasonic C-scan in both the VSD production facility and the laboratory research facility. X-ray analysis again did not reveal delaminations or other flaws. Ultrasonic inspection in the production facility reproduced essentially the same minor porosity indications in the 14-ply region as previously obtained in Phase II, reference 2. However, using laboratory transducers and different frequencies (based on Phase III development work), nearly all of the previous indications disappeared and the part appeared sounder than originally thought. Ultrasonic examination of corner and joggle regions also indicated soundness throughout. Strength data provided below, revealed no low strength material in the previous questionable areas.

A cutting plan was prepared to define the location of tension, flexure, photomicrograph, NDE standards, etc. The extent of this plan is illustrated by the photograph in Figure 89. Many of the specimens shown (those identified by X and U) were used as standards for NDE. The other, smaller specimens were for mechanical or physical property testing. The lower portion of the leading edge, including the lugs (marked H_R in Figure 89) was used in the support lug thermal tests of Task 3, Section 1.3. This testing consisted of exposure of the RPP to the entry temperature, first at one-atmosphere ambient conditions, and then for two cycles



SPECIMENS EVALUATED

- | | |
|-----------------------|------------------------|
| - 2 LUGS | - 8 NDE STANDARDS |
| - 5 FLEXURE | - 2 INPLANE SHEAR |
| - 6 TENSION | - 2 CORNER ANGLE |
| - 3 COMPRESSION | - 3 INTERLAM TENSION |
| - 2 RIVET TENSION | - 3 INTERLAM SHEAR |
| - 6 DENSITY | - 10 MICROSCOPIC EXAM. |
| - 6 COATING THICKNESS | |

FIGURE 89 DESTRUCTIVE EVALUATION OF PHASE II LEADING EDGE

at 10 mm Hg in a nitrogen environment. Heating at one-atmosphere may have been a severe exposure for the RPP, since it feasibly could have produced some material degradation from oxidation. However, judging from strength data of the lower portion of the leading edge compared with the upper portion, no obvious degradation occurred (Table 14).

Porosity, density, thickness, and coating thickness measurements are summarized in Table 13. Flexure bar control specimens, distributed around the part during coating, were examined for comparison with the leading edge. The data is also shown in Table 13.

Examination of thickness and density data reveals that the leading edge thickness per ply varied from 0.0122 to 0.0138 in. which is reasonable since the nominal design value was 0.013 in. /ply. Control specimen data shows more compaction since the per ply thickness excursion on those specimens was 0.0119 to 0.0122 in. /ply. Bulk density on both the leading edge and control specimens is higher than anticipated, being in the 92-104 lb/ft³ range. Previous flat panel data indicated 88-90 lb/ft³ would be a reasonable density, so it appears that either greater debulking, or higher reimpregnation efficiency was experienced on the panel and its control specimens.

Apparent porosity of the leading edge and control specimens cover roughly the same range, with the control specimens showing slightly lower porosity in the extreme.

The coating thickness goal was to achieve an 0.020 inch thick coating over the entire part, which, according to Phase II design criteria, would have provided a 100-mission life with at least 0.010 inch of coating remaining. Average coating thickness measurements in Table 13 shows that on the external surface of the part (mold side) only one measurement (0.018 in.) falls below the 0.020 in. desired, and this is within the 0.010 in. safe allowance at the life limit of the part. A thinner coating was experienced on the inner surface of the part (bag side), which is protected from direct air impingement. Improvement can be made by directing more heat to the backside of the part during coating. The control specimens

TABLE 13 PHYSICAL PROPERTIES PHASE II LEADING EDGE & CONTROL SPECIMENS

S/N 2 COUPONS						
Sample No.	Plies	Apparent Porosity %	Bulk Density g/cc	Total Thickness in.	Coating Thickness Bag Side Average in.	Coating Thickness Mold Side Average in.
2 Rib	12	20.7	1.62	0.155	0.018	0.028
3 Lug	17	13.6	1.56	0.208	0.024	0.028
5 Skin, Lwr.	14	17.9	1.48	0.194	0.018	0.033
6 Skin, Upr.	12	19.6	1.58	0.158	0.019	0.036
9 Rib	12	16.3	1.49	0.156	0.016	0.018
10 Lug	17	13.9	1.53	0.216	0.024	0.022

CONTROL TEST SPECIMEN (COATING ON EDGES REMOVED)						
Specimen No.	Plies	Apparent Porosity %	Bulk Density g/cc	Total Thickness in	Coating Thickness Bag Side, in.	Coating Thickness Mold Side, in.
S2-9	13	13.2	1.56	0.155	0.021	0.021
S2-10	13	19.3	1.50	0.159	0.024	0.024
S2-5	13	12.2	1.53	0.155	0.019	0.019
S2-6	13	15.9	1.66	0.156	0.025	0.025
S2-2	13	11.3	1.55	0.155	0.017	0.019
S2-3	13	12.7	1.55	0.159	0.021	0.017

TABLE 14 MECHANICAL STRENGTH COMPARISON PHASE II LEADING EDGE
(AVERAGE VALUES)

Property	Direction	Plies	Phase II Leading Edge, S/N-2	S/N-2 Control Specimens 13-Ply psi	SRI Data Phase II 13-Ply psi	Battelle Data Phase II 13-Ply psi
Tension	Warp	12	7575 psi	--	8660	7246
	Fill	12 14	3340 psi 3205 psi	--	4525	3202
Flexure	Warp	14	13550 psi	18140	14375	14612
	Fill	12 14	7150 psi 7200 psi	--	13210	8045
Compress	Warp	12	11730 psi	--	11520	--
Shear (In-Plane)	Warp	14	3360 psi	--	--	--
Interlam. Shear	--	12	2363 psi	--	2195	--
Interlam. Tension	--	12	533 psi	--	487	686
Lug Strength	Cross	17	833 lb	--	--	--
Rivet Tension	--	--	94 lb	--	--	--
Angle Moment	Fill	12	13.7 in- lb	--	--	--

reflect the lower end of the coating range but the mold side of the part has a greater excursion on thickness than the control specimens. These thicknesses were measured by microscopic examination.

Microscopic examination of 10 specimens from various areas of the leading edge showed no difference of coating or substrate from previous examinations of flat panel material, so in this respect the leading edge is normal.

Average strength data obtained from the leading edge is summarized in Table 14 along with comparative data from the control specimens, Southern Research Institute (SRI) test data obtained in Phase II, and Battelle data measured on Phase II material. Observations to be made from the data include the following:

- (1) There is little difference between the 12 and 14-ply strengths of the leading edge, and the data is consistent.
- (2) Leading edge strength data agrees closely with the Battelle data within a reasonable tolerance, e. g. , within 13% for inplane stresses.
- (3) Control specimens show higher flexure strength than the part, possibly due to thinner coating or higher compaction (per ply thickness). The control specimens show higher strength than the average Phase II data from either SRI or Battelle.
- (4) Tension-fill and flexure-fill strengths of the leading edge are significantly below those achieved in SRI testing but they are comparable to the data Battelle measured.
- (5) Interlaminar tensile strength is in the region of previous VSD measurements. SRI data is low because of specimen configuration, reference (2), and Battelle data is higher than VSD has measured on Phase II material.

In general when both Battelle and SRI data are taken together, the Phase II leading edge strength is considered comparable to the flat panel

test specimens. This is encouraging, since the leading edge and the material tested by SRI and Battelle do not yet represent a mature system and scatter is expected. For design purposes VSD uses a scatter band of $\pm 33\%$ to establish design allowables, so on this basis the leading edge component strength looks favorable.

Lug strength, rivet strength, and corner angle bending strength data have no comparable SRI or Battelle values to compare against. However, Phase II lug tests of 13-ply flat panel material varied between 485 and 603 lb with the average being 535 lb (reference (2)). Ratioing by ply thickness results in a predicted strength of 700 lb average failing load for 17-ply material to compare against the 833 lb average tested on the leading edge lugs. Therefore, leading edge fabrication appears acceptable.

Angle bending moment is compared against a calculated interlaminar tension stress, which is the mode of failure in the tests conducted. For the 13.7 in. -lb measured, calculated interlaminar tension stress is 560 psi, which compares very favorably with flat specimens taken from the leading edge and flat panels.

Average rivet tension failing load reported in Table 14 computes to be a failing stress of 1220 psi, which, when compared against rivet tensile data from Phase II, reference (2), looks reasonable. Phase II data varied between 627 and 158 psi tensile stress.

Elastic modulus data is shown in Table 15 for the Phase II leading edge, SRI, and Battelle Phase II test data. In some cases the leading edge data is higher, and in others, lower than flat panel data, but even SRI and Battelle data for flat panels are not in total agreement. It appears that better elastic modulus measurement techniques are required for better correlation.

In conclusion the strength values obtained at various locations within the leading edge are fairly consistent with expected values. The data is generally within the tolerance band of data generated by SRI and Battelle in Phase II. The S/N 2 VSD data falls closer to the Battelle data,

TABLE 15 ELASTIC MODULUS COMPARISON, PHASE II LEADING EDGE
(AVERAGE VALUES)

Property	Direction	Plies	ELASTIC MODULUS - 10^6 PSI		
			Phase II Leading Edge, S/N-2	SRI Data Phase II 13-Ply	Battelle Data Phase II 13-Ply
Tension	Warp	12	1.30	1.87	1.71
	Fill	12	1.81	1.47	1.37
		14	2.50		
Flexure	Warp	14	1.91	1.50	1.43
	Fill	12	0.98	1.24	0.72
		14	0.86		
Compression	Warp	12	1.79	2.11	--

which is lower than SRI data. It appears that fabricated components will have property values comparable to those obtained in separate element testing using flat panel stock.

TASK 8 - NON-DESTRUCTIVE EVALUATION OF COATING THICKNESS

The RPP substrate, which provides the structural integrity of the leading edge, is protected from oxidation during entry by a coating, which is formed by coating materials that have diffused into, and reacted with, the outer surfaces of the laminate. The coating so produced is of finite thickness and oxidizes or is eroded at a very slow rate during the 100-mission life of the Shuttle. The initial thickness of the coating is sized to meet the 100-mission life with a suitable margin. To ensure that the design coating thickness is achieved during manufacture, and to gain assurance that sufficient coating remains during the operational life of the Shuttle, it is desirable to be able to measure coating thickness directly on the part in question and be able to do this, not only on the production line, but also on the flight line. The objective of this task, therefore, was to establish an NDE technique for determining coating thickness at various locations on RPP components. This task involved: (1) the determination of an acceptable method for measuring coating thickness on representative flight hardware components; (2) an assessment of the accuracy of the selected method; and (3) definition of procedures for coating thickness measurements for production control, final acceptance, and post-flight inspections. In conjunction with this effort, established NDE techniques for judging component integrity were refined so that the experimental specimens could be judged representative of quality material. Details of this investigation are presented in Appendix A. 1.

Test specimens were processed in accordance with existing production methods and procedures. All specimens were inspected radiographically and ultrasonically during the various stages of processing and in the final coated condition. Three NDI methods of measuring coating thickness were evaluated, these being: (1) eddy current, (2) beta-backscatter, and (3) ultrasonics. A round robin approach was utilized to obtain coating thickness measurement data from three independent NDT laboratories. The round robin participants were: Oak Ridge National Labs,

Los Alamos Scientific Labs, and LTV's NDI labs. The Phase Master, developed by the Oak Ridge National Labs, and the Nortec NDT-8 were used in evaluating the eddy current method. An instrument designed and built by the Los Alamos Scientific Labs was utilized to evaluate the beta-back-scatter method. Short pulsed ultrasonic equipment developed by LTV was employed to evaluate the ultrasonic method. Overall guidance for the Task 8 effort was obtained through the consultation services of Mr. R. W. McClung, who is the Group Leader of the NDT Group at Oak Ridge.

Three rounds of data measurement were conducted utilizing the three NDT laboratories and the previously cited methods. Nine panels, 20 plies in thickness, were processed to the RPP-3 stage. Each of the nine panels was identified and sectioned to make five 4.0 x 6.0 inch specimens and two 3.0 inch diameter discs for a total of 63 test specimens. Two uncoated specimens were obtained from each of the nine panels. The first of these was gained by not submitting the specimens to the coating process, while the second was attained by machining the coating off the fully processed specimens. These specimens served as a bare material reference control, and to determine whether or not any changes in the characteristics of the substrate occurred during the coating process. All other specimens were processed to obtain three nominal coating thicknesses, namely:

- (1) minimum expected - 0.010 inch, (2) mid-range - 0.030 inch, and (3) maximum expected - 0.050 inch.

Two coated specimens from each of the nine panels were subjected to a simulated reentry environment utilizing the plasma arc facility at NASA-JSC. Another coated specimen from each of the nine panels was heat treated in order to determine if further exposure to heat cycles would cause additional changes in the substrate that would affect the coating thickness measurements. Table 16 presents further details with respect to specimen allocations in addition to the schedule for shipment of specimens to the respective NDT labs. Following the first round of data gathering, a statistical model was developed from the data furnished by each laboratory and from the optical coating thickness

TABLE 16 SCHEDULE OF SPECIMENS SHIPMENT

ROUND/SPECIMEN/LAB																														
Panel No.	Round 1 - 1 Sept. '72						Round E(1) 18 Sept. '72						Round 2A 29 Sept '72						Round 2B 6 Oct '72						Round 3 20 Oct '72					
	1	2	3a	3b	4	5	6	3a	3b	4	2	1	2	3a	3b	4	1	2	3a	3b	4	1	2	3a	3b	4	5	6		
	O	L	V	O	L	V	O	N	N	M	M	V	O	N	N	M	O	L	V	O	L	V	L	V	O	L	V	O		
1	O	O	O	O	O	O	O	N	N	M	M	V	V	N	N	M	O	L	V	O	L	V	L	L	L	L	L	L		
2	L	L	L	L	L	L	L	N	N	M	M	O	O	N	N	M	L	V	O	L	V	V	V	V	V	V	V	V		
3	V	V	V	V	V	V	V	N	N	M	M	L	L	N	N	M	V	O	L	V	V	O	O	O	O	O	O	O		
4	O	O	O	O	O	O	O	N	N	M	M	V	V	N	N	M	L	V	O	L	V	L	L	L	L	L	L	L		
5	L	L	L	L	L	L	L	N	N	M	M	O	O	N	N	M	L	V	O	L	V	V	V	V	V	V	V	V		
6	V	V	V	V	V	V	V	N	N	M	M	L	L	N	N	M	L	V	O	L	V	O	O	O	O	O	O	O		
7	O	O	O	O	O	O	O	N	N	M	M	V	V	N	N	M	L	V	O	L	V	L	L	L	L	L	L	L		
8	L	L	L	L	L	L	L	N	N	M	M	O	O	N	N	M	L	V	O	L	V	V	V	V	V	V	V	V		
9	V	V	V	V	V	V	V	N	N	M	M	L	L	N	N	M	L	V	O	L	V	O	O	O	O	O	O	O		

O = Oak Ridge
 L = Los Alamos
 V = VSD
 M = VSD for Heat Treat and Thickness Measurement
 N = NASA for Plasma Arc Test Exposure

(1) Round E is set up to show availability

measurements (actuals) from one section of each of the nine panels. The accuracy of the methods and techniques being evaluated was determined from this model. The balance of the data was then taken, a sample of the specimens was sectioned, and the coating thickness was optically measured. A statistical sample of the total data was then compared to the model.

The ultrasonic pulse echo technique proved entirely too inaccurate to obtain useful data primarily because of surface and interface roughness, and the high attenuation properties of the coating. It was dropped after initial measurements demonstrated the approach to be fruitless. Beta backscatter, likewise, proved to be too insensitive for the desired accuracy, and was certainly less accurate than the eddy current technique.

Only the eddy current method proved to have acceptable accuracy and it uses battery operated, lightweight, readily portable equipment. Further, calibration can rapidly be made using a sample of RPP with the coating machined away, and plastic shims of various thicknesses to accurately establish standoff distances.

Statistical analysis of thickness measurement data showed that coating thickness could be measured within an accuracy of ± 0.0052 in. with 95% probability of non-exceedance, using eddy current equipment operating at 1.6 MHz. This tolerance band is reduced to ± 0.0037 in. with 5 MHz eddy current equipment and should reduce even further if equipment operating up to 15 MHz is employed. This accuracy was obtained over a coating thickness range of 0.010 in. to 0.060 in.

The data plot for the 1.6 MHz equipment is shown in Figure 90, while corresponding data using 5 MHz equipment is shown in Figure 91. This demonstrates the improvement to be realized at the higher frequency. Note that while the meter scales read differently, this does not influence the resultant data, as each meter is calibrated with plastic shims as noted above. The actual thickness measurements were made on sectioned specimens using a microscope at 60x magnification. Each data point

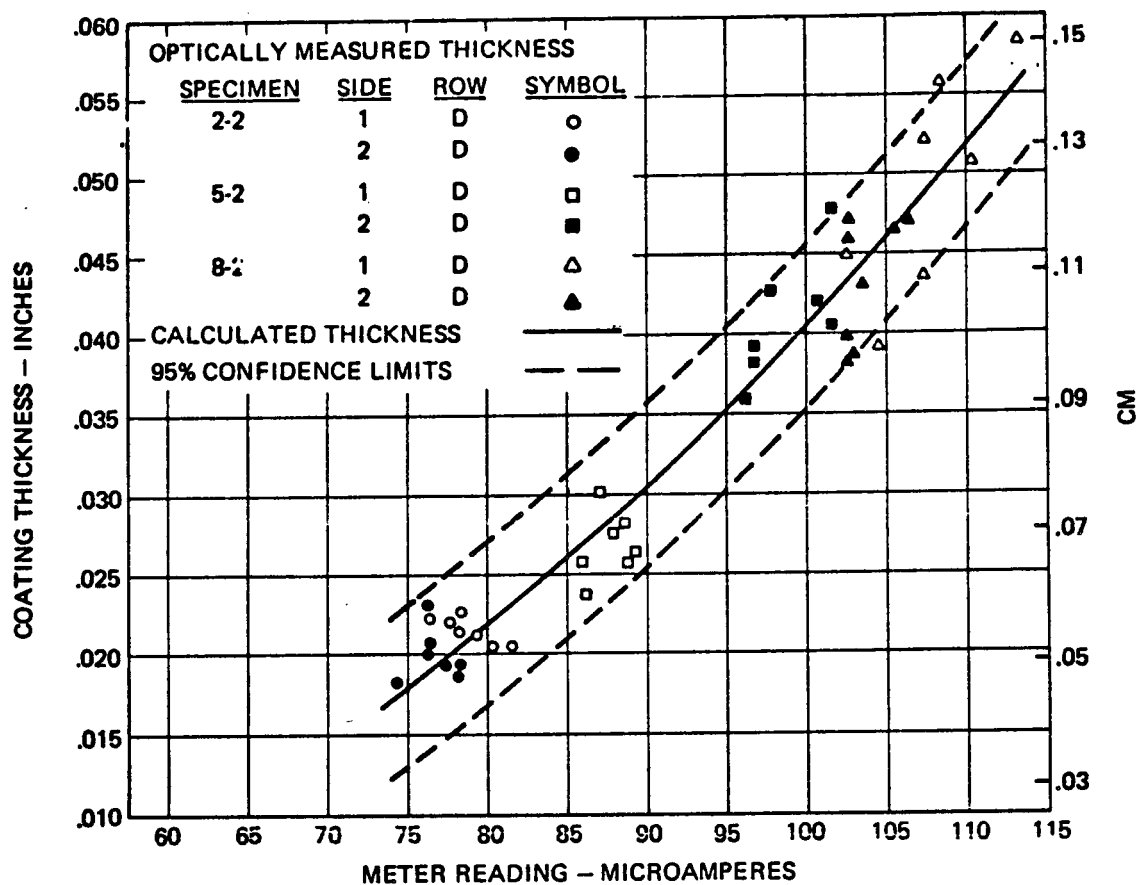


FIGURE 90 EDDY CURRENT STATISTICAL MODEL - 1.6 MHZ EQUIPMENT

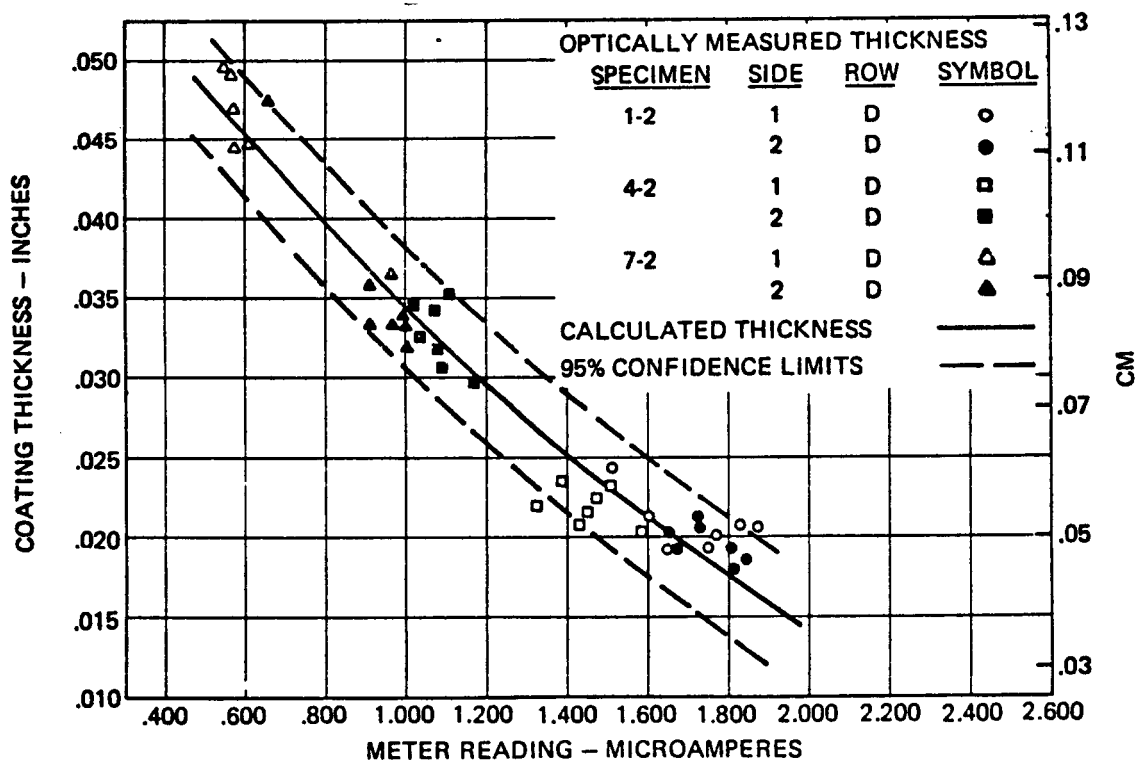


FIGURE 91 EDDY CURRENT STATISTICAL MODEL - 5 MHZ EQUIPMENT

represents an average of ten measurements made in an 0.25 in. length (equal to the diameter of the eddy current probe). The calculated thickness correlation line was established using a least mean square curve fit while the dashed lines indicate the computed tolerance band for 95% probability of non-exceedence.

The significance and desirability of the eddy current technique is readily apparent for the leading edge, both in production and in field operations.

Crazing of the silicon carbide coating on RPP-3 has been a normal characteristic of the material system, since the program inception. All data generated in the Phase II program, Reference 2, was based on crazed material. These tests included plasma arc exposure, 100-mission thermal/oxidation strength tests, fatigue, and static load strength. None of these tests showed that coating crazing produced a significant performance restriction within the 100-mission life requirement of the Shuttle. However, the crazed surface could produce undesirable subsurface oxidation, which would result in lowered laminate strength or reduced coating adhesion. This task, therefore, sought to better understand the crazing phenomenon, and develop techniques to minimize or eliminate its occurrence.

This task consisted of laboratory investigations of the variables related to the coating system and its associated processes. To permit the reduction or elimination of coating crazing that is normally experienced on coated RPP, a more thorough understanding of the chemistry involved was required. The effort included a historical examination of previously coated specimens to compare the degree of crazing with processing, generation of basic information such as coefficients of thermal expansion, identification of coating material constituents - possible reactions and reaction products for the constituents involved, and experiments involving substrate preparation and processing modifications to eliminate crazing. The extent of the effort accomplished is shown in Figure 92. The program approach was based upon coating and substrate preparation investigations conducted at VSD and drawing upon outside knowledge of coating starting materials details, thermodynamic and reaction mechanisms information, as well as analytical support. The following summarizes the tasks accomplished. Details are presented in Appendix A. 2.

1.9.1 CRAZING HISTORY

In order to establish the extent of the coating crazing, an examination of specimens from prior coating runs was made. Specimens coated in 24 in. diameter horizontal and 12 in. diameter vertical furnaces were examined. Retort sizes were evaluated for size effect on the craze

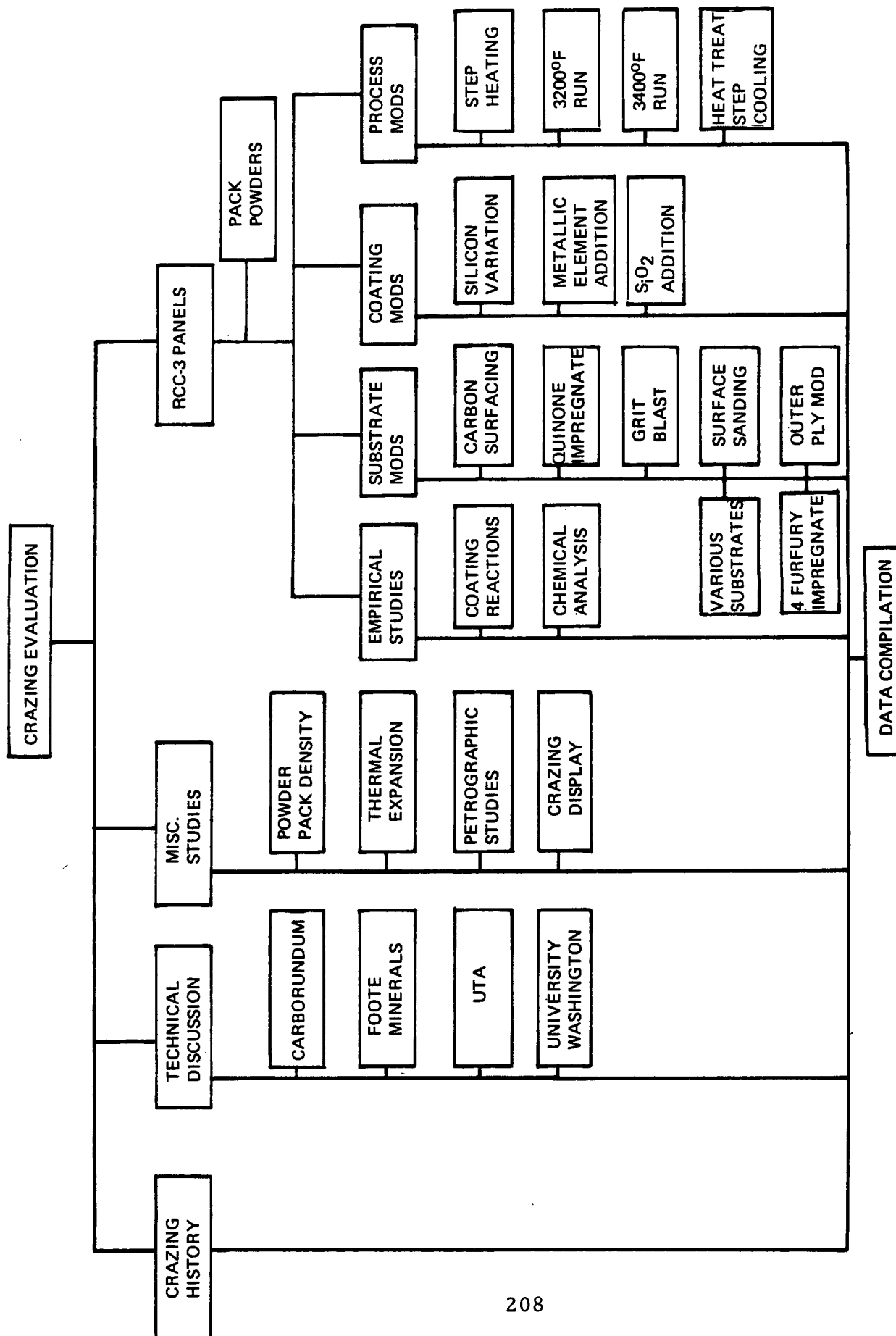


FIGURE 92 CRAZING EVALUATION PROGRAM TASK FLOW TABLE

pattern. Packing methods were studied to relate apparent pack density to the craze pattern. Examination of the data revealed no pattern or single factor that would lead to the cause or elimination of crazing.

1.9.2 TECHNICAL DISCUSSIONS WITH OUTSIDE CONSULTANTS

Trips were made to discuss these technical aspects of the coating process with persons knowledgeable in the field of high temperature chemistry or with experts in the technology of coatings for carbonaceous materials. Of particular assistance was Dr. P. Shaffer of the Carborundum Research Department who was most helpful in discussions dealing with the chemistry of silicon carbide and the effects of small concentrations of impurities during its formation. The chance for a thermal expansion mismatch between the substrate and a silicon carbide coating was considered to be a real possibility which could give rise to a crazing condition within the coating. The possibility of elemental diluents for silicon carbide which might influence its thermal expansion properties was discussed since it was concluded that small doping quantities would not be significantly effective. Larger injected amounts would probably alter the refractoriness of the silicon carbide, changing its high temperature performance capability.

Mr. John Warnach, Plant Manager of Foote Mineral Company's silicon metal powder plant at Wennatchee, Washington, was briefed on VSD's coating process. It was suggested that the purity level factor of silicon might be influential with respect to coating crazing if diffusion coefficients or silicon vapor pressure were controlled by contaminant level concentrations. This was deemed as probably not valid as many different lots of silicon powder have been used and crazing has been noticeable when standard processing is employed.

Dr. Burke Burkart of the Geology Department of the University of Texas at Arlington was also introduced to the problem area. As another possibility for the crazing phenomena, it was suggested that a possible stress was set up within the coating layer if the silicon carbide grains had competed for nucleation sites and growing room was limited sufficiently to

cause crystal growth misalignment. Petrographic examinations made by Dr. Burkart of thin coating sections, however, showed a rather uniform crystal structure which would indicate less strain than that initially anticipated to cause the typically observed crazed pattern.

1.9.3 UNIVERSITY OF WASHINGTON INVESTIGATIONS

The University of Washington, with Dr. J. Mueller as principal investigator, was placed under contract to analytically evaluate the coating process to determine what aspects of the high temperature chemistry, if any, could best be varied to control the crazing phenomena. Analytical determinations were made for reaction products formed under known process conditions and using characterized starting materials. A series of fired and unfired samples was examined. Combinations of starting materials and small size graphite retorts were prepared and heat treated in standard, high temperature fire and low temperature fire coating cycles. These samples were utilized to study the interaction between the graphite retort, RPP-3 substrate, and pack materials. To complement these investigations, a Knudson cell mass spectroscopy study was provided by the NASA-Lewis Research Center to determine the prevalent gas species produced during the high temperature coating cycles.

Experimental findings from these analyses were as follows: (1) the Al_2O_3 fraction of the pack material is a reaction (not inert) chemical member of the system. Aluminum and aluminum oxygen gas species were found by mass spectroscopy of Knudsen Cell products by Dr. Kohl of the NASA-Lewis facility, (2) reactions are occurring in the pack, e.g., silicon melting, SiO_2 and Al_2O_3 reacting with Al(g) species and SiC , (3) reactions are occurring at the RPP-3 interface, e.g., Al_2O_3 with carbon to form Al(g) species and carbon oxides, and coating reactions between various gas phases of silicon with carbon to form the SiC coating, (4) metallic silicon, and to a lesser extent aluminum, are present in the initial coated surface but are vaporized or reacted upon further heat treatment. As another part of their investigation, the University of Washington, in studying the

differential expansion characteristics of the coating and the carbon substrate concluded that sufficient mismatch existed to be the cause of crazing. They postulated that this might be due to firing shrinkage after the coating is formed or to thermal expansion mismatch.

1.9.4 CHEMICAL ANALYSIS

To further characterize the starting materials used in the experiments of this task, semi-quantitative analyses were performed at the Coors Spectrographic Laboratory. The materials analyzed included: (1) Al_2O_3 , (2) silicon, (3) silicon carbide, (4) carbon char, (5) graphite fibers, (6) RPP-3 substrate, (7) coated RPP-3 and (8) heat treated coated RPP-3. Of the 38 metallic elements sought, 13 were detected in sufficient amounts to quantitize. Two of these 13, Al and Si, are in the system from the alumina and silicon metal powder fractions of the pack. Four (Ca, Fe, Mg, B) appear to concentrate in the coating, becoming part of the coating system. These concentrations of contaminants in the coating have not proved detrimental to the performance of the coating. Heat treatment tends to reduce the contaminant amount in the coating. Seven (Cr, Cu, Mn, Ni, Ti, V, Ga) apparently remain in the pack material. The major source of contaminants is the silicon metal powder and constitutes the one site for improvement if contamination proves to be a problem.

Five non-metallic elements were sought. Oxygen was found in all specimens. The 3.3% found in the RPP-3 substrate showed that the substrate carries a significant amount of oxygen into the pack. Its role in the process would be oxidative in nature and could provide a cleaning action during the coating process or raise the oxidation state of the silicon and silicon carbide to a stable oxide level. The hydrogen content was found to be small in the powders and the coating systems, but rather significant in the RPP-3 substrate. Nitrogen concentration follows essentially the same trend as hydrogen, being high in the RPP-3 substrate. The overall high concentration of oxygen, hydrogen, and nitrogen could mean that thermal decomposition products of incomplete resin charring still remains in the

RPP-3 substrate, or alternately, carbon sorption of these gases. Sulfur determinations indicate that small amounts are to be found in the alumina and silicon metal powder pack materials which do not show up in the coating. Fluorine determinations show that fluoride transport of silicon can be ruled out as a prime working mechanism during the coating process.

1.9.5 THERMAL EXPANSION

Thermal expansion measurements at VSD indicated, as shown below, that a noticeable expansion difference exists between the RPP-3 substrate and the siliconized coating applied in the VSD coating process.

DIFFERENTIAL EXPANSION RATIO AT 3000°F BARE RPP-3 AND COATING

Direction	Condition		Ratio
	Bare	Coating	
Warp	1.472	2.634	1: 1.84
Fill	1.575	2.465	1: 1.57

The true magnitude of this difference is not known, but could be the basis for the observed coating crazing phenomena. When the coating is formed on RPP-3 at 3100°F, there are probably no stresses, but as the materials cool to room temperature, the SiC shrinks more than the carbon. The coating goes into tension and fractures in stress relief, forming the crazing pattern. A stress calculation was made assuming coating thicknesses of 0.010 in. and 0.020 in. The theoretical values obtained are shown below:

<u>Coating Thickness (in.)</u>	<u>Calculated Stresses (psi)</u>	
	(SiC) Tension	(c-c) Compression
0.010	210,000	3,100
0.020	560,000	6,000

The handbook ultimate tensile stress of SiC is approximately 5000 psi and the calculated values exceed this by about two orders of magnitude. Using the ultimate tensile stress for SiC, the distance between cracks was calculated to be about 1.1 mm. While this does not exactly correspond to the observed values of 1.5 and 3 mm for fill and warp directions, it does tend to indicate

that thermal expansion mismatch is a prime suspect for the crazing phenomena.

1.9.6 MATERIAL SYSTEM MODIFICATIONS

1.9.6.1 Substrate Modifications

The experiments to modify the RPP-3 substrate in order to more nearly match the siliconized coating to reduce crazing were selected and conducted to cause the least amount of basic change to the substrate. These included: (1) addition of carbon filler powder to the surface of a standard RPP-3 composite, (2) impregnation with graphitizable char producing naphtha quinone and quinone derivative polymers, (3) light grit blasting of RPP composite surface, (4) sanding of RPP-3 composite surface, and (5) outer ply modification by means of substitute carbon reinforcement fabrics. Essentially none of these approaches were effective in reducing or eliminating the coating crazing phenomena.

1.9.6.2 Coating Modifications

Coating experiments modifications were made to affect only the siliconized RPP-3 coating layer. The experiments involved material additions or silicon modifications to the standard 10% Al_2O_3 - 60% SiC - 30% Si pack. Metallic element additions were made with aluminum, chromium, titanium, boron, and iron. Chemical compound additions were made with silicon dioxide. Variations of the silicon metal content from 25 to 39 weight percent with variations of the Al_2O_3 content between 1 to 15 weight percent did not appreciably affect the craze pattern on the coated RPP-3 specimens. Additions of 0.8% aluminum, or 1.9% titanium, or 0.6% boron to the standard

pack mix reduced the craze pattern to a point where it became distinctly visible only under 30x magnification for the titanium and aluminum adjusted pack mixes, while the boron experimental results were entirely free of crazing when examined under magnification up to 60x. In contrast iron and chromium additions were ineffective and the crazing pattern was essentially the same as on the standard coated specimen. It is believed that the effect imposed on the coating system by the aluminum, titanium, and boron to reduce crazing is not basically a chemical union with the SiC coating layer, but rather one of providing a thermal expansion gradient interface zone which smooths out the mismatch between the substrate and coating. This would tend to reduce crazing. In parallel, other experiments indicate that relief from crazing may be obtained by additions of near 1% SiO₂ to the standard pack fired at higher than 3250°F. This experiment was the first clear indication that oxides of silicon were important factors in the coating mechanism.

1.9.6.3 Process Modifications

Process modifications involving variations in the coating ramp time, coating temperatures different from the standard cycle, and step cooling after heat treating were evaluated. Results indicate that crazing can apparently be diminished to a more acceptable level by adjustments to provide hesitations - one hour hold at 2500°F - in the heat-up portion of the coating cycle. Step cooling after heat treating seems to maintain the craze pattern to a visibly acceptable level. Coating temperatures at 3400°F produced coated specimens that do not need heat treating for good plasma performance.

1.9.7 SUMMARY OF RESULTS

The investigations of this task yielded results indicating that the observed coating crazing phenomena is due to the thermal expansion mismatch between the coating and carbon substrate when processed under standard pack mix and coating conditions. However, as can be seen in the

following summarization, the magnitude of the crazing phenomena can be significantly reduced by adjustment of the firing cycle ramp time or by boron or silicon dioxide additions to the pack material.

DEGREE OF CRAZING IMPROVEMENT

Systems	Crazing Visibility Level			
	1X (1)	10X (1)	30X (1)	60X (1)
Standard Coating	Slightly Crazed	---	---	---
Step Heating	Not Crazed	Not Crazed	Crazed	---
SiO ₂ Additions	Not Crazed	Not Crazed	Crazed	---
Boron Additions	Not Crazed	Not Crazed	Not Crazed	Not Crazed

(1) X = Optical Magnification

The ramp time variation of one hour hold at 2500°F is the easiest influential factor to incorporate into the present coating procedure, while the boron or silicon dioxide additive approach needs further evaluation prior to incorporation. Verification coating runs showed the merit of the ramp time hold technique. Strength and oxidation resistance performance of these siliconized RPP-3 specimens were equal to or better than equivalent specimens coated in a run with no ramp time hold. Because of the good results of this investigation, the ramp time hold technique has been integrated into the standard coating firing cycle.

Investigations performed in this task demonstrated that crazing can be significantly reduced by certain process modifications, and may be essentially eliminated through minor coating modifications. The latter will, however, require more extensive investigation to evaluate the full performance and potential of silicon dioxide or boron additions to the coating.

1.10 TASK 10 - FABRICATION OF THICK PLY LAMINATES FOR
NASA TEST

Like Task 5 the purpose of this task was to fabricate four 10 inch x 12 inch x 34 ply RPP panels from which specimens were extracted for NASA-JSC and Battelle (under contract to NASA) test. These panels were fabricated using standard VSD Spec 307-7-7 material and the process defined in Figure 49. These panels were processed together with those of Task 11 (Section .11) and Task 14 (Section .14).

Two furnace runs in the 24" diameter furnace were needed to coat the Task 10 panels, the Task 14 panels, and the 3 inch diameter plasma discs for Task 11. The reproducibility between these two runs as represented by the average weight gain during coating of the four (13-ply) flexure strength control specimens in each run was excellent.

The average weight gain during the first run was 29.5% while the second run had a weight gain of 29.8%. Both of these results compare very favorably with the projected weight gain of 30.7% based on the planned time-temperature profile for the furnace runs. Another set of 13-ply control specimen in the second run had an average weight gain of 30.5%. This indicates that reproducibility from run to run can be achieved. In general, there was very little visible crazing on these parts.

The panels and parts from both coating runs were heat treated at the same time. Heat treatment of the panels did not increase the visible crazing on most of the parts. Weight of the full-size panels was essentially unchanged by the heat treatment procedure while most of the small parts had a slight weight loss, which is normal.

The control specimen flexure strength test result from these runs were as follows:

<u>Thickness</u>	<u>Panel No.</u>	<u>Strength, psi</u>		<u>Strength, psi</u>	
		<u>As-Coated</u>		<u>After H. T.</u>	
		<u>1st Run</u>	<u>2nd Run</u>	<u>1st Run</u>	<u>2nd Run</u>
13 ply	DR 5	14,300	16,800	14,050	15,450
	(11-1)		20,050		16,650
20 ply	11	21,300	28,000	19,950	22,950
34 ply	10 C/T				23,320

Good strength values are indicated. Plasma arc performance was also satisfactory.

The following specimens were fabricated to size and shipped to Battelle for test:

Type	Direction	Overall Size (Inches)	No. of Pieces
Tensile	Warp	5.9 x 1.5	9
	Fill	5.9 x 1.5	9
Shear In-Plane	Warp	5.9 x 1.5	9
Shear Interlam	Warp	5.9 x 1.5	9
Flexure	Warp	5.9 x 1.0	9
	Fill	5.9 x 1.0	9
Compression	Warp	2.6 x 1.0	9
	Fill	2.6 x 1.0	9
Interlam Tension	-	0.75 dia.	9
Diffusivity	-	1.0 x 4.0	1
Emittance	-	1.5 dia.	2
CTE	Interlam	0.35 dia.	18
	Warp	0.44 x stock x 1.75	4
	Fill	0.44 x stock x 3.5	2
Control and NDE	--	Spare Stock	1

Since the testing of these specimens by Battelle is under direct contract to NASA-JSC, the results are not presented herein, except as required for more complete evaluation of Tasks 13 and 14.

In addition to the above, six coated 1.25 in. dia. plasma arc test specimens were fabricated and sent to NASA-LRC for their evaluation.

1.11 TASK 11 - FABRICATION OF 13-PLY LAMINATES FOR
NASA TEST

In addition to thick laminate material supplied under Tasks 5 and 10, 13-ply specimens were supplied under this task. Four 13-ply panels were fabricated using the standard 307-7-7 spec material and the thick laminate process described in Figure 49. As noted in Section 1.10, these panels were processed along with the 34-ply material. However, they were coated and heat treated in the small diffusion furnace.

The following specimens were fabricated and delivered for testing by the noted NASA facility under this task:

<u>Type Specimen</u>	<u>Size</u>	<u>No. Fabricated</u>	<u>For Test By</u>
Plasma arc	1.25 in. dia.	40 coated 6 bare	NASA-LRC NASA-LRC
Plasma arc, control	1.25 in. dia.	6 bare	NASA-LRC
Emittance	1.225 in. square	6 coated	NASA-LRC
Graphite holders	- - -	26 coated only	NASA-LRC
Plasma arc	3 in. dia.	6 coated	NASA-ARC
Plasma arc, control	3 in. dia.	6 bare	NASA-ARC

1.12 TASK 12 - FABRICATION OF ONE ADDITIONAL FAILSAFE
LEADING EDGE

Two deliverable failsafe leading edges were fabricated as part of Task 1, while an additional RPP leading edge was fabricated as Task 12. The purpose of this article was to destructively test it for comparison against flat panel test data (Task 14) and control specimens.

Of the three units fabricated to satisfy the requirements of this contract, unit N-2 was designated for this task. This leading edge was fabricated in accordance with the manufacturing and quality control processes described in Task 1. It was the second unit to be layed up and cured, but was the third to be coated. Dimensional data on the number 2 leading edge panel is provided in Figures 55, 56, 57, and 59. It is generally more accurate than the first unit fabricated and layup progressed much more smoothly with a minimum of squawks.

Following RPP-3 pyrolysis, average strength of the control flexure bars was 17,200 psi, indicating slight strength deficiency from the minimum of 18,000 psi set for acceptance. Strength improvement to bring the part up to specification level was obtained by a special impregnation. This consisted of soaking each of the flanges in furfuryl alcohol for a period of one hour (no vacuum or pressure impregnation was employed) and brush coating all other areas with furfuryl alcohol. This approach, rather than a complete vacuum pressure impregnation cycle, was employed because it was demonstrated in flat panel trials that a complete impregnation after RPP-3 processing would cause delamination in the thicker regions; and it was also determined by experiment that the furfuryl alcohol would satisfactorily soak through the thin flanges. The adequacy of only a brush coat in the thicker areas was justified on the basis that impregnation efficiency has been found to be higher in thick material, probably due to less evaporation from the interior of the material. The validity of the approach taken is shown by the satisfactory strengths obtained in the destructive evaluation of this leading edge as reported under Task 13.

Following pyrolysis control panel flexure strength was increased to an average of 19,100 psi which is acceptable. Two aspects of this operation are worth noting: (1) when processing RPP parts, it is more important that the final part meet desired strength and density rather than be controlled solely to a specific number of impregnation/pyrolysis cycles, and (2) it is possible to improve the strength of the material after RPP-3 processing to meet specification requirements by special impregnation processing.

N-2 leading edge was selected for the acoustic noise test discussed in Section 1.1.1. No damage other than the wallowing out of the attachment holes was noted. NDE examination following acoustic test revealed no failures or delaminations. X-ray radiography, and ultrasonic-through-transmission were used to check the part. Bonded joints for the T-seals were sound. Normal coating crazing was observed by x-ray, and porosity or voids were apparent at each of the rib/spar intersections as noted in Task 1. These do not appear to be structural problems because of the low loads at these intersections, but correction is still required. Filling during layup and/or improved corner debulking should eliminate voids.

Results of the destructive evaluation of this leading edge are covered under Task 13, Section 1.13.

1.13 TASK 13 - DESTRUCTIVE EVALUATION OF A PHASE III
FAILSAFE LEADING EDGE

The purpose of this task was to determine by destructive test the quality of an RPP failsafe leading edge fabricated in Phase III and to compare the results against flat panel test data and control bars fabricated along with the selected leading edge.

Leading edge N-2 was selected for this study, because it represented a degree of fabrication experience, being the third unit fabricated, after the trial leading edge and unit N-1. NDE examination revealed no apparent deficiencies other than the rib/spar corner voids noted in Section 1.12, but these areas were not to be tested. As noted in Task 12, this leading edge was subjected to 100-minutes of acoustic testing at 163 db OA and required beefed-up lug regions to meet the 100-mission acoustic environment.

The cutting plan for this unit is illustrated in Figure 93.

The number and type of examinations made are enumerated below:

- 6 Tension
- 6 Flexure
- 6 Compression
- 4 Interlaminar shear
- 6 Interlaminar tension
- 6 Coating thickness
- 6 Bulk density

Density and coating thickness measurements for the leading edge and control bars, coated with the leading edge, are shown in Table 17. Control specimens with the suffix (N2) in the sample identification number were processed along with the leading edge from layup through coating, while specimens with the suffix (14-3) identification were processed with the leading edge through coating only.

The bulk density of the leading edge varies between 88 lb/ft^3 and 94 lb/ft^3 ($1.41 - 1.50 \text{ gm/cc}$) which is closer to expected values than the Phase II leading edge, Section 1.7. The thinner ply control specimens show a

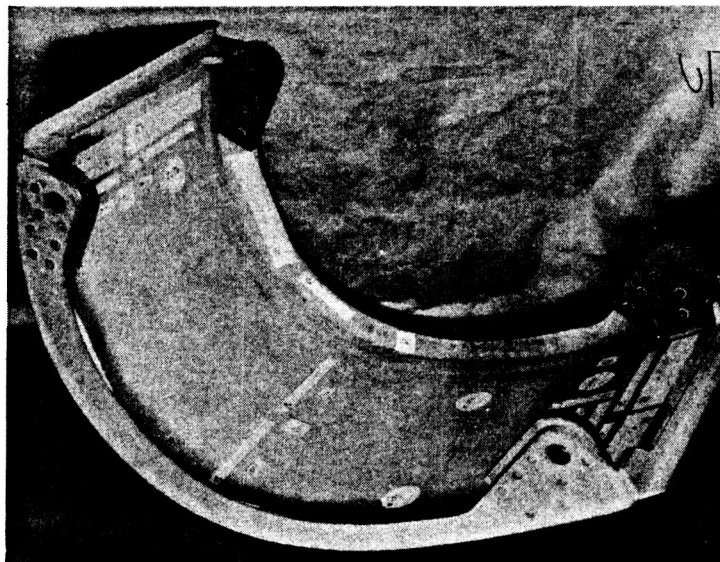
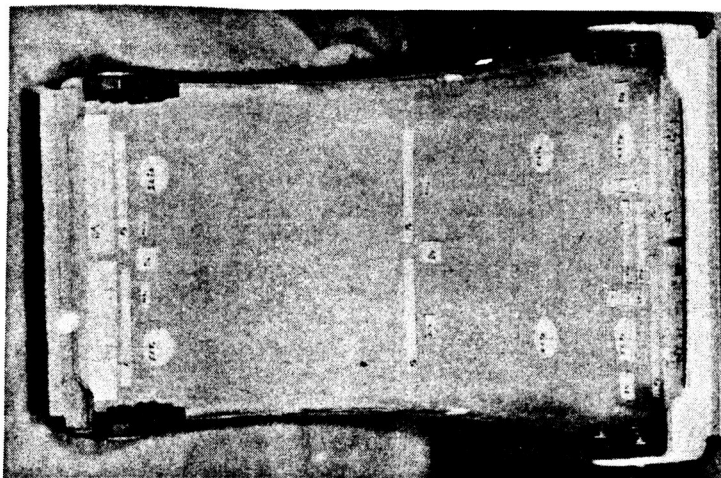
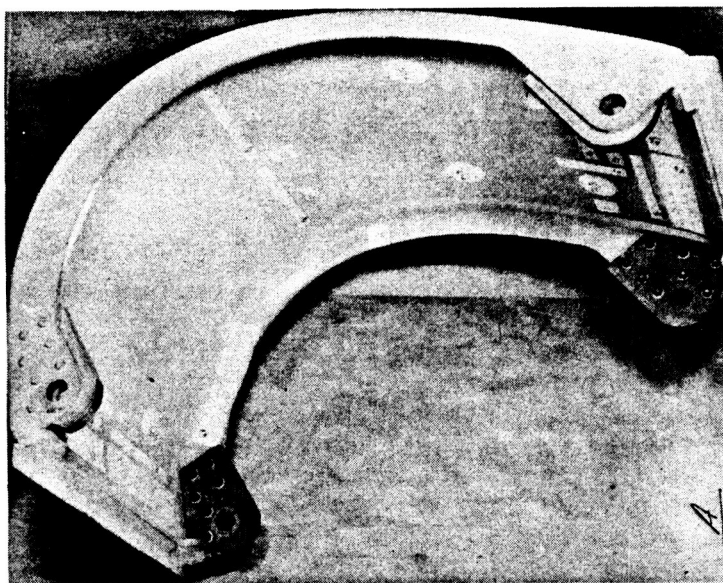


FIGURE 93 CUTTING PLAN - DESTRUCTIVE TEST PHASE III LEADING EDGE

TABLE 17 PHYSICAL PROPERTIES
PHASE III LEADING EDGE AND CONTROL SPECIMENS

N-2 COUPONS					
Sample No.	Plies	Bulk Density gm/cc	Total Thickness in.	Avg. Coating Thickness, in.	
				Bag Side	Mold Side
D1 Lwr Skin	21	1.50	0.265	0.020	0.023
D2 Lwr Skin	21	1.48	0.268	0.020	0.025
D3 Skin	34	1.42	0.443	0.023	0.028
D4 Upr Skin	16*	1.41	0.222	0.020	0.026
D5 Rib	12*	1.48	avg. 0.183	0.028	0.024
D6 Rib	12*	1.45	avg. 0.188	0.029	0.030

* Estimate within one ply, due to specimen extraction in area of splice or ply termination.

CONTROL TEST SPECIMENS					
Sample No.	Plies	Bulk Density	Total Thickness	Avg. Coating Thickness, in.	
				Bag Side	Mold Side
S10-(N2)-N6	13	1.64	0.163	0.032	0.028
S10-(N2)-N8	13	1.63	0.165	0.040	0.032
S10-(14-3)-2	13	1.62	0.162	0.032	0.030
S10-(14-3)-4	13	1.58	0.164	0.030	0.030
S10-(N2)-N7	13	1.60	0.159	0.033	0.032

high density (99 to 102 lb/ft³ (1.58 - 1.64 gm/cc)) primarily because of the greater proportion of coating.

Per ply thickness of the leading edge (exclusive of those sections where total thickness varied in the specimen because of ply termination) varied little, ranging only between 0.0126 and 0.0130 in. /ply. This is a narrower band than experienced on the Phase II leading edge. The control specimens are somewhat more compacted, being in the range 0.0115 to 0.0127 in. /ply. Experience has shown that per ply thickness will be slightly greater for thick laminates than for thinner ones due to relative debulking efficiencies.

This N-2 leading edge was the last to be coated and final adjustments were made in heat conduction paths to ensure more uniform heating during this process. Coating thickness data in Table 17 reflects the improvement affected. Thicknesses do not fall below the 0.020 in. desired, while the upper limit of 0.030 in. represents a satisfactory and expected variation. The mold side (exterior of part), as experienced with the other two Phase III leading edges, has the thicker coating, which is acceptable because the mold side is exposed to the airflow during entry while the bag side is in a stagnant environment. Control specimens have somewhat thicker coating, but these have to be placed in non-optimum locations in the existing coating retort and are not necessarily the best guide to part coating thickness. In production coating thickness of the actual component would be checked using the eddy current technique (Section 1.8), rather than relying upon control specimens. The measurements shown in Table 17 were by microscopic examination of sectioned specimens. Nevertheless, control specimens are still required to measure strength and plasma arc test performance. To obtain more representative control specimens, better retort design and specimen placement is needed.

Strength measurements made on the leading edge are summarized in Table 18. In general, if the Phase III leading edge strengths are compared with the Phase II leading edge strengths, reported in Section 1.7,

TABLE 18 MECHANICAL STRENGTH
PHASE III LEADING EDGE

Property	Direction	Location	Plies	Thickness In.	Failing Strength, PSI	Elastic Modulus, 10 ⁶ PSI
Tension	Warp	Rib	12	0.168	9280	2.90
		Rib	12	0.168	8730	2.22
	Fill	Upper Skin	16	0.194	5430	2.24
		Upper Skin	16	0.195	5020	2.11
		Lwr. Skin	20	0.253	5960	1.62
Flexure	Fill	Lwr. Skin	20	0.255	5970	1.40
		Upper Skin	16	0.198	11800	1.42
		Upper Skin	16	0.197	13100	1.37
		Lwr Skin	21	0.271	16100	1.81
		Lwr. Skin	21	0.266	14900	1.69
Compress.	Warp	Stag. Skin	34	0.460	17200	1.96
		Stag. Skin	34	0.456	18100	2.14
		Rib	12	0.175	13300	2.62
		Rib	12	0.168	12300	2.17
		Lwr. Skin	21	0.270	13000	1.96
	Fill	Lwr. Skin	21	0.271	12900	1.83
		Lwr. Skin	21	0.270	11000	1.67
		Lwr Skin	21	0.271	10100	1.43
		Upper Skin	16	0.204	3380	--
		Upper Skin	16	0.205	3660	--
Interlam Shear	--	Stag. Skin	34	0.439	5390*	--
		Stag. Skin	34	0.440	6000*	--
		Upper Skin	16	--	475	--
		Upper Skin	16	--	383	--
		Lwr Skin	21	--	425	--
Interlam Tension	--	Lwr Skin	21	--	415	--
		Lwr Skin	30	--	395,	--
		Lwr Skin	30	--	400	--

it is found that in all cases with the exception of interlaminar tension the Phase III strength levels exceed those of the Phase II leading edge. This is not surprising since the Phase III panel is thicker than the Phase II unit and therefore the coating influence on strength is not as large. It is encouraging that the strengths are so high.

Similarly, elastic moduli are higher in the Phase III article than those measured on the Phase II unit. The significance of this is not clear at this time but it should be remembered that there has been a wide scatter in elastic modulus measurements in past testing. The Phase III leading edge does not exhibit this same relatively large scatter.

A comparison of strength data obtained from the Phase III leading edge, data measured by Southern Research Institute (SRI) on Phase III flat panel material (reference Section 1.14) and strength measurements made by Battelle for NASA-JSC on Phase III flat panel material are shown in Table 19. Battelle did not flexure test at room temperature, but the 800°F data is believed comparable to room temperature strengths. Several significant factors are to be noted from this comparison, and are enumerated as follows:

- (1) In general the leading edge strength exceeds flat panel values with the exception of interlaminar tension and compression warp for the thin plies. Interlaminar tension and compression warp strengths are in the region of previously measured values, but the flat panel data is higher than previously obtained.
- (2) Tension strength in the rib flanges (12-ply material) is surprisingly high since this material is not completely layed up in the warp direction due to the manner in which the graphite cloth is tailored to produce a curved flange. Therefore, the strength obtained is encouraging.

TABLE 19 STRENGTH COMPARISON
PHASE III LEADING EDGE

(AVERAGE VALUES)									
Property	Direction	Phase III Leading Edge, N-2		SRI Data Phase III Material		Battelle Data (1) Phase III Material			
		Plies	PSI	Plies	PSI	Plies	PSI		
Tension	Warp	12	9005	13	8150	--	--		
	Fill	16	5225	--	--	--	--		
		20	5965	20	4120	--	--		
Flexure	Fill	16	12450	13	10540	--	--		
		21	15500	--	--	--	--		
		34	17650	34	12830	34	11570(800°F)		
Compress	Warp	12	12800	13	16430	--	--		
	Fill	21	12950	20	9900	--	--		
		21	10550	20	10030	--	--		
Interlam Shear		16	3520	20	1920	--	--		
Interlam Tension		16	429	--	--	--	--		
		21	420	20	697	--	--		
		30	397	34	645	34	630 (R. T.)		

(1) Preliminary data

- (3) The difference between interlaminar shear, data obtained by SRI and that from the leading edge is probably more a function of test technique than material properties. Leading edge data was obtained with a short beam shear specimen, while the flat panel data was measured on compression-shear specimens with a small cross-sectional area. Therefore, no conclusive comparisons can be made.

In summary the data obtained from the Phase III leading edge demonstrates that high strength can be obtained in a component, that within expected tolerances meets or exceeds data derived from testing of flat panels.

1.14 TASK 14 - THICK LAMINATE PROPERTY DETERMINATION

Previous strength data measured on coated RPP was confined to 13-ply material because this was the thickness region of primary interest for the Phase II leading edge design. However, with the failsafe concept of Phase III, thicknesses as great as 34 plies were required. The purpose of this task was to evaluate the strength performance of the thicker ply material. The test program was exploratory to determine trends or problems as opposed to generating design data.

To make a more thorough evaluation, two thicknesses were chosen for thick ply evaluation, 20-ply and 34-ply, and were compared against a 13-ply baseline. In addition, a limited amount of data was gathered on bare 8-ply RPP to validate the oxidized leading edge analysis of Task 1. Southern Research Institute (SRI) was chosen for this testing to maintain continuity with the Phase II test data, reference (2). Further, Battelle was selected by NASA-JSC to perform testing of the VSD Phase III 34-ply laminates for NASA (reference Task 10), thus providing a comparison of test techniques.

The thick ply panels for both Task 10 and Task 14 were processed together, and eventually the 34-ply panel material was randomly selected for distribution to SRI and Battelle for testing. SRI performed all machining of specimens from the coated panels provided, while VSD performed most of the machining of specimens for Battelle testing.

Panels were fabricated from 307-7-7 spec material and were processed in accordance with the steps defined in Figure 49. Coating was accomplished in the 24 in. diameter furnace and a one-hour hold was introduced at 2500°F to more evenly distribute heat. This process modification was a result of Task 9 development, and produced coatings that were craze-free to the unaided eye. As noted in Task 10, weight gain during coating was as planned, and strength of control flexure bars was equal to or exceeded expectations. SRI test specimens were taken from three 34-ply panels, two 20-ply panels and two 13-ply panels with each panel measuring 10 in. x 12 in.

Average strength data obtained, which is based on three specimens per data point except as noted, is summarized in Table 20.

Preliminary results from Battelle testing at 800°F, which should be comparable to room temperature values for this material, is shown for comparison. Phase II data, measured by SRI (except for inplane shear which was tested by VSD) is also shown for comparison.

The data is somewhat puzzling, because flexure strength on the 34-ply material is lower than in-house results. For example, 23,320 psi was obtained on a 34-ply control specimen coated along with the thick laminate material (reference Task 10). In addition, Task 1 38-ply thick laminate flexure results were consistently in the 20,000 psi range; and 20-ply specimens coated with the Task 8 material produced strengths of 20,000 psi and above. Further, VSD tests characteristically produced failure on the tension side of the specimen, but both SRI and Battelle note compression failures dominate in their tests. Therefore, the relatively low values obtained by both SRI and Battelle are not totally understood, except that they are supported by the low compression strengths obtained (Table 20).

Similarly, flexure strength in the fill direction for 34-ply material appears low in comparison with the strengths obtained from the Phase III leading edge (Section 1.13), where the average fill direction flexure strength in the 34-ply region of the skin was 17,650 psi. This compares with 12,830 and 11,570 psi average values from SRI and Battelle tests.

The question is whether the differences are due to test technique (e.g., load fixtures, specimen width, load span, support span) or whether they are from material variations. At this point it isn't clear which is correct or if it is a combination of factors. Further testing would be required to analyze this problem.

There is no apparent flexure strength increase with thickened material, as was found in VSD tests, and any differences noted in Table 20 are within the normal scatter band. The 20-ply material produced lower strengths than the 13-ply material, which was surprising, and gave

TABLE 20 STRENGTH DATA
PHASE III COATED RPP

Property	Direction	Plies	Average Failing Stress PSI		
			SRI Phase III	Battelle ⁽¹⁾ Phase III	Phase II (Ref (2))
Tension	Warp	13	9,150	--	8,500
		20	6,330	--	
		34	10,560	9,680	
	Fill	13	4,230	--	4,500
		20	4,120		
		34	5,690	5,470	
Flexure	Warp	13	17,920	--	14,200
		34	17,340	15,060	
	Fill	13	10,540	--	12,200
		34	12,830	11,570	
Compress	Warp	13	16,430	--	11,500
		20	9,900	--	
		34	7,350	9,610	
	Fill	13	15,960 ⁽²⁾	--	11,900
		20	10,030	--	
		34	6,660	9,380	
Shear	Warp	13	4,090	--	3,800
		20	3,210	--	
		34	3,810	3,440	
	Fill	13		--	3,900
		20	3,560	--	
		34	4,230		
Interlam Shear	--	13	--	--	2,200
	--	20	1,920	--	
	--	34	2,040	1,250	
Interlam Tension	--	13	--	--	400
		20	700 ⁽²⁾	--	
		34	650	630(R. T)	

(1) Preliminary data - measured at 800°F except for noted Room Temperature test.

(2) Average of two specimens.

the lowest strength in tension. Data from the N-2 leading edge, Section 1.13, suggests that higher strengths can be produced with 20-ply laminates.

Compression strength decreases with increasing thickness as shown in Table 20, and is consistent in both warp and fill directions. The coating should have some influence on this trend but there is probably some laminate variation, as well, that is contributing to the strength drop off. N-2 leading edge compression data (Section 1.13) indicates higher strength in the warp direction than obtained on flat panels, but fill data is comparable.

The various discrepancies between sets of data suggests that further evaluation is required and probably process controls for the laminate need additional tightening so that higher strength material can be produced routinely. In addition, optimization of test specimen configuration, specimen machining techniques, and test technique need pursuing so that total confidence can be had in the test data.

Interlaminar shear strength is slightly lower than previously obtained, while interlaminar tension is somewhat higher than Phase II test data, and higher than values obtained on the 38-ply material developed in Task 1, Section 1.1.4. The interlaminar strength, which influences compression strength, does not suggest a reason for the sharp decline of compression stress with increased ply thickness. Interlaminar shear stress obtained by Battelle appears unrealistically low and suggests that the test specimen or technique is causing induced tensile stress components which lowers the apparent shear stress.

Examination of the 13-ply data shows that the Phase III material is generally comparable to the Phase II material and perhaps even a little better if compression is used as a guide. It is seen that there is little significant difference between warp and fill compression strengths, possibly due to the influence of the coating. Inplane shear exhibits similar behavior in that warp and fill values obtained are within an expected tolerance band.

Strength of bare RPP, 8-ply thickness, to compare with Task 1 analysis requirements, is given in Table 21. These strengths are well in excess of those used for design in Task 1, Section 1.1.1.

Shear modulus data was measured by torquing flat panels and measuring the induced strains with strain gages. Resultant values of shear modulus are shown in Table 22.

Elastic modulus data for tension, flexure, and compression are shown in Table 23. Tension modulus data follows the strength trend (Table 20) in that the elastic modulus for 20-ply material is lower than for either 13 or 34 ply. Two elastic modulus values are shown for flexure, because there is usually an initial slope of the load-deflection curve that steepens to a second value, presumably when the edges of the crazed coating butt against each other and begin to carry load. For the 13-ply material in the fill direction there was only one slope. Data was in the same range as that obtained on N-2 leading edge, Section 1.13, except that compression-fill modulus is somewhat higher than the values obtained from the leading edge.

In summary the thick flat panel strengths as measured in this task are lower than those determined during laminate process development (Task 1), quality control processing checks (Task 8, 10 and 14), and destructive evaluation of N-2 leading edge (Task 13). This could be due to material variability or test technique, and must be evaluated further for resolution. However, the potential strength capability for thick laminate material is demonstrated by Task 1 and Task 13 data.

TABLE 21 STRENGTH DATA
BARE 8-PLY RPP

Property	Direction	Avg. Strength PSI	Avg. Elastic Modulus, PSI
Tension	Warp	13,450	2.35×10^6
	Fill	7,290	1.43×10^6
Compress	Warp	9,270	3.22×10^6
	Fill	8,850	2.21×10^6
Shear	Warp	4,200	1.07×10^6

TABLE 22 SHEAR MODULUS

Ply Thickness	Condition	Shear Modulus, PSI
8	Bare	1.07×10^6
13	Coated	0.70×10^6
20	Coated	0.68×10^6
34	Coated	0.82×10^6

TABLE 23 ELASTIC MODULUS
PHASE III COATED RPP

Property	Plies	Average Elastic Modulus, 10^6 PSI			
		Warp		Fill	
Tension	13	2.15		1.41	
	20	1.75		1.38	
	34	2.38		1.81	
Flexure ⁽¹⁾	13	1.18	1.91	1.12	1.12
	34	1.71	2.23	1.19	1.42
Compress	13	2.21		--	
	20	2.19		2.16	
	34	2.73		1.82	

- (1) Typical flexural elastic modulus of elasticity showed initial and secondary moduli. First number represents initial, while second number is secondary modulus.

REFERENCES

- (1) Development of a Thermal Protection System for the Wing of a Space Shuttle Vehicle, Phase I Final Report, LTV/VSD Report No. TR143-5R-00044, no date (NASA Contract NAS9-11224).
- (2) Development of a Thermal Protection System for the Wing of a Space Shuttle Vehicle, Phase II Final Report, LTV/VSD Report No. T143-5R-00124, March 1972 (NASA Contract NAS9-11224).
- (3) Oxidation Inhibited RPP Space Shuttle Belly Panel, LTV Report No. T159-5R-00047, dated 31 January 1972.
- (4) Evaluation of Nonmetallic Thermal Protection Materials for the Manned Space Shuttle, Vol. VI (Phase II/Task 2), Final Report, F. P. Kirkhart, W. H. Duckworth, I. M. Grinberg, J. W. Droege, and E. L. Foster, Battelle Columbus Laboratories.
- (5) Draft, Final Report on "Evaluation of Nonmetallic Thermal Protection Materials for Manned Space Shuttle, Vol. IX", W. H. Duckworth, W. C. Chard, K. E. Wilkes, J. H. Peterson, R. A. McCann, and E. L. Foster, Preliminary Results.